

2016-4

Hybrid Optical Fiber Sensors for Smart Materials and Structures

Manjusha Ramakrishnan

Technological University Dublin, manjusha.ramakrishnan@mydit.ie

Follow this and additional works at: <https://arrow.tudublin.ie/engdoc>

Recommended Citation

Ramakrishnan, M. (2016) *Hybrid optical fiber sensors for smart materials and structures*. Doctoral thesis, 2016.

This Theses, Ph.D is brought to you for free and open access by the Engineering at ARROW@TU Dublin. It has been accepted for inclusion in Doctoral by an authorized administrator of ARROW@TU Dublin. For more information, please contact arrow.admin@tudublin.ie, aisling.coyne@tudublin.ie, vera.kilshaw@tudublin.ie.

Hybrid optical fiber sensors for smart materials and structures

A thesis

Submitted for the degree of Doctor of Philosophy

by

MANJUSHA RAMAKRISHNAN



School of Electrical & Electronic Engineering

College of Engineering & Built in Environment

Dublin Institute of Technology

Supervisors: Prof. Gerald Farrell Prof. Yuliya Semenova and

Dr. Ginu Rajan

Dublin, Ireland

April, 2016

To my father, my husband with all my love

Abstract

There has been a rapid growth in the use of advanced composite materials in a variety of load-bearing structures, for example in aviation for structures such as rotor blades, aircraft fuselage and wing structures.

Composite materials embedded with fiber-optic sensors (FOS) have been recognized as one of the prominent enabling technologies for smart materials and structures. The rapid increase in the interest in composite materials embedded with FOS has been driven by numerous applications, such as intelligent composite manufacturing/processing, and safety-related areas in aircrafts.

Research has been focused recently on using several optical sensor types working together to form so called “hybrid optical fiber sensors” in order to overcome the limitations of the individual sensor technologies.

The main aim of the research described in this thesis is to investigate a hybrid sensing scheme that utilizes polarimetric sensors and FBG sensors working in a complimentary fashion to measure multiple physical parameters in a composite material, with a particular focus on measuring the complex indirect parameters thermal expansion and vibration. The research described in this thesis investigates the performance of a hybrid sensing scheme based on polarimetric sensors and FBG sensors after embedding in a composite material. It is shown that the influence of thermal expansion within a composite material on embedded polarimetric sensors is the main source of errors for embedded fiber sensor strain measurements and that for practical strain sensing applications buffer coated PM-PCF are more suitable for embedding in composite. Further, using a buffer stripped PM-PCF polarimetric sensor, a measurement scheme to measure a composite material's

thermal elongation induced strain is proposed. A novel hybrid sensor for simultaneous measurement of strain, temperature and thermal strain is demonstrated by integrating polarimetric sensors based on acrylate coated high bi-refringent polarization maintaining photonic crystal fiber (HB-PM-PCF), and a coating stripped HB-PM-PCF sensor together with an FBG sensor.

Flexible demodulation modules that can be embedded or surface attached is a challenge for composite materials containing fiber-optic sensors. In this thesis an interrogation method that allows intensity domain operation of hybrid sensor is demonstrated. Further focusing towards the miniaturization of the hybrid sensor interrogator, a miniaturized flexible interrogator for the demonstrated hybrid sensing scheme embedded in a composite material is also designed.

Low frequency vibration measurements are performed for glass fibre-reinforced composite material samples with two different strain-sensitive polarimetric sensor types embedded. It is shown that the strain sensitivity of polarimetric sensors limits the vibration measurements to a certain range of vibration amplitudes. A polarimetric sensor based buffer stripped HB-PM-PCF is demonstrated for monitoring the different stages of the curing process for a Magneto-Rheological composite material.

By providing information about multiple parameters such as strain, temperature, thermal strain, vibration amplitude and vibration frequency the proposed and demonstrated hybrid sensing approach has a high potential to change the paradigm for smart material design in the future.


Declaration

I certify that this thesis which I now submit for examination for the award of PhD, is entirely my own work and has not been taken from the work of others, save and to the extent that such work has been cited and acknowledged within the text of my work.

This thesis was prepared according to the regulations for postgraduate study by research of the Dublin Institute of Technology and has not been submitted in whole or in part for an award in any other Institute or University.

The work reported in this thesis conforms to the principles and requirements of Institute's guidelines for ethics in research.

The Institute has permission to keep, to lend or to copy this thesis in whole or in part, on condition that any such use of the material of the thesis be duly acknowledged.

Signature of  _____ Date ____ / ____ /2016____

Candidate

Acknowledgements

The work presented in this thesis has been carried out within the Photonics Research Centre of the Dublin Institute of Technology.

There are numerous people without whose support this thesis would be impossible. Firstly I would like to express the most sincere gratitude to my supervisor, Dr. Gerald Farrell for giving me this opportunity to further my education. I also want to thank him for all his guidance, support with a favorable decision on my maternity related leave issues, patience during my doctoral studies, and for allowing me the freedom to pursue my own ideas and interests. I am deeply indebted to Dr. Yuliya Semenova and Dr. Ginu Rajan for their guidance, comments, encouragement, and willingness to serve as my associate supervisors. I also want to thank both of them for their sincere support by considering the difficulties of a newborn's mother during the most critical stages of doctoral studies.

My sincerer gratitude to members of Faculty of Physics and Faculty of Materials Science, departments of Warsaw University of Technology, Warsaw, Poland for providing facilities to fabricate many composite samples used in the measurements. I would like to extend my sincere gratitude to my publication's co-authors; Anna Boczkowska , Andrzej Domanski', Tomasz Wolinski and Poitr Lesiak for their guidance, and comments. I would like to thank all the partners of Smart Sensors for Engineering Structures (SSES project), (MATERA-ERAnet Project) for their support. Special thanks to Raffel Mikke of Delta company, Poland for facilitating industrial standard composite samples. This is acknowledged and highly valued. I also want to gratefully acknowledge the financial support of

Enterprise of Ireland for this work.

My special thanks and sincere acknowledgement goes to my teachers Prof. V. P. N. Nampoori, Prof. V. M. Nandakumaran, Prof. P. Radhakrishnan, Mr. Madusoodhanan and Mr. Kamalakshan for their constant help and encouragement.

I would like to also extend my sincere thanks to all the faculty, staff and students in Photonics Research Centre for their friendship, technical assistance, and support. I always remember with thanks the help and encouragements I received from my colleagues. It is not possible to write all their names in this page. I wholeheartedly thank Dr. Sithara Pavithram Sreenilayam, Sony, Dr. Sunish James Mathew, Dr. Jinesh Mathew, Ms. Renin Toms and Ms. Shimi Sukumaran for the all helps, nice trips, parties and lovely jokes.

Finally I would like to express my gratitude to those extraordinary people my soul mate my husband, for his enormous help, support and encouragement in every aspect of my life and to my parents and sisters, who raised me and trust me with their endless love. I would like to thank my mother for prayers, scarifies and never ending support. Most importantly, I would like thank my father, who has contributed his life to the family and is one of who motivated me in my tough times. At last not least would like to thank the most effected person of my Doctoral studies, one year old lovely son Ayaan, who stayed well-adjusted during my absence at thesis writing stages.

Above all, I greet with gratitude the Almighty for giving in me the courage to survive the hard times which I went through.

List of publications arising from research

Book Chapters

1. **M. Ramakrishnan**, G. Rajan, Y. Semenova, and G. Farrell. "*Optical Fiber Sensors for smart composite materials structures.*" Advanced Techniques and Applications, CRC Press: New York, K. Iniewski & G. Rajan (Editors), pp.491-520, 2015.

Journal papers

2. **M. Ramakrishnan**, G. Rajan, Y. Semenova, and G. Farrell. "*Overview of Fiber Optic Sensor Technologies for Strain/Temperature Sensing Applications in Composite Materials.*" Sensors, Vol 16(1): 99, 2016.
3. **M. Ramakrishnan**, G. Rajan, Y. Semenova, Y. Zhou, S. Jerrams, and G. Farrell. "*Photonic crystal fibre-based polarimetric sensor for cure monitoring of magnetorheological smart composite material.*" Electronics Letters, Vol 50(15), pp. 1083-1084, 2014 .
4. **M. Ramakrishnan**, G. Rajan, , Y. Semenova, D. Callaghan, and G. Farrell. "*Investigation of the effect of vibration amplitude on vibration measurements of polarimetric fiber sensors embedded in composite beams.*" Smart Materials and Structures, Vol 23(4), pp. 045037, 2014.
5. **M. Ramakrishnan**, G. Rajan, , Y. Semenova, T. Wolinski, A. Domański, and G. Farrell. "*A miniaturized flexible surface attachable interrogator for hybrid*

- optical fiber sensing.* "Microwave and Optical Technology Letters, Vol 56(5), pp. 1167-1174, 2014.
6. **M. Ramakrishnan**, G. Rajan, Y. Semenova, and G. Farrell. *Hybrid Fiber Optic Sensor System for Measuring the Strain, Temperature, and Thermal Strain of Composite Materials.* "Sensors Journal, IEEE, Vol 14(8), pp. 2571-2578, 2014 .
 7. **M. Ramakrishnan**, G. Rajan, Y. Semenova, A. Boczkowska, A. Domański, T. Wolinski, and G. Farrell. *Measurement of thermal elongation induced strain of a composite material using a polarization maintaining photonic crystal fiber sensor.* "Sensors and Actuators A: Physical, Vol 190, pp. 44-51, 2013.
 8. **M. Ramakrishnan**, G. Rajan, Y. Semenova, P. Lesiak, A. Domanski, T. Wolinski, A. Boczkowska, and G. Farrell. *The influence of thermal expansion of a composite material on embedded polarimetric sensors.* "Smart Materials and Structures , Vol 20(12), pp.125002, 2011.
 9. G. Rajan, **M. Ramakrishnan**, Y. Semenova, E. Ambikairajah, G. Farrell, and G. D. Peng. *"Experimental study and analysis of a polymer fiber Bragg grating embedded in a composite material."*Journal of Lightwave Technology, Vol 32(9) , pp. 1726-1733, 2014.
 10. G. Rajan, **M. Ramakrishnan**, Y. Semenova, A. Domanski, A. Boczkowska, T. Wolinski, and G. Farrell. *Analysis of vibration measurements in a composite material using an embedded HB-PM-PCF polarimetric sensor and an FBG sensor.* "Sensors Journal, IEEE, Vol 12(5), pp.1365-1371, 2012.
 11. G. Rajan, **M. Ramakrishnan**, P. Lesiak, Y. Semenova, T. Wolinski, A. Boczkowska, and G. Farrell. *Composite materials with embedded photonic*

- crystal fiber interferometric sensors.*'Sensors and Actuators A: Physical, Vol 182, pp. 57-67, 2012.
12. G. Rajan, **M. Ramakrishnan**, Y. Semenova, K. Milenko, P. Lesiak, A. W. Domanski, T. R. Wolinski, and G. Farrell. *A photonic crystal fiber and fiber bragg grating-based hybrid fiber-optic sensor system.*'Sensors Journal, IEEE, Vol 12(1), pp. 39-43, 2012.
 13. G. Rajan, K. Milenko, Piotr Lesiak, P. Lesiak, A. Boczkowska, **M. Ramakrishnan**, K. Jedrzejewski, A. Domanski, T. Wolinski, and G. Farrell. *A Hybrid Fiber Optic Sensing System for Simultaneous Strain and Temperature Measurement and its Application.*,"Photonics letters of Poland, Vol 2(1), pp. 46-48, 2010.

Conference proceeding papers

1. **M. Ramakrishnan**, G. Rajan, Y. Semenova, and G. Farrell. "*electro-optic modulator based interrogation for a polarimetric fiber sensor for strain and temperature measurements*", Photonics Ireland Belfast, 2013
2. **M. Ramakrishnan**, G. Rajan, Y. Semenova, T. Wolinski and G. Farrell. *A demodulation scheme for a hybrid fiber sensor system for composite materials*", In SPIE Photonics Europe (pp. 843929-843929). International Society for Optics and Photonics, Brussels, Belgium, 2012.
3. **M. Ramakrishnan**, G. Rajan, Y. Semenova, and G. Farrell. "*Characterization of the polarimetric sensors embedded in carbon and glass reinforced composite materials for strain/temperature measurements*", OSA, Photonics 2012, India.

4. **M. Ramakrishnan**, G. Rajan, Y. Semenova, T. Wolinski and G. Farrell. *Comparison of vibration measurements in composite materials using different types of polarimetric sensors.* "In OFS2012 22nd International Conference on Optical Fiber Sensor, pp. 842178-842178, 2012.
5. **M. Ramakrishnan**, G. Rajan, Y. Semenova, P. Lesiak, A. Domanski, T. Wolinski and G. Farrell. "*Design of a flexible electro-optic polymer phase modulator for demodulation of polarimetric sensors*", IOS 2011, Szczyrk, Poland.
6. **M. Ramakrishnan**, G. Rajan, P. Lesiak, Y. Semenova, A. Domanski, T. Wolinski, A. Boczkowska and G. Farrell. "*Detection of thermal expansion of carbon and glass reinforced fiber composite materials using polarimetric and fiber Bragg grating sensors*", ICONTOP-2011, Calcutta, India.
7. **M. Ramakrishnan**, G. Rajan., Y. Semenova, G. Farrell. "*Design of a surface attachable hybrid sensor packaged in polyimide film for engineering applications*", EWOFS-2010, Porto.
8. **M. Ramakrishnan**, G. Rajan., Y. Semenova, G. Farrell. "*Composite Materials with embedded fiber sensors for in-situ structural health monitoring*", WICSM-2010, Dublin.
9. G. Rajan, **M. Ramakrishnan**, Y. Semenova, and G. Farrell. "*Performance analysis of composite materials embedded with optical fiber sensors*," IEEE Sensors Conference 2011, Ireland.

Contents

Smart Structures with Embedded Hybrid Optical Fiber Sensors.....	I
Abstract.....	IV
Declaration.....	VI
Acknowledgements.....	VII
List of publications arising from research	IX
Contents	XII
List of Figures.....	XIX
List of Tables	XXVII
Acronyms	XXVIII
 Chapter 1: Introduction	 1
1.1 Background to the research	1
1.1.1 Introduction to fiber optic sensors	1
1.1.2 Introduction to smart materials and structures	2
1.1.3 Composite materials: structures and types	3
1.1.4 Smart composite structures with embedded fiber optic sensors	7
1.1.5 Optical fiber sensor types	9
1.1.6 Fiber optic polarimetric sensors	10
1.1.7 Fiber Bragg Grating (FBG) sensors	13
1.1.8 Hybrid fiber optic sensor system	15
1.2 Research motivation	18
1.3 Aims and objectives of the research	19

1.4	Research methodology	22
1.5	Layout of the thesis	27
1.6	References	30
Chapter 2: Review of fiber optic Sensor technologies for strain/temperature Sensing in Composite Materials		35
2.1	Overview of fiber optic sensors technologies for strain/temperature sensing applications of composite Materials	37
2.1.1	Introduction	38
2.1.2	Composite materials and demand for the SHM in composite material structures	38
2.1.3	Composite materials with embedded fiber sensors: fabrication methods	42
2.1.4	Composite material degradation associated with embedding of fiber sensors	48
2.1.5	Types of fiber optic sensors for strain / temperature measurements in composite materials	49
2.1.6	Recent trends, issues and future challenges of the OFS technology	76
2.1.7	Conclusion	70
2.1.8	References	80
Chapter 3: Influence of thermal expansion of a composite material on embedded sensors		95
3.1	The influence of thermal expansion of a composite material on embedded polarimetric sensors	96

3.1.1	Introduction	96
3.1.2	Temperature sensitivity of polarimetric sensors	99
3.1.3	Fabrication of composite samples with embedded optical fiber sensors	101
3.1.4	Experimental arrangement	104
3.1.5	Results and discussion	107
3.1.6	Conclusion	114
3.1.7	References	116
Chapter 4: Measurement of thermal elongation induced strain of a composite material using embedded sensor		119
4.1	Measurement of thermal elongation induced strain of a composite material using a polarization maintaining photonic crystal fiber sensor	120
4.1.1	Introduction	121
4.1.2	Methodology of thermal elongation induced strain measurement using a stripped HB-PM-PCF sensor embedded in composite material	124
4.1.3	Fabrication of the composite material sample	126
4.1.4	Experimental arrangement	129
4.1.5	Results and discussions	131
4.1.6	Conclusion	140
4.1.7	References	141
Chapter 5: A multi parameter hybrid fiber optic sensor system and miniaturized interrogator for composite structural health monitoring applications		147

5.1	Hybrid fiber optic sensor system for measuring the strain, temperature and thermal strain of composite material	149
5.1.1	Introduction	150
5.1.2	Principle of operation	153
5.1.3	Experimental demonstration of the hybrid sensor system	159
5.1.4	The hybrid sensor system for strain, thermally induced stain and temperature sensitivities	162
5.1.5	Conclusion	170
5.2	A miniaturized flexible surface attachable interrogator for hybrid optical fiber sensing	171
5.2.1	Introduction	172
5.2.2	Hybrid sensor – methodology	175
5.2.3	The flexible interrogation module	176
5.2.4	Design and fabrication of the proposed flexible interrogator	178
5.2.5	System integration considerations	190
5.2.6	Conclusions	191
5.3	References	192
Chapter 6: Derived applications of polarimetric strain sensing for composite structural health monitoring purposes		198
6.1	Investigation of the effect of vibration amplitude on vibration measurements of polarimetric fiber sensors embedded in composite beams	200
6.1.1	Introduction	202
6.1.2	Theoretical background of polarimetric sensors	205

6.1.3	Fabrication of composite samples with embedded optical fiber sensors	210
6.1.4	Experimental arrangement	213
6.1.5	Results and analysis	215
6.1.6	Discussion	226
6.1.7	Conclusions	226
6.2	A photonic crystal fiber based polarimetric sensor for cure monitoring of magneto-rheological smart composite material	228
6.2.1	Introduction	229
6.2.2	Experiment	230
6.2.3	Principle	232
6.2.4	Results and discussion	233
6.2.5	Conclusions	237
6.3	References	237
Chapter 7: Conclusions and future work		242
7.1	Conclusions from the research	242
7.2	Overall conclusions from the research	250
7.3	Future work	252
7.4	References	255
Appendix A: Statement of contribution		258
Appendix B: Basics of polarimetric sensor		260
Appendix C: Electro-optic modulator based interrogation for a polarimetric fiber		275

Appendix D: Composite materials with embedded optical fiber sensors [278](#)

for in situ structural health monitoring

List of Figures

Figure 1.1 Future smart materials and structures.	3
Figure 1.2. Typically available categories of composite materials.	4
Figure 1.3. A schematic representation of the comparison of linear measurable range and sensitivity of a Panda fiber and a HB-PM-PCF based polarimetric fiber sensor.....	13
Figure 1.4. Schematic of the FBG with incident, transmitted and reflected spectra.	14
Figure 1.5. Schematic of the hybrid polarimetric-FBG sensor system	17
Figure 1.6. Generic experimental setup for hybrid optical fiber sensor characterisation	26
Figure 2.1(a) Use of CF composites by industry, (b) GRP production in Europe for different application industries and (c) development of composite aerospace applications in last 40 years..	41
Figure2.2. Embedding fiber sensors inside composite materials (a) hand layup; (b) pre-preg method, and (c) expert assisted manufacturing of composite part embedded with OFS	43
Figure 2.3 Fiber Bragg grating.	51
Figure 2.4. (a) Measured wavelength shift for the FBG sensors at different deflection values (b) measured wavelength shift for the FBG sensors at different temperatures.....	54
Figure 2.5. (a) Reflection spectra for an FBG written in a HB-PM-PCF with two peaks corresponding to slow axis and fast axis; (b) change in the peak	

separation with transverse strain for FBGs written in MOF and bow-tie type fibers; and (c) change in peak separation with temperature	56
Figure 2.6. Spectral response of a PS-FBG and its interrogation technique based on a narrow band laser signal.	58
Figure 2.7. (a) Temperature-induced wavelength shift of the embedded polymer and silica FBGs and its comparison with free-space FBGs; (b) measured 1.5 dB bandwidth of polymer FBG and 3 dB bandwidth of silica FBG at different temperatures.....	60
Figure 2.8. Wavelength shifts of the polymer and silica FBGs with deflection in the middle of the composite material	61
Figure 2.9. (a) One of the typical EFPI sensor design; and (b) schematic experimental arrangement for the EPFI sensor	63
Figure 2.10. (a) Experimentally measured strain using embedded EFPI sensor during three point bending test in a composite; (b) Responses of the of photonic crystal fiber based sensors embedded in the composite material sample during deflections based on three point bending test; and (c) at different temperatures of the composite sample.....	64
Figure 2.11. Schematic of the sensor based on a Sagnac interferometer..	66
Figure 2.12. Responses of the HB-PM-PCF based SI sensor embedded in the composite material sample during deflections based on three point bending test.....	67
Figure 2.13 (a) Experimental setup for measurements with fiber optic polarimetric sensors in intensity domain; and (b) Change of the polarization of fiber optic polarimetric sensors as a function of strain applied to a composite sample.....	69

Figure 2.14. Micro bend sensor concept	70
Figure 2.15. The temporal profiles corresponding to (a) loading and (b) optical signal attenuation.....	71
Figure 2.16. Strain measured by the optical fiber bonded to a composite sample for various loading conditions.	73
Figure 2.17. Egress optical fiber with connector.....	77
Figure 2.18. Automated optical fiber placement system.	79
Figure 3.1. (a) Pre-strained optical fiber sensors; (b) Fiber sensors at the layer 1 & layer 5 of the composite material; (c) Composite material with embedded sensors just after fabrication; and (d) Cured composite material sample trimmed to the desired shape.....	102
Figure 3.2. Cross sectional view of highly-birefringent fibers (a) Panda fiber (b) HB-PM-PCF.	103
Figure 3.3. Schematic (cross sectional view) of sensors positioned in layer 1 and layer 5 of the 8-layer composite material sample.....	104
Figure 3.4. Schematic of the experimental arrangement for composite material sample with embedded polarimetric sensors.	105
Figure 3.5. Experimental setup to apply temperature changes to the composite material sample.....	106
Figure 3.6. Observed phase shift in coating-stripped HB-PM-PCF fibers for a temperature variation from 0 to 65 ⁰ C (a) in free space; and (b) after embedding.	108
Figure 3.7. Observed phase shift in coated HB-PM-PCF fibers for a temperature variation from 0- 65 ⁰ C (a) free space; and (b) after embedding.	109
Figure 3.8. Observed phase shift in coating-stripped Panda fibers for a	

temperature variation from 0- 7 ⁰ C (a) free space (b) after embedding	111
Figure 3.9. Observed phase shift in coated Panda fibers for a temperature variation from 0-7 ⁰ C (a) free space; and (b) after embedding.....	112
Figure 3.10. Comparison of the temperature sensitivity of (a) HB-PM-PCF polarimetric sensors; and (b) Panda polarimetric sensors.	114
Figure 4.1. Schematic of the composite material sample with embedded fiber sensors.	128
Figure 4.2. Fabricated (a) carbon-epoxy, (b) E glass-epoxy, and (c) E glass- unsaturated polyester resin composite samples.	128
Figure 4.3. Schematic of the experimental arrangement for composite material sample with embedded polarimetric sensors.	130
Figure 4.4. Experimental setup to apply temperature changes to the composite material sample.....	130
Figure 4.5. Observed phase shift for stripped HB-PM-PCF sensors embedded in different composite samples for temperature variation from 0 to 65 ⁰ C.	133
Figure 4.6. TGM measurements data plotted for temperature ranges from 0 to 65 °C.....	134
Figure 4.7. TGM measurements of composite samples over temperature range 0– 1000 °C.....	137
Figure 4.8. Comparison of theoretical predictions with experiment, (a) carbon- epoxy, (b) E glass-epoxy, and (c) E glass-unsaturated polyester resin composite samples.	139
Figure 5.1. Schematic of the hybrid polarimetric-FBG sensor system.	155

Figure 5.2. Diagram of the super imposed spectral response of an FBG with edge response of TFF at 30 ⁰ C, 35 ⁰ C, & 45 ⁰ C.	157
Figure 5.3. Figure 5.3 a) Schematic of the composite material sample with embedded fiber sensors and (b) Fabricated composite sample.	160
Figure 5.4. Spectral response of the TFF filter with a linear edge response from 1549.7 nm to 1550.3 nm.	162
Figure 5.5. Changes in the output intensity for the individual sensors in a strain range from 0 to 580 $\mu\epsilon$	165
Figure 5.6. The FBG reflected spectrum at different temperatures.	167
Figure 5.7. Changes in intensity at the FBG sensor output with temperature... ..	167
Figure 5.8. (a) Optical intensity versus temperature experimentally measured for coating-stripped and acrylate coated HB-PM-PCF sensors over a temperature range from 20 ⁰ C to 50 ⁰ C, (b) Optical intensity versus estimated thermal for the coating-stripped HB-PM-PCF sensor.	169
Figure 5.9. The schematic of the proposed flexible interrogation module.	177
Figure 5.10. Schematic of fabrication of the proposed flexible interrogator	179
Figure 5.11. The layout of the 1x6 channel AWG.	181
Figure 5.12. Simulated optical transmission of the AWG.	181
Figure 5.13. Optimization rib height for single mode operation.	183
Figure 5.14. Inverted Rib waveguide structure of MZI - EO modulator.	183
Figure 5.15. a) Layout of 2x2 MZI EO modulator with vertical offset values of S bend & electrode voltages; and (b) Layout and length of waveguides of 3dB splitter/combiner.	184
Figure 5.16. Simulated phase change of $-\pi/2$ for an electrode voltage of - 1.5 Volt and interaction length of 1 cm..	185

Figure 5.17. Simulated optical field amplitude at P2 of MZI- EO device.	186
Figure 5.18. The fabrication steps for the flexible AWG device (a) Releasing layer and flexible polyamide substrate patterning; (b) AWG device fabrication; (c) Dicing; and (d) Device lift-off.	187
Figure 5.19. The fabrication steps for the flexible MZI-EO device (a) Releasing layer and flexible polyimide substrate, bottom electrode patterning; (b) MZI-EO device fabrication; (c) Dicing; and (d) Device lift-off.	189
Figure 5.20. (a) thin film type flexible interrogation module after fabrication; and (b) SEM image of the rib waveguide structure of AWG device.	190
Figure 6.1. Schematic of the three-point bending of the composite material sample	209
Figure 6.2. Schematic of cross sectional view of a composite material with embedded sensors.	211
Figure 6.3. Cross sectional view of highly-birefringent fibers: (a) Panda fiber (b) HB-PM-PCF.	210
Figure 6.4. Fabricated composite material sample.	212
Figure 6.5. Schematic of the experimental arrangement used to apply vibration analogous to three-point bending on the composite material sample with embedded polarimetric sensors	213
Figure 6.6. Shaker frequency response profile without loading samples measured using an accelerometer for applied frequencies from 0 to 100 Hz.	214
Figure 6.7. The time domain response (a), (b), and (c), and FFT spectrum (d), (e), and (f) of HB-PM-PCF fibers embedded in a 21.5 cm long composite sample at 2 Hz, 10 Hz, and 20 Hz vibration frequencies.	216
Figure 6.8. The time domain response (a), (b), and (c), and FFT spectrum (d), (e),	

and (f) of PM-Panda fibers in 21.5 cm composite sample at 2 Hz, 10 Hz, and 20 Hz vibration frequencies..	216
Figure 6.9. (a) The peak-to-peak vibration amplitude using non-optical measurement, the peak-to-peak output intensity variation of (b) HB-PM-PCF, and (c) Panda fiber for applied frequencies form 0 Hz to 20 Hz.....	219
Figure 6.10. Comparison of the peak-to-peak intensity amplitude variation and applied frequencies for Panda and HB-PM-PCF with non-optically measured response for sample composite sample having length 47.5 cm	225
Figure 6.11. (a) Optical fiber sensors placed within mould; (b) Halbach Array; and (c) Cured MRE composite with optical fiber sensors.....	231
Figure 6.12. (a) Proposed experimental setup for cure monitoring of MRE; and (b) the MRE sample cure monitoring using HB-PM-PCF and FBG sensors.	234
Figure A.1 Three state of polarization (a) linear; (b) circular; and (c) elliptical	261
Figure A.2 Representation of optical field components in space	266
Figure A.3 Representation of polarization ellipse in the rotated ξ - η coordinate system	267
Figure A.4 Representation the degenerate polarization states with mathematical conditions	267
Figure A.5 Representation of the Poincaré sphere in Cartesian and spherical coordinates.	271
Figure A.6 Visual representation of degenerate state and SOP on the surface of the Poincaré sphere.	272

Figure A.7 (a) polarimetric sensor response without an EOM, and (b)	
polarimetric sensor response with an EOM.	276
Figure A.8. Multilayer composite layout	281
Figure A.9. Fabricated composite samples with embedded sensors.	282
Figure A.10. Schematic of the hybrid sensor using polarimetric sensors and fiber	
Bragg grating sensors	282
Figure A.11. Experimental setup to apply strain to the composite material.....	283
Figure A.12. Observed phase change in the Poincare sphere for Panda fibres with	
applied strain of 1500 $\mu\epsilon$ (a) Encore- 0/0 ply(3); (b) Polyester-0/45	
ply(3); (c) Polyester 0/0 ply(3); and (d) Polyester 0/0 ply(2)	284
Figure A.13. Observed phase change in the Poincare sphere for HB-PM-PCF	
fibres with applied strain of 1500 $\mu\epsilon$; (a) Encore 0/0 ply (3), (b)	
Polyester 0/45 ply (3), (c) Polyester 0/0 ply (3), (d) Polyester 0/0 ply	
(2).	285
Figure A.14. Measured FBG wavelength shift with applied strain for different	
ply configurations	285
Figure A.15. Observed phase change in the Poincare sphere for Panda fibres for	
temperature variation from 0 $^{\circ}\text{C}$ to 45 $^{\circ}\text{C}$ (a) Encore 0/0 ply (3); (b)	
Polyester 0/45 ply (3); (c) Polyester 0/0 ply (3); and (d) Polyester 0/0	
ply (2).	287
Figure A.16. Temperature response of the HB-PM-PCF fiber polarimetric sensor	
.....	287
Figure A.17. Measured FBG wavelength shift with applied temperature for	
different ply configurations.....	288

List of Tables

Table 1.1 Comparison of the most common types of sensors for strain measurements in composite materials.....	8
Table 1.2. Comparison of the most common types of sensors for temperature measurements in composite materials.....	9
Table 2.1. Comparison of OFSs.....	75
Table 4.1. Composite material sample details	126
Table 4.2. Comparison of sensitivity to temperature variation for stripped and non-stripped HB-PM-PCF in free space and after embedding in to E glass-unsaturated polyester composite sample.	132
Table 4.3. Experimental thermal expansion induced phase shift, Strain sensitivity and corresponding thermal expansion coefficient.	135
Table 4.4(a). The Physical properties of reinforcement fibre.....	137
Table 4.4(b). The physical properties of reinforcement matrix.....	138
Table 6.1. Comparison of experimentally and theoretically calculated values of the maximum measurable vibration amplitude of Panda fiber for different sample lengths.....	223
Table 6.2. Rate of change of Phase shift for HB-PM-PCF sensor and rate of change of Bragg peak shift for FBG.....	235
Table A.1. Comparison of strain sensitivity of the composite samples.....	289
Table A.2. Comparison of temperature sensitivity of the composite samples..	289

ACRONYMS

SHM	Structural Health Monitoring
OFS	Optical Fiber Sensor
FBG	Fiber Bragg Grating
MEMS	Micro electromechanical Systems
HB-PM-PCF	High-Birefringent Polarization Maintaining Photonic Crystal Fiber
dB	Decibel
rad	Radians
WDM	Wavelength Division Multiplexing
TFF	Thin Film Filter
AWG	Arrayed Waveguide Grating
EO-MZI	Electro-Optic Mach-Zehnder interferometer
TGA	Thermo-Gravimetric Analysis
CTE	Coefficient of Thermal Expansion.
PS-FBG	Phase-Shifted Fiber Bragg Grating
PFBG	Plastic Fiber Bragg Grating
TFBG	Tilted Fiber Bragg Grating Bit Error Rate
MOF	Microstructured Optical Fiber
PM	Polarization Maintaining
MR	Magneto-Rheological
ER	Electro-Rheological
CFP	Carbon Fiber Plastic
GFP	Glass Fiber Plastic
FOG	Fiber Optic Gyro
PDMS	Polydimethylsiloxane
RI	Refractive Index
FSR	Free Spectral Range
PA	Phased array
CMOS	Complementary Metal–Oxide–Semiconductor
RIE	Reactive Ion Etching
GUM	Guide to the expression of Uncertainty in Measurement

RTV	Room Temperature Vulcanized
SOP	State of Polarizatio
EM	Electro Magnetic

Chapter 1

Introduction

This chapter introduces the background, motivation, and objectives of the research, and an overview of the thesis layout.

This thesis presents the outcomes of a number of interconnected investigations of a hybrid optical fiber sensor system utilizing both polarimetric fiber sensors and fiber Bragg grating (FBG) sensors embedded in a composite material. The outcomes can be used in the smart composite materials industry and in a variety of composite structure applications, for example, in the aerospace and wind energy industries for structural health monitoring of helicopter blades, aircraft parts, wind rotor blades, etc.

1.1 Background to the research

1.1.1. Introduction to fiber optic sensors

Optical Fiber Sensors (OFS) offer several advantages over their conventional electronic counterparts as they:

- are not susceptible to electro-magnetic interference;
- carry no risk of explosion in volatile atmospheres and are chemically passive;
- offer the possibility of remote operation, over tens of kilometers if required;
- offer the possibility of multiplexing of multiple sensors in the same fiber;

- possess inherent corrosion resistance;
- have compact size and weight;
- offer high measurement accuracy.

The advantages of OFS mentioned above have resulted in a significant interest in their application in smart composite materials. Such smart composite materials with embedded sensors have the potential to change the paradigm for material design in the future.

1.1.2. Introduction to smart materials and structures

A smart material in principle can react and change in response to external conditions or stimuli similar in many ways to the abilities of a human body. In order to realize this capability a smart material needs to incorporate three components: sensors, processing unit and actuators. These three components of a smart material mimic the three parts of a human nervous system: nerves, brain and the muscles as shown in Figure 1.1.

In reality truly smart materials that incorporate all of three of the components above do not yet exist, but work is ongoing on each of the components and on their integration into a single whole. Structural health monitoring (SHM) systems utilizing fiber based sensors have been implemented for many years for traditional “non-smart” materials. Where the smart material is incorporated into a load-bearing structure, then SHM can be implemented using the data drawn from the sensors, with the processing unit used to optimize the operation, maintenance, repair, and replacement of the structure based on reliable and objective data.

Smart materials and structures are widely used in many different applications to

develop intelligent products in the aerospace, IT, automobile, space and military industries.. Some of the examples of smart materials and structures include composite materials with surface attached or embedded sensors, Electro-Rheological (ER) materials, and Magneto -Rheological (MR) Materials. Composite materials embedded with OFSs have been recognized as one of the prominent enabling technologies for smart materials and structures. The rapid increase in the interest in composite materials embedded with OFS has been driven by numerous applications, such as intelligent composite manufacturing / processing, and safety-related components in aircraft.

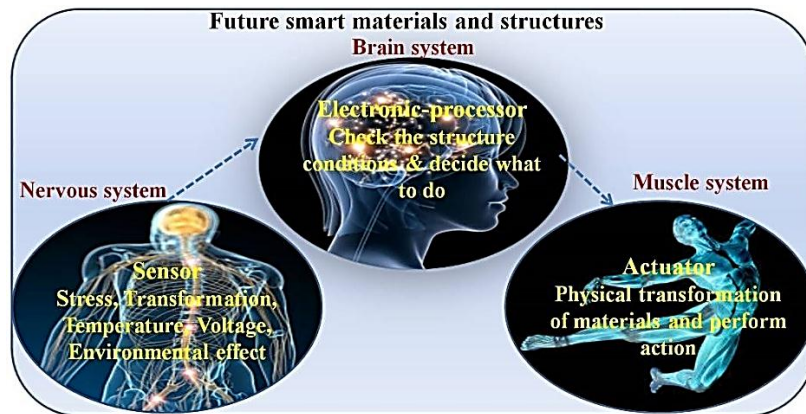


Figure 1.1. Future smart materials and structures

1.1.3. Composite materials: structures and types

In general, a composite material usually consists of two or more constituent materials. The two constituent parts of composite materials are reinforcement and matrix [1.1]. The constituent materials have very different properties but work together to give the composite mechanical properties that are superior to those of the constituent materials. Typically available categories of composite materials are shown in Figure 1.2. Figure 1.2 shows that the three main categories of composite materials are particle-reinforced, fibre-reinforced and structural-reinforced

composite material. The two common sub-categories of particle-reinforced composite materials are large particle reinforced and dispersion strengthened particle-reinforced composite materials. The two common sub-categories of fibre-reinforced composite materials are continuous and discontinuous fibre-reinforced composite materials. Again the discontinuous fibre-reinforced composite materials can be either comprised of either aligned or randomly oriented discontinuous fibre-reinforcement. The two common sub-categories of structural composite materials are laminates and sandwich paneled composite materials.

The two types of composite materials that are chosen for this research are particle-reinforced, and fibre-reinforced composite materials. The reason for these choices are explained later. Furthermore, in the following paragraphs of this section gives a more detailed description of particle-reinforced, and fibre-reinforced composite materials.

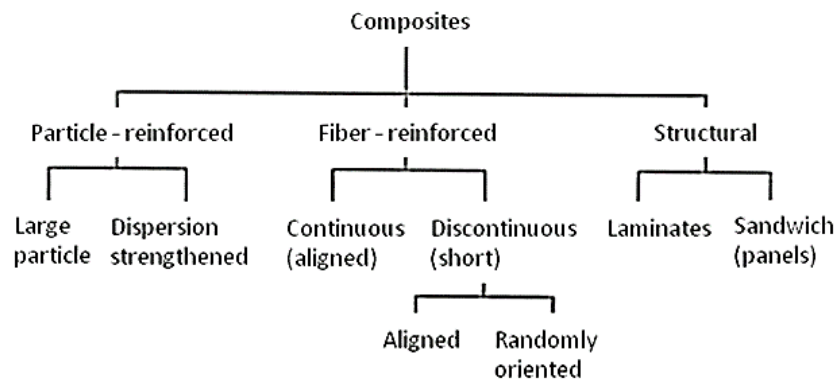


Figure 1.2. Typically available categories of composite materials. (Courtesy www.engineeringcivil.com/)

Fiber-reinforced composites are mainly categorized into two types: glass fibre and advanced fibre. There are different kinds of glass fibres available that are made of different kinds of glass, ranging from normal silica glass to high purity quartz glass and each of these glass fibres offers its own set of properties. There are also

advanced fibre materials that offer higher strength and higher stiffness but with low weight. Boron, silicon carbide, carbon, Aramid (Kevlar® or Twaron®), polyamide, nylon, self-reinforced polymer fibres (for example, Curv®, Pure®, Tegris®), basalt fibre, natural fibres (for example, flax, jute, coir, hemp, cotton etc) are examples of such advanced fibres. These reinforcement fibres can be arranged in a woven, knit braided or non -woven style.

Particle reinforced composite materials also have two constituents: reinforcement and matrix [1.1]. Particle reinforced composites are typically used not for their strength, which is lower than that of fibre reinforced composites, but rather because particle reinforcement can improve the electrical or magnetic properties of a non-conductive or non-magnetic matrix material. Particle-reinforced composites are further classified into large particle and dispersion-strengthened composites. Large particle composites contain large reinforcement particles and particle-matrix interactions cannot be treated at an atomic or molecular levels as in the case of conventional composites. Large-particle composites generally consist of the matrix material and fillers. The fillers modify or improve the properties of the material. An example of a large-particle composite is concrete, which is composed of cement (the matrix), and sand and gravel (the particulates).

For dispersion-strengthened composites, particles are much smaller with diameters between 0.01 and 0.1 μm (10 and 100 nm). In particle reinforced composites the particles can have quite a variety of geometries, but they should be of approximately the same dimension in all directions. For effective reinforcement, particles should be small and evenly distributed throughout the matrix. The volume fraction of the two phases influences the behavior of composites; mechanical properties are enhanced with the increase of particulate content. An example of

such materials is a magnetorheological (MR) materials. MR materials consist of micron size (typically 3 to 5 microns) magnetically permeable particles suspended in a non-magnetic medium [1.1]. The commercial and engineering applications of MR materials are in automobiles, polishing machines, exercise equipment, medical and prosthetics devices etc.

Matrix materials are generally divided into two categories: thermo sets and thermo plastics. Thermo set matrices are the most common, being low cost and solvent resistant. The curing process in the thermo sets is an irreversible chemical process. The most common type of a thermo set is epoxy resin which possesses superior performance and is relatively low cost. Thermo plastic based matrices can be softened by heating to an elevated temperature. Then to form a thermo plastic composite material, the softened matrix is mixed with the reinforcement fibre, a process which is reversible. The most common thermo plastic is polypropylene which has a limited temperature range of up to 150°C.

For a composite manufacturer it is important to select an appropriate fibre reinforcement taking in to account the end user's application for the fabricated composite structure.

In this thesis optical fiber sensors were embedded within two types of fibre reinforced composite materials which were fabricated by combining E-glass fibre laminate reinforcement and carbon fibre reinforcement with epoxy resin. Also, by considering the emerging importance of such smart materials, a part of this thesis is focused on the investigation of the cure process of MR composites using embedded optical fiber sensors.

1.1.4. Smart composite structures with embedded fiber optic sensors

Composite material structures are extensively used in the aerospace, marine, aviation and civil engineering industries, because of their advantages of high strength and stiffness with lower weight [1.1]. During the operational life time composite material structures can commonly suffer fatigue, damage and/or catastrophic failures. There are a wide variety of condition monitoring needs for composite materials, that span their lifecycle from fabrication to decommissioning. Examples are cure process monitoring during manufacturing, vibration measurements, and detection of delamination and cracking while in service etc. In most cases the key requirement is to measure either strain or temperature or both parameters, although there is also on occasion a need to measure other parameters, such as humidity, corrosion, chloride ion concentration etc., depending on the application.

For strain measurements, the most common types of sensors employed in composite materials are piezo-resistive sensors and optical fiber sensors [1.2]. The advantages and disadvantages of these most common types of sensors employed for strain measurements in composite materials are listed in Table 1.1. From Table 1.1 it is clear that optical fiber sensors have a number of advantages over their electronic counterparts.

For temperature measurement the common types of sensors employed in composite materials are optical fiber sensors, thermo resistive sensors and thermo-electric sensors [1.2]. The advantages and disadvantages of each of the sensor types are summarized in Table 1.2, and again it is clear that optical fibers sensors possess a number of inherent advantages.

Table 1.1 Comparison of the most common types of sensors for strain measurements in composite materials

Sensor Type	Advantages	Disadvantages
Piezo-resistive	1) Capable of recognizing static forces 2) Can be mounted on surface of a composite	1) Cannot be embedded in the composite structure 2) Susceptible to external sources of electrical noise and temperature
Optical	1) Not susceptible to electromagnetic interference 2) Multiplexing capability 3) Can be embedded in composite structure or with suitable protection surface attached	1) Require fiber optic cable and ingress/egress connections. 2) Require relatively complex source/detector and interrogation module 3) Can be temperature dependent

Table 1.2. Comparison of the most common types of sensors for temperature measurements in composite materials

Sensor Type	Advantages	Disadvantages
Optical	1) Not susceptible to electromagnetic interference 2) Multiplexing capability 3) Optic fiber can be embedded in composite structure	1) Require fiber optic cable and ingress/egress connections. 2) Require source/detector and interrogation module.
Thermo resistive	1) Typically cheaper than other sensors 2) Easy implementation	1) Resistance versus temperature is non linear 2) Limited temperature range
Thermo-electric	1) Offer high temperature measurements than thermo resistive sensors 2) Cheaper than all other temperature sensors	1) Measured temperature drift over time

From the comparisons above, it can be concluded that optical fiber sensors are the sensing technology which is both immune to electro - magnetic interference and also allows for embedding in composite structures. Unlike electronic SHM systems, the main advantage of optical fiber sensors is that the embedded optical fiber sensors can act as a “nervous system” for the material without perturbing the

structural integrity and mechanical strength of glass/carbon fibre reinforced composite materials, due to the comparable size of the optical fibers with that of the reinforcement fibres.

While OFS have had considerable success in composite sensing, there are issues that need to be addressed further, for example the long-term sensing ability of OFS in field conditions and the effects of aging have not been fully established. OFS are fragile in some configurations, while another common concern is the optical connectors which connect the embedded optical fiber with the external data recording system, which are considered to be the weakest element within the OFS system. A detailed description of challenges and recent advances in embedded optical fiber sensors are presented in Chapter 2.

1.1.5. Optical fiber sensor types

A variety of optical fiber sensor types have been reported for strain/temperature measurements in composite materials, including FBG sensors [1.3], interferometric fiber optic sensors [1.4], polarimetric sensors [1.5], distributed fiber optic sensors [1.6] and hybrid fiber optic sensors [1.7, 1.8]. A detailed overview of the various OFS employed strain/temperature measurements¹ in composite materials is explained in Chapter 2. In the sections that follow a brief overview is included for completeness sake of the two specific types of sensors that are employed in the research described in this thesis. In addition, the concept of a hybrid fiber sensing system, which employs the two sensor types, is introduced.

¹ A more detailed overview of the fiber optic sensing technologies for strain/temperature in composite materials is presented in the following Chapter 2.

1.1.6. Fiber optic polarimetric sensors

The polarization properties of light propagating through an optical medium can be affected by stress, strain, pressure and temperature acting on the medium [1.5, 1.9]. Polarization modulation is the phenomenon utilized in polarimetric sensor². In fiber optic polarimetric sensors, the impact of the local environment is sensed by means of detecting changes in the state of polarization of light. Fiber optic polarimetric sensors are realized using a special type of optical fibers so called highly birefringent polarization maintaining (HB-PM) fiber.

The polarimetric fiber sensors realized in this thesis are based on two types of HB fibers: polarisation maintaining Panda fiber (PM-1500-HP) [1.10] and polarization maintaining photonic crystal fiber (PM-1500-01) [1.11].

In terms of the underlying physical phenomena, the phase of the guided wave through a HB fiber of length L is given by [1.12]:

$$\phi = \beta L = n_{eff} k_0 L \quad 1.1$$

where β is the propagation constant, n_{eff} is the effective refractive index,

$k_0 = \frac{2\pi}{\lambda_0}$ is the wave vector, and λ_0 is the wavelength. The phase difference between

the two polarizations of the fundamental mode guided by the HB fiber of length L thus can be expressed by [1.12]:

$$\Delta\phi = \Delta\beta L = \Delta n_{eff} k_0 L \quad 1.2$$

When the fiber is subjected to an external mechanical strain ϵ , both the fiber length and effective refractive indexes for each of the polarized modes will be effected resulting in a measurable phase difference [1.13]. A key parameter for any sensor

² A detailed description of “Basics of polarimetric sensor” is presented in Appendix B.

is sensitivity. For polarimetric sensors it is possible to calculate the sensitivity based on the optical-mechanical properties of the fiber. However given the wide variety of fiber geometries possible, the common practice that has evolved is to experimentally determine the sensitivity of a HB optical fiber polarimetric sensor, particularly for more exotic fiber geometries. The sensitivity of a polarimetric sensor of length L can be written as [1.12],

$$S = \frac{2\pi}{TL} \quad 1.3$$

where T is an experimental parameter describing the amount of strain or temperature required to induce a 2π phase shift in the polarized light.

Polarimetric sensors can be also operated in intensity domain by using polarizer/analyser and photodetector arrangement. One can analyse the intensity domain operation of the polarimetric sensor using Jones matrices method³ as explained below.

For fiber optic polarimetric sensor based measurements, a primary requirement is to use birefringent fiber type fibers in which the two orthogonally propagating modes are polarized and are similarly excited. This can be achieved with the help of a polarizer. The polarizer is set to adjust the orientation of the input polarization at an angle 45° to one of the main axes of the birefringent fiber. The intensity after the analyzer will be [1.12],

$$I(\lambda) = E^2 = \frac{I_0}{2} (1 + \cos(\Delta\phi)) \quad 1.4$$

where I_0 is the total output power. Therefore, as equation 1.4 shows, changing the state of polarization will alter the intensity seen by the detector in a sinusoidal

³ A detailed description of representation of polarization using Jones matrices is presented in Appendix 2: Basics of polarimetric sensor.

fashion. In order to guarantee a linear response for the polarimetric sensor for a wide range of applied strains/temperature, it is important to choose the operating point of the polarimetric sensor in the linearly varying quadrature region with the help of a polarizer-analyzer arrangement. An important consequence of this for polarimetric fiber sensors for strain/temperature measurements is that the sensor's response range is thus limited to the extent of the linear region. As an example, schematic in Figure 1.3 illustrates the comparison of the linear response ranges and corresponding strain sensitivities for a Panda fiber and a High-Birefringent Polarization-Maintaining Photonic Crystal Fiber (HB-PM-PCF), the fiber types used in this thesis. From Figure 1.3, it can be seen that the linear measureable range of the HB-PM-PCF polarimetric sensor is larger than that of the Panda fiber [1.14] and hence a wider range of strains can be measured using a HB-PM-PCF polarimetric sensor. Another advantage of the HB-PM-PCF over conventional PM fibers is its low temperature sensitivity [1.14, 1.15]. Given these advantages, in this thesis, while Panda fiber based sensors are used for comparative purposes, and HB-PM-PCF based polarimetric sensors are used for strain measurements.

Fiber optic polarimetric sensors can be embedded in composite materials to measure the average strain / temperature over the sensor length [1.13, 1.14] and it is also possible to select the strain / temperature sensitivity of the sensors by selecting a PM fiber type with an appropriate birefringence and length [1.15]. However, it is important to note that for localized/point strain/temperature measurements, particularly within large composite structures, polarimetric sensors cannot be employed as such sensors measure only average strain over the length of the sensing fiber. A further issue for polarimetric sensors for strain measurement is that they require a means to set a zero strain reference, in effect the measurement

system must know the polarization state at which the applied strain is zero. As regards temperature-strain cross sensitivity, by using specific HB-PM fiber based polarimetric sensors it is possible to realize temperature insensitive strain measurement.

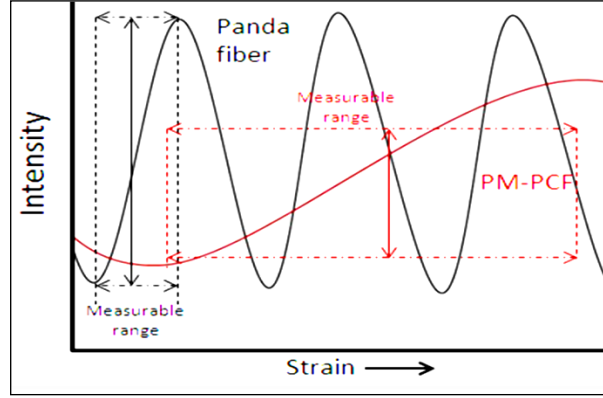


Figure 1.3. A schematic representation of the comparison of linear measurable range and sensitivity of a Panda fiber and a HB-PM-PCF based polarimetric fiber sensor

1.1.7. Fiber Bragg Grating (FBG) sensors

FBGs are the most commonly employed fiber optic sensors in SHM applications for composite materials [1.16]. As shown in Figure 1.4, an FBG consists of an optical fiber in which a periodic refractive index variation so called grating region is fabricated or written. The grating reflects a wavelength of light that is sensitive to local variations in temperature or strain. The light reflected back due to the periodic variations of the core refractive index with a central (Bragg) wavelength given by [1.3]:

$$\lambda_B = 2n_0\Lambda \quad 1.5$$

where n_0 is the effective refractive index of the fiber core and Λ is the grating pitch. External parameters such as strain and temperature can influence the refractive index and periodicity of the FBG and hence it can be used to measure such

parameters.

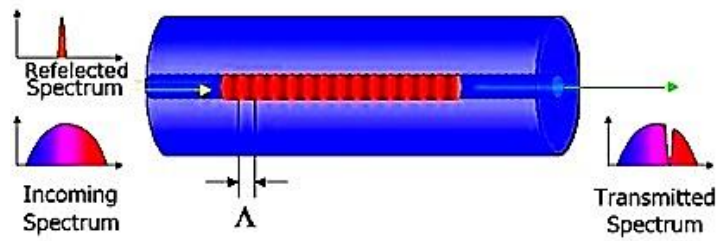


Figure 1.4. Schematic of the FBG with incident, transmitted and reflected spectra

The strain sensitivity of the Bragg wavelength arises from the change in the pitch of the fiber grating due to strain and changes in the refractive index arising from the strain-optic effect. When a strain is applied to the grating, the reflected Bragg wavelength changes. In practice the applied strain value can be estimated from the measurement of the reflected wavelength change due to the applied strain. The typical strain sensitivity of a silica FBG at 1550 nm is $\sim 1.2 \text{ pm}/\mu\epsilon$ [1.8]. Commonly FBGs are used to measure axial strain in the longitudinal direction as this provides the highest strain sensitivity. Bragg wavelength shift can also occur due to changes in temperature. The temperature sensitivity of the Bragg wavelength arises from the change in the grating pitch associated with the thermal expansion of the fiber, and the change in the refractive index arising from the thermo-optic effect. The typical temperature sensitivity of an FBG at 1550 nm is $\sim 11.6 \text{ pm}/^\circ\text{C}$ [1.8].

FBGs respond strongly to both strain and temperature, thus when interrogating the sensor it is necessary to take account of both effects. For temperature measurements alone, the FBG must remain unstrained, typically by embedding the sensor in a reference point, such as a capillary, that isolates the sensor from local strain. The thermal expansion of the buffer coating material also has an influence on the FBG response. To minimize the effect of the buffer coating polyimide coated

FBGs are considered to be an attractive option as they have practically negligible expansion coefficient.

For strain measurements using FBG sensors, compensating techniques are essential to avoid temperature effects. Different methods are available for discrimination between strain and temperature information from an FBG sensor including the dual-wavelength superimposed FBG method [1.17], combined FBG and long-period grating method [1.18], different cladding-diameter FBG method [1.19], FBG Fabry-Perot interferometer method [1.20], special types of FBG method [1.21-1.22], dual-wavelength fiber laser [1.23], embedded FBG [1.24], fiber Raman laser with an etched FBG [1.25], combined method of co-doped fiber and grating-based technique [1.26-1.27], fiber-optic Fizeau interferometric sensor [1.28], and hybrid optical fiber sensing scheme by combining a HB-PM polarimetric sensor with an FBG sensor [1.8].

1.1.8. Hybrid Fiber Optic Sensor System

One of the highlights of the research presented in this thesis is the design and development of a novel hybrid sensor by combining polarimetric fiber sensors together with fiber Bragg grating sensors for simultaneous measurement of strain, temperature and thermal strain in a composite material. Conventionally, FBGs are deployed in composite materials for strain and temperature sensing in a large range of applications [1.8]. However, as was outlined in section 1.1.6, one of the most significant limitations of FBG strain sensors is their high intrinsic temperature cross-sensitivity and the difficulty of measuring strain and temperature simultaneously. The Polarimetric HB-PM fiber based fiber-optic sensors described in section 1.1.5 utilize polarization (phase) modulation within fibers to sense external perturbations. It is known that HB polarimetric sensors can have negligible

temperature sensitivity [1.14]. Thus each sensor type has advantages but also disadvantages and the purpose of a hybrid sensing scheme is to use the sensors together so that the disadvantages are mitigated.

A hybrid optical fiber sensing scheme implemented by combining a HB-PM polarimetric sensor and an FBG sensor was reported earlier by Rajan et. al [1.8] for simultaneous strain and temperature measurements. In this thesis the hybrid sensing scheme based on the combination of HB-PM polarimetric sensors and an FBG has been chosen as the foundation for the research. The hybrid sensing system developed and reported in [1.8] had the disadvantage that the cross-sensitivity issues between thermal strain and temperature during simultaneous strain / temperature measurements within composite materials was not taken into consideration. To overcome this limitation in this thesis a new method for simultaneous strain, temperature, and thermal strain measurement has been proposed and investigated by using a hybrid sensing approach that involves an FBG sensor combined with a stripped HB-PM-PCF sensor and a buffer coated HB-PM-PCF polarimetric sensor. The advantage of the HB-PM-PCF over conventional PM fibers is that the polarimetric sensor based on a HB-PM-PCF can give a linear response for a wide range of applied strains and is insensitive to temperature variations.

In order to provide a context for material later in the thesis, this section finishes with a brief overview of the operating principle of a hybrid sensing system. To provide such an overview it is useful to start by considering the experimental arrangement used to demonstrate such a system, as shown in Figure 1. 5 [1.8]. A 3-dB coupler is used to split the signals between the FBG sensor and the polarimetric sensor. The HB-PM-PCF used was a buffer stripped PM-1550-01 and

the polarized output of the HB-PM-PCF was observed at a wavelength of 1550 nm with the use of a wavelength drop filter. The fiber ends of the HB-PM-PCF were spliced to standard single mode fiber (SMF28) by means of a conventional fusion splicer and the loss for both splices was approximately 2 dB per splice. A polarizer and an analyzer at the input and output were used to obtain the strain and temperature induced change in the state of polarization.

A fiber circulator was used to direct the reflected signal from the FBG to the edge filter. The wavelength filter is used to convert the strain and temperature induced wavelength variation from the FBG into an intensity change. Two photodiodes at the outputs were used to measure the intensity variations.

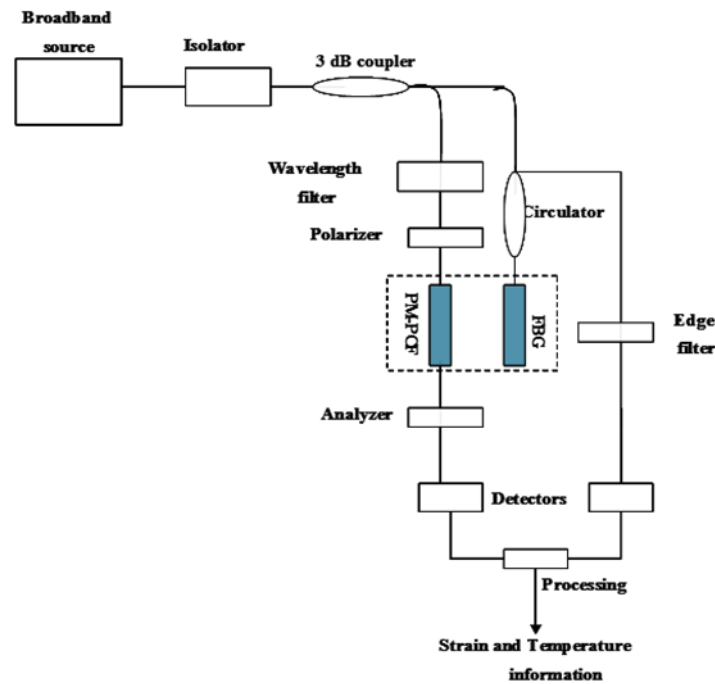


Figure 1. 5 Schematic of the hybrid polarimetric-FBG sensor system

From the Equation 1.4 it is clear that the output signal of a polarimetric sensor is a periodic function of the external strain and the period of this function can be adjusted by choosing an appropriate length for the sensing fiber. Thus by choosing

the appropriate length of the HB-PM-PCF, a linear transmission response with strain can be obtained within a certain strain range of interest. The sensor's response is independent of temperature. To obtain the temperature information the hybrid system utilizes an FBG sensor in a complementary fashion to the polarimetric sensor. The FBG sensor system and the polarimetric sensor system are calibrated for strain and temperature independently. Assuming S_s is the strain sensitivity for both the polarimetric and FBG sensors and S_t is the temperature sensitivity for the FBG sensor, the corresponding intensity variations due to strain and temperature for both sensors can be written in the form of the characteristic matrix below,

$$\begin{bmatrix} \Delta I_1 \\ \Delta I_2 \end{bmatrix} = \begin{bmatrix} \Delta S_s & 0 \\ \Delta S_s & \Delta S_t \end{bmatrix} \begin{bmatrix} \Delta \varepsilon \\ \Delta T \end{bmatrix} \quad 1.6$$

The inverse of the above matrix will yield the strain and temperature information simultaneously. Matrix (1.6) can also be used for sensors with different strain sensitivities by including a sensitivity factor.

1.2 Research Motivation

The field of fiber sensing in composites has received a lot of attention in recent years. A key requirement for sensors in a composite material is that they should be able to sense the influence of multiple physical parameters, such as thermal expansion, stress, strain and temperature, effectively differentiate between these parameters and be able to eliminate the errors induced by factors such as non-uniform strain distribution within the composite etc. Additionally, given the variety of physical environments that composites can be used in, the measurement of complex indirect parameters such as thermal expansion and vibration, is also very

important.

The hypothesis underpinning this research is a that by careful selection of a combination of sensors that work in a complementary fashion, it is possible to measure multiple physical parameters, where the parameters being measured can also include complex indirect parameters.

The motivation for this research is to investigate whether a hybrid optical fiber sensing scheme can demonstrate that the hypothesis above is correct.

1.3 Aim and objectives of the research

The core aim of this research is to investigate a hybrid sensing scheme that utilises sensors working in a complimentary fashion to measure multiple physical parameters, where the parameters being measured include complex indirect parameters thermal expansion and vibration, all in a composite material.

The specific objectives of the research that seek to meet the aim above are as follows:

I. Investigate the influence of thermal expansion in a composite material on the embedded optical fiber sensors

As a precursor to measuring thermal expansion, it is necessary to better understand the influence of thermal expansion on sensors embedded in composite materials. There are no investigations to date on how embedding influences the performance of embedded polarimetric sensors. For this investigation polarimetric sensors based

on buffer-coated and buffer-stripped high birefringent polarization maintaining fibers are selected. Polarimetric sensors based on buffer coated HB-PM-PCF are proven temperature insensitive in free space and thus any thermal response from this type of sensor after embedding in a composite material will reveal a dependency on thermal expansion of the composite material. This investigation underpins the next objective to identify the most suitable polarimetric sensor for measuring thermal expansion.

II. Demonstrate the measurement of thermal expansion of a composite material using an embedded polarimetric sensor

This objective involves a demonstration of the measurement of the complex indirect parameter, thermal expansion. In practice by controlling the fabrication process the measurement of the specific parameter "thermal elongation induced strain" in a composite material will provide information about the thermal expansion characteristics of the composite material. For this investigation polarimetric sensors based on buffer-stripped HB-PM-PCF are selected. The reason for selecting buffer-stripped HB-PM-PCF based polarimetric sensor for this investigation is that this particular type of polarimetric sensor is temperature insensitive in free space and thus any phase changes of the buffer-stripped HB-PM-PCF polarimetric sensors after embedding in composite material will be due to thermal elongation induced strain of the composite material. This investigation involves the temperature induced phase changes of the buffer-stripped HB-PM-PCF polarimetric sensors embedded in carbon-epoxy, E glass-epoxy and E glass-unsaturated polyester resin composite material samples. This investigation also involves comparison of the theoretically calculated and experimentally measured values of thermal elongation induced strain of carbon-epoxy, E glass-epoxy, and E

glass-unsaturated polyester resin composite specimens. This investigation also has the added benefit of potentially improving the accuracy of applied strain measurements in composite materials.

III. Develop a novel hybrid sensor for simultaneous measurement of strain, thermal strain and temperature

This objective involves investigation of thermal elongation induced strain sensitivity, axial strain sensitivity and the temperature sensitivities of a combination of sensors: a buffer-coated HB-PM-PCF polarimetric sensor, a buffer-stripped HB-PM-PCF polarimetric sensor and a polyimide coated FBG sensor that are embedded in E-glass-unsaturated polyester resin composite material samples. The investigation also seeks to establish the characteristic sensitivity matrix for the hybrid sensor and characterize the hybrid sensor for simultaneous measurement of axial strain, temperature and thermal strain of a composite material.

IV. Analyze different types of polarimetric sensors for vibration measurements

This involves investigation of the vibration amplitude range over which the polarimetric sensors can provide accurate information about the vibration frequency range and amplitude. A motivation for this is that in the lead up to catastrophic failure, large amplitude vibrations are known to be common. For this purpose a comparison of composite material samples embedded with polarimetric sensors based on Panda type fiber and HB-PM-PCF types will be carried out and analysed in several glass fiber reinforced composite samples with different lengths embedded with polarimetric sensors.

V. Develop efficient cure monitoring sensor based on stripped HB-PM-PCF

This involves investigation of performance of a polarimetric sensor and an FBG sensor both embedded in a MRE smart composite material during its curing process, and investigation of the stress/ strain induced responses of buffer stripped HB-PM-PCF and FBG sensor during the different stages in the composite curing process

1.4 Research methodology

This thesis is presented as a series of linked journal publications contained within the core chapters of the thesis. Given the requirements for journal papers, a description of the methodology may not always be presented. This section therefore provides a brief overview of the methodology employed in this research. The methodology employed throughout the research undertaken typically consisted of a sequence of steps as follows:

1). Carrying out an in-depth analysis of sensor operation and characteristics using existing published knowledge

Such studies were undertaken a number of times over the course of the research, most frequently involving an investigation: a) of SOP variation of the light through HB-PM fibers/ polarizer / analyzers etc., b) of spectral characteristics of FBG based temperature sensors with different coatings, c) of a hybrid sensing approach, and d) of interrogation methods for intensity domain operation of hybrid sensor. The studies utilized the existing published knowledge as a foundation.

2). Utilizing and customizing existing techniques to fabricate the composite materials with embedded fiber sensors.

In this thesis the composite materials with embedded fiber sensors are fabricated in a laboratory environment using on so called hand layup and pre-preg layup methods. The hand layup method process involved the following steps: (a) shaping the laminate, (b) stacking reinforcement fibers or fabrics one over another, by applying the matrix resin in between them, (c) curing (or polymerization) of the resin matrix, and (d) shaping the sample. The pre-preg layup method involves the following steps: (a) stacking of multiple composite pre-preg laminates one over another, and (b) curing by applying heat and/or pressure. The moulding/curing processes were undertaken using a vacuum-bag assisted by a hot plate. Before the curing process, both for the hand-layup and the pre-preg layup methods, the optical fiber sensors were embedded within a carefully selected layer. Depending on the nature of the investigation, the layer chosen be either the layer at the center of the material or at the surface of the sample. In every case pre-strain was applied to ensure that the optical fibers remained free of bends. The spacing between adjacent optical fiber sensors, precise positioning of FBG sensors, and pre-strain to optical fibers are adjusted using optical post assemblies and 25 mm travel translation stages.

3) Developing the necessary numerical simulations needed for experimental verification/ predictions

Such numerical predictions and simulations are performed throughout the thesis research work. This involved the development of a Matlab based programme to measure Thermal expansion coefficient (CTE), an Ansys based tool to find natural frequencies of composite samples, and a number of simulations using the Opti Beam Propagation (BPM) Software for designing flexible waveguide based interrogation systems. All Numerical / simulation studies were performed on a personal computer with Intel® Core™ 2 Duo CPU E7200 @ 2.53 GHz, 2 GB

RAM and 500 GB hard disk storage.

4) Developing an experimental setup and use this setup to compare and verify the predictions of the model/simulations with experimental results.

a. Temperature control

Composite material samples with embedded optical fiber sensors are subjected to temperature variations over a range from 0 to 65 °C, by using a Peltier cooler (Model No. PE-127-20-15-U from Radionics, Ltd). To increase the surface area of the Peltier cooler to match that of the composite sample, a thermally conductive aluminium plate having thickness 1.2 mm was placed on top of the Peltier cooler and attached with a thermally conducting paste. A time interval of 20 minutes is used between each step temperature variation in order to ensure a uniform temperature distribution within the composite sample. The Peltier cooler temperature is controlled using Thorlabs ITC510 temperature controller with the thermistor feedback sensor attached to the surface of the aluminium plate. The temperature controller allows one to set and maintain a fixed temperature over a 0 to 70 °C operation range, with an accuracy of 0.1 °C.

b. Applied strain control

A three-point bending setup is used for applying strain to the composite sample and the average applied strain is calculated analytically. A translation stage (PT1/M from Thorlabs, Inc) with a 25 mm long standard micrometer and 10 µm resolution is used to apply deflection at the middle of the composite sample. The distance between the fixed clamps placed is equal to the sensor length and the strain step is limited by the resolution of the translation stage used to apply strain.

c. Optical characterization of the sensors

The generic experimental setup that was used for extracting hybrid sensor's response during the strain/temperature measurements within the composite is as shown in Figure 1.6. The generic setup composed of a light source, polarization controller /polarimeter system, and an FBG interrogation systems.

The part of the experimental setup used for the characterization of polarimetric sensors consists of a tunable laser (Tunable laser is a Nettek OSICS ECL1560 external cavity laser) as a light source, - a polarization control and analysis module, which was either combination of polarization controller DPC5500 Module (Thorlabs) and polarimeter IPM5300 Module (Thorlabs) or a combination of a polarization controller FPC560 (Thorlabs) and an in-line polarizer/ analyzer ILP1550PM-FC(Thorlabs), with an optical power meter. The optical power meter (PXIT 306) was integrated into a PXI platform (PXIR 800A) and was controlled with LabVIEW based programs. Input light from the laser source is launched to the polarimetric sensors with its linear polarization at 45^0 relative to the slow axis of the optical fiber by using a polarization controller / in-line polarizer. The output fiber from the composite material is connected to polarimeter / polarization analyzer, and is recorded by a high speed optical power meter (which has the capability to measure 10,000 samples per second). As fiber splicing can induce changes in the polarization state the PM fibers were connected to standard SMF patch chords without splicing, with free ends connected to the polarization control system by means of adjustable key connector for PM fibers 30125D1 - FC/PC (Thorlabs).

When conducting the strain/temperature measurements with an FBG sensor, the FBG peak wavelength shift was recorded either using a Smartscan FBG interrogator from Smartfibers or using a customized wavelength to intensity

measurement technique. The Smartscan FBG interrogator had a wavelength range of 40 nm (1528 – 1568 nm) and 2 channels with inbuilt lasers / detectors. Thus separate source detectors were not needed. A maximum of 8 FBG sensors could be simultaneously interrogated with a frequency up to 2.5 kHz with a repeatability better than 1 pm.

The customized wavelength to intensity measurement technique utilized a thin film optical fiber and an optical power meter (PXIT 306) controlled with a custom LabVIEW based program. A fiber circulator was used to direct the reflected signal from the FBG to the thin film filter. The filter was used to convert the wavelength variation in the reflected signal from the FBG into intensity changes in a calibrated fashion. Each FBG sensor utilized a single channel of an 8-channel thin film based Wavelength Division Multiplexing (WDM) demultiplexer designed originally for a 200 GHz channel spacing dense WDM system, sourced from Laser 2000 (UK)..

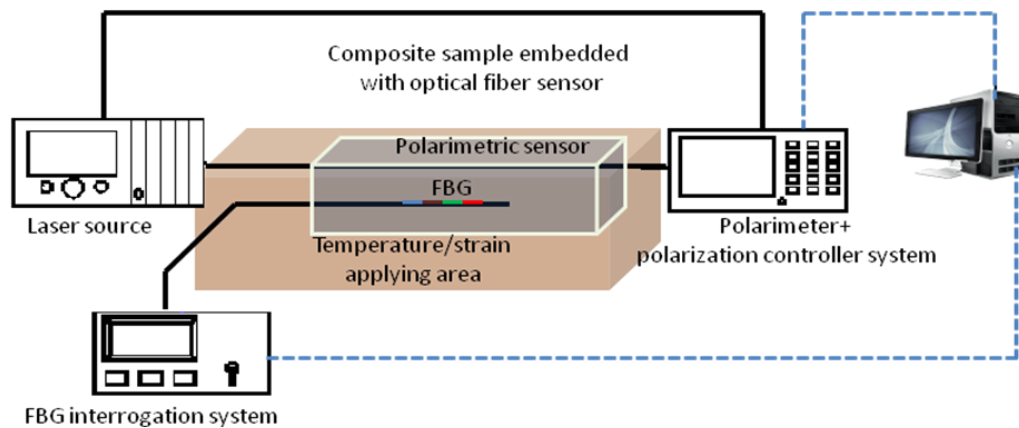


Figure 1. 6 Generic experimental setup for the hybrid optical fiber sensor characterisation.

5) Performance comparison and verification of experimental results with theoretical predictions

This critical step is repeated many times in different experiments and involves an in-depth examination and comparison of numerical predictions and the experimental results, including an assessment of the likely sources of errors and

measurement limitations. For example, the CTEs of different types of composite materials are numerically predicted using Classical Laminate Theory (CLT) together with Thermo Gravimetric Analysis (TGA). The performance of polarimetric sensors embedded in composite materials with different CTEs are compared. The numerically predicted CTE values of different composite materials are compared and verified with experimentally measured thermal strain values.

1.5 Structure of the thesis

This thesis represents my research work and that for it developed a series of linked journal publications to and for community. The publications are all first author publications by the author of this thesis. As the research was carried out within a research group, there are several authors for each publication. A signed statement from all the co-authors is included in Appendix A, confirming that the first author undertook all aspects of the research described in each paper, including preparation and submission of the paper, with the support and advice of the co-authors.

Chapter 1 is this introduction chapter which introduces the research area, the motivation, research objectives and outlines the whole structure of the thesis.

Chapter 2 presents overview of the various aspects of previously developed fiber optic sensor sensing technologies for strain / temperature measurements in composite materials. Chapter 2 is an introductory chapter to the chapters of this thesis which follow and is based on a published review paper.

Chapter 3 presents an experimental analysis of the influence of the thermal expansion of a composite material on both buffer coated and buffer stripped polarimetric sensors used for temperature measurements. The experimental studies showed that that thermal expansion of the composite material is the main source of

errors in strain/temperature measurement using embedded polarimetric fiber sensors and that for more accurate strain / temperature measurements buffer coated polarimetric fiber sensors are the more appropriate candidate. The study also found that the buffer stripped HB-PM-PCF polarimetric sensor after embedding in the composite material shows a significant phase change due to the thermal elongation of the composite material and this investigation provide a foundation for measuring the Coefficient of Thermal Expansion (CTE) value of a composite material in Chapter 4.

Chapter 4 presents a numerical and experimental analysis aimed at the development of a measurement scheme to quantify composite material's thermal elongation induced strain using a buffer stripped HB-PM-PCF sensor. The thermal elongation induced phase change of a stripped PM – PCF sensor embedded in different types of composite materials with three different CTE values are studied. The experimentally measured thermal elongation induced strain of the composite materials is compared with the theoretically calculated CTE values. The theoretical and experimental investigations showed good agreement. The thermally induced strain measurement scheme developed in Chapter 4 provides the basis to resolve the thermal strain induced errors found during the strain measurements using an embedded hybrid sensor presented in Chapter 5.

Chapter 5 presents a hybrid sensor configuration by combining several sensors for simultaneous measurement of strain, temperature and thermal strain in a composite material. This chapter presents a means of implementing a common intensity domain interrogation scheme for the hybrid sensor. This chapter also presents the design of a miniaturized thin film type interrogator for future SHM applications of the proposed hybrid sensor.

Chapter 6 presents two derived applications of the proposed strain measurement technique using polarimetric sensors. The two applications discussed in this chapter are: (1) means to monitor vibrations within a composite structure that can lead to harmful structural damage, and (2) means to monitor the cure process during composite manufacturing.

Chapter 7 summarizes the main conclusions and key results of this thesis and presents a brief overview of possible future research directions.

Three more appendices are also provided. Appendix B provides basics of polarimetric sensor. Reference is made to a conference publication (contained in Appendix C) by the author of this thesis which details the electro-optic modulation for polarimetric fiber sensor based strain and temperature measurements. Finally, a subsidiary objective of this thesis is to determine the influence of complex secondary parameters of the composite material on the embedded sensors. Such studies form the basis of future work of determining the influence of the composite stiffness parameter on an embedded polarimetric sensor and reference is made to this in Appendix D. Appendix D is another conference publication by the author of this thesis on the influence of composite materials ply configuration on the embedded optical fiber sensors and is a good example of the influence of the structure of the composite material, hardness and ply configurations which can cause variations in embedded optical sensors strain / temperature sensitivities.

1.6 References

- 1.1 D. P. Garg, M. A. Zikry, and G. L. Anderson. "Current and potential future research activities in adaptive structures: an ARO perspective." *Smart materials and structures* 10.4: 610, 2001.

- 1.2 X. E. Gros. "Current and Future Trends in Non-Destructive testing of Composite Materials", *Ann. Chim. Sci. Mat*, 25, 539-544. 23,2000.
- 1.3 W. Du, X. M. Tao, H. Y. Tam, and C. L. Choy. "Fundamentals and applications of optical fiber Bragg grating sensors to textile structural composites." *Composite Structures* 42, no., 217-229, 1998.
- 1.4 Y. J. Rao. "Recent progress in fiber-optic extrinsic Fabry–Perot interferometric sensors." *Optical Fiber Technology* 12, no. 3, 227-237, 2006.
- 1.5 V. M. Murukeshan, P. Y. Chan, O. L. Seng, and A. Asundi. "On-line health monitoring of smart composite structures using fiber polarimetric sensor." *Smart materials and structures* 8, no. 5, 54, 1999.
- 1.6 H. Murayama, K. Kazuro, N. Hiroshi, S. Akiyoshi, U. Kiyoshi. "Application of fiber-optic distributed sensors to health monitoring for full-scale composite structures." *Journal of Intelligent Material Systems and Structures*, 14, 3-13. 30, 2003.
- 1.7 R. Montanini, L. d’Acquisto. " Simultaneous measurement of temperature and strain in glass fiber/epoxy composites by embedded fiber optic sensors: I Cure monitoring.” *Smart Materials and Structures*, 16, 1718. 82, 2007.
- 1.8 G. Rajan, M. Ramakrishnan, Y. Semenova, M. Karolina, P. Lesiak, A. W. Domanski, T. R. Wolinski, G. Farrell. "A Photonic Crystal Fiber and Fiber Bragg Grating-Based Hybrid Fiber-Optic Sensor System." *Sensors Journal*, IEEE 12.1: 39-43. 58, 2012.

- 1.9 T. R. Woliński, "I Polarimetric optical fibers and sensors." *Progress in Optics*, 40, 1-75, 2000.
- 1.10 T. S. Yu Francis, and Y. Shizhuo. "Fiber Optic Sensors." Marcel Dekker Inc., New York ,2002.
- 1.11 <http://www.thorlabs.com/thorcat/6500/PM1550-HP-SpecSheet.pdf>.
- 1.12 http://www.thorlabs.com/images/Catalog/V19_13_FiberOpt.pdf.
- 1.13 A. W. Domanski, R. W. Tomasz, J. B Wojtek. "Polarimetric fiber optic sensors: state of the art and future." International Conference on Interferometry '94, International Society for Optics and Photonics, 1994.
- 1.14 T. R. Woliński, P. Lesiak, A. W. Domański. "Polarimetric optical fiber sensors of a new generation for industrial applications." *Technical Sciences*, 56, 2008.
- 1.15 V. M. Murukeshan, P. Y. Chan, L. S. Ong, A. Asundi. "Effects of different parameters on the performance of a fiber polarimetric sensor for smart structure applications." *Sensors and Actuators A: Physical*, 80, 249-255. 23, 2000.
- 1.16 W. Du, X. M. Tao, H. Y. Tam, C. L. Choy. " Fundamentals and applications of optical fiber Bragg grating sensors to textile structural composites." *Composite Structures* 42, 217-229. 37, 1998.
- 1.17 M. G. Xu, J. L. Archambault, L. Reekie, J. P. Dakin," Discrimination between strain and temperature effects using dual-wavelength fibre grating sensors." *Electronics letters*, 30, 1085-1087. 39, 1994.

- 1.18 K. B. Samer, T. Sun, K. T. V. Grattan. " Simultaneous measurement of temperature and strain with long period grating pairs using low resolution detection." *Sensors and Actuators*, 144, 83-89. 38, 2008.
- 1.19 S. W. James, M. L. Dockney, R. P. Tatam. "Simultaneous independent temperature and strain measurement using in-fibre Bragg grating sensors." *Electronics Letters*, 32, 1133-1134, 1996.
- 1.20 R. D. Oliveira, C. A. Ramos, A. T. Marques. "Health monitoring of composite structures by embedded FBG and interferometric Fabry-Perot sensors." *Computers and Structures*, 86, 340-346. 41, 2008.
- 1.21 B. O. Guan, H. Y. Tam, X. M. Tao, X. Y. Dong. "Simultaneous strain and temperature measurement using a superstructure fiber Bragg grating." *Photonics Technology Letters, IEEE*, 12, 675-677. 44, 2000.
- 1.22 C. Sonnenfeld, S. Sulejmani, T. Geernaert, S. Eve, N. Lammens, G. Luyckx, V. Eli, H. Thienpont, " Microstructured optical fiber sensors embedded in a laminate composite for smart material applications." *Sensors*, 11, 2566-2579, 2011.
- 1.23 D. Liu, N. Q. Ngo, S. C. Tjin, X. Dong. "A dual-wavelength fiber laser sensor system for measurement of temperature and strain." *Photonics Technology Letters, IEEE* 19.15, 1148-1150, 2007.
- 1.24 L. Jin, W. Zhang, H. Zhang, B. Liu, J. Zhao, et al. "An embedded FBG sensor for simultaneous measurement of stress and temperature." *Photonics Technology Letters, IEEE* 18.1, 154-156, 2006.

- 1.25 A. Tran, T. Van, Y. G. Han, Y. J. Lee, et al. "Performance enhancement of long-distance simultaneous measurement of strain and temperature based on a fiber Raman laser with an etched FBG." *Photonics Technology Letters, IEEE* 17.9: 1920-1922, 2005.
- 1.26 S. Pal, Y Shen, J Mandal, T Sun, et al. "Simultaneous measurement of strain (to 2000 $\mu\epsilon$) and temperature (to 600° C) using a combined Sb-Er-Ge-codoped fiber-fluorescence and grating-based technique." *Sensors Journal, IEEE* 5.6, 1462-1468, 2005.
- 1.27 P. Cavaleiro, F. M. Araujo, L. A. Ferreira, et al. "Simultaneous measurement of strain and temperature using Bragg gratings written in germanosilicate and boron-codoped germanosilicate fibers." *Photonics Technology Letters, IEEE* 11.12, 1635-1637, 1999.
- 1.28 A. C. L. Wong, P. A. Childs, and G. D. Peng. "Multiplexed fibre Fizeau interferometer and fibre Bragg grating sensor system for simultaneous measurement of quasi-static strain and temperature using discrete wavelet transform." *Measurement Science and Technology* 17.2, 384, 2006.

Chapter 2

Review of Fiber Optic Sensor Technologies for Strain/Temperature Sensing in Composite Materials

In the introduction chapter, a hybrid fiber optic sensor scheme⁴ is described, by integrating a temperature insensitive polarimetric fiber sensor and a fiber Bragg grating sensor, which is capable of simultaneous measurement of the strain and temperature. The area of fiber sensing in composites has received a lot of attention in recent years. A number of sensor types have emerged but all of the sensors face common challenges when embedded in a composite. A common theme for example is that when a fiber optic sensor is embedded in a composite material, the sensor is influenced in various ways by the physical parameters of the composite material such as thermal expansion, and non-uniform strain distribution within the composite etc. It is useful therefore, prior to describing the detailed research undertaken for this thesis, to provide an overview of fiber optic sensing in composites. This review chapter presents such an overview of the various aspects of existing fiber optic sensor sensing technologies, previously developed for strain / temperature measurements in composite materials.

In this chapter an overview is provided, detailing the different types of most

⁴ G. Rajan, M. Ramakrishnan, Y. Semenova, K. Milenko, P. Lesiak, A. W. Domanski, T. R. Wolinski, and G. Farrell. "A photonic crystal fiber and fiber bragg grating-based hybrid fiber-optic sensor system." *Sensors Journal*, IEEE, Vol 12(1), pp. 39-43, 2012.

commonly used composite materials, the relevance of different types of OFS in terms of embedding in composite materials, recent trends, issues, future challenges as well as an overview of earlier reported OFS sensors for strain / temperature measurements in composite materials. The primary aim of this review and its underpinning literature survey is to enable an analysis and comparison of various aspects of sensing in composites, such as the properties of different types of commercially available composite materials, the methods for embedding OFSs in to composite materials.

2.1 Overview of fiber optic sensors technologies for strain/temperature sensing applications of composite materials⁵

Keywords: Fiber optic sensor, composite materials, strain / temperature sensing, smart materials, structural health monitoring.

Abstract: This research work provides an overview of the different types of OFS that can be used with composite materials and also their compatibility with and suitability for embedding inside a composite material. An overview of the different types of OFS used for strain/temperature sensing in composite materials is presented. Recent trends, and future challenges for OFS technology for condition monitoring in smart composite materials are also discussed. This comprehensive review provides essential information for the smart materials industry in selecting of appropriate types of OFS in accordance with end-user requirements.

⁵ M. Ramakrishnan, G. Rajan, Y. Semenova, and G. Farrell. "Overview of Fiber Optic Sensor Technologies for Strain/Temperature Sensing Applications in Composite Materials." *Sensors*, Vol 16(1): 99, 2016

2.1.1. Introduction

Composite material structures [2.1] are widely used in the aerospace, marine, aviation, transport, sport/leisure and civil engineering industries [2.1]. Composite material structures are frequently subjected to external perturbations and varying environmental conditions which may cause the structures to suffer from fatigue damage and/or failures, and thus require real time structural health monitoring (SHM). Diagnostics processes and condition monitoring of composite structures is usually carried out during their working life [2.2]. The goal of such diagnostics is to detect, identify, locate and assess the defects that may affect the safety or performance of a structure. Sensors that are commonly employed for SHM are resistance strain gauges, fiber optic sensors, piezoelectric sensors, eddy current sensors, and micro-electromechanical systems (MEMS) sensors [2.3]. Traditional nondestructive evaluation techniques such as ultrasonic inspection, acoustography, low frequency methods, radiographic inspection, shearography, acousto-ultrasonic and thermography are effective for SHM of composite materials and structures, but frequently it is difficult or impossible to use such nondestructive evaluation techniques in an operational structure due to the size and weight of the systems [2.4]. OFS on the other hand are suitable candidates for SHM of composite materials during operation since they are capable of achieving the goals of diagnostics as well as condition monitoring and being very compact in size can also be embedded into such structures, acting in many ways as the equivalent of a human nervous system [2.5]. Previous investigations of OFS embedded in composite structures indicate that OFS technology is capable of monitoring stress/strain, temperature, composite cure process, vibration, humidity, delamination and cracking and thus has great potential for condition monitoring of

a variety of composite materials applications [2.6, 2.7].

Recognizing the increase in the use of composite structures and the need for them to perform “smart” functions, such as sensing and actuation, this paper for the first time presents a comprehensive overview of recent advances in the area of OFS technology for condition monitoring involving strain and temperature measurements in composite materials and also quantities such as thermal expansion. An overview of different types of most commonly used composite materials and their properties is given in Section 2. Then the demand for the SHM in composite material structures is discussed in Section 3, following which the common fabrication methods of composite materials with embedded fiber sensors are detailed in Section 4 while the issues of composite degradation associated with embedding of fiber sensors are discussed in Section 5. An overview of different types of fiber sensors for strain/temperature measurements in composite materials is presented in Section 6. The recent trends, issues and future challenges of the OFS technology are discussed in Section 7.

2.1.2. Composite materials and demand for the SHM in composite material structures

In this section, various classifications of typical composite materials and their properties are discussed. In general, fibre composite materials have two constituent materials; reinforcement fibres and a matrix [2.8] that when combined together can produce a material with properties superior to those of the constituent materials. It is known that the mechanical properties of a composite material differ depending on the matrix and the reinforcing materials used to fabricate the composite [2.8 2.,9]. The functions of the matrix in a composite material are: to transfer the load

to the reinforcement fibres; to provide temperature resistance and chemical resistance and to maintain the reinforcement fibres in a fixed orientation [2.10].

The second constituent of a composite material is the reinforcement fibre [2.9].

The composite material's tensile properties, stiffness and impact resistance are influenced by the type of the fibre reinforcement [2.10]. As regards applications, fibre reinforced composite materials are commonly used for the fabrication of various structural parts such as aircraft tails, wings, fuselages, propellers, helicopter rotor blades, wind turbine blades, in the construction industry and as components in racing cars, boats, *etc.* [2.7]. One of the key challenges in the design of a composite structural part in many applications is the need to achieve a fail-safe design solution, which requires optimisation of multiple parameters. Typically given the performance specifications for a composite part [2.9], the areas that need optimisation are: the selection of most appropriate reinforcement and matrix constituents to satisfy the requirements for strength and stiffness of the particular composite part with a minimum weight; the selection of the composite part's geometry; a careful analysis of stress distribution within the part; the minimization of moisture ingress; optimization of toughness and an analysis of failure modes. Prior to opting for a particular design for mass production the manufacturer also needs to consider the repeatability of the composite part's performance specification, ease of production, cost efficiency and quality assurance mechanisms [2.10–2.12]. Finally, even though the designed structural part is optimised for fail-safe performance, there is a possibility of damage during operation in extreme environmental conditions and mechanical failure of the structure due to external perturbations [2.3] and this necessitates the requirement for non-destructive structural health monitoring techniques throughout the lifetime of the composite

structural part.

The demand for SHM in composites is in the first instance driven by the increased use of composite materials. The widespread use of carbon reinforced fibre plastics (CRP) and glass fibre reinforced plastic (GRP) composite based structural parts has significantly increased in application areas such as aircraft, sport vehicles, wind turbines, and infrastructure constructions, because of the inherent advantages of composite materials. For example, in aircraft the advantages are well known: lighter weight for the aircraft, reduced requirements for maintenance and increased passenger comfort [2.13]. The use of composite materials in aircraft is growing, as shown in Figure 2.1a–c. Aircraft that utilize a high proportion of lightweight composite materials consume less fuel and result in a high cost benefit that yields energy savings up to 18%. Some existing commercial aircraft models such as the Boeing 787 and Airbus A350 are comprised of *circa* 50% composite materials by weight. Market research conducted in 2013 by Jahn and Witten indicates that there will be a growing demand for such aircraft in the coming years [2.14]. Figure 2.1 a,b shows the overall use of CFP composites by different industries and GRP production in different European industries respectively.

The driving force behind the need for SHM in composite materials is the necessity to monitor composite parts during operation, for safety and early detection of failure. During a typical 20-year service life, composite structures such as wind turbine blades, helicopter blades, construction parts and aircraft parts are subjected to static and dynamic lift, drag and inertial loads over a wide range of temperatures and often severe environmental conditions.

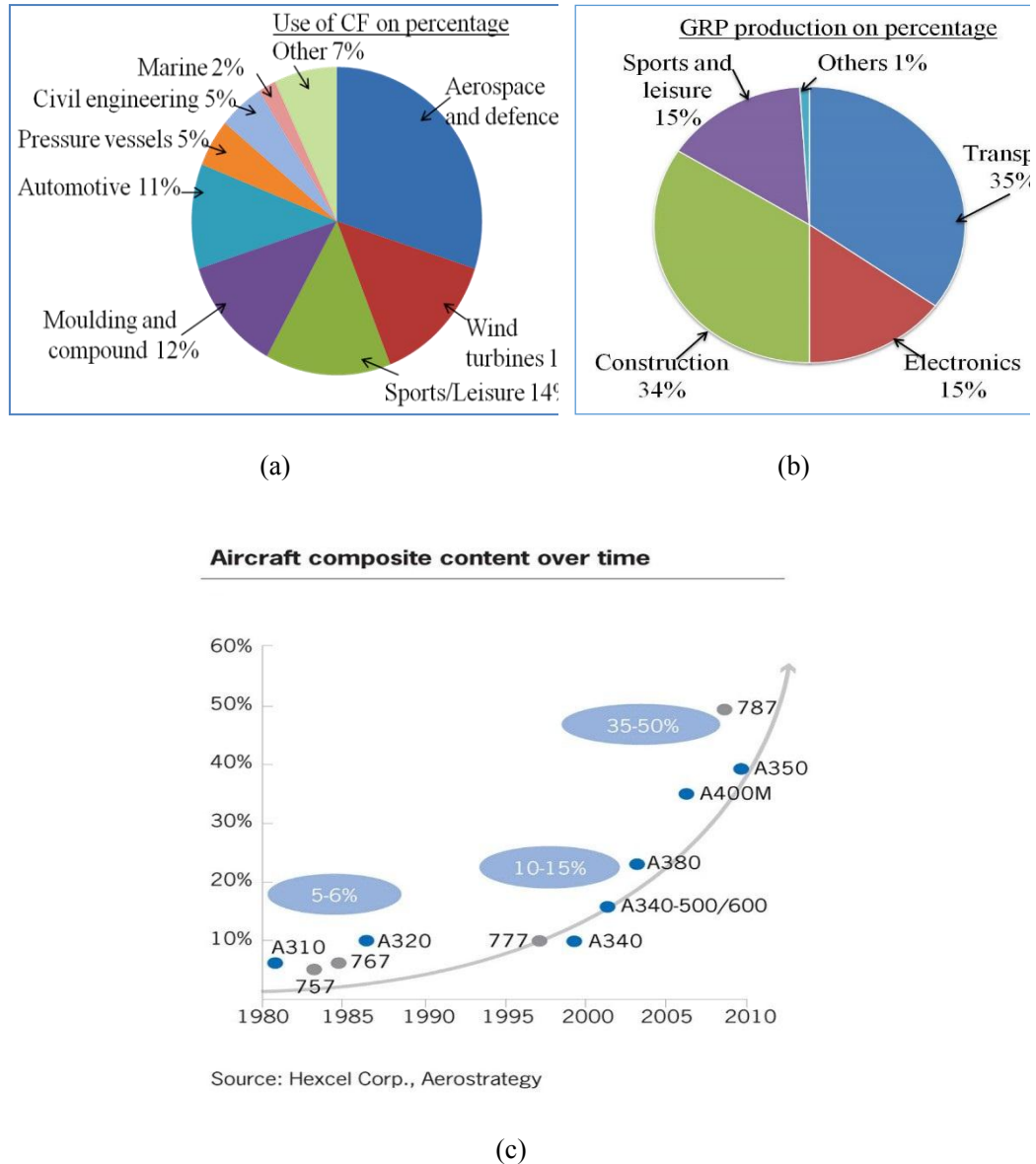


Figure 2.1. (a) Use of CF composites by industry [2.14]; (b) GRP production in Europe for different application industries [2.14] and (c) development of composite aerospace applications in last 40 years (source data from *Hexcel Corp. Aerostrategy*).

As the growth in production and use of composite parts has increased, the composite industry has increasingly focused on damage/failure free composite structures and non-destructive techniques for SHM over a part's life time. Compared to conventional non-destructive sensing techniques, optical fiber sensors have achieved wide acceptance due to their attractive properties such as small size, immunity to electromagnetic interference and low cost [2.1]. Optical

fiber sensors embedded in various structures are very useful for strain/temperature monitoring [2.2] applications in extreme environmental conditions. For example, issues such as bend loading in aircraft wings and bridges can be monitored and avoided by implementing smart composite structures with embedded fiber optic sensors. Also more complex sensing needs can be met, such as the detection of the formation of ice on the wings of an aircraft by implementing smart composite structures with embedded fiber optic sensors within the wings material. Monitoring of the wing bend or loading due to ice accumulation combined with temperature data can improve the efficiency of the aircraft's de-icing systems. As a result, it can be concluded that smart composite materials with embedded fiber optic sensors can significantly enhance the safety of advanced machines, structures and devices.

2.1.3 Composite materials with embedded fiber sensors:

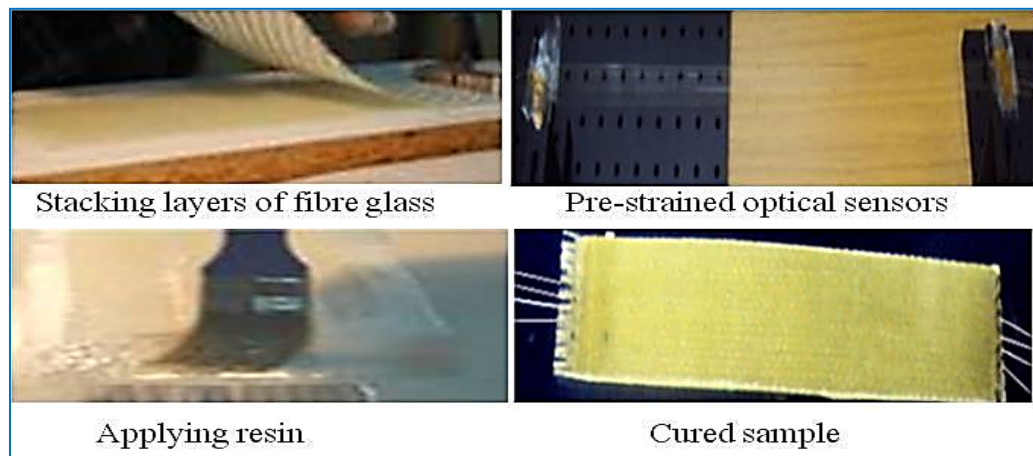
fabrication methods

This section discusses the commonly employed sample fabrication methods for composite materials with embedded OFS.

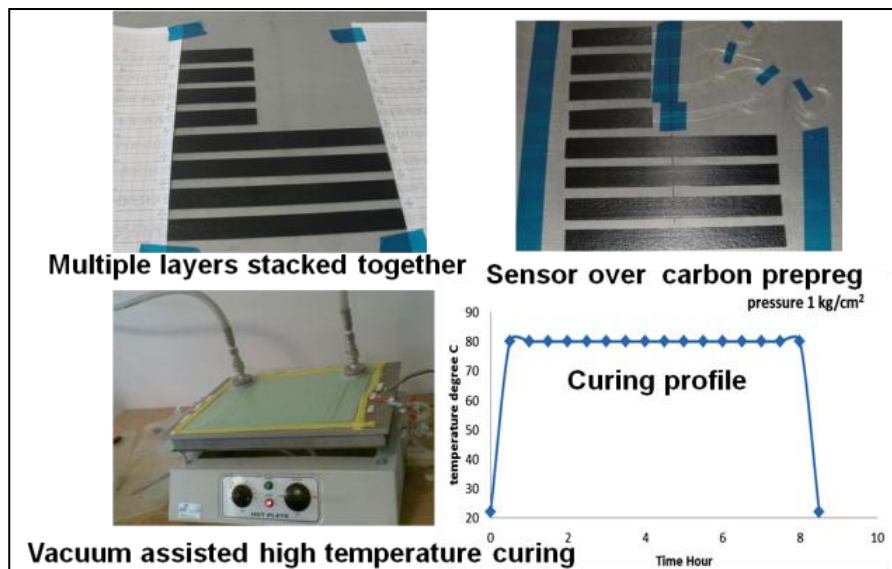
A. Fabrication method of composite samples embedded with OFS by hand layup and pre - preg layup methods

The most common fabrication processes adopted by laboratory based and small scale industrial manufacturers are the expertise intensive hand layup and pre-preg layup [2.15] methods. The hand layup method is a process for arranging fiber-reinforced layers in a laminate and shaping the laminate to fabricate the desired part. For this the reinforcement fibers or fabrics are stacked one over another by applying the matrix in between them. After stacking, curing (or polymerization) of the resin matrix of the multiple laminate layered composite, the sample can be shaped as per the manufacturer's specifications. Pre-pregs are single laminates of

“pre-impregnated” composite fibers with a matrix material such as epoxy resin. In the pre-preg layup method, multiples of composite pre-preg laminates are stacked one over another and the curing can be done unaided or by applying heat and/or pressure. The moulding process can be either vacuum—bag moulding, or an autoclave moulding. Typical autoclave curing conditions involve a temperature range from 120 °C to 200 °C with an applied pressure up to 100 psi (~6.89 kPa).



(a)



(b)



(c)

Figure 2. 2. Embedding fiber sensors inside composite materials (a) hand layup; (b) pre-preg method, and (c) expert assisted manufacturing of composite part embedded with OFS

For embedding optical fibers in samples prepared by both the hand—layup and the pre-preg layup methods the process is similar as follows: before the curing process optical fibers are placed on the corresponding composite layer and some pre-strain is applied to make sure the optical fibers remain free of bends [2.16]. Positioning of the optical sensor is highly application specific and depends on the location of the areas where parameters need to be monitored. For example, for applied strain and temperature measurements of composite material structures it is reported that optical fiber sensors were embedded within the furthest layer from middle layer to achieve the highest measurement sensitivity [2.17]. The different steps for embedding optical fiber sensors by the hand layup and pre-preg methods are shown in Figure 2.2 (a) and (b) respectively. For larger composite parts, optical fibers can be embedded manually with expert assistance as shown in Figure 2.2 (c), but for large scale production of smart composite structure materials embedded with optical fiber sensors, automated robotic systems can be used. One of the most important concerns while embedding OFS inside composite structures is their influence on the structural integrity of the composite part. In the next section have

been detailed some methods to reduce the risk of composite material degradation and to maintain the structural integrity of the composite material structures with embedded sensors.

B. Rotating filament wound pressure cylinder with OFS

Fabrication details of E-glass fibre reinforced composite based pressure cylinders with OFS was reported earlier [2.18] for the composite parts with cylindrical shapes. In this method a machine assisted filament winding process in the circumferential direction is used. Continuous E-glass roving reinforcement fibre with different orientation angles can be used to achieve a defined length for the fabricated pressure cylinder. The winding angle $\pm 55^\circ$ with respect to the cylinder's long axis is the classical winding angle for pressure vessels, where circumferential stress is twice the value of axial stress. The machine assisted filament winding process operates in such a way that at both ends of the cylinder there are zones of reinforcing fibers, placed at an angle of 90° to the cylinder axis. For embedding OFS in to the composite cylinders, a specifically designed mandrel with a winding machine rotary is co-operated with a rotating filament winding machine. The matrix material is applied during the winding process. The matrix material used is a mixture of Araldite LY 5052 epoxy and hardener HY 5052. The samples are cured at temperature 50°C for 900 min. More detailed explanation of this particular method is given in reference [2.18]. A fabrication method for a pressure cylinder made of carbon fibre reinforced epoxy pre-preg embedded with OFS was reported in [2.19]. In this method the carbon fibre reinforcement is wound using a machine assisted rotating filament. The optical fibre is embedded between the first and second plies of the laminate sequence. Pre-stressed optical fibres are drenched in epoxy resin and are wound onto a water-soluble mandrel after which the vessel is

cured in an oven. The winding of the pressure vessels consists of five layers in total: in which two polar windings with winding angles of 12.7° and 16.5° and three hoop windings with a winding angle of approximately 90° . The optical fibre is carefully embedded during the winding process of the vessel in the outer 90° winding, parallel to the reinforcing fibres.

C. Composite panels embedded with OFS

A laboratory level fabrication method of composite panels with embedded OFS using specially designed Resin Transfer Molding (RTM) apparatus is reported earlier [2.20–2.22]. The specially designed RTM apparatus allows for different types of mold designs with variable mold thicknesses. An automatic control system is used for the resin injection process and a transparent glass top is provided for visual monitoring of resin flow. Automated control of curing temperature as well as the mold part temperature is achieved by using thermocouple sensors with an automated water temperature controller. The OFSs are embedded into the perform itself. The ingress/egress parts of optical fibers that enter into the composite panels are at an angle close to 90° relative to the component's surface. A thin bended hypodermic tube is placed around the optical fiber such a way that the bend radius of the hypodermic tube is carefully chosen to avoid the possibility of fiber fracture. To protect the optical fibers from the disturbances due to the reinforcement preform, a tapered silicon stopper is fitted in a hole in the mold and the hypodermic tube passes through this stopper. Thus the ingress/egress is sealed and is capable of withstanding a resin injection pressure of approximately 0.75 bar.

D. Braided composites embedded with OFS

A method to co-braid optical fibers into braided composites is also reported [2.23]. The reported advantage of this method is that the embedded optical fibers will not

cause large resin pockets in the material. In this method, optical fibers are incorporated as an axial yarn so that the optical fibers run straight as well as parallel with respect to the specimen braiding direction. The structural reinforcement fibres are then braided around the optical fibers. The types of OFS that are reported incorporated with such braided composites are the Fabry-Perot fiber optic sensor, polarimetric optical fiber sensor, and the Bragg grating fiber optic sensor. A special RTM molding dye is designed to protect the optical fibers from any damage during the curing process. The RTM process is used for composite fabrication using a release agent, Epoxy 828 resin, and a curative. The temperature of the molding process is 85 °C, at the pressure of 0.1 MPa. Carbon fibre is used as reinforcement and the specimens are braided with a fiber volume fraction of 50%.

E. OFS stitched carbon fibre preforms for advanced composite structures

Incorporating optical fibers during carbon fibre based preform fabrication itself is promising and has been reported earlier [2.24]. In this method optical fibers were stitched into each fiber preform along the middle plane of the laminate. OFS stitched carbon fibre preforms were successfully demonstrated for condition monitoring as well the resin advancement monitoring through the preform during the infusion. For monitoring the resin advancement, a reference optical fiber was placed as near as possible to the infusion tube in order to determine the entry time of the resin as a reference point to allow interpretation of the OFS generated data [2.24].

2.1.4. Composite material degradation associated with embedding of fiber sensors

One of the major concerns when embedding OFSs in composite materials is the

degradation of the composite material's mechanical properties and also the possible increase in the probability of failure due to the presence of embedded optical fibers [2.25]. Various studies have been carried out to analyse the influence of the embedded OFS on composite material tensile/compressive strength, stiffness, inter laminar fracture toughness, and fatigue resistance, etc. It is reported that having embedded optical fibers passing through or parallel to ply-drops in a laminate does not have any significant effects on the static strength of the laminate [2.26, 2.27]. This is valid even for optical fibers placed in the most critical locations. In principle any potential degradation of strength and the modulus of a composite material will be a function of the orientation of the optical fiber relative to the nearest plies, the overall thickness of the laminate, the optical fiber diameter, and type of protective coating on the optical fiber [2.26]. Degradation becomes increasingly severe with an increasing angle between the optical fiber and ply directions. Another issue is the larger diameter of the optical fiber (with its buffer coating) compared to the ply fibers of the composite. In general, commercially available optical fibers have diameters from 125 μm to 230 μm , which is about ten to fifteen times larger than the average E-glass fiber or carbon fiber. Embedding the optical fiber perpendicularly to the direction of the reinforcement fibres can result in appearance of characteristic “eye” patterns or “pockets” within the resin, which act as defect centers in the composite part that could ultimately lead to premature failure in the form of delamination [2.27]. However, testing conducted at a number of labs worldwide concluded that such delaminations were insignificant if the OFS density was low. It reported that if the optical fiber is laid along the direction of reinforcement fiber there is a uniform consolidation around the optical fiber with minimum defects and thus the laminate's mechanical parameters are least affected

[2.6, 2.26–2.29]. Also the optical fibers laid along the direction of fiber reinforcement have limited influence on the mechanical behavior of the composite structure because of optical fiber's own inherent load carrying ability [2.26].

An analysis [2.6] on the flexural strength of a composite material, embedded with OFSs, that bears tensile loading showed that the flexural strength did not suffer any noticeable degradation when the OFS were embedded in the tensile region either in the longitudinal direction or in the transverse direction. For compressive loading, the situation is similar if the sensor is embedded in the longitudinal direction but it is found that if the OFS is embedded in the transverse direction with respect to the compressive region, the flexural strength is degraded significantly [2.30]. In order to realize SHM for composite material components in many applications it is essential to measure the strain and temperature of composite materials and in the next section there is discussion of the different types of OFS strain and temperature sensors that can be embedded in composite materials.

2.1.5. Types of fiber optic sensors for strain/temperature measurements in composite materials

There are a wide variety of applications of fiber optic sensors in composite materials, including vibration measurements, cure process monitoring, temperature measurements, thermal expansion measurements, detection of delamination/debonding, three dimensional strain measurements, thermal strain measurements, relative humidity measurements and detection of cracking, *etc.* [2.31–2.34]. For all these applications the key requirement is to measure either strain or temperature or both parameters. In this section the different types of OFS are discussed that can be used with composite materials to measure

strain/temperature when embedded inside a composite material. The different types of OFS reported for strain/temperature measurements in composite materials are FBG sensors [2.35–2.37], interferometric fiber optic sensors [2.38], polarimetric sensors [2.39], fiber optic micro bend sensors [2.40], distributed sensors (using techniques such as Rayleigh scattering, Raman scattering, and Brillouin scattering) [2.41,2.42] and hybrid sensors [2.43–2.45]. The aim of this review is to provide essential information for the smart materials industry in selecting of appropriate types of OFS in accordance with the end-user requirements and applications.

A. Fiber Bragg grating sensor for composite materials

FBGs are the most commonly employed fiber optic sensors in SHM applications for composite materials [2.35–2.37]. A fiber Bragg grating sensor comprises of a grating region with a periodic change in refractive index in the core region of an optical fiber. Such a periodically modulated refractive index structure enables the light to be coupled from the forward propagating core mode into a backward propagating core mode generating a reflection response, as shown in the schematic illustrating the principle of an FBG provided in Figure 2.3 [2.46]. The light reflected due to periodic variations of the refractive index of the Bragg grating with a central wavelength given by [2.46],

$$\lambda_B = 2n_0\Lambda \quad 2.1$$

where n_0 is the effective refractive index of the guided mode in the fiber core and Λ is the grating pitch.

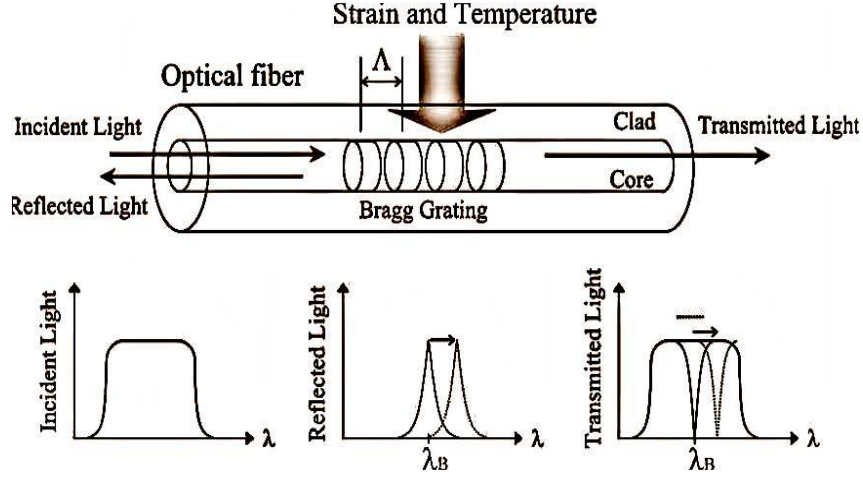


Figure 2.3. Fiber Bragg grating

The strain sensitivity of the Bragg wavelength arises from the change in the pitch of the fiber grating due to strain and changes in the refractive index arising from the strain-optic effect. When a strain is applied to the grating, the Bragg reflected wavelength changes. The wavelength shift $\Delta\lambda_s$ for a value of elongation ΔL is given by [2.46],

$$\Delta\lambda_{\epsilon} = \lambda_B \cdot \left(\frac{1}{\Lambda} \frac{\partial \Lambda}{\partial L} + \frac{1}{n_0} \frac{\partial n_0}{\partial L} \right) \cdot \Delta L \quad 2.2$$

In practice the applied strain value can be estimated from the measurement of reflected wavelength as it changes due to applied strain. The typical strain sensitivity of an FBG at 1550 nm is $\sim 1.2 \text{ pm}/\mu\epsilon$.

Bragg wavelength shift can also occur due to changes in temperature. For a temperature variation of ΔT , the corresponding wavelength shift $\Delta\lambda_T$ is given by [2.46],

$$\Delta\lambda_T = \lambda_B \cdot \left(\frac{1}{\Lambda} \frac{\partial \Lambda}{\partial T} + \frac{1}{n_0} \frac{\partial n_0}{\partial T} \right) \cdot \Delta T \quad 2.3$$

The temperature sensitivity of the Bragg wavelength arises from the change in the

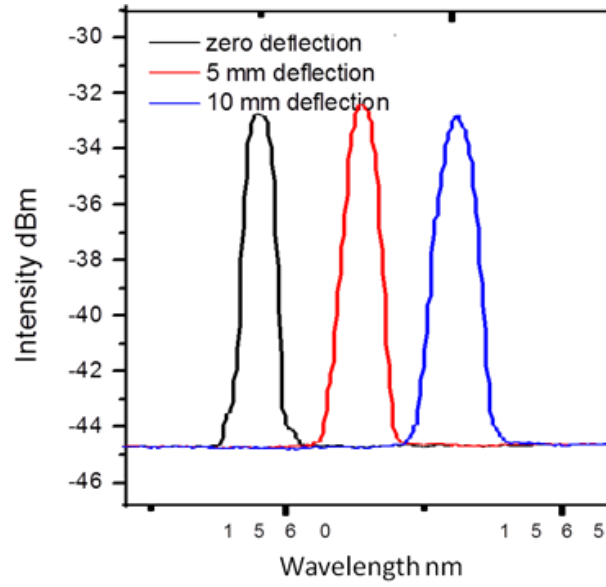
grating pitch associated with the thermal expansion of the fiber, and the change in the refractive index arising from the thermo-optic effect. Thus Equation [2.3] can be also written as [2.46],

$$\Delta\lambda_T = (\alpha_0 + \beta_0) \cdot \lambda_B \cdot \Delta T \quad 2.4$$

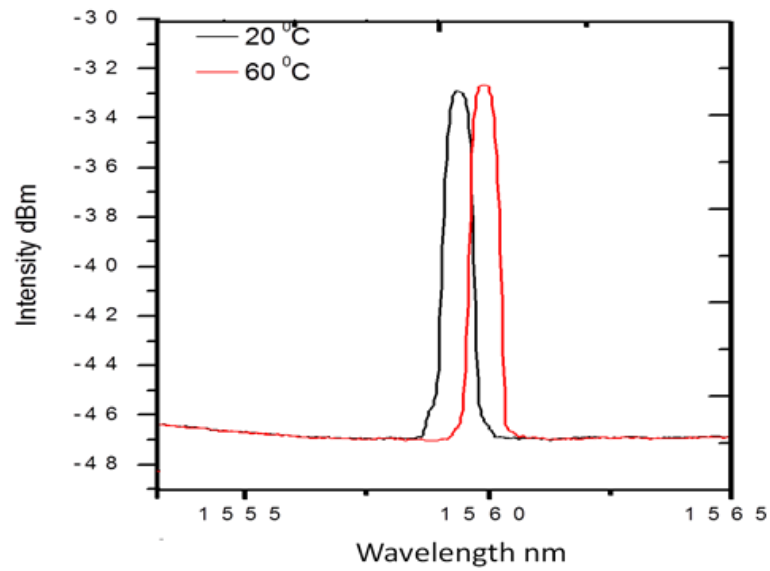
where α_0 is the coefficient of thermal expansion (CTE) of the fiber, and β_0 is the fiber refractive index variation with temperature, respectively. The values of α_0 and β_0 are constants for silica optical fiber, and are $0.55 \times 10^{-6}/^\circ\text{C}$, and $6.6 \times 10^{-6}/^\circ\text{C}$, respectively. The typical temperature sensitivity of an FBG at 1550 nm is ~ 11.6 pm/ $^\circ\text{C}$. Commonly FBGs are used to measure axial strain as well as temperature. This is because axial strain sensitivity is effectively higher as the change in the FBG pitch is directly proportional to the applied longitudinal strain. The measured wavelength shift of the embedded FBG sensors for different deflection values during a three-point bending strain test on composite material is shown in Figure 4a. The measured wavelength shift of the embedded FBG sensors at different temperatures of composite materials is shown in Figure 2.4(b). One can see that a red shift of the Bragg wavelength arises as a result of an increase in temperature. Other than standard Bragg gratings with a uniform period, there are chirped gratings with a gradual period variation [2.47], and Tilted Fiber Bragg gratings (TFBG) [2.47] with gratings written at an angle to the fiber axis are also employed for strain temperature measurements in composite materials. The chirped FBG sensor has a gradual distribution of the grating period [2.48]. This variation in the grating period provides a one-to-one correspondence between the wavelength in the spectrum and the position of the gauge section within composite material, which is the significant advantage of chirped FBG sensors over the conventional FBG sensors [2.48]. The main disadvantage of conventional FBG sensors is the

cross-sensitivity between temperature and strain. In a different manner from conventional FBGs, the wave vector of a TFBG has a certain angle with respect to the fiber axis; making the resonance wavelengths of core mode and cladding mode sensitive to temperature, while their transmission power is temperature-independent [2.49]. Thus based on these unique characteristics of TFBG, it is possible to achieve simultaneous discrimination of mechanical perturbations and temperature [2.47, 2.49]. Different methods have been reported by other authors to compensate for the cross-sensitivity effects between temperature and strain; these methods include introduction of a reference FBG [2.50], dual-wavelength superimposed FBGs [2.51], different cladding diameter FBGs [2.52], combined FBG and a long-period grating [2.53], combination of an FBG and a Fabry-Perot interferometer [2.54], and superstructure FBG method [2.55].

It has also been reported that for coating stripped FBGs thermal expansion of a composite material as well as the non uniform strain can cause Bragg peak distortion and broadening [2.28, 2.56]. The strain components acting in different directions within the composite structure can be measured using multiplexed FBGs [2.57]. In addition, a non-isotropic strain distribution within the composite material can be measured by using an FBG written in a micro-structured high birefringence fiber [2.58].



(a)



(b)

Figure 2.4. (a) Measured wavelength shift for the FBG sensors at different deflection values (b) measured wavelength shift for the FBG sensors at different temperatures.

[2.56].

A. FBG written in micro-structured fibers as a sensor for composite materials

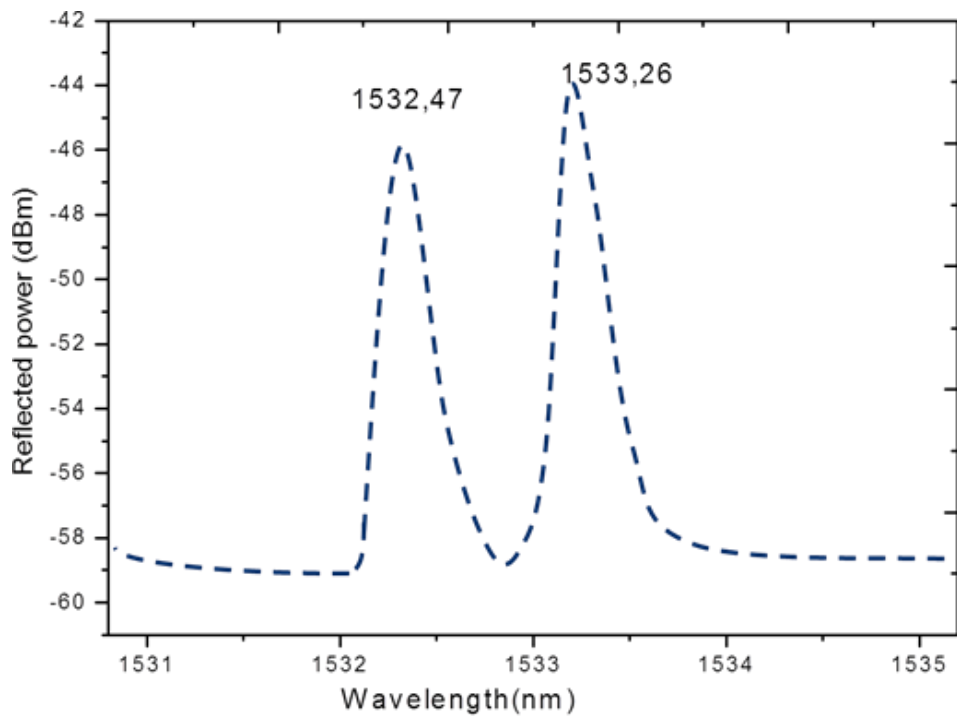
A conventional FBG sensor's primary response is to an axial strain but the

transverse strain also has some influence on the FBG sensor's response [2.57, 2.59]. But it is difficult to discriminate axial strain and transverse strain from the FBG spectral response. For strain mapping in some SHM applications, for example, for the detection of damage, cracks, delamination etc a multi axial strain measurement is required. This in turn results in the importance of development of a sensing scheme that provides measurements of axial strain together with transverse strain. It is reported that FBGs written in the highly birefringent (HB) fibers and high birefringent micro-structured fibers (HB-MOF) have real potential to measure transverse strain and axial strain simultaneously [2.58, 2.60]. As represented in Figure 5a, an FBG written in a highly birefringent fiber displays two Bragg peaks, corresponding to both orthogonally polarized modes. The change of the Bragg peak separation depends on the phase modal birefringence variation induced by transverse load and temperature. The properties of an MOF and its sensitivity to different measurands are determined by the type of the fiber used. However it is reported that FBGs written in HB fibers such as the bow-tie type have the disadvantage of greater temperature and strain cross sensitivity [2.59].

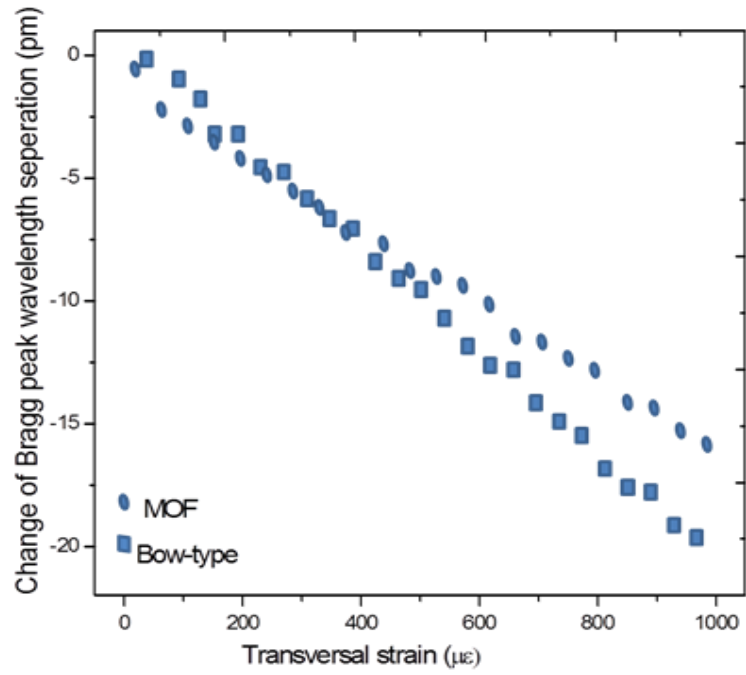
The cross-sensitivity issue can be resolved by writing FBGs in low temperature sensitive MOFs, such as HB-PM-PCF. For example, a comparison response of the embedded FBG sensors written in conventional birefringent optical fibers (bow-tie) and a HB-PM-PCF when the composite material is exposed to controlled mechanical and thermal loads are presented in Figure 5(b), and (c), respectively.

For the FBG in a bow-tie type fiber the Bragg peak separation varies in accordance with the transverse strain and temperature as shown in Figure 5(b), and (c). However in the case of an FBG in a low temperature sensitive MOF, the Bragg peak separation varies with transverse strain only. A temperature independent axial

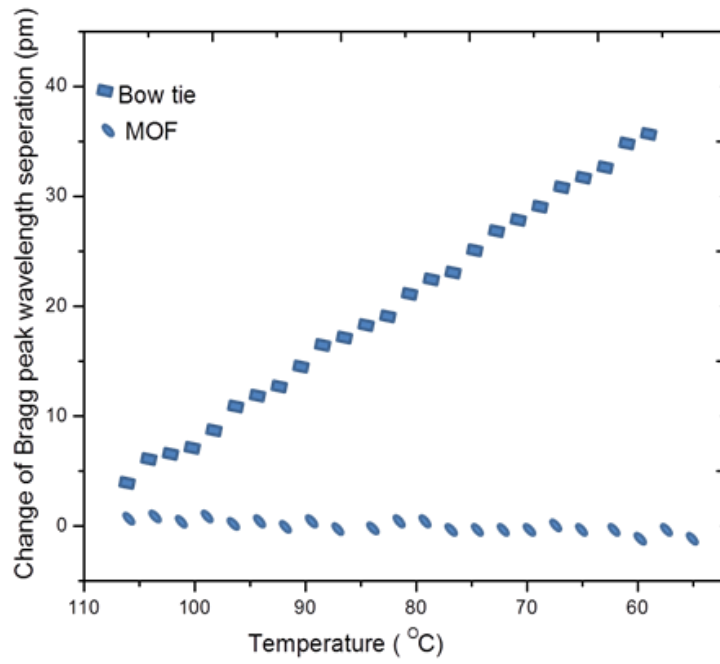
strain and transverse strain measurement in a composite material can be carried out using an FBG written in a HB-PM-PCF [2.60]. It is also reported that the two Bragg peaks in the case of an FBG written in HB-PM-PCF are farther separated than for an FBG in a bow-tie fiber and therefore FBGs written in MOF/HB-PM-PCF allow for more accurate measurements of the peak wavelengths and thus are more suitable for composite material sensing applications despite high splice loss induced lower reflectivity of the grating [2.58, 2.60].



(a)



(b)



(c)

Figure 2.5. (a) Reflection spectra for an FBG written in a HB-PM-PCF with two peaks corresponding to slow axis and fast axis; (b) change in the peak separation with transverse strain for FBGs written in MOF and bow-tie type fibers; and (c) change in peak separation with temperature [2.60].

B. Phase-shifted FBGs for composite materials

The Phase-Shifted FBG (PS-FBG) sensor together with its interrogation system is proven as one of the high sensitive methods for acoustic emission (AE) measurement [2.61]. PS-FBGs are widely used in optical fiber communications and optical fiber sensing applications as a wavelength multiplexer and also as a strain sensor. The extremely sharp resonance in the transmission spectrum of the PS-FBG enables it to develop a high sensitivity interrogation system capable of measuring very small strain changes, even at high acoustic frequencies. A typical transmission spectrum of a PS-FBG interrogated using a tunable laser is shown in Figure 2.6. It has been demonstrated that using this method microscale strains can be measured and thus the sensor is suitable for AE sensing in composite structures [2.61].

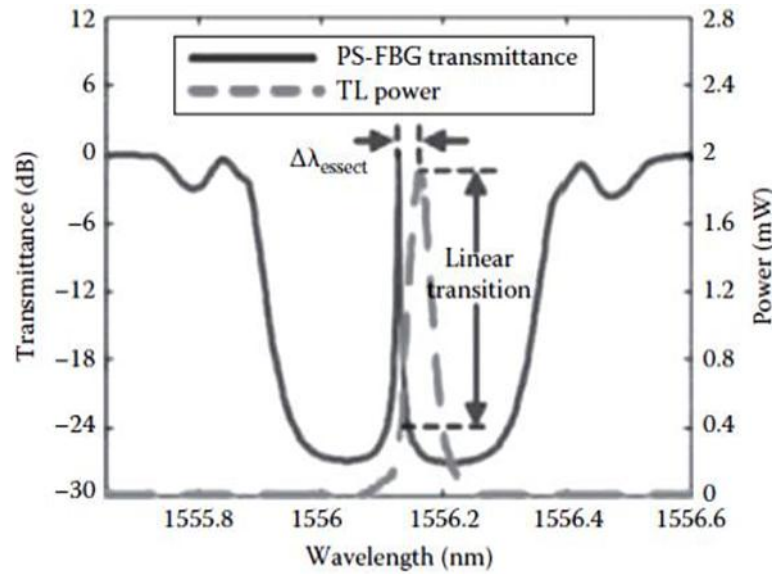


Figure 2.6. Spectral response of a PS-FBG and its interrogation technique based on a narrow band laser signal [2.61].

A.3. Polymer FBG sensor for composite materials

For composite materials, the attractive characteristics of polymer FBGs include

their high temperature sensitivity, large strain range, and the absence of buffer coating [2.62– 2.64]. These distinct features of the polymer FBGs might provide some advantages over standard silica FBGs in measuring some of the parameters of the composite materials.

Rajan *et al.* conducted studies with polymer FBGs embedded in glass-reinforced composite materials [2.65]. For the polymer FBG embedded in composite materials, due to temperature change, spectral broadening is observed together with the shift in the peak reflected wavelength. The observed wavelength shifts of the polymer FBG embedded in a glass-reinforced composite and its comparison with silica FBG and free-space FBG sensors are shown in Figure 2.7(a). A blue shift in the wavelength is observed for the polymer FBG due to the negative thermo-optic coefficient, while a red shift is observed for the silica FBG. The observed temperature sensitivity of the embedded polymer FBG is $-92.28 \pm 2 \text{ pm}/^\circ\text{C}$, which is close to the free-space temperature sensitivity of $-90 \pm 6 \text{ pm}/^\circ\text{C}$. The change in the bandwidth of the reflection spectra of the polymer FBG at different temperatures and its comparison with silica FBG is shown in Figure 2.7(b). It can be seen that the bandwidth of the polymer FBG increases as the temperature increases. The measured bandwidth change for the embedded polymer FBG within the temperature range of 30°C – 45°C was $8.5 \text{ pm}/^\circ\text{C}$. Therefore, from the observed spectral broadening and distortion, it can be concluded that the thermal expansion induced stress is effectively transferred to the polymer fiber and can be measured using a polymer FBG. It is assumed that the reason for this is the absence of a buffer coating for the polymer fiber, which results in a direct transfer of the surrounding physical phenomena to the core and cladding of the

polymer fiber. Stress induced by localized microbends in the composite material could also contribute to the chirping effect. The strain sensitivity of the embedded polymer FBG and its comparison with silica FBG is shown in Figure 8. From the figure, it can be seen that the strain sensitivity of the embedded polymer and silica FBGs are very close in value to each other. In free space, the polymer FBG had a slightly higher strain sensitivity (1.340 ± 0.015 pm/ $\mu\epsilon$) compared to that of silica FBG (1.2 ± 0.01 pm/ $\mu\epsilon$). The similarity in the measured strain sensitivity of the embedded silica and polymer FBGs underlines the fact that longitudinal strain in the composite is not effectively transferred to the polymer fiber. This can be attributed to the differences in mechanical properties of the polymer fiber and the composite material, which resulted in the mechanical strain not being effectively transferred to the polymer FBGs as compared to the case of silica FBG. Polymer FBG has the potential to measure temperature and thermal expansion of the composite material simultaneously.

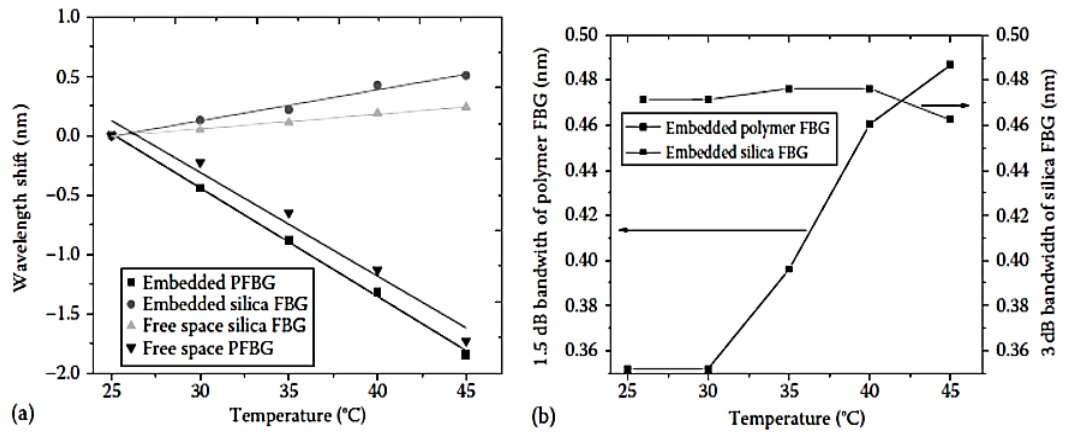


Figure 2.7. (a) Temperature-induced wavelength shift of the embedded polymer and silica FBGs and its comparison with free-space FBGs; (b) measured 1.5 dB bandwidth of polymer FBG and 3 dB bandwidth of silica FBG at different temperatures [2.65].

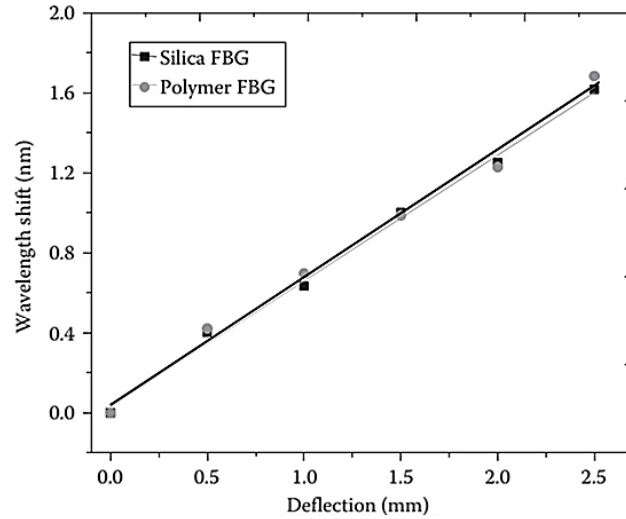


Figure 2.8. Wavelength shifts of the polymer and silica FBGs with deflection in the middle of the composite material [2.65].

B. Interferometric fiber sensors for composite materials

Interferometric fiber sensors [2.66] can also be employed for strain/temperature measurements in composite materials and this is discussed in detail in this section. There are different types of interferometric fiber sensors which differ in their operating principles and strain/temperature sensing characteristics [2.38]. Among the interferometric fiber sensors most commonly employed for composite sensing applications are: extrinsic Fabry-Perot interferometers (EFPI), micro-hole collapsed modal interferometers and Sagnac fiber loop mirror (FLM) sensors.

A Fabry-Perot interferometer (FPI) generally comprises of two parallel reflecting surfaces separated by a certain distance [2.66]. One of the EFPI sensors is illustrated in Figure 9(a). In an extrinsic FPI sensor, the interference occurs due to the multiple superposition of both reflected and transmitted beams at two parallel surfaces [2.38, 2.66]. It is possible to tune the intensity of the interferometric modes of an EFPI sensor by varying the gap between the two reflecting surfaces [2.66]. The reflection or transmission spectrum of an

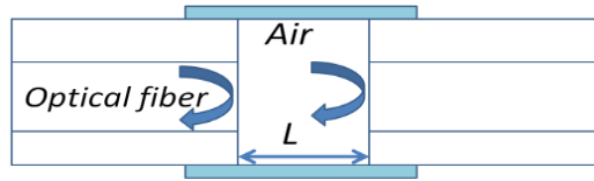
FPI is a wavelength dependent intensity modulation of the input light spectrum, resulting from the optical phase difference between the reflected and transmitted beams [2.66, 2.67]. The maxima and minima of the modulated spectrum indicate that both reflected and transmitted beams, at that particular wavelength, are in 2π phase and 2π out-of-phase, respectively. The optical phase difference between reflected or transmitted beams at a particular wavelength of the FPI is basically specified as [2.66],

$$\delta = \left(\frac{2\pi}{\lambda} \right) n 2L \quad 2.5$$

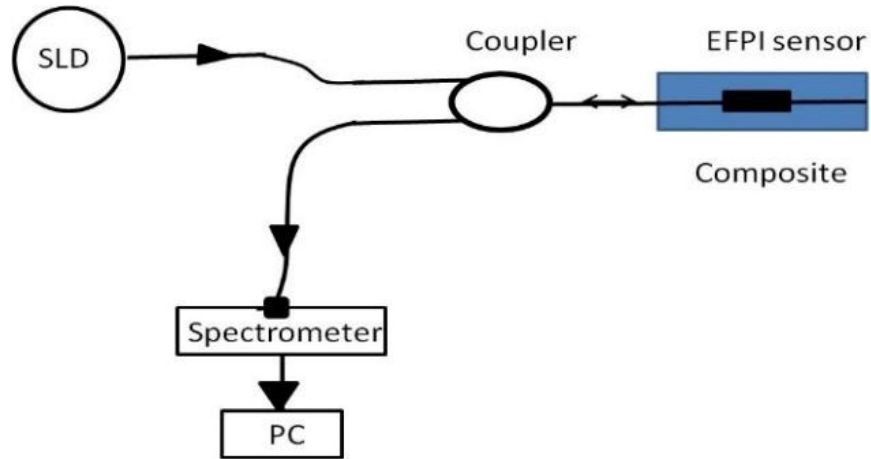
where λ is the wavelength of incident light, n is the refractive index (RI) of cavity material, and L is the length of the cavity.

The schematic experimental arrangement of the EPFI sensor is as shown in Figure 9b, which comprises of a superluminescent light diode (SLD) source, a coupler and a spectrometer. Any applied longitudinal strain to the FPI sensor alters the physical length of the cavity, which results in a phase difference between reflected or transmitted beams. By measuring the shift of the wavelength spectrum, the strain applied to the FPI can be measured. It is found that the shorter the optical path difference (OPD) the larger will be the free spectral range (FSR), resulting a wider dynamic range for a sensor [2.38, 2.67]. Therefore, the dynamic range of the sensor can be tuned by varying the cavity length which in turn changes the OPD of the FPI sensor [2.68]. Figure 10(a) illustrates experimentally measured strain using embedded EFPI sensor during the three point bending test of a composite material sample [2.56]. Moreover, EFPI sensors based on photonic crystal fibers have proved to be good candidates for measurements of axial strain in composite materials since their

sensitivity to temperature is insignificant [2.38, 2.69].

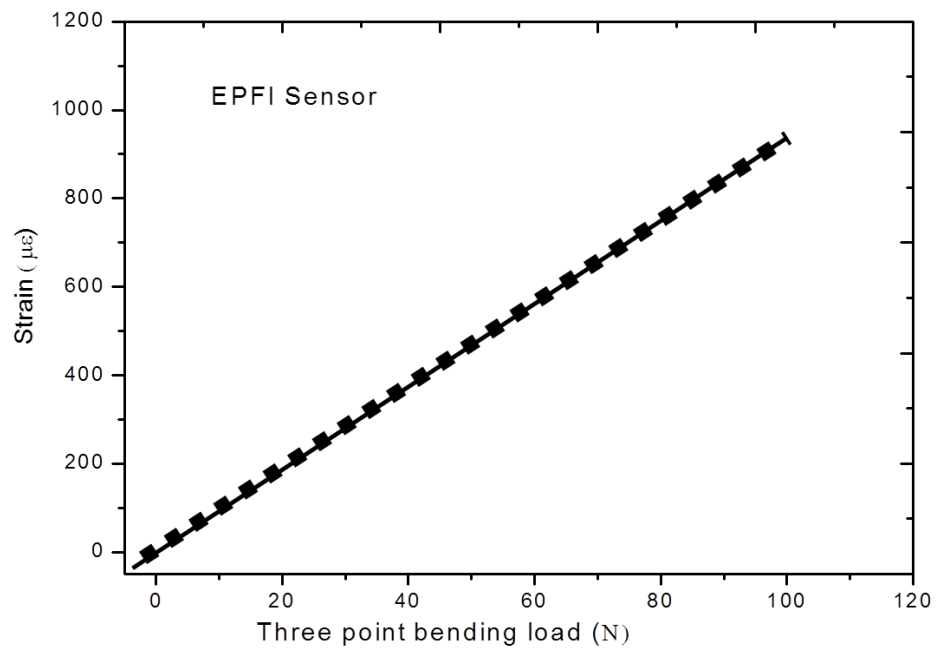


(a)

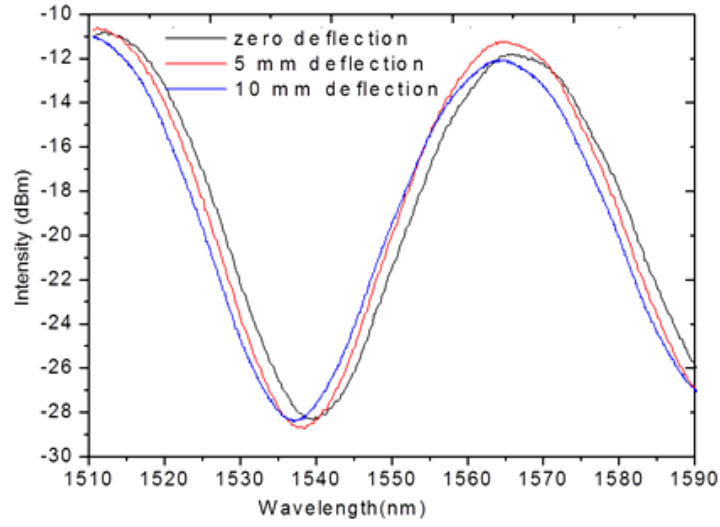


(b)

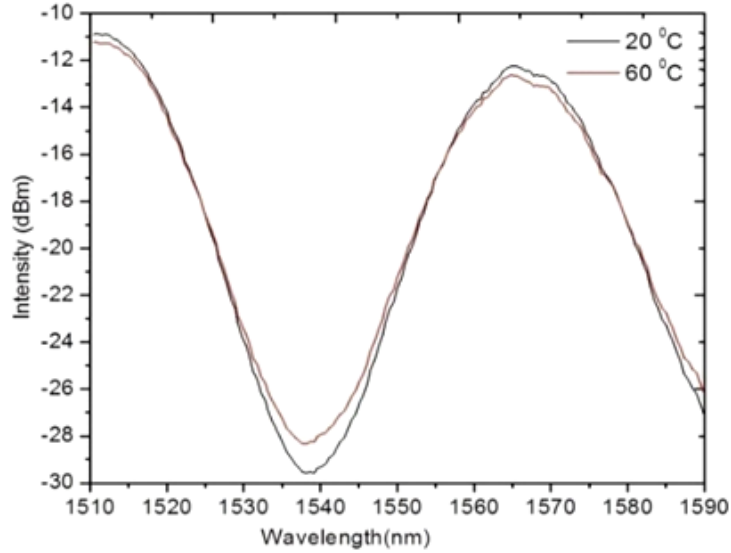
Figure 2.9. (a) One of the typical EFPI sensor design; and (b) schematic experimental arrangement for the EFPI sensor [2.70].



(a)



(b)



(c)

Figure 2.10. (a) Experimentally measured strain using embedded EFPI sensor during three point bending test in a composite [2.69]; (b) Responses of the of photonic crystal fiber based sensors embedded in the composite material sample during deflections based on three point bending test [2.70]; and (c) at different temperatures of the composite sample [2.56].

Recent advancements in the area of HB-PM-PCF sensors [2.38, 2.56] have opened new possibilities for the development of temperature insensitive micro-

hole collapsed photonic crystal fiber modal interferometric sensors. Micro-hole collapsed photonic crystal fiber modal interferometers can be used for localised strain measurements in a composite material. Micro-hole collapsed photonic crystal fiber modal interferometers can be fabricated by fusion slicing of a HB-PM-PCF section between two standard single mode fibers. During the splicing process, at both ends of the HB-PM-PCF section, the holes of the HB-PM-PCF are collapsed in a microscopic region. The first collapsed region allows for the excitation of multiple modes in the HB-PM-PCF and at the second collapsed region at the other end the modes recombine and thus the HB-PM-PCF section forms an interferometer [2.56]. It is reported that temperature independent strain measurement in composites is possible using such a micro-hole collapsed photonic crystal fiber interferometer fabricated from a micro-structured HB-PM-PCF fiber (LMA-10) [2.56]. An example of the output of a micro-hole collapsed modal interferometer embedded in composite beam undergoing three point bending deflection is shown in Figure 2.10(b) [2.69]. Figure 2.10(c) illustrates that such a sensor embedded in a composite material has very low temperature dependence [2.56].

Fiber optic Sagnac interferometers (SIs) are another promising candidate for composite material sensing applications. In a fiber optic SI input light is split into two parts propagating in the opposite directions by a 3 dB fiber coupler and these two counter-propagating beams are combined again at the same coupler as shown in Figure 2.11 [2.66]. The fabrication of such an interferometer can be simply achieved by connecting the ends of a conventional 3 dB coupler. High birefringent fibers (HB) or polarization maintaining fibers (PMFs) are typically utilized as sensing fibers since HB fibers maximize the

polarization-dependence of the signal within the SIs. In order to control the input light polarization a polarization controller (PC) is connected to the sensing fiber. The signal at the output port of the fiber coupler is a result of interference between the beams polarized along the slow axis and the fast axis. The phase of the interference is simply given as,

$$\delta_{SL} = \frac{2\pi}{\lambda} BL \quad 2.6$$

where $B = |n_f - n_s|$ is the birefringent coefficient of the sensing fiber, L is the length of the fiber, n_f and n_s are the effective indices of the fast and slow modes.

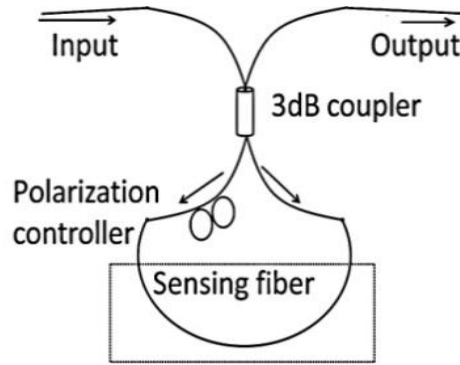


Figure 2.11. Schematic of the sensor based on a Sagnac interferometer.

Fiber optic-based SIs can be used for measuring parameters such as strain, temperature, pressure, twist, *etc.* Such fiber optic based SIs provide the value of the sensed parameter averaged over the length of the sensor. However, a disadvantage of the SI is its significant temperature strain cross-sensitivity [2.66]. It is reported that the temperature strain cross-sensitivity issue can be eliminated by employing low temperature sensitive HB-PM-PCF [2.56]. The output of a low temperature sensitive HB-PM-PCF based SI sensor embedded in composite beam undergoing three point bending deflection is shown in Figure 2.12 [2.56]. Such low temperature sensitive high birefringent fiber

based SIs are an appropriate option for measuring strain acting on a composite material over the length of the sensing fiber.

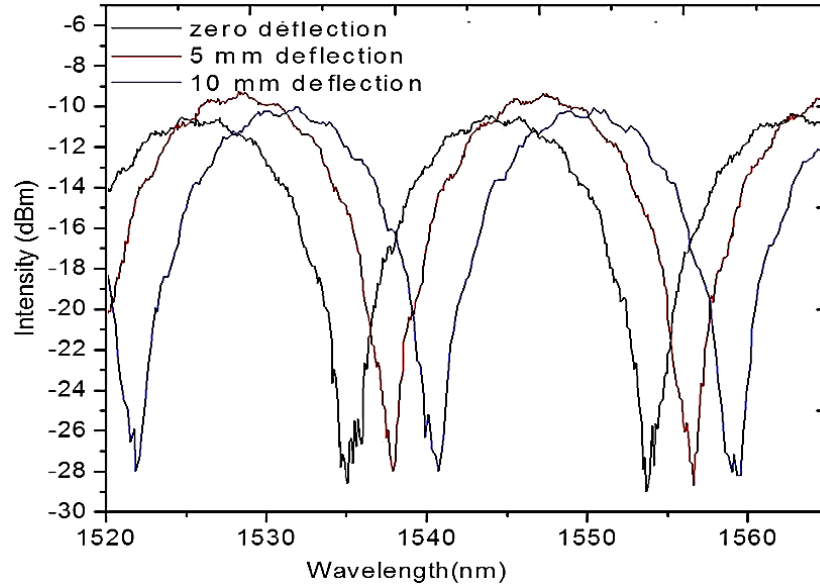


Figure 2.12. Responses of the HB-PM-PCF based SI sensor embedded in the composite material sample during deflections based on three point bending test [2.56].

C. Optical fiber polarimetric sensors for composite materials

The polarization properties of light propagating through an optical can be affected by stress, strain, pressure and temperature acting on a measuring fiber and in a fiber polarimetric sensor, the polarization change is detected to retrieve the sensing parameter [2.71, 2.72]. A symmetric deformation effect or temperature variation in a single-mode fiber influences the propagation constant (β) for every mode because of the changes in the fiber length (L) and the refractive indices of the core and the cladding [2.39, 2.73]. Under the influence of a longitudinal strain (ϵ) and at a constant temperature, for polarimetric sensors the change in the phase difference can be written as [2.73],

$$\delta(\Delta\Phi) = \frac{\partial(\Delta\beta)}{\partial\epsilon/T} \delta L \quad 2.7$$

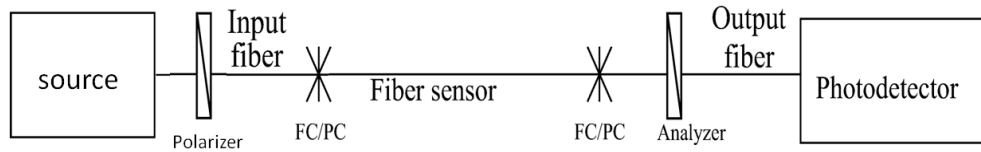
Fiber optic polarimetric sensors can be realized by different types of PM fibers

such as Panda fiber, bow-tie type fiber, side-hole fibers and PM-HB MOF fibers. Fiber optic polarimetric sensors can be embedded in composite materials to measure the average strain/temperature over the sensor length [2.39,2.73]. It is possible to vary the strain/temperature sensitivity of fiber optic polarimetric sensors by selecting a PM fiber type with appropriate birefringence and length [2.74, 2.75].

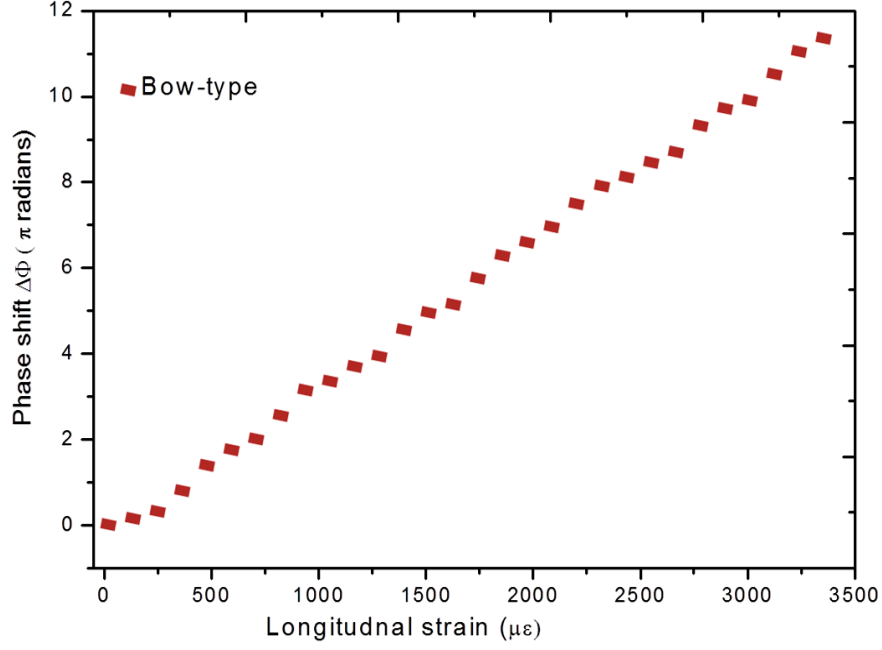
For fiber optic polarimetric sensors the phase difference between the two orthogonal polarizations, can be extracted using an experimental setup consisting of a tunable laser source and a polarimeter/polarization control system [2.76]. Fiber optic polarimetric sensors can be also operated in intensity domain with the help of a polarizer-analyzer arrangement and the experimental setup for operation in intensity domain is shown in Figure 2.13(a). For polarimetric sensors the change in the output intensity at a wavelength λ due to externally applied longitudinal strain can be described by the formula [2.73],

$$I_s(\lambda) = \frac{I_0}{2} [1 + \cos(\Delta\Phi)] \quad 2.8$$

where, I_0 is the input initial intensity.



(a)



(b)

Figure 2.13. (a) Experimental setup for measurements with fiber optic polarimetric sensors in intensity domain [2.66]; and (b) Change of the polarization of fiber optic polarimetric sensors as a function of strain applied to a composite sample [2.76].

For such polarimetric sensors operating in the intensity domain periodic variations in the output intensity can be associated with applied strain or temperature [2.77]. It is reported that low strain sensitive polarimetric sensors such as HB-PM-PCF polarimetric sensor guarantee a linear response for a wide range of applied strain values [2.77]. The change of the polarization of fiber optic polarimetric sensors based on bow tie type fiber as a function of strain applied to a composite sample is as shown in Figure 2.13(b). Moreover, the insignificant temperature sensitivity of HB-PM-PCFs make them the most appropriate candidates for composite strain measurements [2.77, 2.78]. However, for local strain/temperature measurements of large composite structures polarimetric sensors cannot be employed as the polarimetric sensors measures average strain over the length of the sensing fiber.

D. Fiber Optic Micro Bend Sensors

Fiber optic micro bend sensors are capable of measuring parameters such as pressure, acceleration, displacement, temperature and strain [2.40, 2.79, 2.80]. Microbending is typically caused by defects and small geometrical perturbations in the optical fiber. The curvature of radius of microbends is in the order of micrometers. Microbends cause coupling between propagating and radiation modes [2.40] which results in the loss of intensity of the light propagating through the fiber. Figure 14 shows the concept underpinning a typical microbending sensor. Fiber optic micro bend sensor is typically formed by passing the fiber between two sets of corrugations as shown in Figure 2.14.

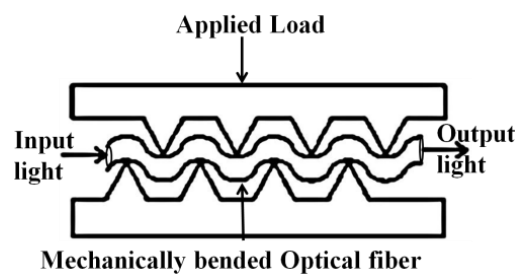
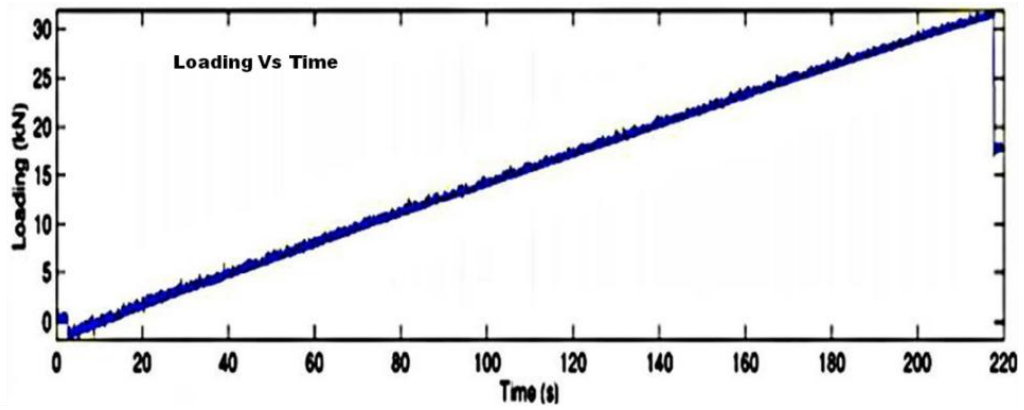
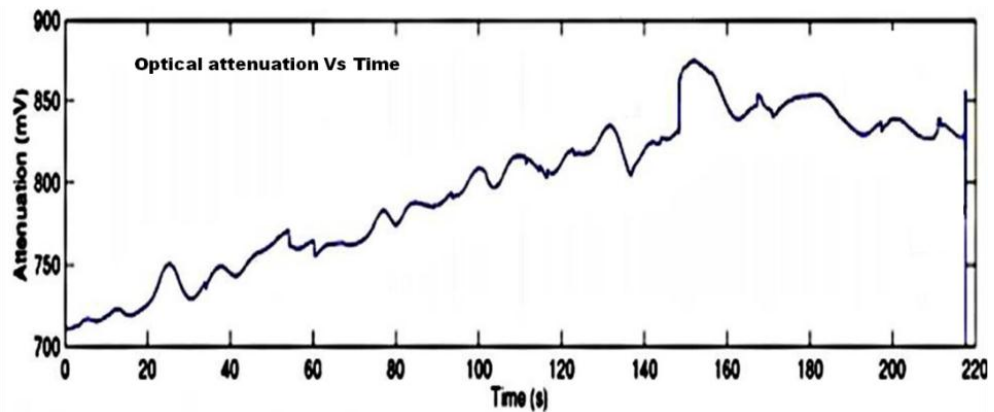


Figure 2.14. Micro bend sensor concept [2.40].

Delamination or cracking in the layers of a composite produces corrugations in that cause microbending in an embedded optical fiber. Specifically, during delamination of a multilaminated composite structure the stress fields in a damaged layer and an undamaged layer are different. The higher stress level in the damaged layer causes the optical fiber to micro-bend in the material resulting in the attenuation of the output, and therefore this method can be used to measure the strain field due to delamination in a composite material [2.40]. As an example the temporal profile of loading in the composite material and the corresponding optical signal attenuation are shown in Figure 2.15.



(a)



(b)

Figure 2.15. The temporal profiles corresponding to (a) loading and (b) optical signal attenuation [2.40].

Another method of damage detection using the fiber optic micro bend sensor utilizes mechanical/acoustic waves propagating in the composite material [2.80, 2.81]. When a mechanical wave hits an optical fiber, it bends the fiber locally and so some coupling between propagating and radiation modes may appear. As a result, temporal features in the measured optical signal can be related to stress waves released by delamination, matrix cracking or reinforcing fibre rupture [2.40]. The main disadvantage of micro bend sensors is their low accuracy which makes them unsuitable for precise stress measurements.

E. Distributed fiber optic sensors.

Distributed fiber-optic sensors (DFS) are capable of providing a continuous measurand profile over the length of the optical fiber and thus are very promising for strain/temperature measurements in large structures such as bridges, buildings and pipelines [2.41, 2.82, and 2.83]. However, given the nature of composite structures, the length is normally limited to 80 m or less with a strain or temperature requirement of at least 1 °C or 20 $\mu\epsilon$ with a few centimeters resolution. DFSs are categorized into several types based on the sensing technology employed and the related physical effect underpinning the operating principle: (i) optical time-domain reflectometry (OTDR) and optical frequency-domain reflectometry (OFDR), both based on Rayleigh scattering; (ii) Raman optical time-domain reflectometry (ROTDR) and Raman optical frequency-domain reflectometry (ROFDR), both based on Raman scattering; and (iii) Brillouin optical time-domain reflectometry (BOTDR) and Brillouin optical frequency-domain reflectometry (BOFDR), both based on Brillouin scattering [2.84–2.86].

OTDR and OFDR are the first generation of fiber optic distributed sensors, based on the use of Rayleigh scattering to reflect the attenuation profiles of long-range optical fiber links [2.83, 2.84]. An example of strain measurement by OFDR technique for various loading conditions is shown in Figure 2.16.

An optical pulse is launched into an optical fiber and the power of the Rayleigh backscattered light is detected using a photo detector as the light pulse propagates along the fiber link [2.85]. The frequency based Brillouin method can provide rapid strain/temperature sensing [2.87, 2.88]. BOFDR can be employed to measure strain/temperature variations as small as 1 °C or 20 $\mu\epsilon$ with few centimeters of resolution [2.88–2.90]. For BOFDR based long distance measurements single-

mode fibers are used [2.89, 2.91]. ROTDR is an appropriate candidate for temperature measurements in composites since the intensity ratio between anti-Stokes components and Stokes components of the ROTDR response provides information about temperature [2.88]. ROTDR can be employed to measure temperature variations as small as 0.1 °C with a few meters of resolution [2.87, 2.88]. Multimode fibers are commonly used for ROTDR based short distance measurements [2.89].

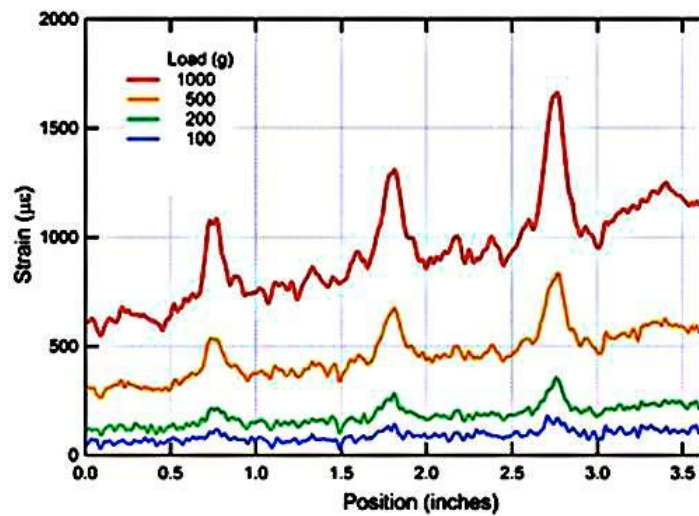


Figure 2.16. Strain measured by the optical fiber bonded to a composite sample for various loading conditions (data redrawn from *Luna Engineering Note EN-FY1317*).

In the case of composite strain/temperature measurements from the above mentioned categories of DFS, an appropriate sensing technology can be selected based on the application and its requirements, specifically BOFDR is more suitable for strain measurements and ROTDR is more suitable for temperature measurements in a composite material [2.88, 2.89, and 2.91]. Other than the technologies mentioned above, quasi-distributed optical fiber sensors can be realized by multiplexing a number of grating-based sensors [2.85].

F. Hybrid sensing approaches for simultaneous strain and temperature measurements in composite materials

In most practical applications of composite materials, the key requirement is to measure more than one parameter. For example, for SHM applications in composite parts such as helicopter rotor blades, wind turbines and aircraft structures a simultaneous monitoring of temperature and strain is frequently necessary. Several OFSs such as FBGs, PM polarimetric sensors, etc are capable of measuring strain and temperature, but there is always an issue of accurate discrimination between these two influencing factors [2.35, 2.37]. One of the simplest and promising methods for simultaneous measurement of strain and temperature in composite parts is the hybrid fiber optic sensing approach; in this two or more OFS operate in a combined manner to eliminate the disadvantages of individual OFSs providing accurate and independent strain/temperature information [2.92]. Many researchers have investigated different hybrid sensing approaches for simultaneous strain and temperature measurements such as using a combination of FBG sensors with various type sensors such as long period gratings (LPG) [2.55, 2.92], Fabry-Perot interferometer sensors [2.54], PCF modal interferometers [2.93], and fiber loop mirrors using a small core micro-structured fiber [2.94]. Sensors based on gratings written in micro structured fibers and standard optical fibers have also been reported for discrimination between strain and temperature [2.95]. Previously reported a hybrid approach which involves an FBG sensor and a HB-PM-PCF polarimetric sensor for simultaneous measurement of strain and temperature [2.96] of composite materials. In the context of composite structures, the temperature sensitivity of a OFS can be influenced by the thermal strain of the composite material [2.16]. Sensors based on stripped HB-PM-PCF

based polarimetric fibers have been reported for thermal strain and thermal expansion measurements in composite materials [2.15]. A hybrid optical fiber sensor embedded in a composite material which is capable of discriminating between strain, temperature and thermal strain has great potential for future OFS based SHM applications.

In the previous sections have detailed the major types of OFS used for strain and temperature measurements in composite materials. Appropriate sensor selection for any application is only possible by identifying the particular features of all OFS. The OFS types discussed in this review are compared in Table 2.1.

Table 2.1. Comparison of OFSs.

OFS Technology	Advantages	Disadvantages	Remarks	Main Applications
Standard FBGs	Most accepted technology,		Typical strain sensitivity	Strain, temperature,
	allows for point measurements of strain and temperature	Temperature and strain cross sensitivity issues	$\sim 1.2 \text{ pm}/\mu\epsilon$ and typical temperature sensitivity $\sim 11.6 \text{ pm}/^\circ\text{C}$	vibration, cure process, localized damage, <i>etc.</i>
FBGs written in MOF		FBGs written in bow-tie fibers have temperature		
	Can discriminate both axial and transverse strain components of composite material with insignificant temperature sensitivity	and strain cross sensitivity. But FBGs written in MOF have lower strain sensitivity compared to FBGs written in bow-tie fibers.	The cross-sensitivity issue can be resolved by using FBGs written in low temperature sensitive MOFs	Multi directional strain sensing, localized damage, <i>etc.</i>
Interferometric fiber optic sensors	Possesses higher temperature and strain sensitivities and are flexible in terms of size	Temperature and strain cross sensitivity issue, brittle sensor	The cross-sensitivity issue can be resolved by using low temperature sensitive MOFs	Strain, temperature, vibration, cure process, localized damage, <i>etc.</i>

Polarimetric sensors	Sensitivity can be tuned by choosing different optical fiber types and sensor lengths	Difficult to measure strain/temperature at localized points, provide information averaged over the sensor's length	The cross-sensitivity issue can be resolved by using low temperature sensitive HB-PM-PCF	Strain, temperature, vibration, cure process, <i>etc.</i>
Fiber optic micro bend sensors	Can measure continuous strain profile in a composite material using single optical fiber	Low accuracy	Output signal is strongly attenuated by any mechanical wave propagating in the composite material	Delamination and damage detection
Distributed sensors	Can measure continuous strain/temperature profile in a composite material using single optical fiber	For better resolution require the use of spectral demodulation techniques that are expensive and bulky	Appropriate sensing technology can be selected based on the application and its requirements	Strain, temperature, delamination, damage detection
Hybrid sensors	Two or more OFS operate in a combined manner to eliminate the disadvantages of individual OFSs providing accurate and independent strain/temperature information	Since two or more sensors are employed complicated interrogation methods are needed	Capable of discriminating beten strain, temperature and thermal strain	Strain, thermal strain, temperature, vibration, cure process, damage point, <i>etc.</i>

2.1.6 Recent Trends, Issues and Future Challenges of the OFS

Technology

Embedding OFS inside composite materials is a minimally invasive technique; but for industrial applications still there exist a few issues which are under investigation and in this section discuss those challenging issues.

One of the challenges with composite structures embedded with OFS is the provision of a reliable method for connecting the interrogation systems to the

sensor [2.97, 2.98]. Custom designed connectors with ingress/egress optical fiber ends are promising technique, and one example of such a connector is shown in Figure 2.17. However, such egress optical fibers with connectors may cause the composite to become brittle at the edges of the structure [2.99]. Also edge trimming of the composite after the connector installation is impossible. Free space coupling is more promising than surface and edge mounted connectors [2.100]. For example, in [2.101] a novel method of free-space passive coupling of light into FBG sensors is reported which consists of an angled 45° mirror integrated directly into the fiber. Also to resolve the connection issues associated with ingress/egress optical fiber ends of L-shaped composite a reconnection technique is established by situating the optical fiber connector on a 6-axis automatic stage together with the assistance of CCD camera [2.102].

The second issue is the structural damage to the composite material due to the fact that optical fibers have larger diameter compared to reinforcement fibers. As a solution researchers are considering new optical fibers with a reduced diameter and an optimized coating. One example of such fibers is a thinner optical fiber with 80 micron diameter known as Draw Tower Grating (DTG) fiber, which should be less invasive when embedded within a laminate composite structure [2.103].



Figure 2.17. Egress optical fiber with connector.

Another issue related to embedding of OFS in a composite part in weight or space sensitive applications is the large size of conventional OFS interrogators which could present difficulties for sensing of composite parts that for example are in constant motion, such as helicopter rotor blades and wind turbine structures [2.104]. To an extent this issue can be resolved by adopting miniaturized interrogation modules based on photonic integrated circuits (PIC) or flexible polymer waveguides [2.105, 2.106]. Such surface attachable flexible interrogators allow for integration of photo detector arrays with wireless communication technology and thus have strong potential in smart sensing of composite parts in motion.

Finally, it must be recognised the OFS embedding procedure is often a labor intensive task. Therefore, ideally it requires a reliable automated optical fiber placement system that matches well with the existing industrial composite production processes. Several composite manufactures, such as for example Airborne, have introduced automated fiber placement systems that provide control over embedding depth, pre-strain, position and alignment. Such an all automated fiber placement system is shown in Figure 2.18. The biggest challenge in using most of automated OFS embedding systems, is that it is difficult to ensure an adequate repeatability of the OFS placement. In addition, during such an automated fabrication process the safety of delicate areas of OFS (such as grating written area of FBG, spliced and buffer coating removed areas of sensing optical fiber, *etc.*) and control over the alignment of specialized optical fibers such as micro structured optical fibers are not well assured. Thus, an automated fiber placement system together with an X-ray based micro controlled tomography could be a suitable solution for quality control of the embedded OFS and a realistic option for appropriate alignment of optical fibers for future smart sensing applications.

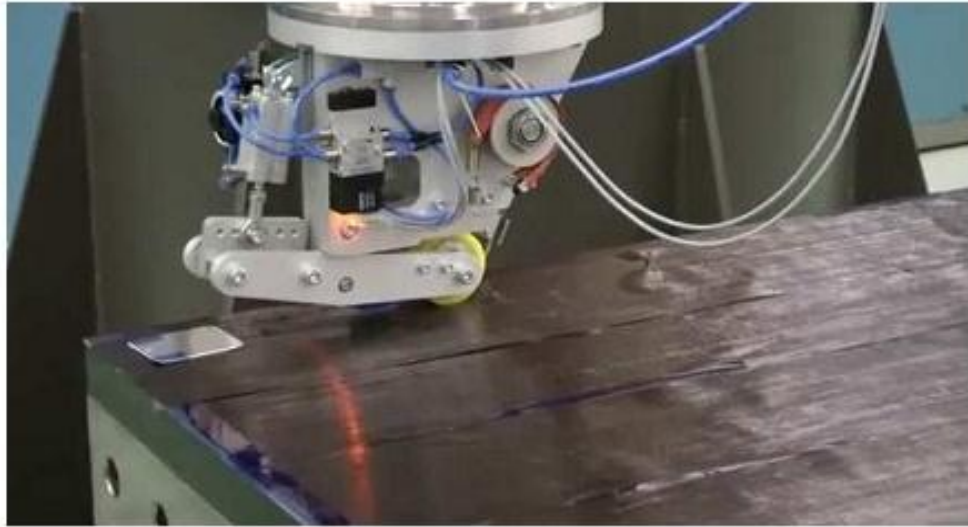


Figure 2.18. Automated optical fiber placement system (from “*Airborne: the future in composites*” website).

2.1.7. Conclusion

This chapter presents a comprehensive overview of the OFS sensors used for strain/temperature sensing of composite materials. This review article provides essential information regarding many aspects, including different types of composite materials, properties, and their performance, the relevance of OFS for composite material sensing applications, future challenges of embedded OFS and recent trends. Embedded OFS have proved themselves useful to smart sensing applications of composite materials in wide range of areas that include aerospace, structural, civil and the sports industry. Extensive research and development continues worldwide and will inevitably make this technology more commercially viable, more standardised and more beneficial to society in general.

2.1.8. References

- 2.1. D. P. Garg, M. A. Zikry, and G. L. Anderson. "Current and potential future research activities in adaptive structures: an ARO perspective." *Smart materials and structures* 10.4: 610, 2001.
- 2.2. D. Balageas. "Introduction to structural health monitoring." *Structural Health Monitoring*; ISTE: London, UK, pp. 16–43, 2006.
- 2.3. J. Cai, L. Qiu, S. Yuan, L. Shi, P. Liu, Liang, D. "Structural Health Monitoring for Composite Materials." *Composites and Their Applications*: InTech: Rijeka, Croatia, 2012.
- 2.4. YK Zhu, GY Tian, RS Lu, H Zhang, "A review of optical NDT technologies." *Sensors* 2011, 11(8), 7773-7798, 2011.
- 2.5. XE Gros. "Current and Future Trends in Non-Destructive testing of Composite Materials." *Ann. Chim. Sci. Mater.*, 25(7), 539–544, 2000.
- 2.6. X. W. Ye, Y. H. Su, J. P. Han. "Structural health monitoring of civil infrastructure using optical fiber sensing technology: A comprehensive review." *The Sci. World J.* Volume 2014, Article ID 652329, 2014.
- 2.7. A. Méndez, A. Csipkes, "Overview of fiber optic sensors for NDT applications." *Nondestructive Testing of Materials and Structures*, Springer Netherlands: Dordrecht, The Netherlands, pp. 179–184, 2013.
- 2.8. D.D.L. Chung. "Composite Materials: Science and Applications", 2nd ed., Springer-Verlag London: London, UK, 2010.
- 2.9. D. Hull, T.W. Clyne. "An Introduction to Composite Materials." Cambridge University Press: Cambridge, UK, 1996.

- 2.10. A.K. Kaw. "Mechanics of Composite Materials." CRC Press: Boca Raton, FL, USA, 2005.
- 2.11. A.R. Bunsell, R. Jacques. "Fundamentals of Fibre Reinforced Composite Materials." CRC Press: Boca Raton, FL, USA, 2005.
- 2.12. G. Fernando. "Sensors and Composites: Requirements, Opportunities and Complexity." Presented at the 1st International Workshop on Embedded Optical Sensors for Composite Materials, Ghent, Belgium, 7–8 October, 2013.
- 2.13. M. Kaufmann. "Composite Materials: State-of-the-art and Future Challenges." Presented at the 1st International Workshop on Embedded Optical Sensors for Composite Materials, Ghent, Belgium, 7–8 October, 2013.
- 2.14. W. Elmar, J. Bernhard. "Composites Market Report 2014." Available online: http://www.eucia.eu/userfiles/files/20141008_market_report_grpcrp.pdf (accessed on 13 January 2016)
- 2.15. M. Ramakrishnan, G. Rajan, Y. Semenova, A. Boczkowska, T. Wolinski, A. Domański, G. Farrell. "Measurement of thermal elongation induced strain of a composite material using a polarization maintaining photonic crystal fiber sensor." *Sens. Actuators A Phys.*, 190, 44–51, 2013.
- 2.16. M. Ramakrishnan, G. Rajan, Y. Semenova, P. Lesiak, A. Domanski, T. Wolinski, A. Boczkowska and G. Farrell. "The influence of thermal expansion of a composite material on embedded polarimetric sensors." *Smart Mater. Struct.* 20(12), 2011.

- 2.17. P. Lesiak, M. Szeląg, D. Budaszewski, R. Plaga, K. Mileńko, G. Rajan, Y. Semenova, G. Farrell, A. Boczkowska, A. Domański, T. Woliński. "Influence of lamination process on optical fiber sensors embedded in composite material." *Measurement*, 45, 2275–2280, 2012.
- 2.18. J. Degrieck, W. D. Waele, P. Verleysen. "Monitoring of fibre reinforced composites with embedded optical fibre Bragg sensors, with application to filament wound pressure vessels." *NDT&E Int.*, 34, 289–296, 2001.
- 2.19. H. Hernández-Moreno, F. Collombet, B. Douchin, D. Choqueuse, P. Davies, J.G. Velázquez. "Entire life time monitoring of filament wound composite cylinders using Bragg grating sensors: I. Adapted tooling and instrumented specimen." *Appl. Compos. Mater.*, 16, 173–182, 2009.
- 2.20. C. Keulen, B. Rocha, M. Yildiz, A. Suleman. "Embedded fiber optic sensors for monitoring processing, quality and structural health of resin transfer molded components." *J. Phys. Conf. Ser.*, 305, 2011.
- 2.21. G. Bektaş, T. Boz, C.J. Keulen, M. Yıldız, C. Öztürk, Y.Z.; Menciloğlu, A.Suleman. "Fiber Bragg grating and etched optic sensors for flow and cure monitoring of resin transfer molded composite structures." In *Proceedings of the 18th International Conference on Composite Materials (ICCM18)*, Jeju Island, Korea, 21–26 August 2011.
- 2.22. F. Tuccillo, V. Antonucci, A.M. Calabro, M. Giordano, L.Nicolais. "Practical and theoretic analysis of resin flow in vacuum assisted resin transfer molding processes." *Macromolecular Symposia; WILEY-VCH Verlag: Campania, Italy, Volume 228*, pp. 201–218. 2005.

- 2.23. S. Yuan, R. Huang, Y. Rao, "Internal strain measurement in 3D braided composites using co-braided optical fiber sensors." *J. Mater. Sci. Technol.* 20, 199–202, 2004.
- 2.24. V. Antonucci, M. Esposito, M. R. Ricciardi, M. Raffone, M. Zarrelli, M. Giordano, "Permeability characterization of stitched carbon fiber preforms by fiber optic sensors." *Express Polym. Lett.* 5, 1075–1084, 2011.
- 2.25. D. W. Jensen, J. Pascual. "Degradation of graphite/bismaleimide laminates with multiple embedded fiber-optic sensors." *Proc. SPIE*, 1370, 1990.
- 2.26. D.C. Lee, J.J.;Lee, Yun, S.J. The mechanical characteristics of smart composite structures with embedded optical fiber sensors. *Compos. Struct.* 32, 39–50, 1995.
- 2.27. J. Güemes, J.S. Perez. "Fiber Optics Sensors." *New Trends in Structural Health Monitoring*, Springer: Vienna, Austria, pp. 265–316, 2013.
- 2.28. G. Luycks, E. Voet, N. Lammens, J. Degrieck. "Strain Measurements of Composite Laminates with Embedded Fibre Bragg Gratings: Criticism and Opportunities for Research." *Sensors*, 11(1), 384–408, 2011.
- 2.29. W. Błazejewski, P. Gąsior, J. Kaleta. "Application of Optical Fiber Sensors to Measuring the Mechanical Properties of Composite Materials and Structures." *Advances in Composite Materials, Ecodesign and Analysis*, InTech: Rijeka, Croatia, 2011.
- 2.30. L. Emmanwori, K.N. Shivakumar. "Structural performance of composite laminates with embedded fiber optic sensor under tension and compression

- loads.” In Proceedings of the 43rd Annual Conference of American Institute of Aeronautics and Astronautics, Denver, CO, USA, 22-25 April 2002.
- 2.31. C.C. Ciang, R.L. Jung, J.B. Hyung. “Structural health monitoring for a wind turbine system: A review of damage detection methods.” *Meas. Sci. Technol.*, 19(12), 2008.
 - 2.32. G. Zhou, L.M.Sim. “Damage detection and assessment in fibre-reinforced composite structures with embedded fibre optic sensors-review.” *Smart Mater. Struct.*, 11(6),2002.
 - 2.33. R. D. Sante. “Fibre Optic Sensors for Structural Health Monitoring of Aircraft Composite Structures: Recent Advances and Applications.” *Sensors*, 15, 18666–18713, 2015.
 - 2.34. S. Minakuchi. “From Material Characterization to Product Quality Control: Applicability of Fibre-Optic Sensors to Composites Process Monitoring.” Presented at the 1st International Workshop on Embedded Optical Sensors for Composite Materials, Ghent, Belgium, 7–8 October 2013.
 - 2.35. W. Du, X.M. Tao, H.Y. Tam, C. L. Choy. “Fundamentals and applications of optical fiber Bragg grating sensors to textile structural composites.” *Compos. Struct.*, 42, 217–229, 1998.
 - 2.36. R. D. Sante, L. Donati, E. Troiani, P. Proli. “Reliability and accuracy of embedded fiber Bragg grating sensors for strain monitoring in advanced composite structures.” *Met. Mater. Int.*, 20, 537–543, 2014.

- 2.37. K.T. Lau. "Structural health monitoring for smart composites using embedded FBG sensor technology." *Mater. Sci. Technol.*, 30, 1642–1654, 2014.
- 2.38. Y.J. Rao. "Recent progress in fiber-optic extrinsic Fabry-Perot interferometric sensors." *Opt. Fiber Technol.*, 12, 227–237, 2006.
- 2.39. V. M. Murukeshan, P.Y. Chan, L.S.Ong, A. Asundi. "On-line health monitoring of smart composite structures using fiber polarimetric sensor." *Smart Mater. Struct.*, 8(5), 1999.
- 2.40. L. Rippert, P. Jean-Michel, W. Martine, V. H. Sabine. "Fibre optic sensor for continuous health monitoring in CFRP composite materials." *Proc. SPIE*, 4693, 2002.
- 2.41. H. Murayama, K. Kazuro, N. Hiroshi, S. Akiyoshi, U. Kiyoshi. "Application of fiber-optic distributed sensors to health monitoring for full-scale composite structures." *J. Intell. Mater. Syst. Struct.*, 14, 3–13, 2003.
- 2.42. J. M. L. Higuera, L. R. Cobo, A. Q. Incera, A. Cobo, "Fiber optic sensors in structural health monitoring." *J. Lightwave Technol.*, 29, 587–608, 2011.
- 2.43. F.F. Gerard. "Fibre optic sensor systems for monitoring composite structures." In *Proceedings of the RP Asia 2005 Conference*, Bangkok, Thailand, 25–26 August 2005.
- 2.44. R. Montanini, L. d'Acquisto. "Simultaneous measurement of temperature and strain in glass fiber/epoxy composites by embedded fiber optic sensors: I. Cure monitoring." *Smart Mater. Struct.*, 16(5), 2007.

- 2.45. B. Glisic, D. Inaudi. "Fibre Optic Methods for Structural Health Monitoring". 1st ed., John Wiley & Sons, Ltd.: Southern Gate, Chichester, UK, 2007.
- 2.46. K.O. Hill, G. Meltz. "Fiber Bragg grating technology fundamentals and overview." J. Lightwave Technol., 15, 1263–1276, 1997.
- 2.47. K. Raman, "Fiber Bragg Gratings." Academic Press: Cambridge, MA, USA, 1999.
- 2.48. S. Yashiro, T. Okabe, N. Toyama, N. Takeda. "Monitoring damage in holed laminates using embedded chirped FBG sensors." Int. J. Solids Struct., 44, 603–613, 2007.
- 2.49. X. Dong, H. Zhang, B. Liu, Y. Miao, "Tilted fiber Bragg gratings: Principle and sensing applications." Photonic Sens., 1, 6–30, 2011.
- 2.50. Y. Zhao, L. Yanbiao. "Discrimination methods and demodulation techniques for fiber Bragg grating sensors." Opt. Lasers Eng., 41, 1–18, 2004.
- 2.51. M. G. Xu, J. L. Archambault, L. Reekie, J. P. Dakin. "Discrimination between strain and temperature effects using dual-wavelength fibre grating sensors." Electron. Lett., 30, 1085–1087, 1994.
- 2.52. S. W. James, M. L. Dockney, R. P. Tatam. "Simultaneous independent temperature and strain measurement using in-fibre Bragg grating sensors." Electron. Lett., 32, 1133–1134, 1996.

- 2.53. K. B. Samer, T. Sun, K. T. V Grattan. "Simultaneous measurement of temperature and strain with long period grating pairs using low resolution detection." *Sens. Actuators* 2008, 144, 83–89.
- 2.54. R. D. Oliveira, C. A. Ramos, A.T. Marques. "Health monitoring of composite structures by embedded FBG and interferometric Fabry-Perot sensors." *Comput. Struct.*, 86, 340–346, 2008.
- 2.55. B.O. Guan, H.Y. Tam, X.M. Tao, X.Y. Dong. "Simultaneous strain and temperature measurement using a superstructure fiber Bragg grating." *IEEE Photonics Technol. Lett.*, 12, 675–677, 2000.
- 2.56. G. Rajan, M. Ramakrishnan, P. Lesiak, Y. Semenova, T. Wolinski, A. Boczkowska, G. Farrell, "Composite materials with embedded photonic crystal fiber interferometric sensors." *Sens. Actuators A Phys.* 182, 57–67, 2012.
- 2.57. M. Kreuzer. "Strain Measurement with Fiber Bragg Grating Sensors.", HBM: Darmstadt, Germany, 2006.
- 2.58. C. Sonnenfeld, S. Sulejmani, T. Geernaert, S. Eve, N. Lammens, G. Luyckx, V. Eli, H. Thienpont. "Microstructured optical fiber sensors embedded in a laminate composite for smart material applications." *Sensors*, 11(3), 2566–2579, 2011.
- 2.59. J. A. Guemes, J. M. Menendez. "Response of Bragg grating fiber-optic sensors when embedded in composite laminates." *Compos. Sci. Technol.*, 62, 959–966, 2002.

- 2.60. G. Luyckx, E. Voet, T. Geernaert, K. Chah, T. Nasilowski, W. D. Waele, et al. "Response of FBGs in microstructured and bow tie fibers embedded in laminated composite." *IEEE Photonics Technol. Lett.*, 21, 1290–1292, 2009.
- 2.61. A. I. Azmi, S. Deep, S. Wenjuan, C. John, D. P. Gang. "Performance enhancement of vibration sensing employing multiple phase-shifted fiber Bragg grating." *J. Lightwave Technol.*, 29, 3453–3460, 2011.
- 2.62. D. J Webb. "Polymer optical fibre Bragg gratings." *OSA Tech. Dig.*, 2012.
- 2.63. K. Kalli, H. L. Dobb, D. J. Webb, K. Carroll, C. Themistos, M. Komodromos, G. D Peng, Q. Fang, I. W Boyd. "Development of an electrically tuneable Bragg grating filter in polymer optical fibre operating at 1.55 μm ." *Meas. Sci. Technol.*, 17, 3155–3164, 2007.
- 2.64. W. Zhang, D. J. Webb, G. D. Peng. "Investigation in to time response of polymer fibre Bragg grating based humidity sensors." *J. Lightwave Technol.*, 30, 1090–1096, 2012.
- 2.65. G. Rajan, M. Ramakrishnan, Y. Semeonva, E. Ambikairajah, G. Farrell, G. D. Peng. "Experimental study and analysis of a polymer fibre Bragg grating embedded in a composite material." *J. Lightwave Technol.*, 32, 1726–1733, 2014.
- 2.66. B. H. Lee, Y. H. Kim, K. S. Park, J. B. Eom, M. J. Kim, B. S. Rho, H. Y. Choi. "Interferometric fiber optic sensors." *Sensors*, 12, 2467–2486, 2012.
- 2.67. E. Udd, W. B. Spillman. "Fiber Optic Sensors: An Introduction for Engineers and Scientists-." 2nd ed., John Wiley & Sons, Hoboken, NJ, USA, 2011.

- 2.68. T. Liu, M. Wu, Y. Rao, D. A. Jackson, G. F. Fernando. "A multiplexed optical fibre-based extrinsic Fabry-Perot sensor system for in-situ strain monitoring in composites." *Smart Mater. Struct.*, 7(4), 1998.
- 2.69. J. S. Leng, A. Asundi. "Structural health monitoring of smart composite materials by using EFPI and FBG sensors." *Sens. Actuators A Phys.*, 103, 330–340, 2003.
- 2.70. G. F. Fernando, T. Liu, P. Crosby, C. A. Doyle, D. B. Martin, B. Ralph, R. Badcock. "A multi-purpose optical fibre sensor design for fibre reinforced composite materials." *Meas. Sci. Technol.*, 8, 1997.
- 2.71. T. R. Woliński. "Polarimetric optical fibers and sensors." *Prog. Opt.*, 40, 1–75, 2000.
- 2.72. A.W. Domanski, R. W. Tomasz, J. B. Wojtek. "Polarimetric fiber optic sensors: State of the art and future." *Proc. SPIE*, 2341, 1994.
- 2.73. T. R. Woliński, P. Lesiak, A. W. Domański. "Polarimetric optical fiber sensors of a new generation for industrial applications." *Tech. Sci.*, 56, 125–132, 2008.
- 2.74. J. Ma, A. Asundi. "Structural health monitoring using a fiber optic polarimetric sensor and a fiber optic curvature sensor-static and dynamic test." *Smart Mater. Struct.*, 10, 181–188, 2001.
- 2.75. W. D. Hogg, D. T. Roderick. "Polarimetric fibre optic structural strain sensor characterisation." *Proc. SPIE*, 1170, 542–550, 1990.
- 2.76. A. W. Domański, P. Lesiak, M. Karolina, A. Boczkowska, D. Budaszewski, Ertman, S. Woliński, T. R. "Temperature-insensitive fiber

- optic deformation sensor embedded in composite material.” *Photonics Lett. Pol.*, 1, 2009.
- 2.77. D. H. Kim,; J. U Kang. “Analysis of temperature-dependent birefringence of a polarization-maintaining photonic crystal fiber.” *Opt. Eng.*, 46, 2007.
 - 2.78. V. M. Murukeshan, P. Y. Chan, L. S.Ong. A. Asundi. “Effects of different parameters on the performance of a fiber polarimetric sensor for smart structure applications.” *Sens. Actuators A Phys.*, 80, 249–255, 2000.
 - 2.79. J. W Berthold. “Historical review of microbend fiber-optic sensors.” *J. Lightwave Technol.*, 13, 1193–1199, 1995.
 - 2.80. N. K. Pandey, B.C.Yadav, “Embedded fibre optic microbend sensor for measurement of high pressure and crack detection.” *Sens. Actuators A Phys.* 128, 33–36, 2006.
 - 2.81. M. Wevers,; L. Rippert, J. M. Papy,; S. van Huffel, “Processing of transient signals from damage in composite materials monitored with embedded intensity-modulated fiber optic sensors.” *NDT&E Int*, 39, 229–235, 2006.
 - 2.82. S. Adachi. “Distributed optical fiber sensors and their applications.” In *Proceedings of the SICE Annual Conference, Tokyo, Japan, 20–22 August 2008*.
 - 2.83. M. Niklès. “Fibre optic distributed scattering sensing system: Perspectives and challenges for high performance applications.” *Proc. SPIE 2007*, 6619, doi:10.1117/12.738349.
 - 2.84. K.T.V. Grattan, T. Sun. “Fiber optic sensor technology: An overview.” *Sens. Actuators A Phys.*, 82, 40–61, 2000.

- 2.85. A. D. Kersey, A review of recent developments in fiber optic sensor technology. *Opt. Fiber Technol.*, 2, 291–317, 1996.
- 2.86. X. Bao, C. Liang. “Recent progress in Brillouin scattering based fiber sensors.” *Sensors*, 11, 4152–4187, 2011.
- 2.87. A. H. Hartog. “Progress in Distributed Fiber Optic Temperature Sensing.” *Environmental and Industrial Sensing. Proc. SPIE 4578*, 2002.
- 2.88. B. Culshaw. “Optical fiber sensor technologies: Opportunities and-perhaps-pitfalls.” *J. Lightwave Technol.*, 22, 2004.
- 2.89. F. Ravet, “Distributed Brillouin Sensor Application to Structural Failure Detection.” *New Developments in Sensing Technology for Structural Health Monitoring*; Springer Berlin Heidelberg: Berlin, Germany, pp. 93–136, 2011.
- 2.90. R. Bernini, A. Minardo, L. Zeni. “Distributed Sensing at centimetre-scale spatial resolution by BOFDA: Measurements and signal processing.” *IEEE Photonics J.*, 4, 48–56, 2012.
- 2.91. X. Zeng, X. Bao, Y. C. Chia, W. B. Theodore, W. B. Anthony, D. D. Michael, F. Graham, L. K. Alexander, V. G. Anastasis, “Strain measurement in a concrete beam by use of the Brillouin-scattering-based distributed fiber sensor with single-mode fibers embedded in glass fiber reinforced polymer rods and bonded to steel reinforcing bars.” *Appl. Opt.*, 41, 5105–5114, 2002.
- 2.92. H. J. Patrick, G. M. Williams, A. D. Kersey, J. R. Pedrazzani, “Hybrid fibre Bragg grating/long period grating sensor for strain/temperature discrimination.” *IEEE Photonics Technol. Lett.*, 8, 1223–1225, 1996.

- 2.93. Dong, B.; Hao, J.; Liaw, C.; Lin, B.; Tjin, S.C. “Simultaneous strain and temperature measurement using a compact photonic crystal fiber inter-modal interferometer and a fiber Bragg grating.” *Appl. Opt.*, 49, 6232–6235, 2010.
- 2.94. R.M. Andre, M.B. Marques, P. Roy, O. Frazao. “Fiber Loop Mirror Using a Small Core Micro-structured Fiber for Strain and Temperature Discrimination.” *IEEE Photonics Technol. Lett.*, 22, 1120–1122, 2010.
- 2.95. O. Frazão, J. P. Carvalho, L. A. Ferreira, F. M. Araújo, J. L. Santos. “Discrimination of strain and temperature using Bragg gratings in microstructured and standard optical fibres.” *Meas. Sci. Technol.*, 16, 2005.
- 2.96. G. Rajan, M. Ramakrishnan, Y. Semenova, M. Karolina, P. Lesiak, A. W. Domanski, T. R. Wolinski, G. Farrell. “A Photonic Crystal Fiber and Fiber Bragg Grating-Based Hybrid Fiber-Optic Sensor System.” *Sens. J.*, 12, 39–43, 2012.
- 2.97. H. K. Kang, J. W. Park, C. Y. Ryu, C. S. Hong, C. G. Kim. “Development of fibre optic ingress/egress methods for smart composite structures.” *Smart Mater. Struct.*, 9(2), 2000.
- 2.98. A. K. Green, M. Zaidman, E. Shafir, M. Tur, S. Gali. “Infrastructure development for incorporating fibre-optic sensors in composite materials.” *Smart Mater. Struct.*, 9(3), 2000.
- 2.99. W.R. Simon, William, R.P. Apparatus for Ingress and Egress of Fiber Optic Sensor Leads from the Surface of Composite Parts and a Method for the Manufacture Thereof. U.S. Patent 6,173,090, 9 January 2001.

- 2.100. D. Kinet, P. Mégret, K. W. Goossen, L. Qiu, D. Heider, C. Caucheteur. “Fiber Bragg Grating Sensors toward Structural Health Monitoring in Composite Materials: Challenges and Solutions.” *Sensors* 14, 7394–7419, 2014.
- 2.101. L. Qiu, K. W. Goossen, D. Heider, E. D. Wetzel. “Nonpigtail optical coupling to embedded fiber Bragg grating sensors.” *Opt. Eng.*, 49, 2010.
- 2.102. S. Minakuchi, T. Umehara, K. Takagaki, Y. Ito, N. Takeda. “Life cycle monitoring and advanced quality assurance of L-shaped composite corner part using embedded fiber-optic sensor.” *Compos. Part A Appl. Sci. Manuf.* 48, 153–161, 2013.
- 2.103. C. Chojetzki, M. Rothhardt, J. Ommer, S. Unger, K. Schuster, H. R. Mueller. “High-reflectivity draw-tower fiber Bragg gratings—Arrays and single gratings of type II.” *Opt. Eng.*, 44, 2005.
- 2.104. D. D. Palmer, R. W. Engelbart, C. M. Vaccaro. “Future Directions Relative to NDE of Composite Structures.” *SAE Tech. Pap.* 2004.
- 2.105. H. Van, G. L. Bram, B. Erwin, M. Jeroen, K. Sandeep, M. Oliver, J. W. David, S. Kate, V. D. Peter, V. S. Geert. “Ultra small integrated optical fiber sensing system.” *Sensors*, 12, 12052–12069, 2012.
- 2.106. J. Missinne, V. S. Geert, V. H. Bram, V. C. Kristof, V. G. Tim, D. Peter, V. Jan, V. D. Peter. “An array waveguide sensor for artificial optical skins.” *Proc. SPIE*, 7221 2009.

Chapter 3

Influence of thermal expansion of a composite material on embedded sensors

A primary aim of the research described in this chapter is to determine the effect of a composite material's thermal expansion on an embedded fiber polarimetric sensor. For this purpose, the fiber polarimetric sensor performance is investigated before and after embedding into the composite material, which would allow one to resolve the main sources of errors during strain measurements taken using an embedded hybrid sensor arrangement.

It is proven that the high birefringent micro structured fibers such as a stripped photonic crystal fiber has insignificant temperature sensitivity in free space and thus can be utilized as a temperature independent strain sensor. Different types of fiber optic sensors employed for strain and temperature measurements in composite material are presented in Chapter 2. The previously published investigations have not dealt with the issue of composite material thermal expansion dependency on the temperature sensitivity of polarimetric sensors. This chapter contributes to achieve this aim by comparing the temperature sensitivities of PM – PCF and Panda type fiber before and after embedding in a composite material. Also dependency of buffer coating of polarimetric sensor on composite material thermal expansion is also investigated by comparing the performance of embedded polarimetric sensors with and without the buffer coating. The outcomes of this piece of research enable one to select the most suitable one for composite

sensing application.

In the presented in this chapter, a composite material sample with polarimetric fiber sensors and FBG sensors embedded in two distinct layers of a multi-layer composite structure is fabricated and characterized. The polarimetric fiber sensors used in this study are based on Panda type polarization maintaining fiber and high-birefringent polarization maintaining photonic crystal fiber (HB-PM-PCF). This chapter shows that thermal expansion of the composite material is the main source of errors for embedded fiber sensor strain measurements. Thus, for practical strain sensing applications buffer coated HB-PM-PCF are more suitable for embedding in composite materials rather than buffer stripped HB-PM-PCF. This is because buffer coated fibers have low temperature sensitivity in free space compared to buffer stripped ones. Since the composite material's physical properties such as thermal expansion influence the embedded sensor performance, therefore the correct selection of the sensor type prior to embedding and their characterization after embedding in the composites are very important for accurate measurements. Also the sensitivity of a sensor depends on the placement of the optical fiber in the multilayered composite structure.

3.1 The influence of thermal expansion of a composite material on embedded polarimetric sensors⁶

Keywords: Photonic crystal fiber sensors, polarimetric sensors, smart structures, composite materials

⁶ M. Ramakrishnan, G. Rajan, Y. Semenova, P. Lesiak, A. Domanski, T. Wolinski, A. Boczkowska and G. Farrell, "Influence of thermal expansion of composite material on embedded polarimetric sensors", Smart Materials and Structures, Vol. 20, No. 12, pp. 125002, 2011.

Abstract: Some of the most critical issues of the influence of the thermal expansion of composite materials on embedded polarimetric sensors for measurements of strain and temperature are studied in this paper. A composite material sample with polarimetric fiber sensors embedded in two distinct layers of a multi-layer composite structure is fabricated and characterized. The polarimetric fiber sensors used in this study are based on panda type fiber and high-birefringent polarization maintaining photonic crystal fiber (HB-PM-PCF). The temperature sensitivities of polarimetric fiber sensors with acrylate buffer coated and buffer stripped polarization maintaining optical fibers are measured in free space and compared to those for embedded in the composite material. It is found that a polarimetric fiber sensor with an acrylate coating embedded in the composite material shows the same response as the one in free space while the coating-stripped fiber polarimetric sensor shows significant temperature sensitivity when embedded in the composite material. This is due to the stress-induced change in birefringence created by the thermal expansion of the composite material, while in the case of a buffer coated fiber, the effect is considerably reduced as the thermal stress is largely eliminated by the buffer coating. The results obtained in this study demonstrated that thermal expansion of the composite material is the main source of error in strain and temperature measurement using embedded polarimetric fiber sensors and that more accurate strain and temperature measurements can be obtained with buffer coated polarimetric fiber sensors.

3.1.1 Introduction

Composite material structures are widely used in the aerospace, marine, aviation and civil engineering industry, because of their superior properties [3.1, 3.2].

Continuous fibre-reinforced composite structures [3.3, 3.4] have attractive properties such as low density, high strength and high stiffness. Additionally, composite materials offer the potential to utilize embedded OFS which make them suitable candidates for smart materials for various applications in aerospace components and civil engineering structures. One or more OFS embedded in a composite material can be used to monitor the condition of the material during the manufacturing process or alternatively to monitor the structural health of the composite part over its operational lifetime and thereby can enhance the reliability and safety of many advanced structures. Embedding OFS in composite materials is possible because their size and weight are comparable to those of the composite fibre reinforcement fabric, allowing them to act as a form of “nervous system” for a composite fiber matrix structure. Integrated OFSs offer many advantages over traditional nondestructive evaluation techniques and surface bonded sensors, such as more reliable data about matrix cracks, point damage and thermo-mechanical behavior.

The fiber optic sensor technology most widely used for structural health monitoring is fiber Bragg grating sensing [3.5]. However, the cross-sensitivity between temperature and strain is a serious disadvantage for many real-life applications. Polarimetric fiber sensing [3.6] technology is a promising candidate for sensing in composites as it offers temperature independence. Additionally, given the availability of an extensive variety of polarization maintaining (PM) fibers and micro-structured highly-birefringent (HB) polarization maintaining fibers, such sensors possess a wide range of sensitivities and are suitable for sensing a variety of parameters, such as strain, temperature, displacement, humidity, etc independently. In comparison with previously reported methods for resolving the

strain and temperature cross-sensitivity issue with polarimetric sensors such as the fiber-optic differential heterodyne sensing scheme [3.7], and fiber-optic dual-technique sensor [3.8], the hybrid sensing approach described in [3.9] based on temperature insensitive HB-PM-PCF offers the advantage of simplicity.

For composite structures most research reports have concentrated on the use of FBGs to measure temperature and strain during the curing process and during structural tests. A few authors have reported interferometric [3.10] and polarimetric sensors [3.11] embedded in composite materials. What has not been well examined in the previous research studies is the impact of the characteristic properties of the composite materials and also the effect of the fiber buffer coating on the characteristics of the embedded fiber sensors. In this paper a detailed investigation is carried out on the influence of thermo-mechanical properties of composite materials on the embedded polarimetric fiber sensors in order to explore the most suitable approach to embedding such sensors in composites. The objective of this research is to ensure consistent and accurate temperature or strain measurements for applications such as wind turbine rotor blades and helicopter rotor blades which operate in varying atmospheric temperature conditions from -20 to 40 °C. The polarimetric fiber sensors used are based on PM-PCF and panda fibers with and without an acrylate fiber buffer coating.

3.1.2 Temperature sensitivity of polarimetric sensors

In a polarimetric sensor [3.12], symmetric deformation or variation in the refractive index induced by temperature influences the propagation constant for every mode because of the changes in the fiber length and the refractive indices of the core and the cladding. This in turn leads to changes in the phase difference between the two

orthogonal polarization states of the fundamental mode.

One can calculate the temperature sensitivity (S) of a HB fiber section with a length L as follows,

$$S = \frac{2\pi}{T_T \cdot L} \quad [\text{rad}/(^{\circ}\text{C} \cdot \text{m})] \quad 3.1$$

where T_T is the temperature change required to induce a 2π phase difference between the two polarizations of the fundamental mode.

The value of the parameter T_T multiplied by the length of the fiber L is a wavelength-dependent constant:

$$L \cdot T_T = \text{const}(\lambda) \quad 3.2$$

This dependence previously established for strain measurements using HB bow-tie fibers, enables a range of possible approaches to realizing polarimetric temperature and strain sensors by utilizing a variety of HB-PM and HB-PM-PCF fibers that are specifically tailored to particular applications.

The two types of polarization maintaining (PM) fibers used in this study are Panda fiber and HB-PM-PCF. In the case of the Panda fiber both temperature and strain lead to a phase difference between orthogonal polarizations of the fundamental mode LP_{01} , while in the case of HB-PM-PCF the phase difference arises only from strain as HB-PM-PCF fibers are proven to have a very low temperature sensitivity [3.13, 3.9] in free space, due to the pure silica structure of PCF.

3.1.3 Fabrication of composite samples with embedded optical fiber sensors

The fibre glass reinforced composite materials for this study are fabricated by the hand lay-up method, with woven glass fiber fabrics as reinforcement bound

together by resin. Samples were prepared with Synolite 1066-P-1, a pre-accelerated, thixotropic, unsaturated polyester resin manufactured by DSM Netherlands having a viscosity of 400 mPa.s, and with a specific gravity of 1.29 at 25 °C. Plain woven Fiberglass fabrics from JPS Composite Materials Corporation with a density of 280 g/m² were used. The dimension of each layer of the fabrics was 215 mm x 120 mm. The fabrication process is as follows: the mould surface is coated with a release agent of an anti-adhesive agent poly vinyl chloride, to prevent sticking the moulded part to the mould surface. The catalyst used is Luperox K1 manufactured by Arkema- France, which is added at a 100:1 resin: catalyst-mix ratio for the hardening process. The first glass fibre reinforcing fabric is placed on the mould and using a brush the fibre fabrics is impregnated with the resin. Then the second layer of the fibre reinforcing fabric is put in place after applying the resin and the process is repeated with subsequent stacked layers until the sample has eight layers of liquid resin and woven reinforcing glass fibre fabrics. The orientation of the fibre glass reinforcement was chosen to provide a 0-0 ply unidirectional configuration. The fabrication process is shown in Figure 3.1.

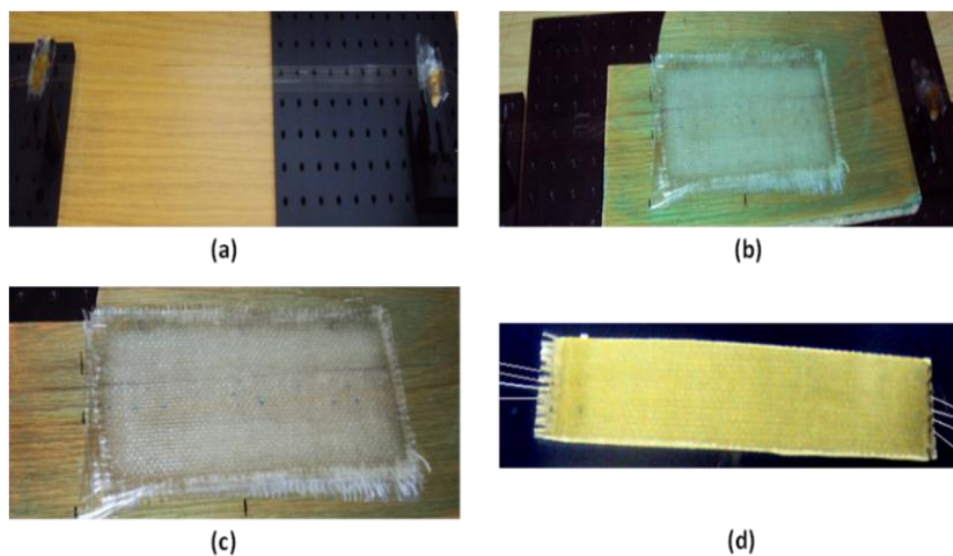


Figure 3.1. (a) Pre-strained optical fiber sensors (b) Fiber sensors at the layer 1 & layer 5 of the composite material (c) Composite material with embedded sensors just after fabrication

(d) Cured composite material sample trimmed to the desired shape

The fifth and the first layers are chosen as the locations for the optical fibers placed at a distance of 2 mm apart from each other. As had been previously observed, since the fiber coating may influence the operation of the sensor, the sensing optical fibers are embedded with and without fiber coating for comparison purposes. During the process of embedding and composite curing, a pre-strain is applied to the optical fibers positioned between the composite layers to make sure the fibers remain straight. The composite material sample is cured at 25⁰ C for about 20 hours. The composite material samples are uniformly cured and then post-cured [3.14] at a temperature of 60⁰ C for about 8 hours to eliminate the presence of any excess moisture or solvents. The sample is then removed from the mould surface. After curing, the samples are trimmed so they all have common dimensions of 215 mm x 40 mm and are 1.8 mm thick.

The polarimetric fiber sensors are realized based on two types of highly birefringent fiber: polarization maintaining Panda fiber (PM-1500-HP) and polarization maintaining photonic crystal fiber (PM-1500-01), having beat lengths of 5.0 mm and <4 mm respectively at an operating wavelength of 1500 nm. Both types of fiber have identical acrylate coatings with geometrical parameters as shown in Figures 3.2(a) and (b) respectively.

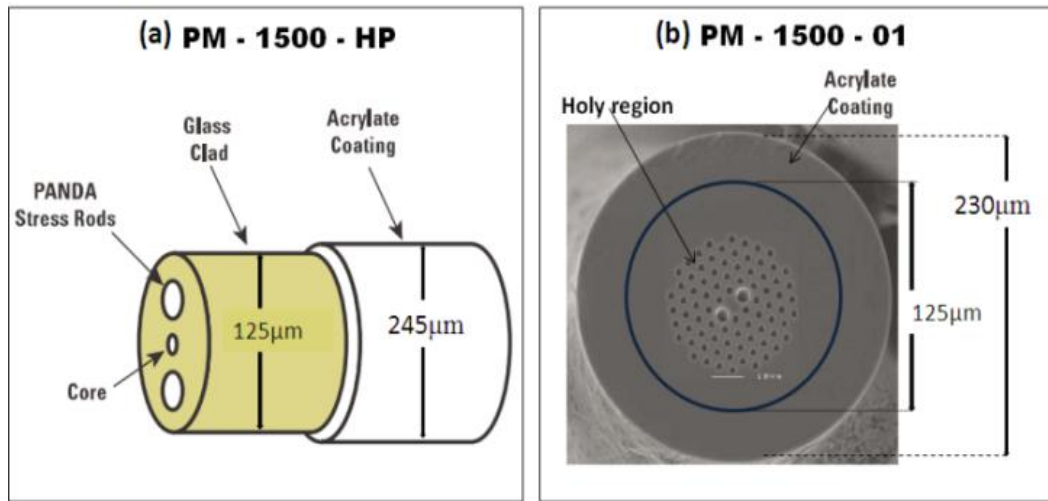


Figure 3.2. Cross sectional view of highly-birefringent fibers (a) Panda fiber (b) HB-PM-PCF

The embedded positions for the fiber optic sensors within the composite sample layers are shown in cross section in Figure 3.3. The HB-PM-PCF polarimetric sensor fiber without a coating is positioned at 17 mm from the left side of the sample. HB-PM-PCF with a coating is positioned 19 mm from the left side of the sample. The Panda polarimetric sensor fiber without a coating is positioned 21 mm from the left side. Finally the Panda fiber with a coating is positioned 23 mm from the left side. Two such sets of identical sensor fiber sets are placed in layer 1 and in layer 5 in order to study the influence of placing the optical sensors in different layers of the composite sample on the sensors performance. Layers 1 and 5 were chosen because they represent the layers closest to the sample surface and the sample centre respectively.

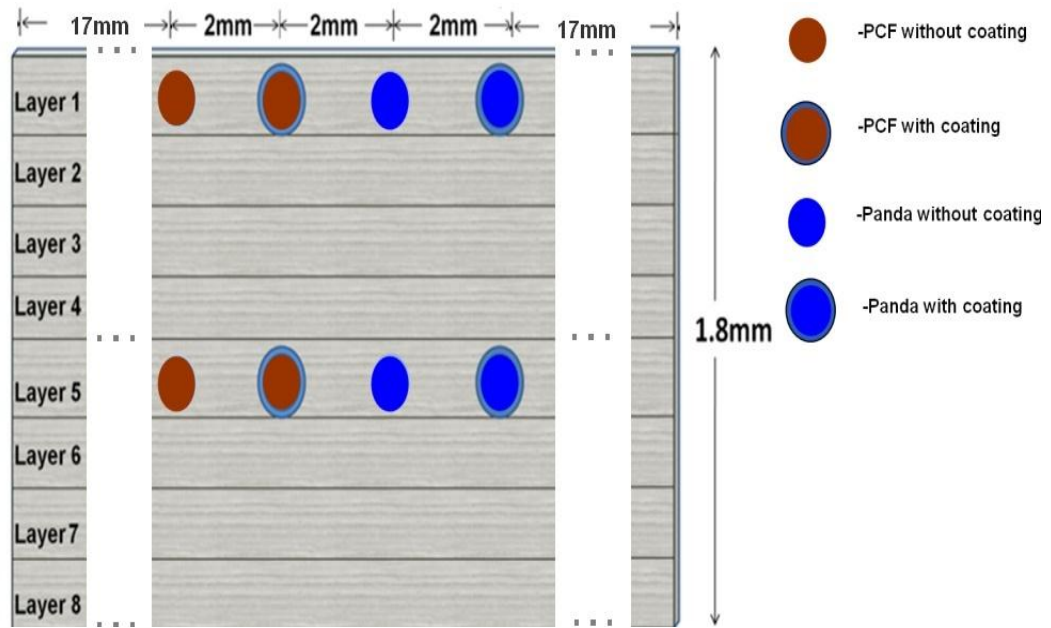


Figure 3.3. Schematic (cross sectional view) of sensors positioned in layer 1 and layer 5 of the 8-layer composite material sample.

3.1.4 Experimental arrangement

To extract the phase difference between the two orthogonal polarizations, the experimental setup shown in Figure 3.4 is used. A tunable laser source with a wavelength of 1550 nm is used as an input source. The temperature sensitivity of the polarimetric sensors is measured by using a polarimeter and polarization control system, TXP 5004 from Thorlabs. The output of the laser source is fed to the polarization controller, so that polarized light is launched into the inputs of the optical fiber sensors. Polarization variations at the outputs are observed by using the polarimeter. It is well known that fiber splicing can induce changes in the polarization state and therefore the response of a polarimetric sensor. Therefore, the PM fibers are connected without the use of splices, with free ends connected to the polarization control system by means of polarization maintaining connector ferrules.

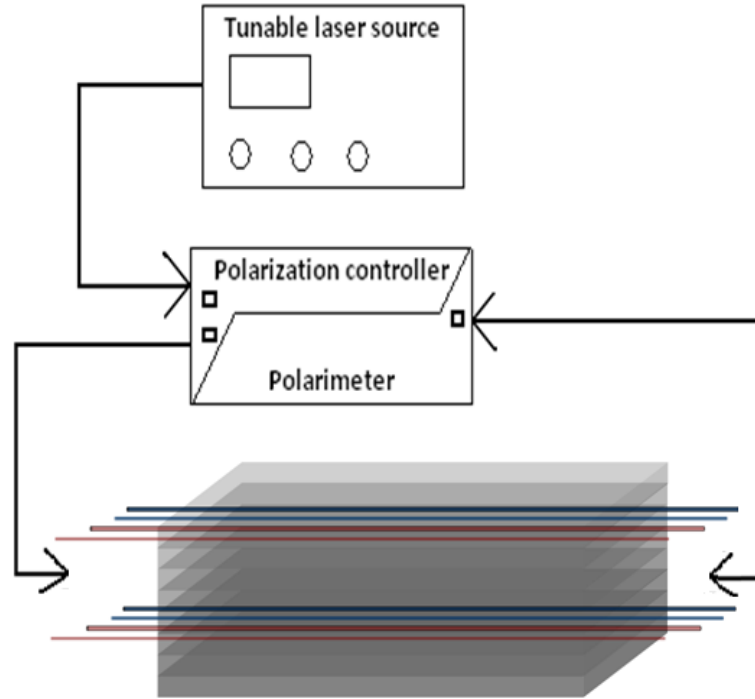


Figure 3.4. Schematic of the experimental arrangement for composite material sample with embedded polarimetric sensors

To study the influence of the thermal expansion of the composite material on the embedded polarimetric fiber sensors, the sample is subjected to temperature variations over a range from 0 to 65 °C, by using a Peltier cooler (Model No. PE-127-20-15-U from Radionics. Ltd) and the experimental set up as shown in the Figure 3.5. To increase the surface area of the Peltier cooler to match that of the composite sample, a thermally conductive aluminium plate with dimensions of 210 mm x 100 mm x 1.5 mm is placed on top of the Peltier cooler, which has a surface area of 62 mm x 62 mm, attached with a thermally conducting paste. A time interval of 20 minutes is used between each 5 °C step temperature variation in order to ensure a uniform temperature distribution in the composite sample. The Peltier cooler temperature is controlled using Thorlabs ITC510 temperature controller with the thermistor feedback sensor attached to the surface of the aluminium plate. The temperature controller offers stability over 0 to 70 °C operation range, with an

accuracy of 0.1°C . The sample is placed on the aluminum plate so that layer 1 is in contact with the plate.

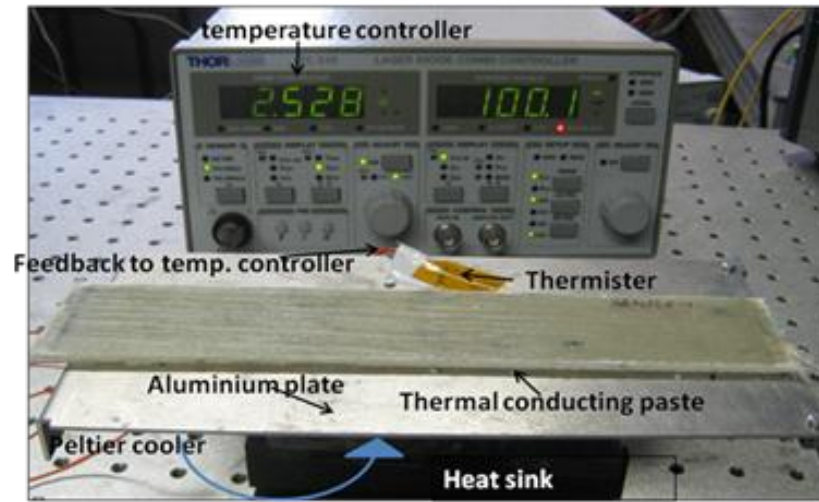


Figure 3.5. Experimental setup to apply temperature changes to the composite material sample

The strain or temperature induced polarization variation is measured using a polarization controller and polarimeter. The State of Polarization (SOP) [2.15] at the input to the polarimetric sensors is adjusted by changing the azimuth and ellipticity at the polarization controller. Initially these values are set so as to achieve the maximum optical power at the polarimeter input. The Poincare sphere is used as a way to graphically represent the polarization transformations. The Poincare sphere is a graphical tool in real, three dimensional space in which the polarization can be uniquely represented by a point on or within a unit sphere centered in a rectangular (x, y, z) coordinate system. The coordinates of the point are the three normalized Stokes parameters describing the state of polarization. Because a state of polarization is represented by a point, a continuous change in the polarization state can be represented as a continuous path on the surface of the Poincare sphere. Thus the strain and temperature response of the polarimetric sensor can be determined by the evaluation of the Poincare sphere.

The polarized light from the source is launched with its polarization at an angle of 45° , to the optical axis of the PM- fiber to ensure equal distribution of optical intensity between the two orthogonal polarizations. The polarimeter provides real time information about the SOP of the polarimetric sensor output, presented graphically as a circular trace on a Poincare sphere with phase change and also numerical values for measurands such as azimuth, ellipticity, Stokes parameters and the intensity of the optical power. The temperature is varied in equal steps, and the variations of the Poincare sphere trace and Stokes parameters are recorded for each step change. The polarization induced phase shift for an applied temperature change is calculated from the Poincare sphere. By extrapolating from the recorded results, the applied temperature needed to obtain one complete circular path on the Poincare sphere (exactly 2π radians) is determined and thus the temperature sensitivity can be estimated.

3.1.5 Results and discussion

A. Temperature response of the embedded HB-PM-PCF sensors

Temperature responses of both coated and coating-stripped HB-PM-PCF polarimetric sensors embedded in the composite material sample are presented in this section. For comparison the temperature responses of the coating-stripped HB-PM-PCF in free space were found before embedding when subjected to a temperature variation from 0 to 65°C and as expected the sensor is found to be effectively temperature insensitive as shown in Figure 3.6 (a).

However, the coating-stripped HB-PM-PCF embedded in the layer 1 of the composite material shows a phase shift of 3.6028 rad, for a temperature variation of 65°C as shown in Figure 3.6(b), resulting in a sensitivity of $0.2578 \text{ rad/m} \times ^\circ\text{C}$,

and for layer 5 a sensitivity of $0.2247 \text{ rad/m} \times ^\circ\text{C}$. Since coating-stripped HB-PM-PCF proved to be insensitive to temperature in free space, it is concluded that the sensitivity when embedded in a composite must be due to strain/stress induced by temperature variations within the composite material or thermal expansion of the composite material.

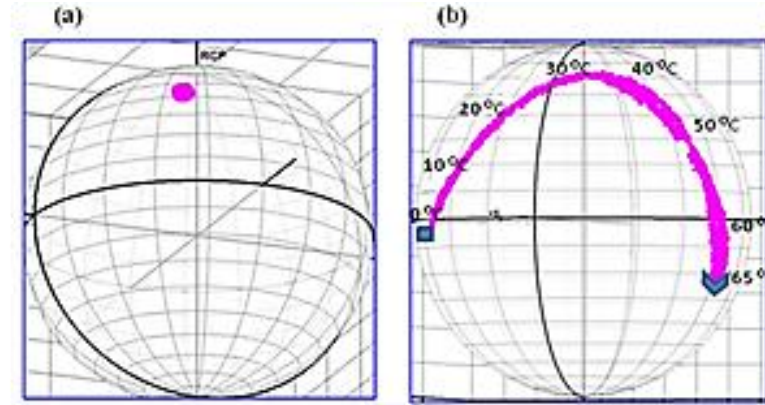


Figure 3.6. Observed phase shift in coating-stripped HB-PM-PCF fibers for a temperature variation from 0 to 65°C (a) in free space (b) after embedding

The process followed above for the coating stripped fibers above was then repeated for the coated HB-PM-PCF fibers. The temperature response of the coated HB-PM-PCF in free space subjected to a temperature variation of $0\text{--}65^\circ\text{C}$ was firstly determined and is shown in Figure 3.7 (a). In the coated HB-PM-PCF, a phase shift of 0.1548 rad is observed for a temperature variation of 65°C , yielding an estimated sensitivity of $0.01108 \text{ rad/m} \times ^\circ\text{C}$. While this value for free space is low, it is non-zero, unlike the coating stripped HB-PM-PCF. When the coated HB-PM-PCF is embedded in layer 1 of the composite material sample (and therefore is in direct contact with the heat source) and is subjected to a temperature variation of 65°C it shows a phase shift of 0.1518 rad (Figure 3.7 (b)), equivalent to a sensitivity of $0.01086 \text{ rad/m} \times ^\circ\text{C}$. For a coated HB-PM-PCF embedded in the layer 5 the temperature sensitivity also yields a comparable low value of $0.0185 \text{ rad/m} \times$

$^{\circ}\text{C}$. Comparing the free space and embedded sensitivities it is clear that for a coated HB-PM-PCF the sensitivity is not unduly affected by embedding, a very different conclusion in comparison to that for the coating-stripped case, where sensitivity increases dramatically after embedding.

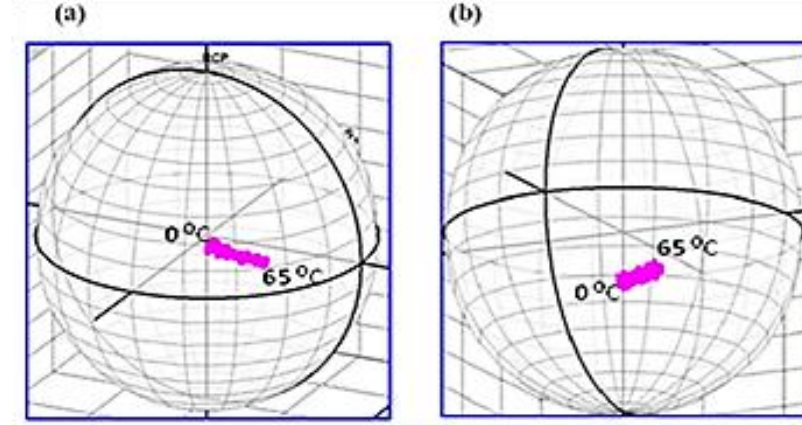


Figure 3.7. Observed phase shift in coated PMPCF fibers for a temperature variation from 0-65 $^{\circ}\text{C}$ (a) free space (b) after embedding

It should be noted that by comparing the performance of coating-stripped and coated HB-PM-PCF in free space from Figure 3.6(a) and Figure 3.7(a), it is observed that there is a minor dependence on temperature for the buffer coated HB-PM-PCF, which is believed to arise due to the temperature sensitive nature of the acrylate coating of the HB-PM-PCF fibers.

The difference in the fiber sensor temperature sensitivity between coating stripped HB-PM-PCF and a coated HB-PM-PCF when embedded in the composite is due to the higher tolerance of the coated HB-PM-PCF to the dominant form of thermal expansion in a composite material, that is transverse expansion. During cooling and heating cycles the SOP followed the same trace indicating the absence of a hysteresis phenomenon, confirming also that the 0-65 $^{\circ}\text{C}$ experimental temperature range lies in the linear thermal expansion region of the composite material, which is reasonable given that the glass transition temperature of the particular cured resin

is above 150 °C. It is identified in [2.16] that composite materials have both longitudinal and transverse expansions, but that the coefficient of transverse thermal expansion is many times higher than that for longitudinal expansion.

The thermal expansion induced stress and strain, causes a change in the birefringence of the HB-PM-PCF and as a result a phase shift between the guiding modes can occur in the case of a buffer stripped HB-PM-PCF embedded in the composite material. However, for the coated HB-PM-PCF sensor, the impact of the thermal expansion of the composite material has a much lower effect as seen in Figure 3.7 and as a consequence the temperature sensitivity of the sensor by comparison to the free space sensitivity does not vary significantly after embedding in the composite material. This immunity to thermal expansion in a buffer coated HB-PM-PCF is due to two reasons: (i) the impact of transverse thermal expansion is eliminated due to strain tolerance provided by the coating material, thus no stress induced birefringence change arises (ii) the coefficient of longitudinal thermal expansion of the glass reinforced general purpose resin based composite is very low [2.17].

B. Temperature response of the embedded panda fiber sensors

The temperature responses of both coated and coating-stripped panda fiber polarimetric sensors embedded in the composite materials sample are presented in this section. A panda fiber based polarimetric sensor is sensitive to both temperature and strain. To analyze temperature sensitivity, the panda fiber samples are subjected to temperature variations without applying any strain.

For the buffer coating stripped case, the temperature responses of the panda fiber in free space and embedded in the layer 1 of the composite material were measured

and show a phase shift of 3.1605 rad and 6.175 rad respectively, when subjected to a temperature variation 0-7 °C, as shown in Figure 3.8(a) and Figure 3.8(b). Note that since panda type fibers are more sensitive compared to HB-PM-PCF, in order to achieve a phase variation within one complete circuit of a Poincare sphere the smaller temperature range of 0-7 °C is used to enable a more direct comparison with the HB-PM-PCF case. A significant change in temperature sensitivity is observed before and after embedding of coating stripped panda fibers into composite materials similar to that of the HB-PM-PCF. The magnitude of temperature sensitivity increased from 2.1 rad/m x °C to 4.1 rad/m x °C. The coating stripped panda fiber that is embedded in the composite layer 5 yielded a temperature sensitivity value of 3.56 rad/m x °C. This difference in the magnitude of the temperature sensitivity before and after embedding confirms the dependence of the coating-stripped panda fiber temperature response on composite material thermal expansion.

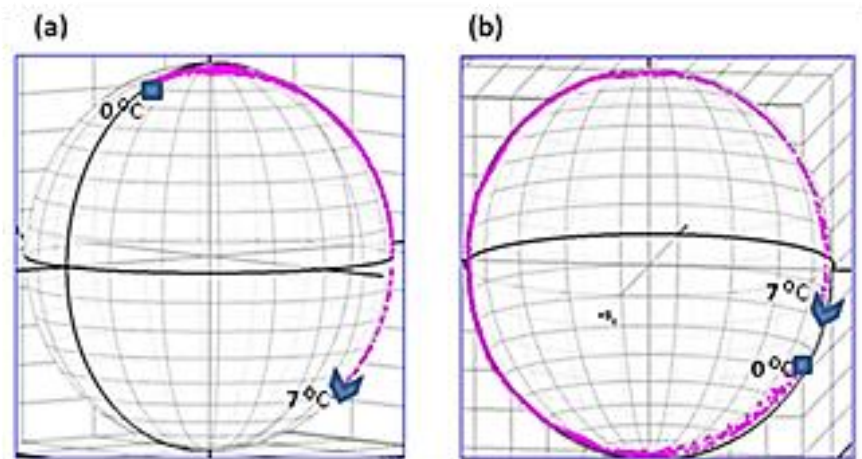


Figure 3.8. Observed phase shift in coating-stripped Panda fibers for a temperature variation from 0- 7°C (a) free space (b) after embedding

For the buffer coated case, investigations were also undertaken for the panda fiber in free space and embedded in the composite material sample. For layer 1 and a

temperature variation of 7°C , there is a phase shift of 3.311 rad and 3.913 rad respectively as shown in Figure 3.9(a) and Figure 3.9(b). The corresponding temperature sensitivities are $2.2 \text{ rad} / \text{m} \times ^{\circ}\text{C}$ and $2.6 \text{ rad} / \text{m} \times ^{\circ}\text{C}$. The coated panda embedded in the composite layer 5 yields a value of $2.34 \text{ rad} / \text{m} \times ^{\circ}\text{C}$. Thus the magnitude of temperature sensitivities for buffer coated panda fiber sensors are comparable in free space and after embedding, from which can conclude that there is no significant influence for coated panda fiber due to the thermal expansion of the composite material.

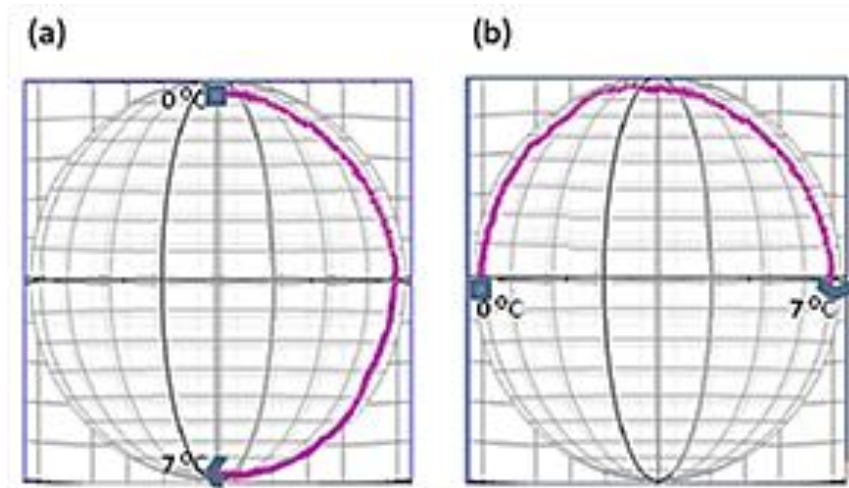


Figure 3.9. Observed phase shift in coated Panda fibers for a temperature variation from 0-
 7°C (a) free space (b) after embedding

Comparing the performance of coating-stripped and coated panda fibers in free space as shown in Figure 3.8. (a) and Figure 3.9. (a) respectively, the reason for the slight increase in temperature sensitivity from 2.1 to $2.2 \text{ rad} / \text{m} \times ^{\circ}\text{C}$ for coated panda fiber in free space is due to the acrylate coating which undergoes a small thermal expansion which induces low levels of stress on the fiber.

A comparison of the temperature responses of embedded panda fiber without a coating Figure 3.8. (b) and with a coating Figure 3.9(b), shows significant difference in sensitivities from $4.1 \text{ rad} / \text{m} \times ^{\circ}\text{C}$ to $2.6 \text{ rad} / \text{m} \times ^{\circ}\text{C}$ respectively. The

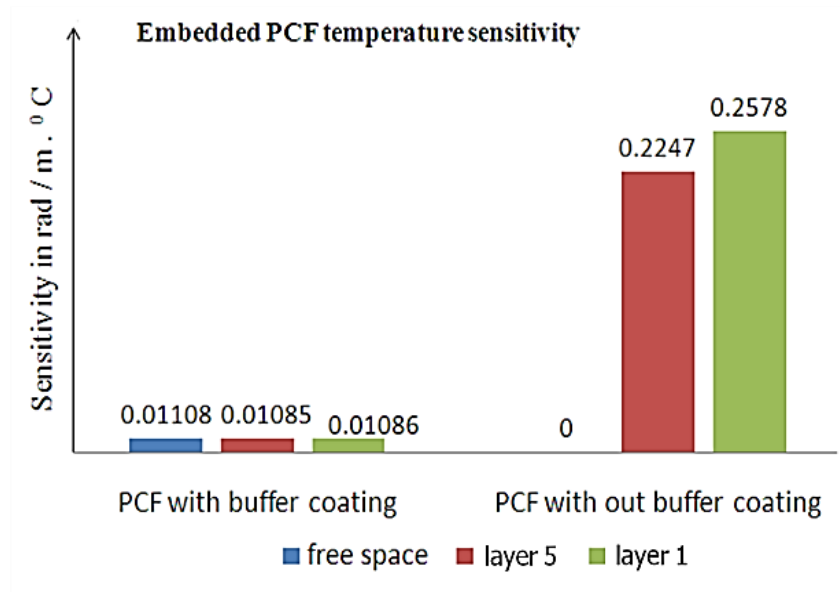
effective temperature sensitivity when embedded of a buffer stripped Panda fiber is significantly higher compared to a coated panda fiber due to the influence of transverse thermal expansion, as explained in section C.

C. Discussion

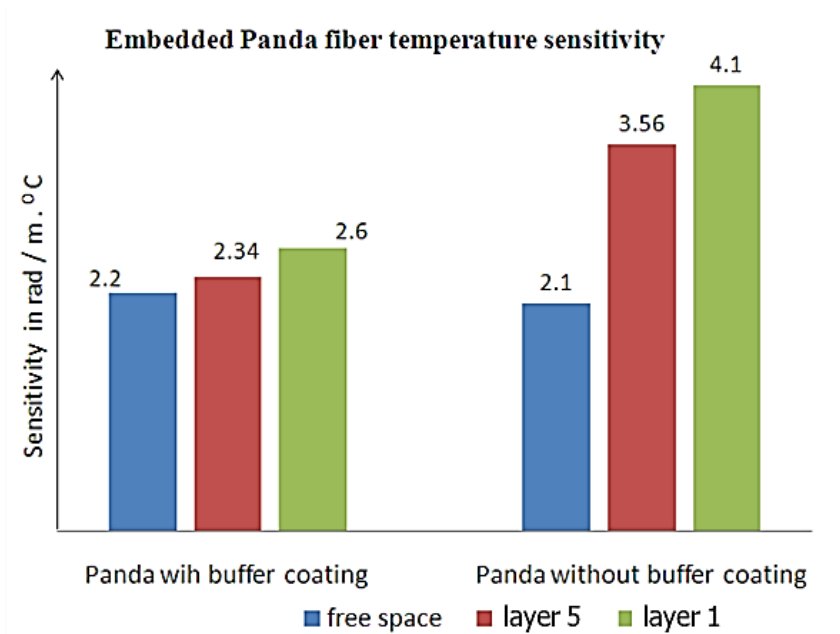
Figure 3.10(a) summarises and compares the temperature sensitivities of HB-PM-PCF sensors in various configurations. It is clear that the presence of a coating preserves the temperature independence of a HB-PM-PCF sensor when it is embedded in a composite. In a similar fashion, Figure 3.10(b) summarises and compares the temperature sensitivities of panda fiber sensors in various configurations. The inherent temperature sensitivity of panda fiber sensors is higher, but once again the presence of a coating, mitigates the effect of thermal induced stress in the composite

A conclusion is that while a coating stripped HB-PM-PCF sensor can be used as a temperature independent strain sensor in free space, it cannot be used for strain measurements in composite materials. The acrylate coated panda sensors can be used for embedding in composites provided a temperature correction is used to increase the accuracy of strain measurements. However, for embedding in composite materials, coated HB-PM-PCF sensors are most effective in delivering temperature insensitive strain measurement.

One final insight from Figure 3.10 is that optical fiber sensors in the outer layer of a composite sample show a higher thermal stress sensitivity due to the fact that the temperature gradually decreases in the direction from the outer layer that is contact with the heat source toward the layer 5, with a consequent reduction in thermally induced stress



(a)



(b)

Figure 3.10. Comparison of the temperature sensitivity of (a) HB-PM-PCF polarimetric sensors; and (b) Panda polarimetric sensors

3.1.6 Conclusion

The vital issues of the influence of composite material thermal expansion on

embedded polarimetric sensors for measurements of strain and temperature are studied in this chapter. The glass-fiber reinforced general purpose resin based composite samples are fabricated and characterized, with polarimetric sensors embedded in two distinct layers of the multi-layer composite structure. The two types of polarimetric sensors studied are based on polarization maintaining photonic crystal fiber and panda fiber. The temperature sensitivities of coated and coating stripped HB-PM-PCF and panda fiber polarimetric sensors are calculated in free space and compared to those embedded in the composite material. From the results it is concluded that a polarimetric sensor with an acrylate coated fiber embedded in the composite material shows the same response as the one in free space, while a coating-stripped fiber polarimetric sensor shows a significant increase in temperature sensitivity when embedded in the composite material, which is due to the stress induced change in birefringence created by thermally induced strain. In the case of coated fiber, the effect is eliminated by the coating. For panda fibers the magnitude of dependency on thermal expansion of the composite material is many times higher than for HB-PM-PCF, because of the cross-sensitivity between temperature and thermal induced strain. From the analysis it is concluded that thermal expansion induced drifts are the main source of errors during temperature and strain measurements using embedded polarimetric sensors. To improve the sensor system accuracy in real-world applications, it is concluded that buffer coated polarimetric fiber sensors are a better choice than buffer stripped fiber sensors.

3.1.7 References

- 3.1 D. D. L. Chung. "Composite materials: science and applications." Springer Publications, 2nd Edition, 2010.
- 3.2 M. Grassi, X. Zhang, and M. Meo. "Prediction of stiffness and stresses in Z-fiber reinforced composite laminates Composite Part A: applied science and manufacturing." vol 33 pp 1653-1664, 2002.
- 3.3 J. K. Kim, D. Z. Wo, L. M. Zhou, H.T. Huang, K.T. Lau, M. Wang. "Advances in Composite Materials and Structures." Key Engineering Materials, vol 334-335, 2007.
- 3.4 D. P. Garg, M. A. Zikry, G. L. Anderson, X. E. Gros, "Current and potential future research activities in adaptive structures- an ARO perspective." Smart Mater. Struct., vol 10. pp .610-623, 2001.
- 3.5 V. D. Marty, P. Ferdinand, E. Bocherens, R. Carbone, H. Beranger, S. Bourasseau, M. Dupont, D. Balageas. "Embedded fiber Bragg grating sensors for industrial composite cure monitoring." Journal of Intelligent Materials Systems and Structures. vol. 9 pp. 785-787,1998.
- 3.6 V. M. Murukeshan, P. Y. Chan, O. L. Seng, A. Asundi. "On-line health monitoring of smart composite structures using fiber polarimetric sensor." Smart Mater. Struct. vol 8, pp 544-548,1999.
- 3.7 T. Yoshino, T. Hashimoto, M. Nara, K. Kurosawa. "Common path heterodyne optical fiber sensors." J. Lightwave Technology, vol. 10 pp. 503–513, Apr. 1992.

- 3.8 M. A. Vengsarkar, W. C. Michie, L. Jankovic, C. Brian and O. C. Richard.
“Fiber-optic dual-technique sensor for simultaneous measurement of strain and temperature”, J. Lightwave Technology, vol. 12, 1994.
- 3.9 G. Rajan, K. Mileńko, P. Lesiak, Y. Semenova, A. Boczkowska, M. Ramakrishnan, K. Jędrzejewski, A. Domański, T. Woliński, and G. Farrell.
“A hybrid fiber optic sensing system for simultaneous strain and temperature measurement and its applications.” Photonics letters of Poland, vol 2 (1) pp 46-48,2010.
- 3.10 J. Villatoro, V. Finazzi, V. P. Minkovich, V. Pruneri, G. Badenes.“Highly sensitive sensors based on photonic crystal fiber modal interferometers.” Journal of Sensors, 2009.
- 3.11 A. Domanski, et.al, “Comparison of Bragg and polarimetric optical fiber sensors for stress monitoring in composite materials.” Acta Physica Polonica, vol .116 p 294, 2009.
- 3.12 T. R. Wolinski, P. Lesiak, A. W. Domanski. “Polarimetric optical fiber sensors of a new generation for industrial applications.” Bulletin Of The Polish Academy Of Sciences Technical Sciences, vol 56, No. 2, 2008.
- 3.13 X. Dong, H. Tam. “Temperature-insensitive strain sensor with polarization maintaining photonic crystal fiber based Sagnac interferometer.” Applied Physics Letters, vol 90(15), 151113, 2007.
- 3.14 N. Delaye, S. Marais. “Characterization of unsaturated polyester resin cured with styrene.” J. Appl.Polym.Sci. 67:695–703,1998.
- 3.15 E. Collett. “Field guide to polarization.” SPIE press, vol 5,2005.

- 3.16 S. R. Reid, G. Zhou, "Impact behavior of fibre-reinforced composite materials and structures." CRC press, October 31, 2000.
- 3.17 T. Stolarski, Y. N. Yoshimoto. "A numerical study on the coefficients of thermal expansion of fiber reinforced composite materials." Composite Structures, vol 78, pp 1-10,2007.

Chapter 4

Measurement of Thermal Elongation Induced Strain of a Composite Material Using Embedded Sensor

It was explained in Chapter 3 that due the thermal elongation of the composite material the buffer stripped HB-PM-PCF polarimetric sensor shows significant phase change when embedded in the composite material. That investigation not only allows for the elimination of errors in analysing information from embedded sensors but importantly it opens up the possibility of measuring the Coefficient of Thermal Expansion (CTE) value of a composite material itself, based on the observed phase change of the embedded buffer stripped polarimetric sensor. This has not been investigated previously and can provide useful information about material properties and improved fabrication.

Thus the primary aim of this chapter is describe the measurement of composite material's thermal elongation induced strain using an embedded polarimetric sensor. Measuring the thermally induced strain of the composite material using a polarimetric sensing scheme will allow one to resolve such the thermal strain induced errors during the strain measurements using an embedded hybrid sensor. In this investigation for thermal induced strain measurements a stripped PM- PCF polarimetric sensor is selected. The reason for selecting the particular type is that the stripped photonic crystal fiber based polarimetric sensor is proven having

insignificant temperature sensitivity in free space. This chapter contributes to achieve this aim by comparing the phase change of the stripped PM-PCF embedded different types of composite materials with three different CTE values. For the research work presented in this chapter, buffer stripped HB-PM-PCF polarimetric sensors are embedded in carbon-epoxy, E glass-epoxy, and E glass-unsaturated polyester resin composite material and are characterized. Controlled fabrication conditions and post fabrication testing is conducted to ensure that residual strain and moisture expansion is absent in the fabricated composite samples. Further thermal elongation induced strain is measured from the stripped polarimetric sensor. This experimentally measured thermal elongation induced strain of the composite materials is compared with the theoretically calculated CTE values. The theoretical and experimental investigations showed good agreement. The outcomes of this piece of research enable one to measure the thermal expansion of a composite material, assuming the material has negligible residual strain and moisture expansion, using a single stripped HB-PM-PCF sensor.

4.1 Measurement of thermal elongation induced strain of a composite material using a polarization maintaining photonic crystal fiber sensor⁷

Keywords Thermal elongation induced strain; High-Birefringent Polarization Maintaining Photonic Crystal Fiber (HB-PM-PCF); Polarimetric fiber sensor; Composite material

⁷ Manjusha Ramakrishnan, Ginu Rajan, Yuliya Semenova, Anna Boczkowska, Andrzej Domański, Tomasz Wolinski, Gerald Farrell, "Measurement of thermal elongation induced strain of a composite material using a polarization maintaining photonic crystal fiber sensor", *Sensors and Actuators A: Physical*, Volume 190, Pages 44-51, 2013.

Abstract: A measurement scheme to measure a composite material's thermal elongation induced strain using a buffer stripped HB-PM-PCF sensor is investigated in this research work. A composite material sample with an embedded HB-PM-PCF based polarimetric fiber sensor is fabricated and characterized. It is found that the buffer stripped HB-PM-PCF polarimetric sensor which is temperature insensitive in free space, shows significant phase change when embedded in the composite material due the thermal elongation of the composite material. The temperature induced phase change of buffer stripped HB-PM-PCF polarimetric sensors embedded in carbon-epoxy, E glass-epoxy, E glass-unsaturated polyester resin composite material samples is measured and the results are used to determine the thermal elongation induced strain over a temperature range from 0 °C to 65 °C. The experimentally measured thermal elongation induced strain of the same samples are found to be $3.648 \times 10^{-5} \text{ } \epsilon / ^\circ\text{C}$, $1.52 \times 10^{-5} \text{ } \epsilon / ^\circ\text{C}$, and $2.42 \times 10^{-5} \text{ } \epsilon / ^\circ\text{C}$. The Coefficient of Thermal Expansion (CTE) estimated theoretically using composite laminate theory shows good agreement with that derived using the HB-PM-PCF sensor. The present investigation offers a simple nondestructive method to determine thermal elongation induced strain in composite structures. It is shown that the method allows the measurement of thermal expansion for those composite materials having negligible residual strain and moisture expansion.

4.1.1 Introduction

Composite materials, in particular continuous fibre-reinforced composite structures [4.1] have many attractive properties such as low density, high strength and high stiffness [4.2, 4.3]. Due to the extensive use of composite materials,

structural health monitoring (SHM) of composites is an important function [4.4, 4.5], which also offers the possibility to develop so-called “smart” composite structures with compact integrated sensors.

In composite structures, knowledge of the thermal expansion behavior is of significant importance in avoiding debonding due to differential thermal expansion stresses. Thermal expansivity and hydro-thermal strain may be measured in various ways, reviewed by James et al. [4.6], but the most common procedure is mechanical dilatometry [4.7]. In order to very accurately measure the linear thermal expansion coefficient of precision items such as gauge blocks, optical interferometer based wavelength measurements [4.8], and interferometric dilatometry [4.9], have been used to obtain deformation values. A displacement measuring interferometric system using a heterodyne scheme [4.10], is another technique that provides high accuracy. However, all of the interferometric systems are very sensitive to their external environment, involve a difficult alignment process and can be physically too large for many applications.

Fiber optic sensor technology is a promising candidate for composite SHM as such sensors can be embedded within a composite material without affecting the mechanical properties of the composite. For SHM applications, the most extensively used technology is FBG sensing [4.11, 4.12, and 4.13]. The measurement of the thermal expansion coefficient using a surface-mounted Bragg-grating sensor is discussed by Lo and Chuang [4.14]. For embedded sensors, an investigation of FBG sensors embedded in carbon-epoxy laminates has been presented by Mülle et al [4.15]. Further, H-I Kim et al [4.16] continued the research on the thermal expansion measurement accuracy of FBG sensors by combining such sensors with a heterodyne interferometer system, and developed a

displacement measuring interferometer (DMI). However, the cross-sensitivity between temperature and strain is a serious disadvantage of FBG sensors for many real-life applications [4.17].

Another promising fiber optic sensing technology for composite materials is called polarimetric fiber sensing [4.18, 4.19]. In this category, a wide variety of polarimetric sensors are available employing polarization maintaining (PM) fibers and micro-structured highly-birefringent (HB) polarization maintaining fibers, which are capable of sensing multiple parameters, such as temperature, strain, displacement, rotation etc.

For many embedded fiber optic sensors, the measurement of thermal expansion is achieved by measuring thermal strain. The specific type of polarimetric sensor using micro-structured polarization maintaining highly-birefringent photonic crystal fiber (PM-HB-PC)F is proven to have very low temperature sensitivity in free space [4.20, 4.21]. But it has been shown that it acquires a significant response with temperature when embedded in a composite material, due to the stress-induced change in birefringence created by the thermal expansion of the composite material [4.22]. It is logical therefore to assume that this sensor could be used as a basis for measuring thermal strain and thus thermal expansion.

When the temperature of a composite sample changes, thermal elongation occurs and it is this elongation that produces thermal strain. However, the thermal elongation of a fiber reinforced composite material is not only caused by the thermal expansion of the resin and reinforcement fiber itself but also as a result of a combination of moisture content expansion and anisotropic expansion points due to non-uniform residue pockets [4.23]. Thus the measurement of thermal expansion of the composite material only by measuring thermal strain is difficult because of

these additional factors. In this present work for more accurate thermal expansion measurement, an attempt is made to eliminate these additional factors by optimizing the sample fabrication techniques.

This study investigates the application of PM-HB-PCF sensors to the measurement of thermal expansion in carbon and glass fiber reinforced composite materials. For thermal expansion measurements carbon-epoxy, E glass-epoxy, E glass-unsaturated polyester resin composite samples with embedded HB-PM-PCF polarimetric sensors are fabricated and are subjected to temperature variations from 0 °C to 65 °C. The measured thermal elongation induced strain is compared to theoretical predictions from Classical Laminate Theory. The sensor can be used for consistent and accurate thermal elongation measurements for composites used in aeronautical applications such as helicopter rotor blades, which operate in varying atmospheric temperature conditions over a temperature range that can exceed 60 °C.

4.1.2 Methodology of thermal elongation induced strain measurement using a stripped HB-PM-PCF sensor embedded in composite material

In HB PM optical fibers, any symmetric deformation effect (X) induced by strain (ϵ) influences the propagation constant β of every fiber optic mode due to changes in fiber length L and the refractive indices of both the fiber core and the fiber cladding. In a single mode regime, this leads to changes in the phase difference $\Delta\Phi = \Delta\beta \cdot L$ between both polarizations of the fundamental LP_{01} mode along the length of the fiber [4.24],

$$\frac{\delta(\Delta\Phi)}{\delta X} = \Delta\beta \frac{\partial L}{\partial \varepsilon} + \frac{\partial(\Delta\beta)}{\partial \varepsilon} L \quad 4.1$$

The strain sensitivity of a HB-PM-PCF polarimetric sensor can be written as [4.25],

$$S = \frac{2\pi}{T_\varepsilon \cdot L} \quad [\text{rad}/(^{\circ}\text{C} \cdot \text{m})] \quad 4.2$$

where T_ε is the applied strain required to induce a 2π phase difference between the two polarizations of the fundamental mode. The value of the parameter T_ε multiplied by the length of the fiber L is a wavelength-dependent constant:

$$L \cdot T_\varepsilon = \text{const}(\lambda) \quad 4.3$$

In the case of stripped HB-PM-PCFs (such as PM-1550-01) the influence of temperature on the birefringence of the fiber is negligible [4.25] in free space and hence the phase change in such a polarimetric sensor will only originate from the induced strain. The origin of the temperature induced response of the stripped HB-PM-PCF sensor after embedding [4.22] in the composite material is due to thermally induced strain over the sample length.

When temperature varies the composite material's thermal elongation is due to a combination of thermal strain caused by thermal expansion of the resin/matrix mixtures, expansion induced by moisture absorption and finally residual strain [4.23]. Since in this study, the composite cure and post-curing cycles are optimised by manufacturers so as to reduce the residual strain, and can be neglected.

$$\varepsilon_{TL} = \Delta\Phi_T / S_\varepsilon \quad 4.4$$

The composite material's thermal elongation results in a stress applied to the stripped HB-PM-PCF which in turn produces a significant phase change. Thus, the thermal elongation induced strain ε_{TL} , averaged over the sample length, can be derived from the observed phase change by knowing the strain sensitivity of

stripped HB-PM-PCF in constant temperature settings and can be calculated as,

$$\varepsilon_{TL} = \Delta\Phi_T / S_\varepsilon \quad 4.5$$

where $\Delta\Phi_T$ is the observed phase change in radians per unit length per unit temperature and S_ε is the strain sensitivity of the HB-PM-PCF sensor embedded in the composite material.

4.1.3 Fabrication of the composite material sample

The glass and carbon fibre reinforced composite material samples are fabricated using two methods: the vacuum assisted prepreg method and hand layup method. Three types of samples are fabricated: carbon-epoxy, E glass-epoxy and E glass-unsaturated polyester resin. The details of the composite material, matrix, fabrication and layup are shown in Table 4.1.

Table 4.1. Composite material sample details

Material	Product ID	Reinforcement fiber	Matrix	Fabrication method	Cure temperature	Cured Vacuum	Ply
Carbon-Epoxy	UD250C STFT109 /33	Carbon unidirectional	FT109-Epoxy	Prepeg vacuum assisted	80°C 8hrs	736mm Hg	[0/0] ₈
E-glass - Epoxy	Hexply M12- 37/G778 1	E Glass Plain fabric	Hexply M12-Epoxy resin	Prepeg vacuum assisted	80°C 8hrs	736mm Hg	[0/0] ₇
E glass - Unsaturated polyester	EG7781	E glass Plain fabric	Unsaturated polyester resin	Hand lay-up method	25°C 24hrs	-	[0/0] ₈

The polarimetric fiber sensors are realized by using a highly birefringent polarization maintaining photonic crystal fiber (PM-1500-01), having a beat length < 4 mm at an operating wavelength of 1550 nm. we have been previously shown [4.22] that the presence or absence of a fiber buffer coating has an influence

on the effect of thermal strain. Thus in order to undertake a more comprehensive study of thermal expansion measurements in a composite material, both HB-PM-PCF fibers with an acrylate buffer coating and without a buffer coating are embedded. The fabrication methods used for the different sample types are outlined below.

A. Prepeg method

This method is used for the carbon-epoxy and E glass-epoxy samples. In the prepeg method, for the glass composite material sample, the reinforcement fabric used is an E-glass fibre fabric of density 299 g/m^2 and epoxy matrix HEXPLYM12. For the carbon composite material sample, unidirectional carbon fibre with a density of 200 g/m^2 and an epoxy matrix UFT109/33 is used. The prepreg laminates were cut into multiple pieces with identical dimensions of $25 \text{ cm} \times 4 \text{ cm}$, to form the plies of the fabricated composite sample. The fabrication process is as follows: the mould surface is firstly coated with a release agent 44-NC, to prevent sticking of the moulded part to the mould surface. The fibre reinforcing prepreg fabric is then placed on the mould. The HB-PM-PCF is placed in the number 1 layer as shown in Figure 4.1. Since the $250 \mu\text{m}$ HB-PM-PCF is laid parallel to the reinforcing fibres as an inclusion in to composite sample and the two ends of the optical fibre are led outside the area of the sample, any additional defects in the laminate are close to zero [4.26]. The HB-PM-PCF fibres were placed 2 mm apart from each other and approx 19 mm from both the ends of the sample. Careful consideration is given to laying down the optical fiber sensors on the prepreg laminates to ensure that the fiber sensors are free of any residual bending and also are parallel to each other. Therefore, before placing the fiber sensors in-situ, a pre-strain is applied to the fiber by fixing both ends of the fibers on a translation stage.

Ideally the top-most or the bottom-most layer exhibits the maximum strain, higher than that of the inner layers. In the present experiment the location in between the first layer and second layer is chosen as the placement layer for the optical fiber sensors in order to reduce the risk of breakage of the fragile fiber sensors. Both glass and carbon fiber reinforced composite samples produced by the prepreg method are cured as per the manufacturer's specifications at an elevated temperature of about 80 °C for a day and at a vacuum of 1 kg/cm². The thickness of the fabricated sample was 2 mm.

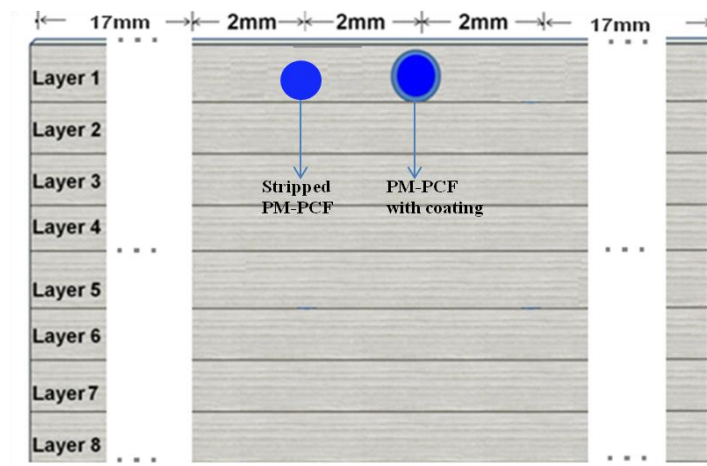


Figure 4.1. Schematic of the composite material sample with embedded fiber sensors.



Figure 4.2 Fabricated (a) carbon-epoxy, (b) E glass-epoxy, and (c) E glass-unsaturated polyester resin composite samples

B. Hand layup method

This method is used for the E glass-unsaturated polyester resin sample. E-glass woven fiber fabrics are used as the reinforcement and a general purpose polyester

resin is used as the matrix. The matrix material is prepared from the polyester resin with a catalyst added to the resin at a rate of 1% by volume. The reinforcement glass woven fabric used has a density of 280 g/m^2 and was cut into 8 pieces with identical dimensions of 20 cm x 10 cm, to form the eight plies of the fabricated composite sample. The HB-PM-PCF sensors are once again embedded in layer 1 as shown in Figure 4.1. The sample is cured as per the manufacturer's specifications at room temperature for a day and then for eight more hours at a temperature circa 60°C . After curing the sample is trimmed to dimensions of 20 cm x 3 cm. The thickness of the fabricated sample was 3.2 mm. An image of the fabricated samples is shown in Figure 4.2.

4.1.4 Experimental arrangement

In order to measure thermal elongation induced strain by extracting the phase difference between the two orthogonal polarizations, the experimental setup used is as shown in Figure 4.3. The experimental arrangement consists of a laser source at 1550 nm, a polarization control system (TXP 5004 from Thorlabs) and polarimeter. To study the influence of thermal expansion of the composite material on the embedded polarimetric fiber sensors, the sample is subjected to temperature variations over a temperature range from 0°C to 65°C , by using a Peltier cooler as shown in Figure 4.4.

The polarization variation of the polarimetric sensor is measured by using a polarization controller and polarimeter. The experimental method adopted to vary the temperature of composite samples and extracting the strain/temperature response of the polarimetric sensor is the same as described in our earlier work [4.22]. The temperature response of the polarimetric sensor can be determined by

evaluating the measured Poincare sphere. A more detailed description of the experimental arrangement is provided in reference [4.22].

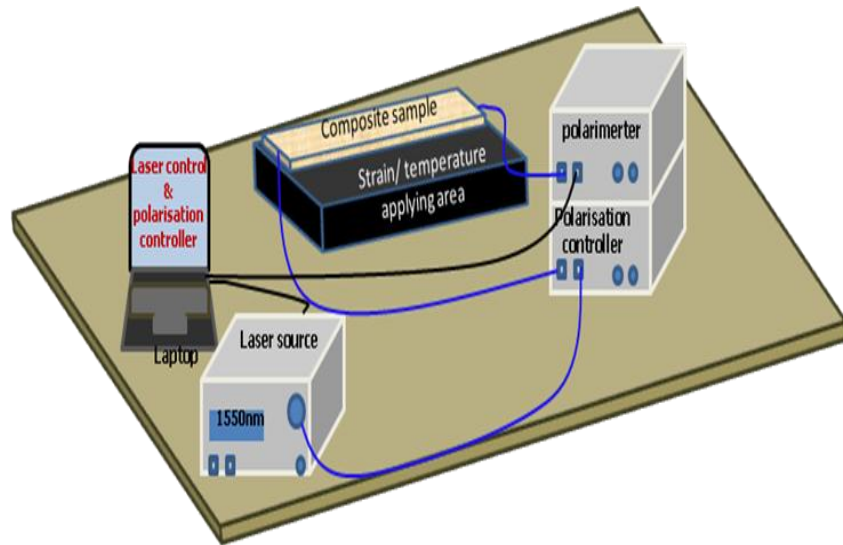


Figure 4.3. Schematic of the experimental arrangement for composite material sample with embedded polarimetric sensors

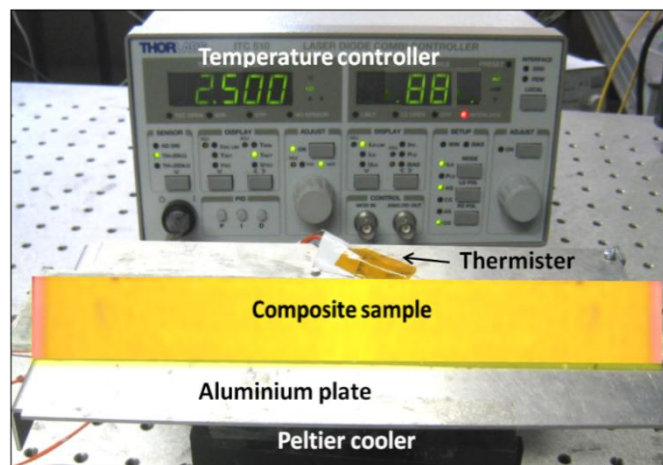


Figure 4.4. Experimental setup to apply temperature changes to the composite material sample.

In this study it is necessary to find the volume fractions of the reinforcement fibres, of moisture and of volatile solvents. The Thermo Gravimetric Analysis (TGA) method [4.27] measures the amount and rate of change in the weight of a material as a function of temperature due to decomposition, oxidation, or dehydration in a

controlled atmosphere at temperatures up to 1000°C. The decomposition temperature of reinforcement fiber fabrics is above 800°C and the resin polymers decompose around 400°C [4.28]. Thus the decomposed weight below 800°C gives the amount of resin in the composite sample. In TGA results, the rate of change in the weight loss with temperature below 150°C indicate mostly indicate the moisture/volatile solvents content [4.27] in the composite sample. In the present study since the sensors are operating in the temperature range below 150 °C and by using TGA any absorbed or excess moisture/ volatile contents with in composite can be observed as weight loss associated with decomposition. In this work a TGA system, Q500 from TA Instruments, with a precision of $\pm 0.1\%$, is used for an accurate determination of the reinforcement fiber volume fraction and thermal stability of composite sample specimens.

4.1.5 Results and discussion

A. Thermal elongation induced strain measurement using HB-PM-PCF

A comparison of the temperature response of buffer stripped and acrylate coated HB-PM-PCF polarimetric fiber sensors in free space and embedded in the composite material are was conducted and published previously [4.22]. From these results it can be concluded that a buffer stripped polarimetric sensor which is temperature insensitive in free space shows a significant increase in its temperature response when embedded in the composite material as shown in Table 4.2. However, the source and implications of this increased response have not been analyzed to date.

To investigate the capability of stripped HB-PM-PCF sensors to differentiate the

thermo- mechanical elongations in different types of composite materials, two identical buffer stripped HB-PM-PCF sensors are embedded in a carbon-epoxy and E glass-epoxy composite specimens and the responses of the sensors are compared in the temperature range from 0⁰C to 65⁰C. A linear variation of the phase shift with temperature is observed over the range from 0⁰C to 65⁰C, in each of the composite specimens as shown in Figure 4.5. Over multiple observations of a cycle of heating followed by cooling, no hysteresis in the measured phase shift was detected. This is reasonable as the 0–65 ⁰C experimental temperature range lies in the linear thermal expansion region of the composite material, given that the glass transition temperature of the particular cured resin is above 150 ⁰C [4.22].

Table 4.2. Comparison of sensitivity to temperature variation for stripped and non-stripped HB-PM-PCF in free space and after embedding in to E glass-unsaturated polyester composite sample.

HB-PM-PCF	free space	after embedding
stripped	0.00002	0.2578
non-stripped	0.01108	0.01086

As discussed in Section 4.1.2 the residual strain and excess moisture content expansion also contributes towards the total thermal elongation. In practical applications, it was found that the maximum moisture absorption (M_{∞}) values for carbon-epoxy, E glass-epoxy, and E glass-unsaturated polyester resin based composites materials are 0.65 %, 0.87% and 0.50% caused by 3.5 days hygrothermic exposure at 95% RH & 50 ⁰C [4.29]. It should be noted that a more detailed treatment of the contribution of moisture content to the total thermal elongation in composite materials is a complex topic beyond the scope of this present investigation.

However, the composite sample fabrication curing and post curing process are optimized to avoid irregular residual strain due to unevenly distributed residue point within the composite [4.30]. It is likely that the moisture content and its influence on the stripped HB-PM-PCF sensor embedded in composite specimens will be very low but to prove this TGA measurements over the temperature range from 0°C to 65°C are undertaken with the results shown in Figure 4.6.

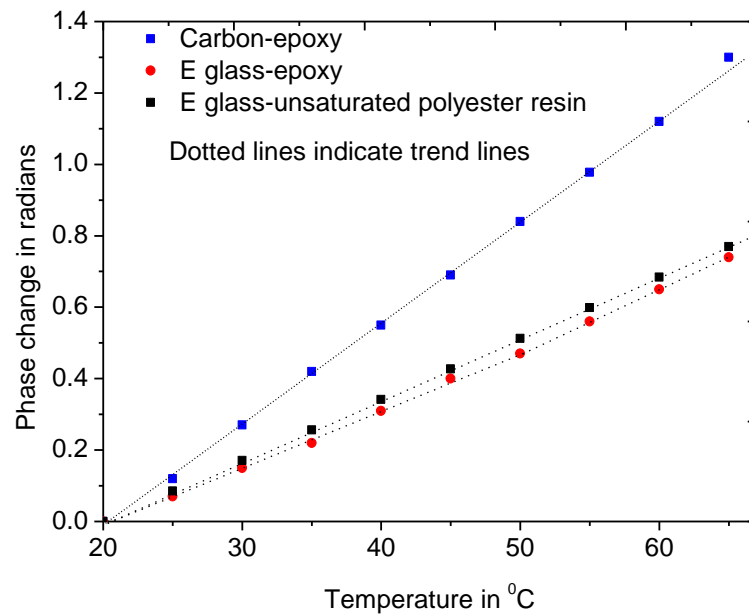


Figure 4.5. Observed phase shift for stripped HB-PM-PCF sensors embedded in different composite samples for temperature variation from 0 to 65 C

It can be seen that the % weight loss for each of the composite samples is indeed very low, with estimated % wt loss values less or equal to 0.02%, 0.01% and 0% for carbon-epoxy, E glass-epoxy, and E glass-unsaturated polyester resin, respectively. Since the percentage of weight loss due to decomposition of the composite constituents is also very low over temperature range 0°C to 65°C , the influence of excess moisture expansion on the buffer-stripped HB-PM-PCF sensor can be neglected. Most commercial composite manufacturing processes are optimized to minimize residual strain and moisture content. The present

investigation provides a simple nondestructive method to determine the thermal expansion for those composite materials having negligible residual strain and moisture expansion. In addition to this, for in-service applications of composite structures subjected to long-term environmental exposure, the method can be adapted to measure valuable information about thermal elongation induced strain in these structures.

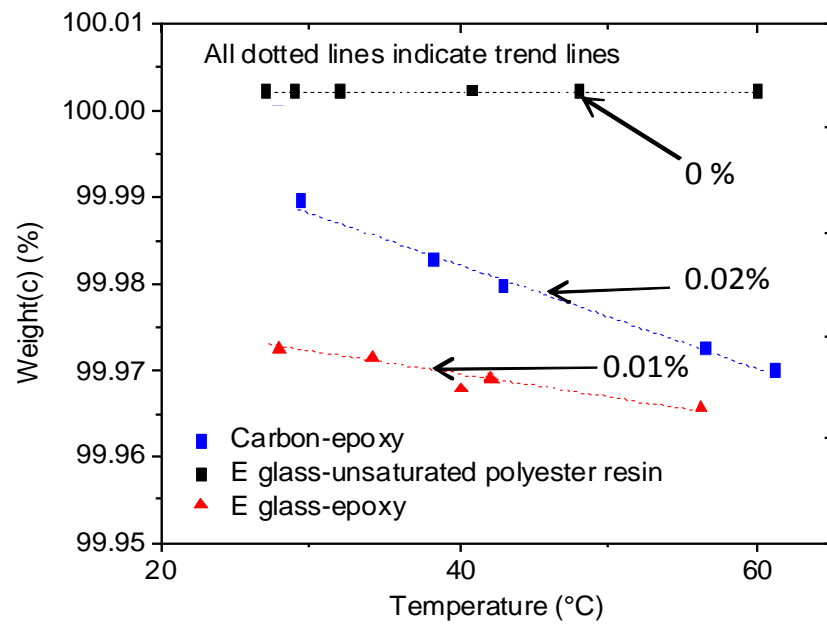


Figure 4.6. TGM measurements data plotted for temperature ranges from 0 to 65 ° C.

The experimental setup utilizes a polarimeter that can accurately detect a phase shift value as low as ± 0.25 degree (or 0.00436 rad). The measured phase shifts and corresponding sensitivities are estimated as 1.3 rad & 0.124 rad/m. $^{\circ}$ C, 0.74 rad & 0.0735 rad/m. $^{\circ}$ C, and 0.7695 rad & 0.0855 rad/m. $^{\circ}$ C for buffer stripped HB-PM-PCF embedded in carbon-epoxy, E glass-epoxy, and E glass-unsaturated polyester resin composite specimens respectively.

In order to convert the measured phase shifts into the equivalent strain values, the strain sensitivity measurements are conducted for buffer stripped HB-PM-PCF sensors in each composite sample at a constant temperature of about 25 $^{\circ}$ C. The

samples are subjected to mechanical stress-induced elongation (ϵ) by applying a deflection at the middle of the sample as detailed in [4.31]. The composite lamination process influences the embedded polarimetric sensor performance [4.32] and thus a strain sensitivity calculation after embedding is essential. Thus the measured strain sensitivities of stripped HB-PM-PCF sensors embedded in carbon-epoxy, E glass-epoxy, and E glass-unsaturated polyester resin composite specimens are 3.39905×10^3 rad/m. ϵ , 4.831518×10^3 rad/m. ϵ , and 3.53093×10^3 rad/m. ϵ respectively.

As described in section 4.1.2 the resultant thermal elongation induced strain on the buffer stripped HB-PM-PCF sensor embedded in the composite materials is calculated by knowing the values of the thermal elongation induced phase shift and strain sensitivity of buffer stripped HB-PM-PCF and the values are presented in Table 4.3.

Table 4.3. Experimental thermal expansion induced phase shift, Strain sensitivity and corresponding thermal expansion coefficient.

Material	Thermal expansion induced phase shift $\Delta\Phi_T$ (rad/m. $^{\circ}\text{C}$)	Strain sensitivity S_{ϵ} (rad/m. ϵ)	Thermal strain of PCF/ Thermal expansion(CTE) α_s^m ($\epsilon/^{\circ}\text{C}$)
Carbon-Epoxy	0.124	3.39905×10^3	3.648×10^{-5}
E glass-Epoxy	0.0735	4.831518×10^3	1.52×10^{-5}
E glass-Unsaturated polyester	0.0855	3.53093×10^3	2.42×10^{-5}

The values of the thermal elongation induced strain on the buffer stripped HB-PM-PCF embedded in carbon-epoxy, E glass-epoxy, and E glass-unsaturated polyester resin composite specimens calculated using this method are $3.648 \times 10^{-5} \epsilon/^{\circ}\text{C}$, $1.52 \times 10^{-5} \epsilon/^{\circ}\text{C}$, and $2.42 \times 10^{-5} \epsilon/^{\circ}\text{C}$ respectively.

B. Modeling of the thermal behavior and comparison with experimental

For the purpose of comparison, the thermal behavior of composite materials can be predicted from the elastic and thermal properties of reinforcement fibers and the matrix material. For modeling of the thermal expansion coefficients the values of the mechanical properties of the reinforcement fibers/ matrices that are obtained from the manufacturer's data sheet together with the fiber volume fraction obtained from the TGA measurements are used, as detailed in Table 4.4(a) and 4.4(b). From TGA results as shown in Figure 4.7, TGA results the V_f values can be estimated as 0.64, 0.69 and 0.47 for carbon-epoxy, E glass-epoxy, E glass-unsaturated polyester resin respectively. In this, theoretical thermal expansion coefficient calculations are carried out using a Classical Laminate Theory (CLT) based composite analysis Matlab tool [4.33, 4.34]. In composite materials the thermal elongations due to thermal expansion are due to the two coefficients of thermal expansion (CTE), longitudinal CTE and transverse CTE. In the direction of the reinforcement fibers, the contribution to the thermal expansion is dominated by the fibers, and the direction perpendicular to the fibers, the contribution to the thermal expansion is dominated by the matrix material [4.35, 4.36]. The theoretically estimated Longitudinal CTE and Transverse CTE of the carbon-epoxy, E glass-epoxy, E glass-unsaturated polyester resin composite specimens are given in Figure 4.8.

The thermal elongation induced strain measured by the buffer-stripped HB-PM-PCF sensor in the carbon reinforced composite is higher than that of either E glass-epoxy samples because of the higher thermal expansion coefficients of the particular carbon fiber used. The fiber volume fraction is higher in the case of E-glass (69%) - epoxy composite compared to the E-glass (47%) - unsaturated

polyester resin composite, resulting in the latter having a higher transverse CTE.

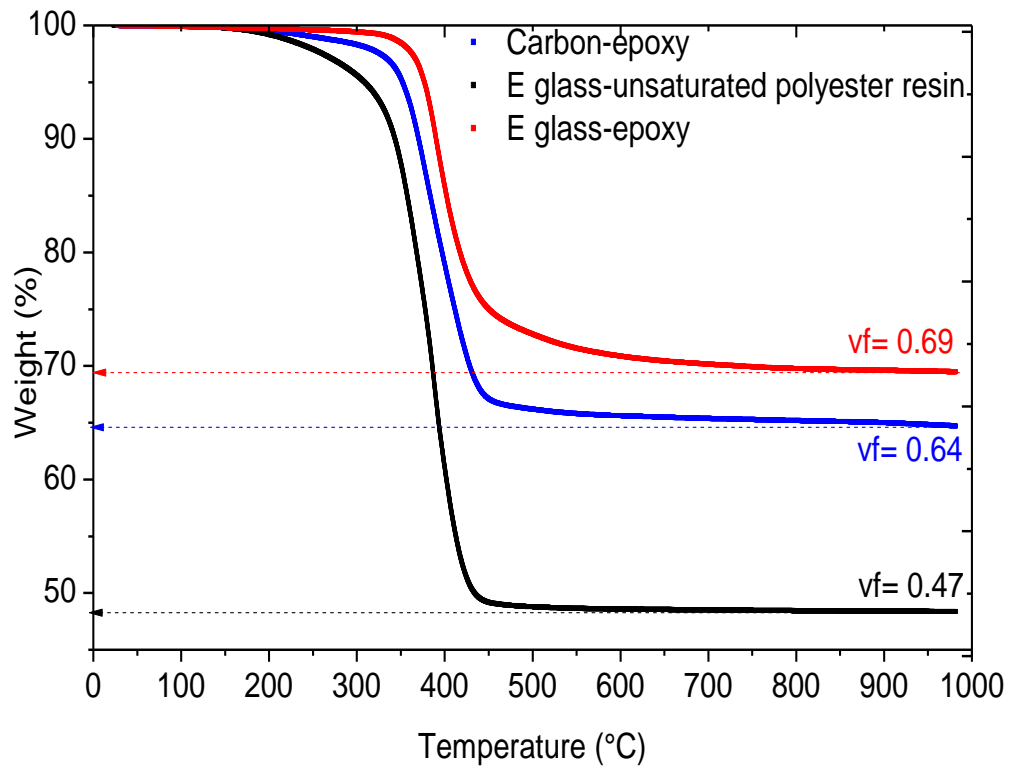


Figure 4.7. TGM measurements of composite samples over temperature range 0–1000 °C.

Table 4.4(a). The Physical properties of reinforcement fibre

Fibre type	E_{lf} (Gpa)	E_{tf} (Gpa)	ν_{12}	$\alpha_{lf} \times 10^{-7}$ (m/m/°C)	$\alpha_{tf} \times 10^{-5}$ (m/m/°C)
Carbon	129	12	0.4	-5.40	3.51
E glass	72.4	72.3	0.28	5.40	1.00

Table 4.4(b). The physical properties of reinforcement matrix.

Composite material	Physical properties of matrix				Fiber volume fraction V_f
	E_m (Gpa)	ν_m	$\alpha_m \times 10^{-5}$ (m/m/°C)	V_m	
Carbon-Epoxy	5.1	0.36	3.55	0.36	0.64
E glass-Epoxy	4.62	0.33	2.145	0.31	0.69
E glass -	4.6	0.36	3.08	0.53	0.47

Unsaturated polyester					
-----------------------	--	--	--	--	--

From the theoretical thermal expansion calculations for the three types of composite specimens (carbon-epoxy, E glass-epoxy, E glass-unsaturated polyester resin composite samples), it was found that for all the samples the CTE along the transverse axis to the reinforcement fibers is highest since along this axis the influence from the reinforcement fibers is the smallest. The longitudinal plane CTE component is significantly lower due to the much higher influence of the reinforcement fibers along the longitudinal axis [4.37].

From the comparison shown in Figure 4.8, it can be seen that the experimental results are in agreement with theoretically estimated transverse CTEs. Although the buffer stripped HB-PM-PCF is sensitive to both transverse and longitudinal thermal deformations, there is negligible contribution from the latter, since the longitudinal CTE component is 10 orders of magnitude lower than that for the transverse CTE component as shown in Figure 4.8.

Thus in summary, it can be concluded that a buffer stripped HB-PM-PCF polarimetric fiber sensor is a suitable candidate for measurement of thermal expansion in composite structures for practical applications.

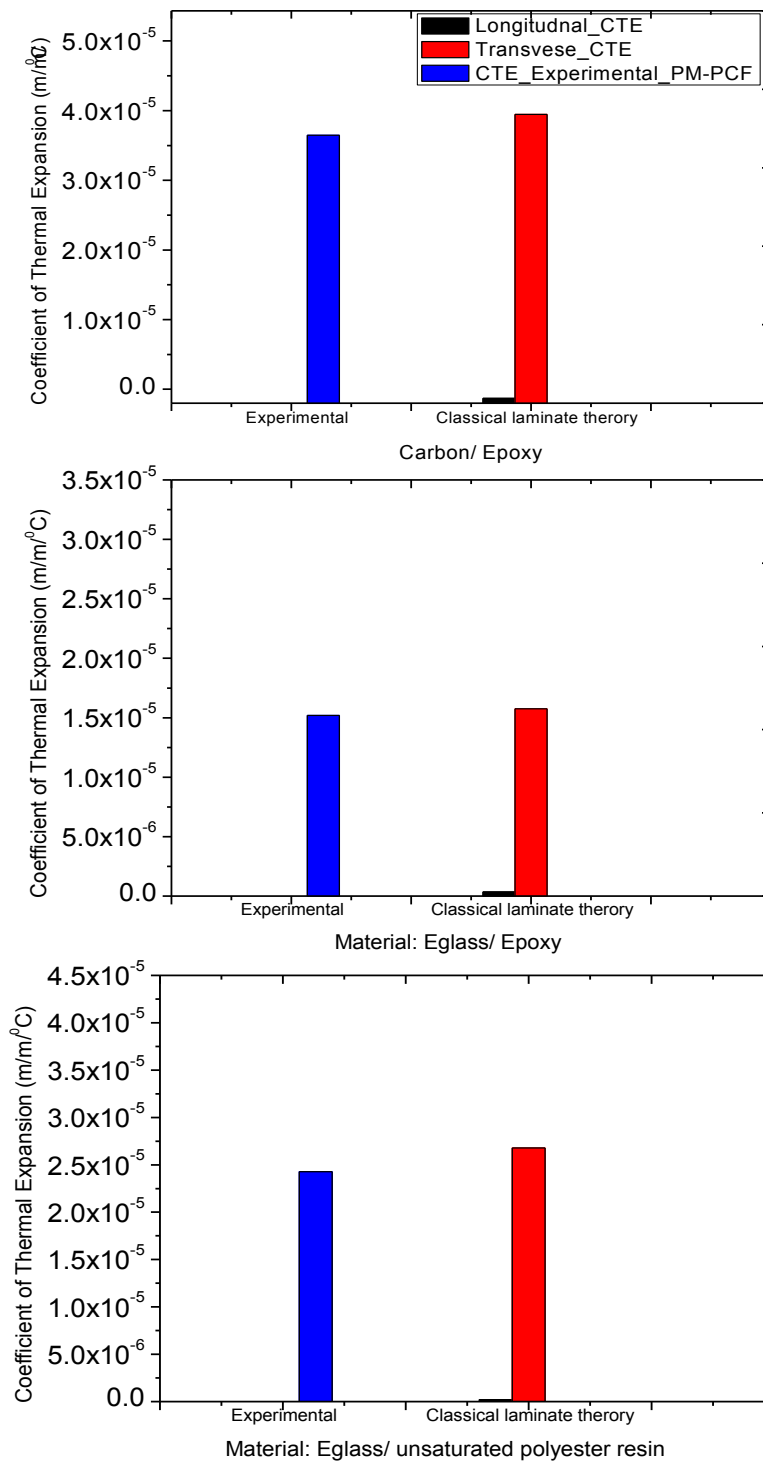


Figure 4.8. Comparison of theoretical predictions with experiment, (a) carbon-epoxy, (b) E glass-epoxy, and (c) E glass-unsaturated polyester resin composite samples.

Given that the sensor gauge length and the sample size used in this study are comparable, the measured thermal elongation induced strain is the average of

thermal strain effectively applied over the sensor region, which is mainly contributed by transverse CTE due to specific characteristics of composite-reinforcement/ matrices chosen for this study. However, in larger composite parts using similar sensors it should be possible to measure thermal expansion at multiple points. The advantages of this type of fiber sensor is that the observed phase change is independent of temperature changes in the composite and exhibits a sensitivity only due to the stress induced from the thermal elongation of the host composite material and thus the thermal strain information can be extracted more accurately than by using temperature cross sensitive sensor types. Potential applications of this sensor are in dental composites, and aircraft composites for selecting materials with a lower thermal strain over the operating temperature range of interest

4.1.6 Conclusion

The measurement of thermal expansion for different types of carbon and glass fiber-reinforced composite materials using embedded optical fiber sensors is reported in this chapter. The embedded HB-PM-PCF sensors successfully detected the thermal elongation induced strain of the host composite materials. The experimentally observed thermal elongation induced strain values of the buffer-stripped HB-PM-PCF embedded in carbon-epoxy, E glass-epoxy, and E glass-unsaturated polyester resin composite specimens are $3.648 \times 10^{-5} \text{ } \epsilon / ^\circ\text{C}$, $1.52 \times 10^{-5} \text{ } \epsilon / ^\circ\text{C}$, and $2.42 \times 10^{-5} \text{ } \epsilon / ^\circ\text{C}$ respectively. A numerical analysis of the coefficient of thermal expansion for the composites was conducted. The CTE values from the numerical analysis correlated well with those from experiments. The stripped HB-PM-PCF sensors showed a higher temperature response in the carbon fibre

reinforced composite material when compared to that of the E-glass fibre reinforced composites because carbon fiber reinforced composites have higher transverse thermal expansion coefficients. From the result⁸ one can conclude that more accurate determination of thermal expansion is possible by eliminating residual strain and moisture expansion. The practical applications of thermal expansion measurement using buffer stripped HB-PM-PCF lie in aeronautical and helicopter structures.

4.1.7 Reference

- 4.1 D. P. Garg, M. A. Zikry, G. L. Anderson, X. E. Gros. "Current and potential future research activities in adaptive structures: an ARO perspective." *Smart Mater. Struct.* 10, 610-623, 2001.
- 4.2 D. D. L. Chung "Composite Materials: Science and Applications." 2nd Edition, Springer Publications, 2010.
- 4.3 M. Grassi, X. Zhang and M. Meo. "Prediction of stiffness and stresses in Z-fiber reinforced composite laminates." *Composite Part A: applied science and manufacturing* 33, 1653-1664, 2002.
- 4.4 X. E. Gros. "Current and Future Trends in Non-Destructive testing of Composite Materials" *Ann. Chim. Sci. Mat* 25, 539-544, 2000.
- 4.5 V. Dewynter-Marty, P. Ferdinand. "Embedded fiber Bragg grating sensors for industrial composite cure monitoring." *Journal of Intelligent Materials Systems and Structures* 9, 785-787, 1998.

⁸ Some of the data presented here is from Corrigendum to "Measurement of thermal elongation induced strain of a composite material using a polarization maintaining photonic crystal fiber sensor", *Sensors and Actuators A: Physical*, Volume 201, Pages 504-5.5, 2013.

- 4.6 J. D. James, J. A. Spittle *et al.* “A review of measurement techniques for the thermal expansion coefficient of metals and alloys at elevated temperatures.” Meas. Sci. Technol. 12, 1-15, 2001.
- 4.7 V. T. Cherepin. “Experimental techniques in physical metallurgy.” (Experimental’ naya Tekhnika v Fizicheskoy Metallovedenii), (Kiev: Tekhnika) p200 (in Russian), 1968.
- 4.8 V. G. Badami and M. Linder. “Ultra-high accuracy measurement of the coefficient of thermal expansion for ultra-low expansion materials.” Proc. SPIE, 4688 469–80, 2002.
- 4.9 E. B. Hughes. “Measurement of the linear thermal expansion coefficient of gauge blocks by interferometry.” Proc. SPIE 2088 179–893, 1993.
- 4.10 J. Cordero, T. Heinrich, T. Schuldt, M. Ghlke, S. Lucarelli, D. Weise, U. Johann and C. Braxmaier. “Interferometry based high-precision dilatometry for dimensional characterization of highly stable materials.” Measurement Science and Technology 20, 095301, 2009.
- 4.11 Y. Fan and M. Kahrizi. “Characterization of a FBG strain gage array embedded in composite structure.” Sensors and Actuators A 121, 297-305, 2005.
- 4.12 B. A. Tahir, J. Ali and R. A. Rahman. “Strain Measurements Using Fibre Bragg Grating Sensors.” American Journal of Applied Science (Special Issue): 40-48, 2005.
- 4.13 K. O. Hill and G. Meltz. “Fiber Bragg grating technology fundamentals and overview” J. Lightwave. Technol. 15, 1263–76, 1997.
- 4.14 Y. L. Lo and H. S. Chuang. “Measurement of thermal expansion coefficients using an in-fibre Bragg-grating sensor.” Meas. Sci. Technol. 9, 1543–7, 1998.

- 4.15 M. Mulle, R. Zitoune, F. Collombet, P. Oliver and Y. H. Grunevald. "Thermal expansion of carbon–epoxy laminates measured with embedded FBGs—comparison with other experimental techniques and numerical simulation." *Composites Part A*, 38, 1414–1424, 2007.
- 4.16 H. Kim, J. Yoon, H. Kim and J. H. Han. "Measurement of the thermal expansion of space structures using fiber Bragg grating sensors and displacement measuring interferometers." *IOP, Meas. Sci. Technol* 21, 085704 - 085713, 2010.
- 4.17 H. I. Kim, J. S. Youn and J. H. Han. "Transverse Strain Effects on the Measurement of the Thermal Expansion of Composite Structure using Surface Mounted Fiber Bragg Grating Sensors." *Journal of Intelligent Material Systems and Structures* 22, 1141-1147, 2011.
- 4.18 V. M. Murukeshan, P. Y. Chan, O. L. Seng and A. Asundi. "On-line health monitoring of smart composite structures using fiber polarimetric sensor." *Smart Mater. Struct* 8, 544-548, 1999.
- 4.19 H. A. Asundi. "Performance analysis of all-fiber polarimetric strain sensor for composites structural health monitoring." *NDT&E International* 39, 320-327, 2007.
- 4.20 X. Dong and H. Y. Tam. "Temperature-insensitive strain sensor with polarization maintaining photonic crystal fiber based Sagnac interferometer." *Applied Physics Letters* 90, 151113-3, 2007.
- 4.21 G. Rajan, K. Mileńko, P. Lesiak, Y. Semenova, A. Boczkowska, M. Ramakrishnan, K. Jędrzejewski, A. Domański, T. Woliński and G. Farrell. "A hybrid fiber optic sensing system for simultaneous strain and temperature

- measurement and its applications.” *Photonics Letters of Poland* 2, 46-48, 2010.
- 4.22 M. Ramakrishnan, G. Rajan. Y. Semenova, et al. “The influence of thermal expansion of a composite material on embedded polarimetric sensors.” *Smart Mater. Struct* 20, 125002 - 125009, 2011.
 - 4.23 A. Rudajevova, S. K u ´dela Jr., S. K u ´dela, P. Luka ´c. “Anisotropy of the thermal expansion in Mg fibre composites.” *Scripta Materialia* 53, 1417–1420, 2005.
 - 4.24 D. H. Kim, and J. U. Kang. “Analysis of temperature-dependent birefringence of a polarization-maintaining photonic crystal fiber.” *Opt. Engg* 46, 1, 2007.
 - 4.25 T. R. Wolinski, P. Lesiak, A. W. Domanski. “ Polarimetric optical fiber sensors of a new generation for industrial applications.” *Bulletin Of The Polish Academy Of Sciences Technical Sciences* 56, No. 2, 2008.
 - 4.26 B. Wojciech, G. Paweł and K. Jerzy. “Application of Optical Fibre Sensors to Measuring the Mechanical Properties of Composite Materials and Structures.” *Advances in Composite Materials - Ecodesign and Analysis*, ISBN: 978-953-307-150-3, 2011.
 - 4.27 ASTM Standard D 3171-99. “Standard Test Methods for Constituent Content of Composite Materials.” *American Society for Testing and Materials*, West Conshohocken, PA, USA, 2004.
 - 4.28 J. K. Park, T. J. Kang. “Thermal and ablative properties of low temperature carbon fiber–phenol formaldehyde resin composites.” *Carbon* 40, 2125–2134, 2002.

- 4.29 M. Sreejith, H. N. Narasimha Murthy, K. S Rai, M. Krishna, S. C Sharma, J. K. Jeena. "Hygrothermic behavior of carbon/vinylester, glass/vinylester, carbon/epoxy and glass/epoxy composites." *Iranian Polymer Journal* 19, 89-103, 2010.
- 4.30 P. Vaddadi, T. Nakamura and R. P. Singh. "Inverse Analysis to Determine Hygrothermal Properties in Fiber Reinforced Composites." *Journal of Composite Materials* 41, No. 3, 2007.
- 4.31 T. R. Woliński, P. Lesiak, R. Plaga, M. Szeląg, *et.al.* "Stress induced in optical fiber sensors embedded in composite materials by the lamination process." *International conference proceedings*, ID: 87483, *Metrologia* 2001, Brazil.
- 4.32 P. Lesiak, A. Boczkowska, D. Budaszewski *et al.* "Influence of the lamination process on the strain sensitivity of the fiber sensors embedded in composite materials." *Proc. SPIE* 7753, 77534, 2011.
- 4.33 L. Aydin, H. S. Artem. "Multiobjective genetic algorithm optimization of the composite laminates as a satellite structure material for coefficient of thermal expansion an elastic modulus." *IEEE* 978-1-4244-3628-6/09, 2009.
- 4.34 Z H. Karadeniz, D. Kumlutas. "A numerical study on the coefficients of thermal expansion of fiber reinforced composite materials." *Composite Structures* 78, 1 - 10, 2007.
- 4.35 R. L. Rich and J. Gaudin. "Design of dimensionally stable composites by evolutionary optimization." *Compos. Struct.* 41, 97–111, 1998.
- 4.36 C. C. Chamis. "Simplified Composite Micromechanics Equations for Hygral, Thermal and Mechanical properties." *SAMPE Quarterly*, 14 – 23, 1984.

- 4.37 X. Deng & N. Chawla. “Three-dimensional (3D) modeling of the thermoelastic behavior of woven glass fiber-reinforced resin matrix composites.” *J Mater Sci* 43:6468–6472,2008.

Chapter 5

A multi parameter Hybrid Fiber Optic Sensor System and Miniaturized Interrogator for Composite Structural Health Monitoring Applications

As it was discussed in Chapter 3, thermal expansion of a composite material is the main source of errors during strain measurements using embedded polarimetric fiber sensors and for more accurate axial strain measurements a buffer coated PM-PCF polarimetric fiber sensor is recommended. It was also shown in Chapter 3 that a buffer stripped HB-PM-PCF polarimetric sensor shows a significant phase change, when embedded in the composite material, due to thermally induced elongation of the composite material, which in turn can induce errors during axial strain measurements using such a stripped HB-PM-PCF sensor. A useful consequence however of the research presented in Chapter 3 is that a stripped HB-PM-PCF polarimetric sensor fiber can be used to quantify thermal elongation induced strain within a composite material. Thus in Chapter 4, a sensor was demonstrated for measurements of thermally induced strain within a composite material, based on a stripped HB-PM-PCF fiber.

Additionally, the investigations in Chapters 3 & 4 open the possibility of developing a novel hybrid sensor for simultaneous measurement of axial strain,

temperature and thermal strain inside a composite material, by combining the buffer coated and buffer stripped HB-PM-PCF polarimetric sensors together with an FBG sensor. This chapter presents an investigation of such a novel hybrid sensor configuration which has not been investigated previously. The sensor operates in the intensity domain by converting the polarization and wavelength information from the polarimetric sensors and the FBG respectively, into detectable intensity variations by using an interrogation scheme comprising of an Electro-Optic (EO) modulator for interrogation of the polarimetric sensor and a Thin Film Filter (TFF) for the FBG sensor. Thus the proposed sensor configuration not only provides simultaneous measurement of axial strain, temperature and thermal strain inside the composite material but also allows for the analysis of data from all the three types of sensors in a common intensity domain. This in turn eliminates the need to provide complex interrogation modules working in different domains (that is intensity, wavelength and phase) for the extraction of sensing parameters.

Sensing of composite materials employed in aerospace components and other similar applications such as in wind turbines frequently involves embedding the fiber sensors in composite parts which are in constant motion. In such applications fiber based connections to an interrogation system mounted remotely are difficult to implement. An alternative is the use of a compact interrogator mounted with the composite part itself, utilizing a wireless approach for communication with the end user. In such cases, a flexible compact integrated interrogation unit with the capability of being embedded into the composite part can provide a portable dynamic sensing system. A fully embedded ultra thin flexible sensing system has been demonstrated [5.1], which was comprised of a single Vertical-Cavity Surface-Emitting Laser (VCSEL), a fiber sensor and a photodetector chip. In future to

realise a fully embeddable hybrid sensing system, the interrogator unit for the hybrid sensor system may need to be designed using flexible rather than rigid waveguides and devices, to allow for embedding in the composite part. Therefore this chapter is also focused on the design, simulation and implementation of a miniaturized flexible interrogator for the hybrid sensing scheme which comprises of an Arrayed Waveguide Grating (AWG) for FBG demodulation and an Electro Optic Mach - Zehnder Interferometric (EO - MZI) intensity modulator. The compact film-type interrogation module with dimensions of 3.4 cm x 0.1 cm x 0.01 cm can be attached to the surface of a composite material or could even be embedded in the material.

In summary then the first objective of the research described in this chapter is to demonstrate a novel hybrid sensor configuration by combining several sensors for simultaneous measurement of strain, temperature and thermal strain in a composite material. The second objective of this chapter is to demonstrate a means of implementing a common intensity domain interrogation scheme for the hybrid sensor. The last objective of this chapter is to describe the design of a miniaturized thin film type interrogator for future SHM applications of the proposed hybrid sensor.

5.1 Hybrid fiber optic sensor system for measuring the strain, temperature and thermal strain of composite materials ⁹

⁹ Manjusha Ramakrishnan, Ginu Rajan, Yuliya Semenova, Gerald Farrell, “Hybrid fiber optic sensor system for measuring the strain, temperature and thermal strain of composite materials”,

Keyword Hybrid sensor; polarimetric sensor; fiber Bragg grating; polarization maintaining - photonic crystal fiber; composite material

Abstract: This work proposes a hybrid optical fiber sensor system for simultaneously sensing the strain, temperature, and thermal strain of composite materials. The hybrid fiber optic sensor system involves a combination of three sensors: a polarimetric sensor based on an acrylate coated polarization maintaining photonic crystal fiber (HB-PM-PCF), a coating stripped HB-PM-PCF sensor and a fiber Bragg grating sensor (FBG). Temperature is sensed using the FBG sensor, axial strain is sensed using the acrylate coated HB-PM-PCF sensor and thermal strain is sensed using the coating stripped HB-PM-PCF. The hybrid sensor system presented operates in the intensity domain by converting the polarization and wavelength information from the polarimetric sensors and the FBG respectively into detectable linear intensity variations. Subsequently by deriving a characteristic matrix for the hybrid sensors, information about temperature, axial strain and thermal strain can be simultaneously determined. An experimental demonstration of the hybrid sensor system is described based on a glass fibre reinforced composite material sample within which the three different sensors are embedded. The proposed sensor configuration can be employed in composite material structural health monitoring (SHM) applications.

5.1.1 Introduction

Optical Fiber sensing (OFS) based measurement of temperature and strain have great potential for application in the structural health monitoring of composite

materials [5.2]. The most widely used OFS type used for strain and temperature measurement in composite materials are fiber Bragg grating (FBG) sensors [5.3]. However, the main disadvantage of employing FBGs as strain and temperature sensors is their high intrinsic temperature cross-sensitivity. Some sensors are intrinsically temperature insensitive, for example Highly Birefringent (HB) polarization-maintaining (PM) fiber based polarimetric sensors can be made temperature insensitive but the measurement of strain requires a means of setting a zero strain reference.

The most common approach to providing temperature measurement for reference purposes or a reference for zero strain involves the use of a second fiber optic sensor. This is commonly referred to as “hybrid sensing”. Many of the hybrid sensing approaches reported to date use combinations of FBGs with various types of sensor such as a long period grating (LPG) [5.4, 5.5], Fabry-Perot interferometer sensor [5.6], photonic crystal fiber (PCF) modal interferometer [5.7], and a fiber loop mirror using a small core micro-structured fiber [5.8]. Sensors based on gratings written in micro structured fibers have also been reported for discrimination between strain and temperature [5.9]. We have previously reported a hybrid approach which involves an FBG sensor and a HB-PM-PCF polarimetric sensor for simultaneous measurement of strain and temperature [5.10].

In the case of OFS embedded in composite structures, a further complication is the influence of thermally induced strain in the composite material. It has been reported earlier that for FBGs written in micro structured fibers exhibits two Bragg peaks due to thermally induced strain of the composite materials [5.11]. We have previously reported that the temperature sensitivity of polarimetric sensors is significantly influenced by the thermally induced strain in composite materials

[5.12] and that this thermally induced strain in the composite material can be measured using a stripped HB-PM-PCF sensor [5.13]

In this paper we propose a new method for simultaneous measurement of applied strain, temperature and thermally induced strain by using a hybrid approach which involves a combination of three different sensors: a polarimetric sensor based on an acrylate coated PM-PCF, a coating stripped HB-PM-PCF, and a fiber Bragg grating sensor. The proposed hybrid sensing scheme provides simultaneous measurement of strain, temperature, and thermally induced strain. The first sensor is a buffer stripped HB-PM-PCF which is insensitive to temperature in free space, but once embedded in a composite material it is affected by the thermal expansion of the composite and therefore is capable of measuring thermally induced strain [5.12]. The second sensor is a buffer coated HB-PM-PCF which is insensitive to thermally induced strain and thus can be used for measurements of external applied strain independently from temperature [5.13]. A third sensor, an FBG, is used for composite material temperature measurements only. An added advantage of a HB-PM-PCF based sensing scheme is that HB-PM-PCFs can offer a linear response [5.14] for a wider range of applied strain by comparison to conventional PM fibers. This novel hybrid approach to sensing has not been exploited before and overcomes the limitations of the individual sensors to implement simultaneous and independent measurement of three different parameters. The principle of operation of the proposed hybrid sensing approach and its experimental demonstration for measurement of strain, temperature and thermally induced strain parameters of a glass reinforced composite material are presented in the following sections.

5.1.2 Principle of operation

In polarimetric fiber sensing [5.14], a symmetric deformation effect in a single-mode fiber influences the propagation constant (β) for every mode because of changes in the fiber length (L) and the refractive indices of the core and the cladding. Under the influence of longitudinal strain (ε) at a constant temperature, for polarimetric sensors the change in the phase difference can be written as,

$$\delta(\Delta\Phi) = \frac{\partial(\Delta\beta)}{\partial\varepsilon} \delta L \quad 5.1$$

HB-PM-PCFs have been proven to be temperature insensitive in free space [5.14] and hence the phase change in such a polarimetric sensor will only originate from the temperature induced strain.

The strain sensitivity of such a HB-PM-PCF of length L can be written as [5.13],

$$S_\varepsilon = \frac{2\pi}{T_\varepsilon L} [\text{rad} / m\varepsilon.m] \quad 5.2$$

where T_ε is an experimental parameter describing the amount of strain required to induce a 2π phase shift of the polarized light.

For an acrylate buffer coated HB-PM-PCFs embedded in the composite material the influence to thermally induced strain is negligible [5.13]. This is due to the fact the transverse CTE induced non uniform strain transfer [5.16] is apparently eliminated due to the presence of the buffer coating. However, a buffer stripped fibre is sensitive to both applied longitudinal strain ε (equation 5.1), and thermal strain ε_{TL} . The dependence of strain measurement on the presence or absence of a buffer layer on HB-PM-PCF fibre embedded in a composite material allows one to distinguish between applied strain and thermally induced strain.

The method for measurement of thermally induced strain using a buffer stripped

HB-PM-PCF is explained in our earlier paper [5.14], which shows that the thermal strain ε_{TL} at zero applied mechanical strain, can be calculated as,

$$\varepsilon_{TL} = \frac{\Delta\Phi_T}{S_\varepsilon} \quad 5.3$$

where $\Delta\Phi_T$ is the observed phase change in radians per unit length per unit temperature and S_ε is the strain sensitivity of the HB-PM-PCF sensor embedded in the composite material.

In general, for polarimetric sensors the change in the output intensity at a wavelength λ due to externally applied longitudinal strain can be described by the formula,

$$I_s(\lambda) = \frac{I_0}{2} [1 + \cos(\Delta\Phi)] \quad 5.4$$

It is possible to select the operating point of the HB-PM-PCF polarimetric sensor in the linearly varying quadrature region with the help of a polarizer-analyzer arrangement. This is to guarantee a linear response for the HB-PM-PCF polarimetric sensor for a wide range of applied strains.

To obtain the temperature information, an FBG sensor is proposed as a complementary sensor to the polarimetric sensors. The schematic of the proposed hybrid polarimetric-FBG sensor system is shown in Figure 5.1.

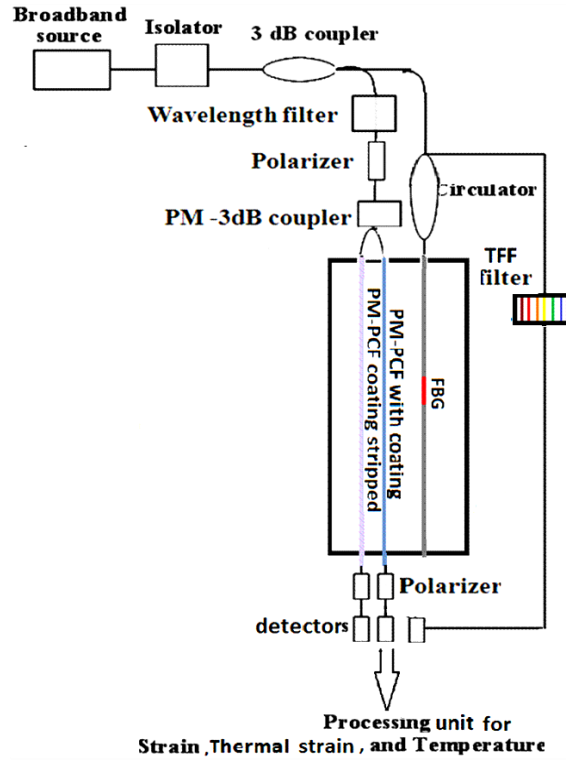


Figure 5.1. Schematic of the hybrid polarimetric-FBG sensor system

The Bragg wavelength of an FBG is given by the expression,

$$\lambda_B = 2n_{eff}\Lambda \quad 5.5$$

where n_{eff} is the effective refractive index of the fiber core and Λ is the grating pitch.

The shift in Bragg Wavelength with strain and temperature can be expressed using,

$$\Delta\lambda_B = 2n_{eff}\Lambda \left\{ \left(1 - \frac{n^2}{2} [P_{12} - \nu(P_{11} + P_{12})] \right) \varepsilon + \left[\alpha + \frac{dn_{eff}/dT}{n_{eff}} \right] \Delta T \right\} \quad 5.6$$

Where ε is the applied strain, $P_{i,j}$ is the Pockel's coefficients of the stress-optic tensor, ν is the Poisson's ratio, α is the coefficient of thermal expansion of specimen and ΔT is the temperature change. Equation 5.6 indicates that both applied mechanical strain, temperature and thermal expansion of the specimen contribute towards Bragg peak wavelength shift.

During temperature measurements of composite materials using embedded FBGs,

the buffer coating of FBGs also plays an important role. For example, it is reported that for coating stripped FBGs, the transverse CTE of composite material can cause non uniform lateral strain, which in turn induces a birefringence and hence peak distortion and broadening [5.16]. However, such peak distortion is not visible in the case of the polyimide coated FBGs embedded in E-glass fibre reinforced composite materials [5.17], supporting the conclusion that the non-uniform lateral strain distribution caused by the transverse CTE of the composite material is eliminated due to the presence of a buffer coating. However, an elevated temperature sensitivity is reported [5.17] due to the additional mechanical strain induced by the CTE of the composite material. In the present hybrid sensing scheme, we employ a polyimide coated FBG for which the Bragg wavelength shifts with both strain and temperature, where the temperature shift is a result of the inherent temperature sensitivity of the FBG plus CTE induced temperature sensitivity.

In the hybrid sensing scheme presented here operating in intensity domain, the FBG wavelength shift due to the strain and temperature is converted into intensity changes by means of a Thin Film Filter (TFF) based FBG interrogator and is explained in detail in our previous work¹⁰ [5.18]. In a TFF based FBG interrogator, the linear edge response region of wavelength filter is designed to overlap the range of peak reflected wavelength variation for the FBG. Thus in the TFF based interrogation scheme, for example when the strain/temperature of the FBG increases, the local peak observed in the superimposed spectral response of the FBG and the edge response region of the wavelength filter, moves towards the

¹⁰ M. Ramakrishnan, G. Rajan, Y. Semenova, T. Wolinski and G. Farrell. "A demodulation scheme for a hybrid fiber sensor system for composite materials", In SPIE Photonics Europe (pp. 843929-843929). International Society for Optics and Photonics, Brussels, Belgium, 2012.

longer wavelength shift region as shown in Figure 5.2. Thus the effective intensity of the peaks changes with changes in the Bragg wavelength following the edge response of the TFF. These changes in intensity, with a suitable calibration, allow one to measure the FBG peak wavelength and thus strain or temperature using only an intensity domain based measurement. For example, when the FBG temperature increases from 30 to 45°C the peak intensity of the spectral response of an FBG increases in line with the edge response of the TFF as shown Figure 5.2.

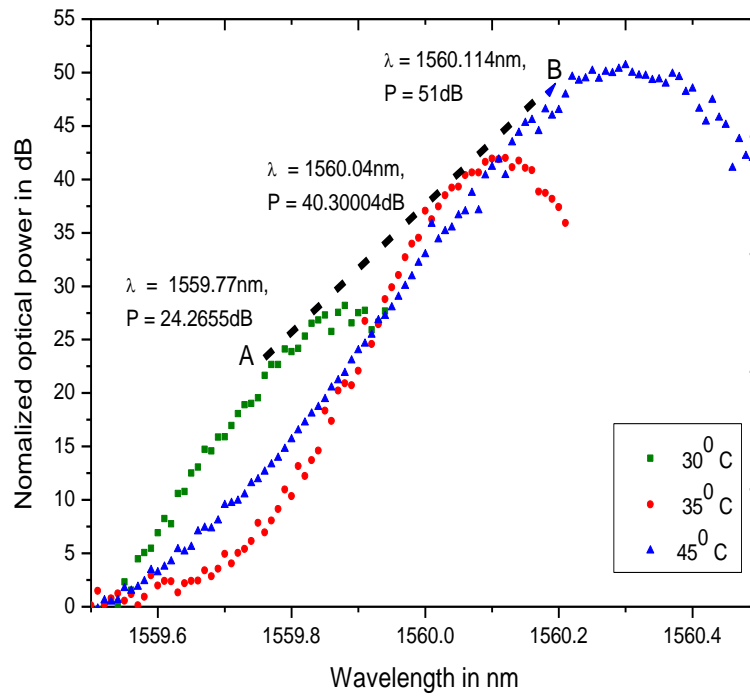


Figure 5.2. Diagram of the super imposed spectral response of an FBG with edge response of TFF at 30°C, 35°C, & 45°C.

The optical intensity of the TFF based demodulation system, which converts the applied strain (ϵ) and temperature (T) information from the FBG sensor into an intensity variation which can be expressed respectively as [5.19]:

$$I_{\epsilon}(\lambda) = I(\lambda_0) + \frac{(I(\lambda_{m\epsilon}) - I(\lambda_0))}{(\lambda_{m\epsilon} - \lambda_0)} (\lambda_{\epsilon} - \lambda_0) \quad 5.7$$

$$I_T(\lambda) = I(\lambda_0) + \frac{(I(\lambda_{mT}) - I(\lambda_0))}{(\lambda_{mT} - \lambda_0)} (\lambda_T - \lambda_0) \quad 5.8$$

where λ_0 is the peak reflected wavelength of the FBG at a constant temperature and zero strain state and $\lambda_{m\varepsilon}$ and λ_{mT} are the wavelengths corresponding to the Bragg peak shifts due to the applied maximum strain and temperature. $I(\lambda_0)$, $I(\lambda_{m\varepsilon})$ and $I(\lambda_{mT})$ are the intensities corresponding to those wavelengths.

From equations 5.7 and 5.8 it is clear that as previously explained the strain and temperature induced wavelength shifts of the reflected signal can be converted into a linear intensity variation within the range of the operating wavelengths.

The responses of FBG sensors and the polarimetric sensors are calibrated for strain and temperature independently. Assume $S_{\varepsilon I}$ is the strain sensitivity for both the stripped and non-stripped HB-PM-PCF polarimetric sensors, $S_{T\varepsilon I}$ is the thermal strain sensitivity of the stripped HB-PM-PCF polarimetric sensor, $S_{T\varepsilon 2}$ is the thermal strain sensitivity of FBG, $S_{\varepsilon 2}$ is the strain sensitivity for the FBG sensor and S_T is the temperature sensitivity for the FBG sensor. Finally, the corresponding intensity variations due to strain, thermally induced strain and temperature for both types of sensors can be written in the form of the characteristic matrix as follows,

$$\begin{bmatrix} \Delta I_1 \\ \Delta I_2 \\ \Delta I_3 \end{bmatrix} = \begin{bmatrix} \Delta S_{\varepsilon 1} & 0 & 0 \\ \Delta S_{\varepsilon 1} & 0 & \Delta S_{T\varepsilon 1} \\ \Delta S_{\varepsilon 2} & \Delta S_T & \Delta S_{T\varepsilon 2} \end{bmatrix} \begin{bmatrix} \Delta \varepsilon \\ \Delta T \\ \Delta T\varepsilon \end{bmatrix} \quad 5.9$$

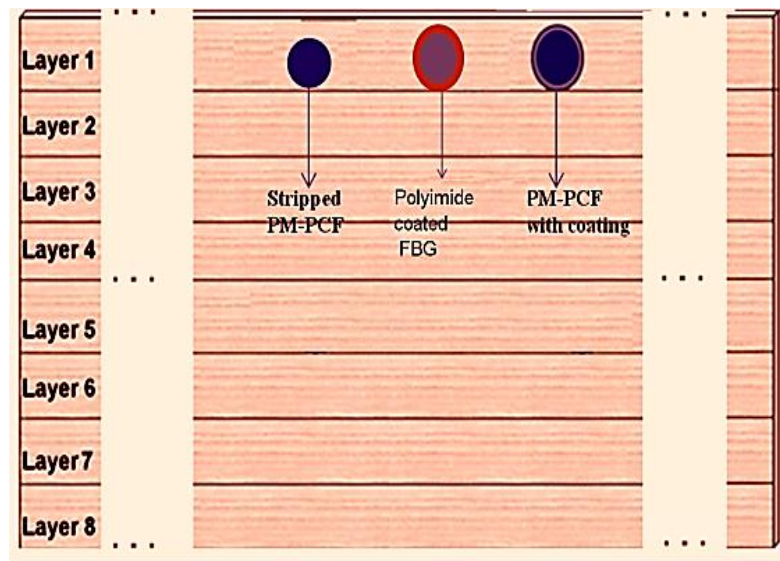
Finding the coefficients of the above matrix will yield the strain, thermally induced strain and temperature information simultaneously. Since the temperature sensitivity of the FBG is different from its free space temperature sensitivity, the FBG must be characterised after embedding into the composite material.

5.1.3 Experimental demonstration of the hybrid sensor system

A. Sample fabrication

The hand-layup [5.13] method is used for fabricating the E glass-unsaturated polyester resin sample. E-glass woven fibre fabrics are used as the reinforcement and an unsaturated polyester resin is used as the matrix. The reinforcement E-glass fibre diameter is $\sim 16\mu\text{m}$. For curing of the resin it is mixed with a catalyst in the volume ratio of 100:1. The reinforcement glass woven fabric used has a density of 280 g/m^2 and is cut into 8 pieces with identical dimensions of $21.5\text{ cm} \times 10\text{ cm}$, to form the eight plies of the fabricated composite sample. The orientation of the fibre glass reinforcement was chosen to provide a 0 - 0 unidirectional configuration. The optical fiber sensors are laid parallel to the reinforcement fibre in layer 1 of the resin, as shown in Figure 5.3(a). The diameter of the optical fibre is either $125\text{ }\mu\text{m}$ (bare) or $230\text{ }\mu\text{m}$ (with a buffer coating), which is about ten to fifteen times greater than the average E- glass fibre diameter ($16\text{ }\mu\text{m}$). In general, due to their compatible load carrying capability, the presence of optical fibres has limited influence on mechanical behaviour [5.20]. Additionally, it was reported earlier that if the optical fiber is laid along the direction of reinforcement fibres there is a uniform consolidation of the resin around the optical fiber with minimum defects and thus the laminate's mechanical parameters are least affected [5.20, 5.21 & 5.22]. However, if an optical fibre is oriented perpendicular to the strength members or fibre reinforcement, this results in formation of a characteristic “eye” pattern area within the resin, which acts as a defect center in the composite part that could lead to premature failure in the form of delamination [5.21]. However even if the sensor fibers are laid perpendicular, it should be noted that testing conducted at a number

of labs worldwide has concluded that the risk of delimitation was not serious unless the sensor fibers were very tightly spaced. The sample is then cured as per the manufacturer's specifications at room temperature for a day and then for 8 more hours at a temperature circa 60 °C. After curing, the sample is trimmed to final dimensions of 21.5 cm x 4 cm. The thickness of the fabricated sample was 0.22 mm. An image of the fabricated sample is shown in Figure 5.3(b). The thickness of the one layer of resin plus reinforcement is ~ 0.275 mm.



(a).



(b)

Figure 5.3 a) Schematic of the composite material sample with embedded fiber sensors and
(b) Fabricated composite sample

B. Experimental setup

An experimental arrangement to demonstrate the hybrid optical fiber sensor system proposed here is as shown in Figure 5.1. A 3 dB coupler is used to split the input

signals between the FBG sensor and the polarimetric sensors. The HB-PM-PCF sensors used were acrylate buffer coated PM-1550-01 and buffer stripped PM-1550-01. The diameters of the polyimide coated FBG sensor, acrylate buffer coated PM-1550-01, and buffer stripped PM-1550-01 are $\sim 180\mu\text{m}$, $230\mu\text{m}$, and $125\mu\text{m}$ respectively.

The polarized outputs of the HB-PM-PCF sensors were observed at a wavelength of 1550 nm with the use of a wavelength filter. A polarizer and analyzer arrangement at the input and output of the polarimetric sensors were used to obtain the strain and temperature induced changes in the state of polarization of the output from the sensors. A fiber circulator was used to direct the reflected signal from the FBG to the TFF. The TFF used to convert the strain and temperature induced wavelength variation from the FBG into intensity changes utilized a single channel of an 8-channel thin film based WDM- Demux [5.6], designed for 200 GHz DWDM channel spacing, sourced from Laser 2000 (UK). The peak wavelength of the FBG used was 1549.7 nm and its length was 1 cm. For the demodulation of the FBG the TFF channel that was closest to the peak Bragg wavelength of the FBG having a linear spectral response from 1549.7 nm to 1550.3 nm was selected, and the selected channel's spectral response is as shown in Figure 5.4.

Three photodiodes were required to measure the output intensity variations from the different sensors. A National Instruments LabVIEW 8.0 based programme was used for real time data processing to obtain the strain and temperature information simultaneously.

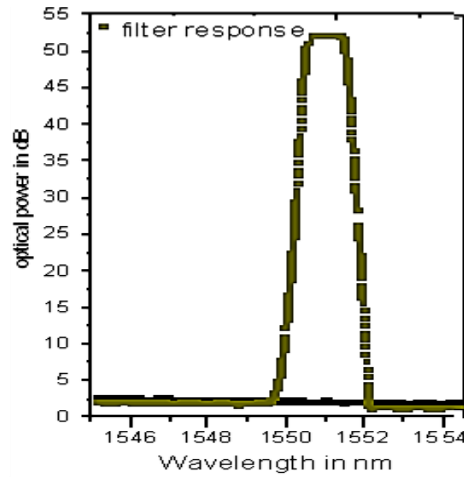


Figure 5.4. Spectral response of the TFF filter with a linear edge response from 1549.7 nm to 1550.3 nm

5.1.4 The hybrid sensor system for strain, thermally induced strain and temperature sensitivities

In order to solve the characteristic matrix of the hybrid sensor (equation 5.9), the strain, temperature and thermal strain sensitivity values has to be calculated. In the following sections the strain, temperature and thermal strain sensitivity measurements are described.

A. Determining the applied strain sensitivity of the sensors

By adjusting the polarizer/analyzer arrangement, polarized light from the source is launched with its polarization at an angle of 45^0 to the optical axis of the PM- fiber. Such a polarizer analyzer arrangement ensures an equal distribution of optical intensity between the two orthogonal polarizations. This polarizer/analyzer arrangement must be kept undisturbed during the strain/temperature measurements for reliable results from the HB-PM-PCF sensors. It was reported that, the embedded polarimetric sensor response is influenced by pre-stress on optical fiber, input light azimuth, optical fiber turns, orientation of the reinforcement fibre and

shape of the composite structure, etc. This is due to the fact that the variation in the elastic properties of the composite structure as well as the shape deformation of embedded polarimetric sensor modifies the birefringence properties of the highly birefringent fiber [5.23]. In this paper the polarimetric sensors are embedded in a flat composite sample as shown in Figure 3(b). A three point bending setup [5.17] is used for applying strain to the composite sample and average applied strain can be calculated analytically [5.17].

For the measurement of strain using FBG sensors, an FBG of 1 cm long is embedded in the composite material. In measuring FBG strain sensitivity the Bragg wavelength variation is converted into an intensity variation using the TFF wavelength filter method detailed in section 5.1.2. The strain is measured by considering the strain sensitivity of the FBG as $1.2\text{pm}/\mu\epsilon$, and the slope of the TFF wavelength filter 70.42 dB/nm . In this experimental demonstration a TFF with a 0.7 nm linear spectral range within the spectral response from 1549.7 nm to 1550.4 nm is used as shown in Figure 5.4. Thus the estimated maximum measurable strain range is 0 to $583.3\text{ }\mu\epsilon$. Experimentally then an incremental strain step of $78\text{ }\mu\epsilon$ was applied to the composite sample with all the three sensors embedded in layer 1 at constant temperature of $20\text{ }^{\circ}\text{C}$, with the applied strain range from 0 to $583\text{ }\mu\epsilon$. As explained in section 5.1.2, the HB-PM-PCF strain sensor can provide a linear intensity response only if its operating point is chosen within the linear quadrature region ($\pi/4$ to $+\pi/4$). The HB-PM-PCF sensor has a larger linear measurable strain range [5.10, 5.14] compared to other high strain sensitive PM fibers such as Panda fiber. For the HB-PM-PCF sensor used here it is known that a phase change of $\pi/2$ will occur for an applied strain value of $2225\text{ }\mu\epsilon$, and that the corresponding strain sensitivity value is $3.53\text{ radians /m.m}\epsilon$ [5.12]. Thus in order to effectively operate

the HB-PM-PCF sensor in its linear quadrature region, an initial setting for the HB-PM-PCF strain measurements is done by adjusting the operating point of the polarizer/analyzer arrangement to ensure that the signal from the HB-PM-PCF sensor for zero strain is at the starting value of the linear quadrature region. This is achieved by rotating the analyzer shown in the Figure 5.1.

In the case of strain measurements in composite materials, an acrylate coated HB-PM-PCF shows negligible temperature dependence [5.13] and thus such an acrylate coated HB-PM-PCF is more suitable to use as a strain sensor in this system. The measured change in intensity for the acrylate coated HB-PM-PCF, the stripped HB-PM-PCF polarimetric sensors and the FBG sensor with applied strain at a constant temperature is shown in Figure 5.5(a), Figure 5.5(b), and Figure 5.5(c) respectively. From the Figure 5.5, it is clear that for all the three type of sensors the intensity variation is monotonic and linear. Both the acrylate coated HB-PM-PCF and the stripped HB-PM-PCF polarimetric sensors showed almost the same sensitivity value of $0.00464 \text{ dB}/\mu\epsilon$ and $0.00467 \text{ dB}/\mu\epsilon$ respectively indicating that buffer coating does not have significant influence on uniform applied strain measurements in E-glass fibre reinforced composites. The FBG sensor showed an applied strain sensitivity value of $0.0862 \text{ dB}/\mu\epsilon$.

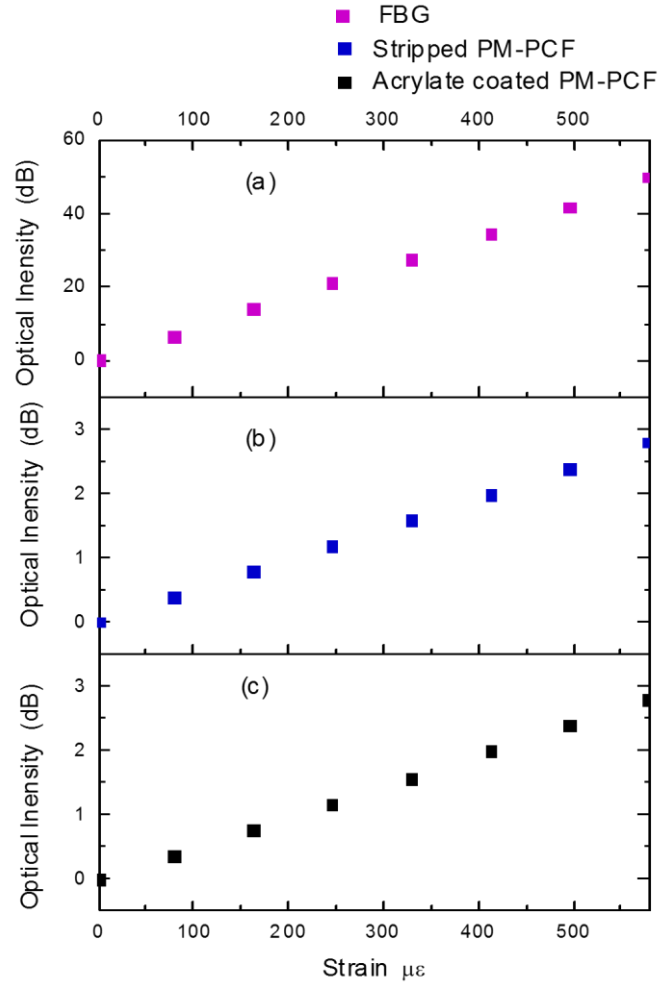


Figure 5.5. Changes in the output intensity for the individual sensors in a strain range from 0 to 580 $\mu\epsilon$

B. Determining the applied strain sensitivity of the sensors

For temperature measurements, the composite sample is attached to a Peltier element driven by a temperature controller. The temperature of the composite sample is varied from 20 $^{\circ}\text{C}$ to 50 $^{\circ}\text{C}$, in the absence of applied strain. While there is no applied strain, lateral strain will arise due to thermal strain within the composite as the temperature varies, which can result in a strong strain non-uniformity between the two orthogonal axes of the optical fiber.

During temperature measurements of the composite sample using a polyimide

coated FBG no splitting of the Bragg reflected spectrum was observed and the FBG reflected spectrum at different temperatures is as shown in Figure 5.6. It is known that if there is a strong strain non-uniformity, the FBG peak can split into two due to birefringence [5.16]. It is also known that if the strain gradient between the two orthogonal axes is small, a spectral broadening of the FBG reflected spectrum can be observed [5.16]. Only a small amount of spectral broadening was observed leading to the conclusion that the non-uniform lateral strain components induced by the CTE of the E-glass composite material do not have significant influence on the reflected spectrum of the FBG.

The intensity domain output of the FBG sensor obtained using TFF interrogator for an applied temperature variation from 20 °C to 50 °C at intervals of 5 °C is as shown in Figure 5.7. The polyimide coated FBG sensor embedded in E glass– reinforced composite material shows an estimated temperature sensitivity of 1.732 dB/°C. Assuming that the free space temperature sensitivity of the FBG is 11.2 pm/°C, and the TFF slope is 70.42 dB/nm, the temperature sensitivity of this FBG in free space in the intensity domain is calculated as of 0.788 dB/°C, significantly less than the embedded value. It is clear therefore that the CTE of the composite material contributed towards an increase in the temperature sensitivity for the embedded FBG sensor. The thermal strain caused an increase in temperature strain sensitivity by a value of 0.944 dB/°C. Considering the TFF filter slope of 70.42 dB/nm and FBG strain sensitivity of 1.2pm/με, the thermal strain sensitivity can be estimated. Thus, the experimentally estimated temperature sensitivity, and the thermal strain sensitivity values for the FBG part of our present hybrid sensor system are 0.788 dB/°C and 0.0845dB/με respectively.

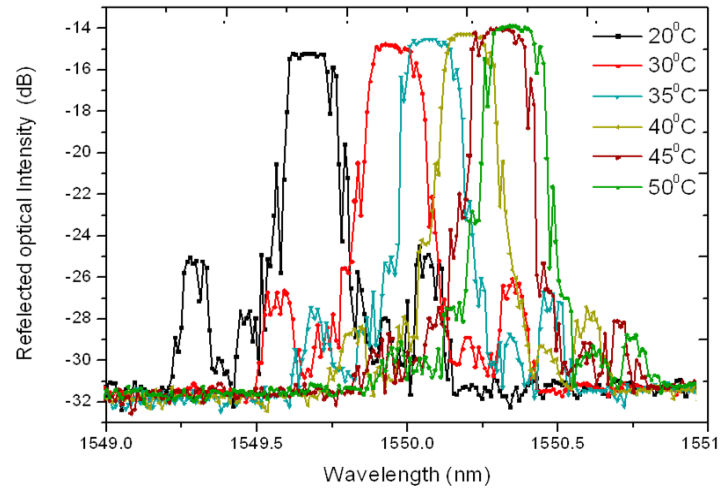


Figure 5.6 The FBG reflected spectrum at different temperatures

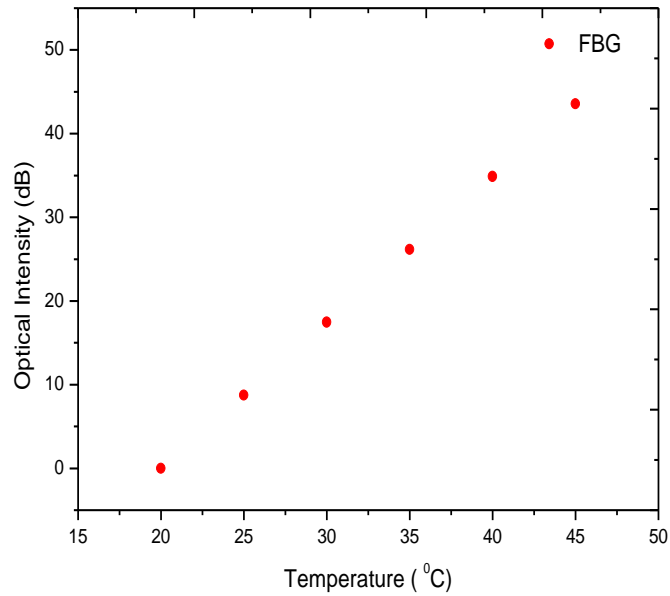


Figure 5.7. Changes in intensity at the FBG sensor output with temperature.

From the experimental results of the polyimide coated FBG, the thermal strain acting on the FBG per degree celcius is only $11.2 \mu\epsilon/^{\circ}\text{C}$. However, the transverse CTE of the E-glass reinforced composite material calculated by classical mechanical analysis [5.13] showed a value of $\sim 26.7 \mu\epsilon/^{\circ}\text{C}$, which is greater than the experimentally observed thermal strain value from polyimide coated FBG. Thus the experimental results confirm that, the influence of thermal strain for polyimide coated FBG is significantly reduced by the strain tolerance of the buffer

coating.

C. Determining the applied strain sensitivity of the sensors

The output intensities of the acrylate coated HB-PM-PCF and the stripped HB-PM-PCF polarimetric sensors for a temperature variation from 20 °C to 50 °C at intervals of 5 °C are as shown in Figure 5.8(a). During temperature measurements in the composite material sample, the HB-PM-PCF with no buffer coating showed significant optical intensity variation due to thermal strain. The observed thermally induced strain influence on the embedded buffer stripped HB-PM-PCF sensor [5.12] is mostly due to transverse thermal expansion of the composite material. The acrylate coated HB-PM-PCF showed only negligible intensity variation, indicating that the buffer coating reduces the influence of non-uniform strain components [5.24] caused by the transverse CTE.

The thermally induced strain sensitivity value was derived from the stripped HB-PM-PCF sensor temperature response on the assumption that the strain sensitivity of the stripped HB-PM-PCF is 0.00464 dB/μ ϵ as was shown in section 5.1.4 A. The experimentally calculated optical intensity response versus thermally induced strain applied to the composite sample with an embedded coating-stripped HB-PM-PCF is as shown in Figure 5.8(b).

The thermal strain sensitivity calculated from the stripped HB-PM-PCF response is estimated as 22.2 μ ϵ /°C for a temperature variation from 20 °C to 50 °C. Further the experimentally calculated thermal strain using a stripped HB-PM-PCF is in good agreement with the simulated results. For the coating-stripped HB-PM-PCF the thermal strain sensitivity value is 0.00462 dB/μ ϵ , while for the acrylate coated HB-PM-PCF the thermal strain sensitivity is negligible having a value only

0.000464 dB/ $\mu\epsilon$. Thus for the acrylate coated HB-PM-PCF, the thermal strain sensitivity is one order less than that of the stripped HB-PM-PCF and this small thermal strain sensitivity of the acrylate coated HB-PM-PCF is most likely due to the thermal expansion of the acrylate coating.

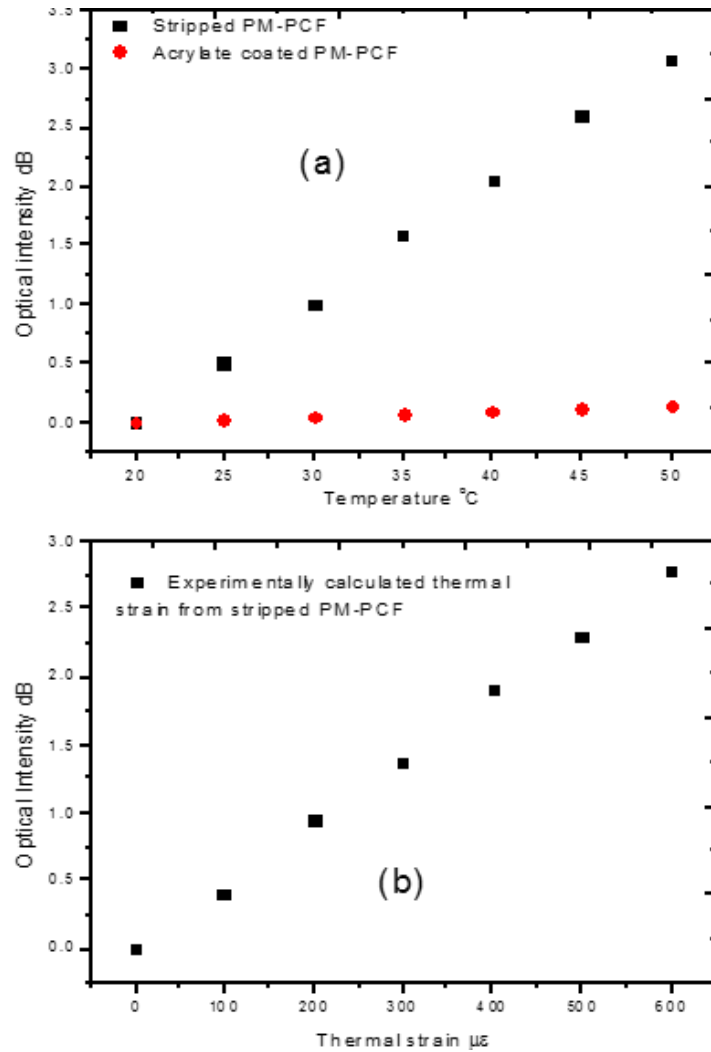


Figure 5.8 (a) Optical intensity versus temperature experimentally measured for coating-stripped and acrylate coated HB-PM-PCF sensors over a temperature range from 20 °C to 50 °C, (b) Optical intensity versus estimated thermal for the coating-stripped HB-PM-PCF sensor.

In summary, the FBG sensor is sensitive to both strain and temperature, the buffer coated HB-PM-PCF polarimetric sensor can be considered as a strain sensor and

the stripped HB-PM-PCF sensor is sensitive to both strain and thermally induced strain. Further, the characteristic matrix derived from the experimentally measured sensitivity values of the three sensors can be written as,

$$\begin{bmatrix} 0.00464\text{dB}/\mu\epsilon & 0 & 0 \\ 0.00467\text{dB}/\mu\epsilon & 0 & 0.00462\text{dB}/\mu\epsilon \\ 0.0862\text{dB}/\mu\epsilon & 0.788\text{dB}/^{\circ}\text{C} & 0.0845\text{dB}/\mu\epsilon \end{bmatrix} \quad 5.10$$

Thus we can conclude that, simultaneous measurement of the strain, temperature and thermal strain can be obtained from the proposed hybrid sensing system by multiplying the transpose of equation 5.9 with the output intensity matrix of equation 5.10.

The proposed hybrid sensor system successfully demonstrated the strain, temperature and thermally induced strain measurements in the composite material. The limitations in the dynamic range of the FBG strain/temperature measurements could be resolved by using customized wavelength filters with wider linear spectral response. We have already completed the design and fabrication of such miniaturized wavelength filters with a wider dynamic range. The proposed hybrid sensor system can be applied for real time monitoring of strain, temperature and thermally induced strain of composite structures in a wide range of end user applications involving composites such as in marine industry, infrastructure industry, aerospace, wind mills, etc.

5.1.5 Conclusion

In this paper a hybrid sensor system is proposed for simultaneously sensing temperature, strain and thermal strain in composite materials and its operation is demonstrated by combining three different sensors: a polarimetric sensor based on an acrylate coated polarization maintaining photonic crystal fiber (HB-PM-PCF),

a coating-stripped HB-PM-PCF sensor, and a fiber Bragg grating sensor, all embedded in an E glass fiber reinforced composite material. Temperature is sensed using the FBG sensor, strain is sensed using the acrylate coated HB-PM-PCF sensor and thermal strain is sensed using the coating stripped HB-PM-PCF. In this paper we also developed a characteristic sensitivity matrix of such a hybrid sensor. Furthermore, we have also demonstrated an interrogation scheme for this hybrid sensor system that converts the polarization and wavelength information from the different sensors into the intensity domain. By detecting the outputs of the three sensors in the intensity domain, information about temperature, axial strain and thermally induced strain can be simultaneously derived. The proposed sensor configuration can be employed in composite material structural health monitoring (SHM) applications.

5.2 A Miniaturized flexible surface attachable interrogator for hybrid optical fiber sensing¹¹

Keyword Hybrid sensor; polarimetric sensor; fiber Bragg grating; arrayed waveguide grating; electro optic Mach- Zehnder interferometric intensity modulator.

Abstract: In this study, we propose a miniaturized flexible interrogator for polarimetric and fiber Bragg grating (FBG) sensors based on a hybrid sensing scheme embedded in composite materials. The flexible interrogation module comprises of an Arrayed Waveguide (AWG) for FBG demodulation and an Electro

¹⁰ Manjusha Ramakrishnan, Ginu Rajan, Yuliya Semenova, Tomasz Wolinski, Andrzej Domański Gerald Farrell, “A miniaturized flexible surface attachable interrogator for hybrid optical fiber sensing”, Microwave and Optical Technology Letters, 56(5), 1167-1174, 2013.

Optic Mach- Zehnder Interferometric (EO-MZI) intensity modulator for polarimetric sensor demodulation. A customized design of the AWG and EO- MZI are presented, and the designed performance resulted in a wide channel spacing of 5 nm and low cross talk of -34 dB between adjacent channels for the AWG, and a low V_{π} voltage of ± 1.5 Volt for the MZI-EO. The method for fabrication of the flexible interrogator device is also presented, based on post processing of platinum coated polyimide substrate. The film type interrogation module is compact, with a size of 3.4 cm x 0.1 cm x 0.01 cm. The surface attachable flexible hybrid sensor interrogator is proposed to integrate with photo detector arrays and wireless communication technology to enhance the competency of hybrid sensing scheme in smart sensing composite parts in motion for applications in aircraft, wind rotor blades, etc.

5.2.1 Introduction

The use of fiber optic sensing based SHM [5.25] for composite structures is well established in applications such as aerospace, infrastructure, marine, wind rotor blades, etc. The interrogation systems traditionally used in field applications of optical fiber sensors are too bulky and cumbersome for applications in composite structures and also are difficult to package. In comparison integrated optoelectronic devices [5.26], commonly found in optical communications systems are significantly smaller and easier to package. For several sensing applications, such as FBGs systems and fiber optic gyros (FOGs) [5.27], interrogation systems based on integrated optical devices have been reported [5.28]. For example, integrated AWGs [5.28] / bandpass wavelength filters are extensively employed as the core of FBG interrogation systems, while integrated optic based (EO) modulators [5.27]

have been shown to be suitable for FOG demodulation purposes.

Sensing for composite materials in some aerospace components and other applications such as wind turbines will frequently involve embedding fiber sensors in parts which are in constant motion. In such applications fiber based connections to an interrogation system mounted remotely are difficult to implement. An alternative is the use of a compact interrogator mounted on the composite part itself which utilizes wireless system to communicate to the end user. For such applications, the ability to attach an integrated interrogation system to the surface of the composite would be an advantage. For this flexible rather than rigid waveguides and devices are more suitable. Flexible optical waveguides [5.29, 5.30] with embedded thin-film vertical-cavity surface-emitting lasers and photo detector arrays have been proposed as solutions to the packaging challenges of large-scale integration for telecommunication applications. However, the potential of such flexible integrated optic devices for optical fiber sensor interrogation purposes has not been fully realized yet.

In this study, a miniaturized flexible interrogation module is prepared for a hybrid sensing [5.31] scheme which can be attached as a “table top” component to a surface of a composite structure. The hybrid sensor is comprised of two types of fiber sensors: a high-birefringence polarization maintaining fiber based polarimetric sensor [5.32] combined with an FBG sensor. Using the hybrid sensor approach, simultaneous measurement of strain and temperature in composite materials has been reported earlier [5.33]. This involves converting the polarimetric and FBG sensors outputs into the intensity domain using edge filters. In my previous conference paper [5.34], an experimental demonstration of the hybrid sensor interrogation module is realised using a commercially available Thin

Film Filter (TFF) based WDM demultiplexer for FBG demodulation and a Lithium Niobate phase modulator for interrogation of polarimetric sensors. The working principle of the flexible AWG based FBG interrogator proposed in this study is similar to that in [5.34]. In principle it is possible to use off-the-shelf dense WDM devices, designed for telecommunication applications, with a channel spacing in the order of 1 nm or less for interrogation of FBG sensors. The limitation of such off-the-shelf devices for this application is their narrow channel spacing, so that a complex algorithm is needed to extract FBG peak shift information. Thus in the flexible interrogation scheme proposed here, the AWG is designed with a wide channel spacing of 5 nm and a small cross talk value of -34 dB between adjacent channels. For a polarimetric sensor, an external perturbation leads to a phase change and an electro-optic phase modulator can be utilized for polarimetric sensors interrogation [5.34]. In this paper, we report for the first time the design and fabrication of a miniaturized flexible interrogation module for a hybrid sensing system for composite materials.

There have been previous reports of flexible waveguide based AWGs [5.35], fabricated by soft moulding of Polydimethylsiloxane (PDMS). However, the processing of PDMS is quite difficult. The fabrication of flexible electro-optic polymer based EO devices by the post lift-off method was reported earlier [5.36], in which a fabricated device is released from a wafer by utilizing the low adhesive property of SU-8 polymer on gold. In this study, the proposed flexible interrogation module is designed based on two polymer waveguide based devices [5.37] an AWG and a Mach-Zehnder interferometric electro-optic (MZI-EO) intensity modulator. The core/cladding polymers of both the MZI-EO device and AWG are selected to facilitate a flexible waveguide based device fabrication. The AWG is based on a

Cyclotene polymer as the core material, while the MZI-EO device utilizes an EO polymer AJL146 [5.38] as the core material.

The paper is organized as follows. The hybrid sensor methodology is described in Section 5.2.2. The detailed explanation of the proposed flexible interrogation module is provided in Section 5.2.3. The simulated performance and proposed fabrication process of the flexible sensor interrogation module are presented in Section 5.2.4. The fabricated interrogator system integration possibilities are discussed in Section 5.2.5.

5.2.2 Hybrid sensor - methodology

In a polarimetric sensor a symmetric deformation effect in a single-mode fiber influences the propagation constant (β) of every mode, which leads to changes in the phase difference between both polarizations of the fundamental mode LP₀₁ [5.32]. The phase difference between orthogonal polarizations induced by the polarimetric sensor, results in a sinusoidal intensity variation, when the sensor output is connected to crossed polarizers. There are different varieties of polarimetric sensors [5.32] involving different types of high-birefringence polarization maintaining fibers. The temperature and strain sensitivity of each of the polarimetric sensor types is different. In the case of a Panda fiber, both strain and temperature changes lead to a phase difference [5.32, 5.33], while in the case of a HB-PM-PCF the phase difference originates only from longitudinal strain and has a very low sensitivity to temperature [5.31].

While polarimetric sensors can provide average strain measurements, they are not suitable for point strain measurements, which are also frequently required. For such measurements, FBGs are commonly employed, but with the problem that the

Bragg wavelength changes with both strain and temperature. By employing a hybrid sensing approach, where both FBG and polarimetric sensors are used, the cross-sensitivity issue of temperature for FBG strain measurements can be eliminated, using the temperature independent strain information from the polarimetric sensors. The average strain and temperature in the sample can also be measured either by comparing the average strain from different types of polarimetric sensors or by taking the average of localized point strains. More details on the simultaneous measurement of average and local strain and temperature in composite materials are discussed in our previous research [5.31, 5.33].

5.2.3 The flexible interrogation module

The experimental setup for a hybrid sensor system and the proposed interrogation demonstration can be realized as shown in Figure 5.9, in which for illustration purposes the case of five FBG sensors and two polarimetric sensors is shown. The setup comprises of a compact distributed feedback laser (working in the wavelength range from 1530 nm to 1570 nm), a fiber optic in-line isolator, a polarization maintaining (PM) 1 x 3 optical fiber splitter, 1550 nm wavelength filters (for polarimetric sensors), an in-line fiber optic polarizer and analyzer, the polarimetric sensors (Panda and HB-PM-PCF), an in- line fiber optic circulator, an FBG array, a flexible hybrid sensor interrogation module (combining the MZI-EO intensity modulator and AWG), an array of photo receivers. The outputs of the receivers could be connected in turn via a wireless link to a data processing unit. We have previously demonstrated [5.34] that it is possible to interrogate both FBGs and polarimetric sensors in the intensity domain using wavelength dependent edge

filters for converting the wavelength changes from FBGs and using EO modulators for converting the phase changes induced by polarimetric sensors into intensity variations. In such a scheme wavelength information from an array of FBGs can be easily converted into the intensity domain using an AWG whose multiple input wavelengths are designed to match the Bragg wavelengths of the FBG sensors [5.28, 5.34]. For interrogation of a polarimetric sensor, its output is connected to the input arm of an MZI electro-optic intensity modulator, the operating voltage of which is chosen in such a way that any change in the output from the polarimetric sensor causes a linear variation of the modulator's output intensity. As a result, any external perturbation of the polarimetric sensor (e.g., strain) is easily converted into linear changes in the output intensity.

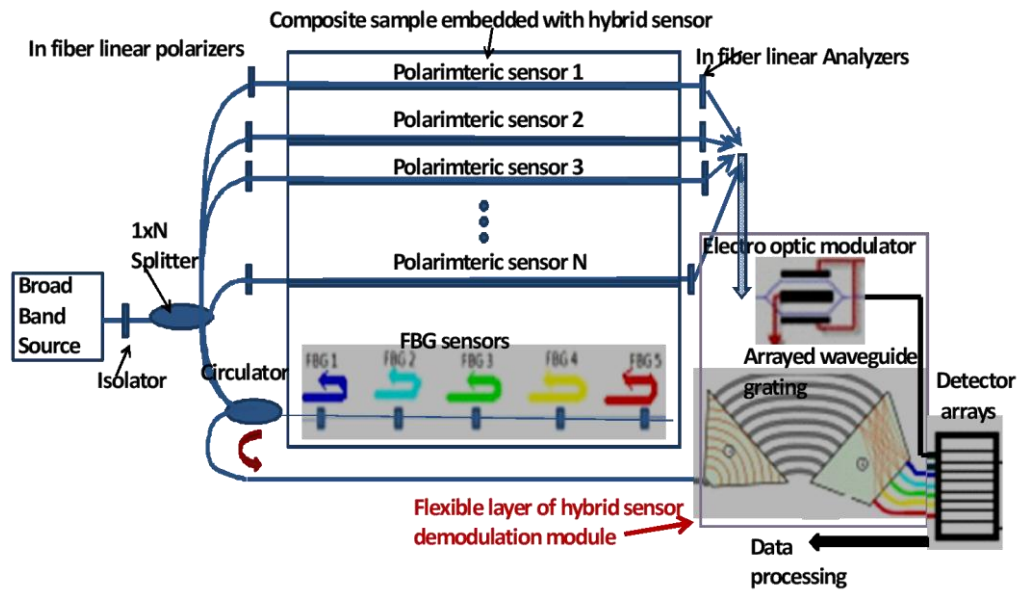


Figure 5.9 The schematic of the proposed flexible interrogation module

It should be noted that a single MZI EO device can be used for interrogation of multiple polarimetric sensors simultaneously using time domain multiplexing. The response of multiple polarimetric sensors can be separated in to time domain by appropriate processing of the detector output. The polarimetric sensors used can be

based on a wide variety of highly birefringent polarization maintaining fibers such as, PANDA fibers, side holed and micro-structured HB-PM-PCF.

5.2.4 Design and fabrication of the proposed flexible interrogator

When implemented as a flexible interrogator, both the MZI-EO device and the AWG are polymer-based optical waveguide devices. The polymer materials for core and cladding of the flexible interrogator are selected based on their adhesion properties and compatibility with existing integrated - optic / CMOS fabrication facilities.

For fabrication of the proposed flexible interrogator a method called the post-lift off method is adopted, in which the low adhesion between polyimide and a layer of platinum is utilized to lift the fabricated device off a silicon wafer used as a base only. Both the MZI-EO device and AWG are fabricated on a common polyimide substrate [5.39] film. A 100 μm thick polyimide layer is flexible and strong enough to support the MZI-EO device and AWG devices. The polyimide substrate also offers better thermal stability due to its good thermal properties [5.40].

A. Design and simulation of a flexible 1x6 arrayed waveguide

In this section a design of a 1x6 channel AWG and its performance optimization achieved using OptiBPM [5.41] and WDM Phasar tools is presented. The optimized AWG is intended for the purpose of FBG sensor interrogation. In the example here a six-channel AWG is designed to suit the interrogation of six FBGs (with matching peak wavelengths). The key requirements while optimizing the design of this 1x 6 AWG are: a wavelength range of 1535 nm to 1565 nm; a wide channel spacing of 5 nm over this wavelength range, with low crosstalk between adjacent AWG channels. Each channel of such of an AWG can be used to convert

a Bragg wavelength shift of up to 2.5 nm for a single FBG sensor into the intensity domain.

The AWG is designed based on UV curable polymers Cyclotene 3022-46 (Microchem) with an RI of 1.535 as the core material andOrmoclad (Microchem) with an RI of 1.522 as the upper/ lower cladding material. Single mode wave propagation is achieved using a rib waveguide structure with a rib height of 4 μm , width of 4 μm and etch height of 1 μm as shown in Figure 5.10. The designed rib waveguide structure offers a low propagation loss <0.05 dB/cm.

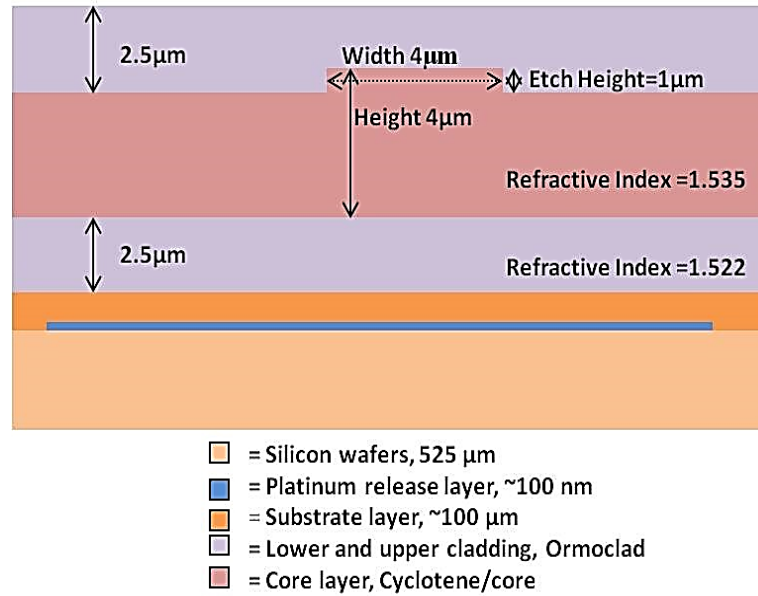


Figure 5.10 Schematic of fabrication of the proposed flexible interrogator

The design parameters used for the custom design the AWG geometry are as follows: the wavelength spacing between AWG channels, center wavelength, and effective index of the waveguide are 5 nm, 1.5425, and 1.5330241, respectively. The custom designed AWG [5.42] layout is as shown in Figure 5.11. The operation of the AWG device is explained in [5.43] as follows. When a mode in the input waveguide enters the input Free Spectral Range (FSR) it becomes divergent. In the phased array (PA) region a spatial separation of different wavelengths occurs by

introducing a length difference between adjacent PA waveguides. Further, a wavelength-dependent angular tilt occurs so the outgoing modes at different wavelengths are coupled to different output ports using the output side FSR. In order match typical commercial fiber dimensions, the gap between the adjacent output channels of the AWG is set to 250 μm as shown in Figure 5.11.

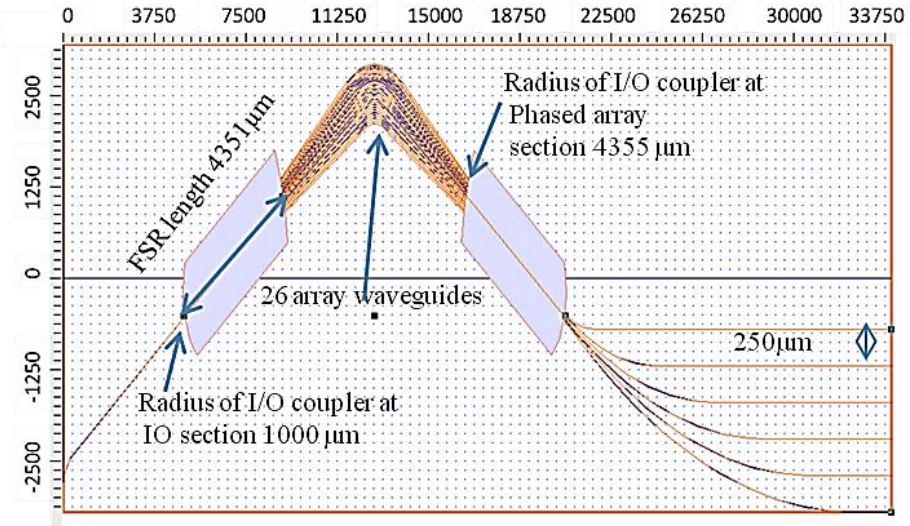


Figure 5.11. The layout of the 1x6 channel AWG

The geometrical parameters of the custom designed AWG are optimized to achieve the performance specification mentioned earlier. The final geometrical parameters of the custom designed AWG are as follows: the number of waveguides in the PA region is 26, the length increment of PA waveguides is 26.254 μm , the PA waveguide separation is 27.107 μm , the minimum distance between waveguides in the PA region is 20 μm , the FSR regions lengths are 4352 μm . The AWG flexible film size is 34 x 6.4 mm. A Gaussian shaped channel response is selected for the AWG and the optimized optical transmission of the AWG for TE polarization is as in Figure 5.12.

Simulation using WDM Phasar shows that the optimized design AWG offers a wide channel spacing of 5 nm (625 GHz) between six channels located at 1532 nm,

1537 nm, 1542 nm, 1547 nm, 1552 nm and 1557 nm, with adjacent channel crosstalk value of -34 dB. For an input of 0 dBm to the AWG the insertion loss is estimated to be less than 10 dB.

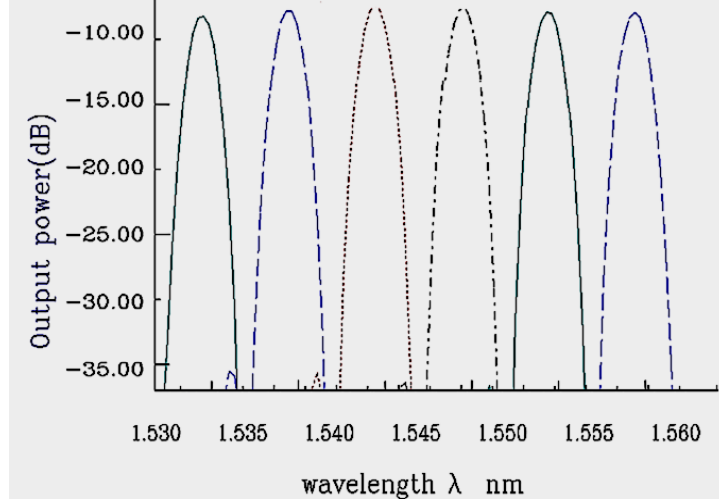


Figure 5.12. Simulated optical transmission of the AWG

B. Design and simulation results for a flexible EO intensity modulator

In this section we present the design of an MZI-EO and results of its performance optimization simulated using Optimode solver and OptiBPM tools. The optimized MZI EO is intended for the purpose of polarimetric fiber sensor interrogation. The key requirements in optimizing the MZI-EO design are that the waveguide should support single mode operation with low propagation loss and a low V_π voltage.

The MZI-EO is designed with a guest-host EO polymer AJ416 [5.38] as the core material, with refractive index of 1.6403 for the TE mode. The reason for selecting the AJ416 polymer as a core material is its key benefits such as high thin film γ_{33} value of 120-130 pm/V, and high stability [5.38, 5.43]. A UV-curable resin Cyclotene 3022-46 with an RI of 1.535 is chosen as the upper/ lower cladding.

In the MZI EO device single mode operation is optimized using an oversized waveguide structure [5.43]. It has been proved in earlier research works that the single-mode condition does not require a thin core layer. Even if the core layer is thick so that it could in principle support several modes in the slab waveguide, it is still possible to design the rib waveguide so as to support only one mode by radiating the higher order modes horizontally into the slab modes [5.43]. For optimizing the rib height for single mode operation, the TE refractive indices of the fundamental (0th order) and higher order modes (1st order and 2nd order) are calculated using the Optimode solver tool for planar waveguides with a 4 μm width for various thicknesses of core layer as shown in Figure 5.13. For the fundamental mode to propagate through the rib region the effective index contrast between the entry rib and side slab sections is $\Delta n_{\text{eff}} = 0.003$ [5.42]. From Figure 5.13, it is obvious that for a 3 μm core thickness, the etch depth of $\Delta T = 0.5 \mu\text{m}$ results in an effective index difference of 0.003. The effective index of the 1st order TE mode for a 3 μm thick center rib region is less than ($n_{1\text{center}} < n_{0\text{center}}$) the effective index of the fundamental mode in a 2.5 μm slab region. Consequently, the higher order mode's propagation through the slab region changes to a single mode operation within the rib waveguide region.

The inverted rib-waveguide structure is adopted for the MZI -EO modulator with a 4 μm width, 3 μm rib height and 0.5 μm etch height as shown in Figure 5.14. The key benefit of such an inverted-rib structure [5.44] is that the rib is processed in the robust cured lower cladding region instead of the core layer, thus reducing the processing requirements for the core layer.

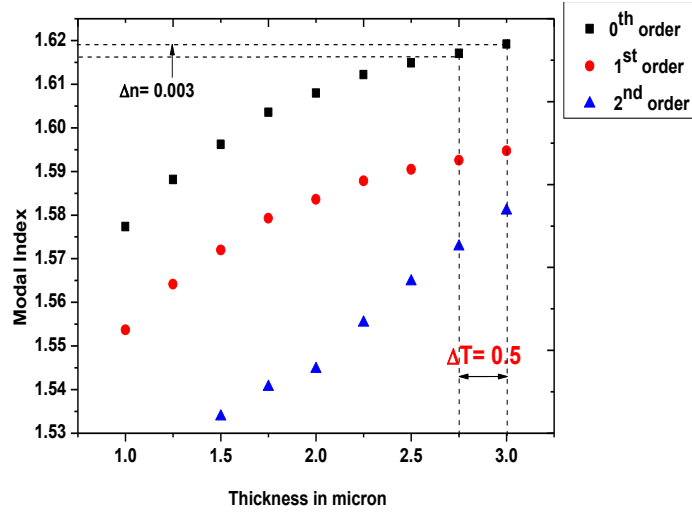


Figure 5.13 Optimization rib height for single mode operation

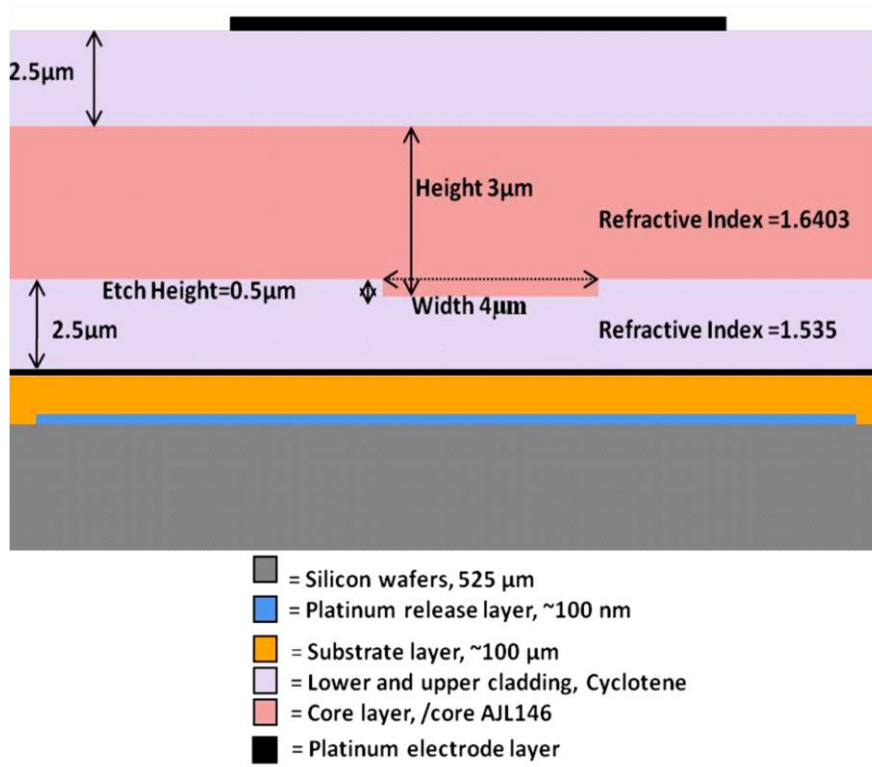
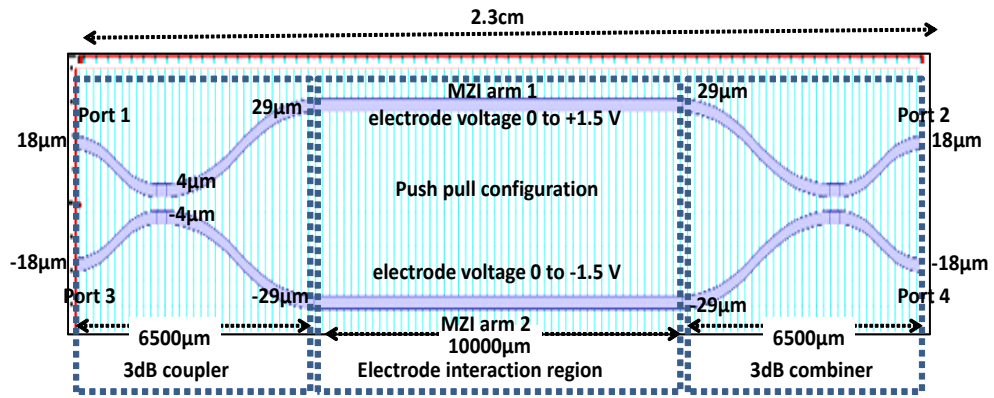


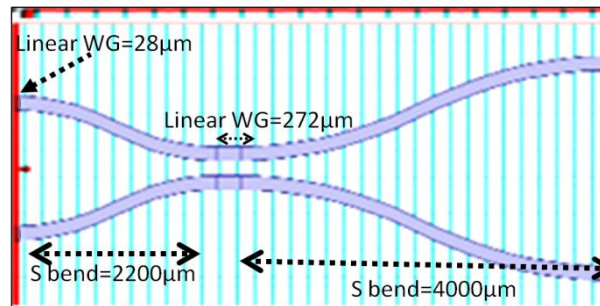
Figure 5.14 Inverted Rib waveguide structure of MZI - EO modulator

The 2x2 MZI EO intensity modulator design is initially laid out using the OptiBPM waveguide layout designer tool and simulation is performed at 1550 nm wavelength using a beam propagation method [5.41]. The MZI EO design consists of a 3 dB splitter, electrode interaction region and a 3 dB combiner as shown in

Figure 5.15(a). Both the 3 dB splitter and 3 dB combiner are identical and have patterns that are mirror images of each other with a length of 6.5 mm. The 3 dB splitter/combiner consists of a linear waveguide, an S bend, coupling linear waveguide and a second S bend region; the length of each region is as shown in Figure 5.15(b). The S bend dimensions are chosen to reduce the losses during switching.



(a)



(b)

Figure 5.15 a) Layout of 2x2 MZI EO modulator with vertical offset values of S bend & electrode voltages, (b) Layout and length of waveguides of 3dB splitter/combiner

Using the Electro optic solver, the phase change of the optical field with applied voltage is simulated. It is observed that a phase change of $-\pi/2$ occurs when an electrode voltage of -1.5 Volt is applied to the linear waveguide with electrode interaction length of 1 cm, as shown in the Figure 5.16. Further, in our MZI-EO

device the electrode configuration is push-pull [5.36], achieved by applying equal and opposite voltages at the two electrode arms of MZI-EO. The push-pull configuration of the MZI-EO device gives maximum possible intensity change for a minimum applied voltage at the electrodes.

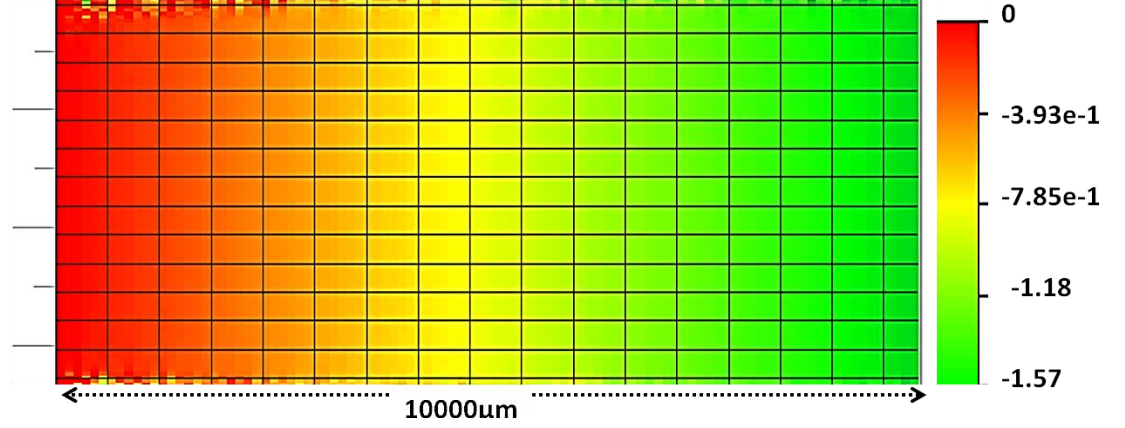


Figure 5.16 Simulated phase change of $-\pi/2$ for an electrode voltage of - 1.5 Volt and interaction length of 1 cm

For the designed MZI-EO device, by applying a +1.5 V to the MZI arm 1 and -1.5 V to the MZI arm 2 as shown in Figure 5.15(a), the optical field at the output port P_2 switches from minimum to maximum. The simulated amplitude at the output port P_2 of the MZI-EO device, with corresponding electrode voltages is shown in Figure 5.17. It is obvious that the $V\pi$ voltage¹² is ± 1.5 V. The total chip size of the optimized MZI-EO device is 23 mm x 0.1 mm, where the electrode interaction regions have a length of 1 cm. The MZI-EO is optimized to achieve the lowest propagation loss of 0.07 dB/cm.

¹² Half wave voltage as shown in Figure 5.17

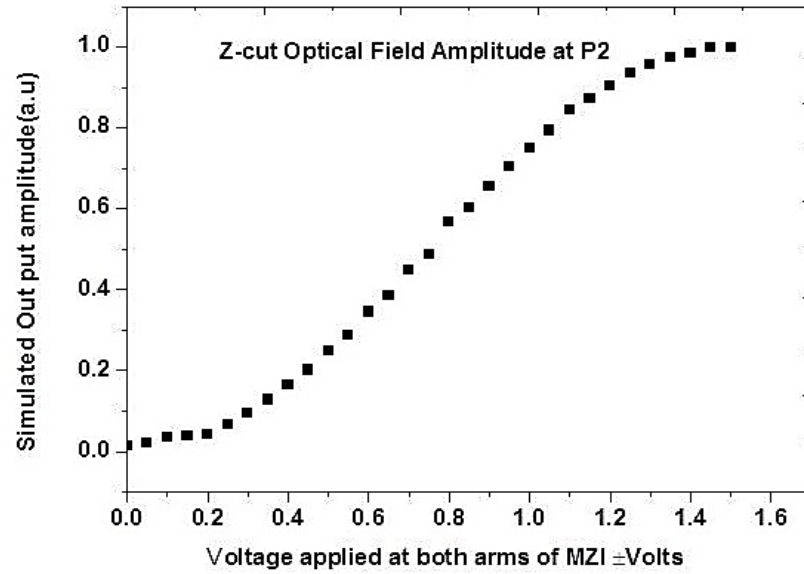


Figure 5.17 Simulated optical field amplitude at P2 of MZI- EO device

C. Proposed fabrication method for the flexible AWG and MZI EO devices

The flexible AWG and MZI-EO are fabricated by the post lift-off method. The AWG/ MZI-EO device structures are processed on the flexible polyimide substrate. Polyimide does not adhere well to platinum [5.38] and this property is utilised for the peeling of the device film. The Polyimide substrate with the fabricated AWG/ MZI-EO can thus be released from the wafer when processing is completed. The actual fabrication of AWG and MZI-EO are very similar, for example the method of patterning of the substrate layer and peeling off the device. Further, the proposed device fabrication method is simpler, and is compatible with existing facilities for complementary metal–oxide– semiconductor (CMOS) [5.45] fabrication. The flexible device fabrication process involves four steps. The releasing layer and the flexible polyimide substrate patterning, the device fabrication, the dicing and the device lift off. The detailed description of these steps for fabrication of the AWG / MZI-EO is as follows:

A. Steps in the fabrication of the flexible AWG

1: Releasing layer and the flexible polyimide substrate patterning

The first step in fabrication is flexible polyimide substrate patterning on a silicon wafer. If a releasing platinum layer is placed in between silicon wafer and polyimide flexible substrate, it is possible to peel off the device after fabrication. However, the flexible polyimide substrate requires a strong base to firmly hold the device during the robust fabrication process. This is ensured by arranging that rectangle corners at the edges of the silicon wafer are left without the platinum layer and thus the platinum releasing layer needs to be sputtered with such a rectangular lift off mask pattern. On top of the platinum releasing layer the 100 μm thick polyimide substrate layer is spin coated. This step is shown in Figure 5.18(a).

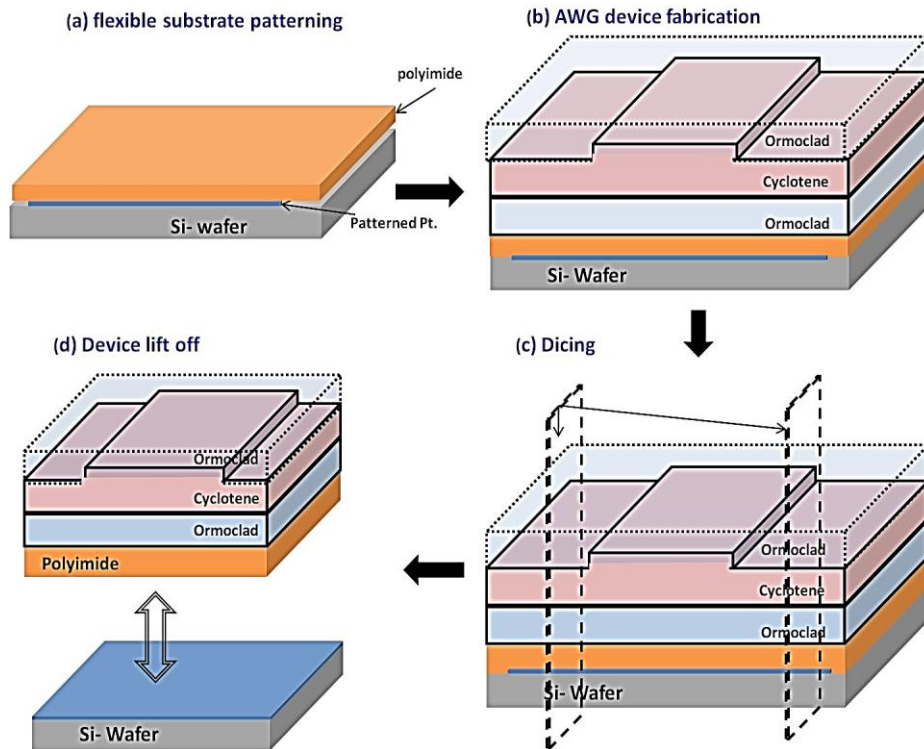


Figure 5.18 The fabrication steps for the flexible AWG device (a) Releasing layer and flexible polyamide substrate patterning, (b) AWG device fabrication, (c) Dicing, and (d) Device lift-off.

2: AWG device fabrication

On top of the polyimide substrate layer the 2.5 μm thick lower cladding material layer (Ormoclad) is spin coated. On top of the lower cladding layer the 4 μm thick core material layer (Cyclotene) is spin coated. Further, with the help of an arrayed waveguide mask pattern, the AWG is patterned on the core layer. The rib waveguide structure of AWG is processed using Reactive Ion Etching (RIE) to achieve a 1 μm etch height. Again, on top of the core material layer (Cyclotene), the 2.5 μm thick upper cladding material layer (Ormoclad) is spin coated. This step is shown in Figure 5.18(b).

3: Dicing

From the four sides, the silicon wafer is diced so as to remove the edges of the silicon layer that are left un-patterned (to hold the device) to facilitate release. This step is shown in Figure 5.18(c).

4: Device lift-off

The last and final step is device lift-off from silicon wafer utilising the low adhesive property of platinum with polyimide. This step is shown in Figure 5.18(d).

B. Steps for fabrication of the flexible MZI-EO

The fabrication steps are as shown in Figure 5.19. Since the steps involved in the fabrication of the MZI-EO device are similar to that of AWG device fabrication, (such as the releasing layer and the flexible polyimide substrate layer patterning, the dicing and the device lift off) these steps are not explained in this section. However, the patterning of the MZI-EO device and the platinum electrode layer are dissimilar to that of a AWG device and these steps are explained as follows.

In the case of the MZI-EO device, the platinum bottom electrode needs to be patterned on top of the polyimide substrate layer. However, the low adhesion of

this bottom platinum electrode layer to the polyimide substrate layer can lead to detachment of the flexible film MZI-EO device from the polyimide substrate layer. Thus, to ensure firm binding of the MZI-EO device on top of the flexible polyimide substrate, the bottom electrode is patterned so that points on the bottom electrode act as anchors for the MZI-EO device.

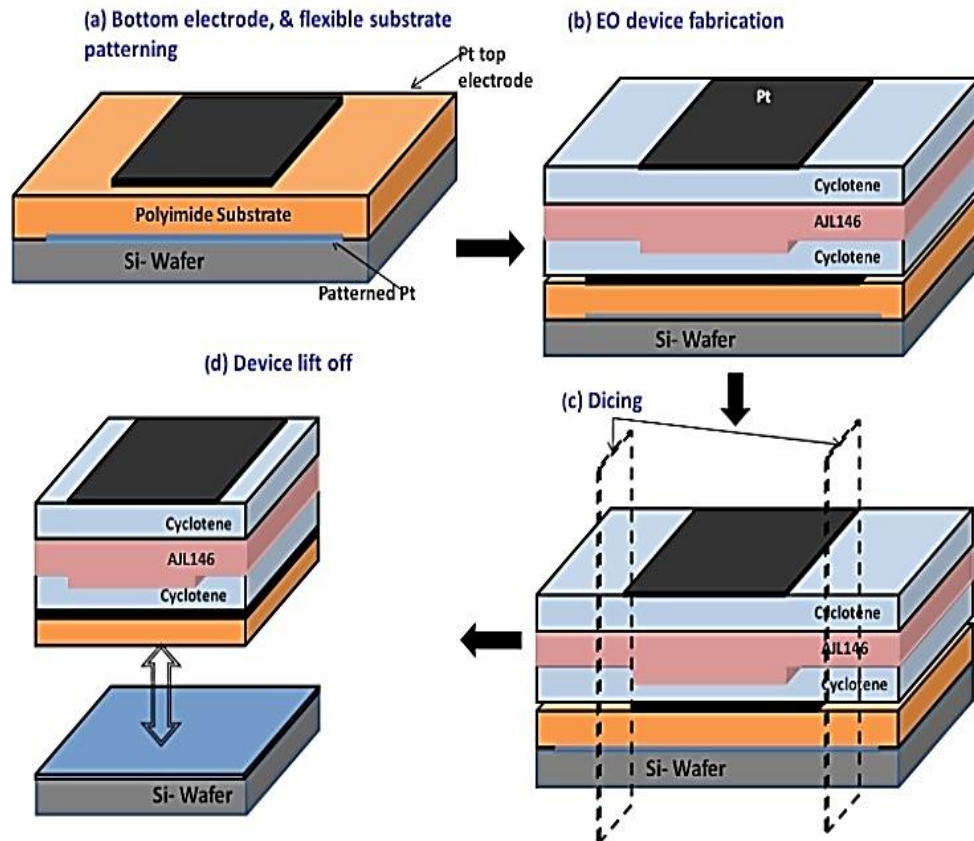


Figure 5.19 The fabrication steps for the flexible MZI-EO device (a) Releasing layer and flexible polyimide substrate, bottom electrode patterning (b) MZI-EO device fabrication, (c) Dicing, and (d) Device lift-off.

1. MZI-EO device fabrication:

On top of the patterned bottom electrode, a 2.5 μm thick layer of Cyclotene is spin coated to form the lower cladding. Through the partial RIE the mask of the MZI-EO device is patterned on the lower cladding layer to achieve 0.5 μm etch height. Since the MZI-EO device is designed with the inverted rib structure,

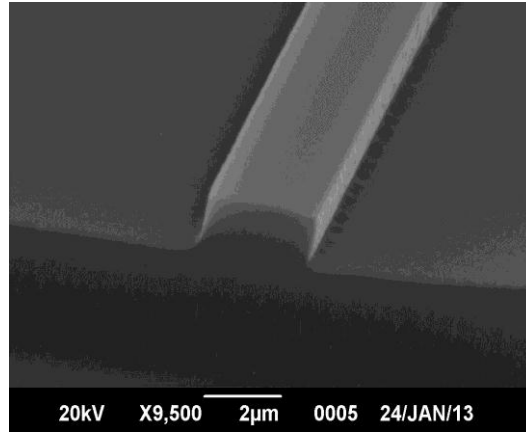
processing is performed on the lower cladding. This reduces processing of the core layer. On top of the lower cladding layer the 3 μm thick core material layer (EO polymer AJL416) is spin coated. Again, on top of the core material layer a 2.5 μm thick upper cladding layer (Cyclotene) is spin coated. Finally, on top of the Cyclotene the upper cladding platinum top electrode is patterned as shown in Figure 5.19(c).

5.2.5 System integration considerations

The flexible interrogation module is in the process of being fabricated, having a size of 3.4 cm x 0.1 cm x 0.01 cm. As an example of current progress the first sample of the interrogation module is shown in Figure 5.20 (a), appearing as a thin film device. A further example is the polymer rib waveguides within the thin film module, shown in Figure 5.20 (b) as a SEM image of the rib structure of the AWG device. It is clear that flexible film interrogator is light weight and miniaturized. Such a surface attachable interrogator has the potential not to add to the mechanical loading of composite structures.



(a)



(b)

Figure 5.20 (a) thin film type flexible interrogation module after fabrication; and (b) SEM image of the rib waveguide structure of AWG device

5.2.6 Conclusions

A miniaturized flexible surface attachable interrogator has been proposed for polarimetric and FBG sensors based hybrid sensing scheme embedded in composite materials. The designed interrogator comprised of two polymer waveguide based devices: an AWG for FBGs demodulation and an EO- MZI intensity modulator for polarimetric sensor demodulation. The simulated performances of the designed AWG and EO- MZI resulted in a wide channel spacing of 5 nm and low cross talk of -34 dB between adjacent channels for the AWG, and a low V_{π} voltage of ± 1.5 Volt for the MZI-EO. The proposed interrogator has been realized as a flexible device using post processing of platinum coated polyimide substrates. The fabricated flexible film type interrogation module is compact, with a size of only 3.4 cm x 0.1 cm x 0.01 cm. Additionally, it has been proposed to integrate the surface attachable flexible hybrid sensor interrogator with photo detector arrays and wireless communication technology to enhance the application of hybrid sensing scheme in smart sensing and SHM of composite parts

in motion for applications in aircraft, wind rotor blades, etc.

5.3 References

- 5.1. H. B. Van, G Lee, E. Bosman, J. Missinne, S. Kalathimekkad, Maskery O, Webb DJ, Sugden K, Van Daele P, Van Steenberge et.al. "Ultra small integrated optical fiber sensing system." *Sensors*, 12.9, 12052-69, 2012.
- 5.2. B. Glisic, D. Inaudi. "Fibre Optic Methods for Structural Health Monitoring." Wiley, 2007.
- 5.3. K. O. Hill, G. Meltz. "Fiber Bragg grating technology fundamentals and overview." *J. Lightwave Technology*. 15. 8, 1263 -1276, 1997.
- 5.4. K. B. Samer, T. Sun, K. T. V. Grattan. "Simultaneous measurement of temperature and strain with long period grating pairs using low resolution detection." *Sens. Actuators A, Phys.*, 144.1, 83 -89, 2008.
- 5.5. H. J. Patrick, G. M. Williams, A. D. Kersey, J. R. Pedrazzani. "Hybrid fibre Bragg grating/long period grating sensor for strain/temperature discrimination." *IEEE Photon. Technol. Lett.*, 8.9, 1223 -1225, 1996.
- 5.6. R. De Oliveira, C. A. Ramos, A. T. Marques. "Health monitoring of composite structures by embedded FBG and interferometric Fabry-Perot sensors." *Comput. Struct.*, 86, 340 -346, 2008.
- 5.7. B. Dong, J. Hao, C. Liaw, B. Lin, S. C. Tjin. "Simultaneous strain and temperature measurement using a compact photonic crystal fiber inter-modal interferometer and a fiber Bragg grating.", *Appl. Opt.*, 49.32, 6232 - 6235, 2010.

- 5.8. R. M. Andre, M. B. Marques, P. Roy, O. Frazao. "Fiber loop mirror using a small core micro-structured fiber for strain and temperature discrimination.", *IEEE Photon. Technol. Lett.*, 22.15, 1120 -1122, 2010.
- 5.9. O. Frazao, J. P. Carvalho, L. A. Ferreira, F. M. Araújo, J. L. Santos. "Discrimination of strain and temperature using Bragg gratings in microstructured and standard optical fibres." *Meas. Sci. Technol.*, 16.10, 2109 -2113, 2005.
- 5.10. G. Rajan, M. Ramakrishnan, Y. Semenova, K. Milenko, P. Lesiak, et al. "A photonic crystal fiber and fiber Bragg grating-based hybrid fiber-optic sensor system." *IEEE Sensors J.*, 12. 1, 39 -43, 2012.
- 5.11. C. Sonnenfeld, "Microstructured optical fiber sensors embedded in a laminate composite for smart material applications.", *Sensors*, 11. 3, 2566 - 2579, 2011.
- 5.12. M. Ramakrishnan, G. Rajan, Y. Semenova, P. Lesiak, A. Domanski, et al. "The influence of thermal expansion of a composite material on embedded polarimetric sensors." *Smart Mater. Struct.*, 20. 12, 125002-1 - 125002-3, 2012.
- 5.13. M. Ramakrishnan, G. Rajan, Y. Semenova, P. Lesiak, A. Domanski, et al. "Measurement of thermal elongation induced strain of a composite material using a polarization maintaining photonic crystal fiber sensor." *Sens. Actuators A, Phys.*, 190, 44 -51, 2013.
- 5.14. T. R. Wolinski, P. Lesiak, A. W. Domanski. "Polarimetric optical fiber sensors of a new generation for industrial applications." *Bull. Polish Acad., Technical Sciences.*, 56. 2, 1 -8, 2008

- 5.15. D. H. Kim and J. U. Kang. "Analysis of temperature-dependent birefringence of a polarization-maintaining photonic crystal fiber." *Opt. Eng.*, 46 .7, 1 -5, 2007.
- 5.16. G. Luyckx, E. Voet, N. Lammens, J. Degrieck. "Strain measurements of composite laminates with embedded fibre Bragg gratings: Criticism and opportunities for research." *Sensors*, 11.1, 384 -408, 2011.
- 5.17. G. Rajan, M. Ramakrishnan, P. Lesiak, Y. Semenova, T. Wolinski et al. "Composite materials with embedded photonic crystal fiber interferometric sensors." *Sens. Actuators A, Phys*, 182, 57 -67, 2012.
- 5.18. M. Ramakrishnan, G. Rajan, Y. Semenova, T. Wolinski and G. Farrell. "A demodulation scheme for a hybrid fiber sensor system for composite materials." *Proc. SPIE*, 8439, 843929-1 -843929-10, 2012.
- 5.19. Q. Wang, G. Farrell, T. Freir, G. Rajan, P. Wang. "Low-cost wavelength measurement based on a macrobending single-mode fiber." *Opt. Lett.*, 31. 12 , 1785 -1787 , 2006 .
- 5.20. D. Lee, J. I. Lee, S. Yun. "The mechanical characteristics of smart composite structures with embedded optical fiber sensors." *Compos. Struct.*, 32. 1, 39 -50, 1995.
- 5.21. A. Giemes, S. P. Julian. "Fiber optics sensors, new trends in structural health monitoring.", *Sensors*, 265. 1, 1 -3, 2013.
- 5.22. B. Wojciech, G. Pawel, K. Jerzy. "Application of optical fibre sensors to measuring the mechanical properties of composite materials and structures." *Adv. Compos. Mate. Ecodes. Anal.*, 11. 1, 1 -27, 2011.

- 5.23. V. M. Murukeshan, P.-Y. Chan, L. S. Ong, A. K. Asundi. "Toward realization of a smart polarimetric sensor." *Proc. SPIE*, 3670, 54 -58, 1999.
- 5.24. P. Lesiak, M. Szelag, D. Budaszewski, R. Plaga, K. Milenko, et al. "Influence of lamination process on optical fiber sensors embedded in composite materials." *Meas., Elsevier Sci.*, 45.9, 2275 -2280, 2012.
- 5.25. E J Friebele, et al. "Optical fiber sensors for spacecraft applications". *Smart Mater. Struct.*, 8, 813–838, 1999.
- 5.26. Won T. Tsang et al. "Integrated Opto-electronics: Practicalities and Potentials." *Proc. of SPIE*, 5624, 2005.
- 5.27. Feng Sun, et al. "Study on the Drift of Modulated Phase in Interference Fiber Optic Gyroscope." *Journal of Computers*, 5. 3, 2010.
- 5.28. Y. Sano, T. Yoshino. "Fast optical wavelength interrogator employing arrayed waveguide grating for distributed fiber Bragg grating sensors." *J. Lightwave Technol.*, 21, 132–139, 2003.
- 5.29. Chulchae Choi, et al. "Flexible Optical Waveguide Film Fabrications and Optoelectronic Devices Integration for Fully Embedded Board-Level Optical Interconnects." *Journal of Lightwave Technology*, 22. 9, September 2004.
- 5.30. E. Bosman. "Optical interconnections embedded in flexible substrates." *Proceedings Symposium IEEE/LEOS Benelux Chapter*, Eindhoven, 2006.
- 5.31. G. Rajan, et al. "A Photonic Crystal Fiber and Fiber Bragg Grating-Based Hybrid Fiber-Optic Sensor System." *IEEE Sensors Journal*, 12. 1, January 2012.

- 5.32. T. R. Wolinski, P. Lesiak, A. W. Domanski. "Polarimetric optical fiber sensors of a new generation for industrial applications." Bull. Pol. Ac.: Tech., 56, 2, 125–132, 2008.
- 5.33. Rajan G, et al. "A hybrid fiber optic sensing system for simultaneous strain and temperature measurement and its applications." Photonics Letters of Poland, 2 .1, 46-48, 2010.
- 5.34. M Ramakrishnan, et. al. "A demodulation scheme for a hybrid fiber sensor system for composite materials." Proc. of SPIE, 8439, SPIE doi:10.1117/12.922627, 2012.
- 5.35. Jung-Gyu Lim, et. al. "Polymeric Arrayed Waveguide Grating Using Imprint Method Based on a Flexible PDMS Stamp." IEEE Xplor, Digital Object Identifier: 10.1109/LEOS.2006.278751, Oct. 2006.
- 5.36. Hyun-Chae Song, et al. "Flexible low-voltage electro-optic polymer modulators." Patent no: US 7,366,363, B290089-048, 2008.
- 5.37. Hong Ma et. al. "Polymer based optical waveguides: materials, processing, and devices." Adv. Mater., 14. 19, 1339-1365, 2002.
- 5.38. Diyun Huang et. al. "Highly efficient EO polymers for low $V\pi$ modulators." Linear and Nonlinear Optics of Organic Materials VIII, Proc. of SPIE Vol. 7049, 70490H, doi: 10.1117/12.795561, 2008.
- 5.39. S.Y. Xiao. "A novel fabrication process of MEMS devices on polyimide flexible substrates." Microelectronic Engineering 85, 452–457, 2008.
- 5.40. Farah, John. "Polished polyimide substrate", United States Patent 6563998, 2003.

- 5.41. OptiBPM, Waveguide optics modeling software system, version 8.0, second edition, Optiwave Inc. 2006.
- 5.42. J Meint K. Smit. " PHASAR-Based WDM-Devices: Principles, Design and Applications." IEEE Journal of Selected Topics in Quantum Electronics, 2, 2, June 1996.
- 5.43. Min-Cheol Oh, et al. "Recent Advances in Electrooptic Polymer Modulators Incorporating Highly Nonlinear Chromophore." IEEE Journal On Selected Topics in Quantum Electronics, 7.5, September/October,2011
- 5.44. Seong-Ku Kim, et al. "Inverted-Rib Waveguide Structure." IEEE Photonics Technology Letters, Vol. 2, February 2003.
- 5.45. O. Brand. "Fabrication Technology" Advanced Micro and Nanosystems." Vol. 2. CMOS – MEMS, WILEY-VCH Verlag GmbH & Co. KGaA, Weinheim, ISBN: 3- 527-31080-0, 2005.

Chapter 6

Derived Applications of Polarimetric Strain

Sensing for Composite Structural Health

Monitoring Purposes

In Chapter 5 it was shown that a hybrid sensor comprising a buffer coated PM - PCF polarimetric sensor, a buffer stripped polarimetric sensor and an FBG sensor embedded in a composite material can be used for simultaneous measurement of axial strain, thermal strain, and temperature of the composite material. In that hybrid sensing scheme, the polarimetric sensor type is used for measuring the strain parameter of the composite material. The measurement of strain is important in many SHM applications, not just as an absolute measurement in itself but also in derived measurement applications. Two important examples of such a use of strain measurement described in this chapter are: (i) as a means to monitor vibrations within a structure, which can lead to crack formation and propagation, and (ii) for composite cure monitoring during manufacture. A precursor to the work related to vibration measurement was a report ¹³ that a PM -PCF based polarimetric sensor, which is proven to show insignificant temperature sensitivity in free space and having a wide dynamic range during strain measurements, is the most suitable

¹¹ Rajan, G., Ramakrishnan, M., Semenova, Y., Domanski, A., Boczkowska, A., Wolinski, T., Farrell, G., "Analysis of Vibration Measurements in a Composite Material Using an Embedded PM-PCF Polarimetric Sensor and an FBG Sensor", DOI: 10.1109/JSEN.2011.2172412, 2011.

candidate for vibration measurements. A second precursor to the work described in the first of the two journal papers that form this chapter was a conference paper ¹⁴ which showed that the vibration amplitude of composite beams influences the accuracy of vibration measurements of highly strain sensitive polarimetric sensors such as Panda fiber sensors. This led to the investigation described in this chapter of the vibration amplitude range over which the polarimetric sensors can provide accurate vibration information. The investigation in this chapter not only shows the dependence of strain sensitivity of polarimetric sensors on the vibration amplitude but also allows one to estimate the vibration amplitude range over which the polarimetric sensors can provide accurate information. The influence of such high amplitude vibrations on the accuracy of polarimetric sensors has not been investigated to date and is significant in that it allows the selection of an appropriate type and length of polarimetric sensor for reliable vibration measurements in composite materials.

In the previous chapters it was shown that embedded stripped PM -PCF sensors can efficiently monitor thermal expansion of a composite material, with the conclusion that a stripped PM - PCF sensor is a better choice for monitoring of the non – uniform internal stress / strain in various applications, such as during composite curing process. Cure monitoring of common composite materials has been previously reported investigation. However, for novel smart materials such as Magneto Rheological (MR) smart composites, cure monitoring using photonic sensors has not been previously reported. MR materials are a class of smart materials having mechanical properties that can be controlled by an external

¹² Ramakrishnan, M., Rajan, G., Semenova, Y., Farrell, G., "Comparison of vibration measurements in composite materials using different types of polarimetric sensors", Proc. SPIE 8421, OFS2012 22nd International Conference on Optical Fiber Sensors, 842178, 2012.

magnetic field [6.1]. As a means of achieving controlled movement/motion of mechanical dampers and brakes, MRs are used in a variety of application areas from medical to automotive and aerospace [6.2, 6.3]. Thus the second derived application of the polarimetric strain sensing discussed in this chapter is monitoring of the cure process stages of Magneto Rheological (MR) smart composites to allow one to achieve more accurate control over the fabrication process.

In summary the first objective of this chapter is to describe an investigation of the vibration amplitude range over which the polarimetric sensors provide accurate information about the vibration frequency. Following on from this, the second objective is to develop an analytical calculation of the maximum allowable vibration amplitude. The last objective of this chapter is to demonstrate a sensor that can identify the non-uniform strain/stress components that evolve during different phases of the composite curing process for MR composites.

6.1 Investigation of the effect of vibration amplitude on vibration measurements of polarimetric fiber sensors embedded in composite beams ¹⁵

Keyword Photonic crystal fiber sensors, panda fiber, polarimetric sensors, vibration measurements, composite materials

Abstract: Glass fiber reinforced composite material beams embedded with two types of polarimetric sensors are fabricated by the hand layup method and characterized. Two types of polarimetric sensors: a high strain sensitive Panda type

¹⁵ M. Ramakrishnan, G. Rajan, , Y. Semenova, D. Callaghan, and G. Farrell. "Investigation of the effect of vibration amplitude on vibration measurements of polarimetric fiber sensors embedded in composite beams." Smart Materials and Structures, Vol 23(4), pp. 045037, 2014.

fiber, and a low strain sensitive polarization maintaining photonic crystal fiber (HB-PM-PCF) are compared for low frequency vibration measurements from 0 Hz to 100 Hz. Different lengths of glass fiber reinforced composite samples with embedded polarimetric sensors are fabricated and compared for different vibration amplitudes and vibration frequencies. The influence of the vibration amplitude of the composite beams on the accuracy of vibration measurements using the two types of polarimetric sensors is investigated. At high amplitude vibrations the low strain sensitive HB-PM-PCF polarimetric sensors offer a wider linear range and thus reproduce the vibration frequency and vibration amplitude accurately. However for high amplitude vibrations the high sensitivity and low dynamic strain range of Panda type fibers result in a multiple-peaks intensity pattern within one vibration cycle which leads to inaccurate vibration frequency and vibration amplitude measurements. The experimental results show that the strain sensitivity of polarimetric sensors limits the vibration measurements to a certain range of vibration amplitudes. The vibration amplitude range over which the polarimetric sensors provide accurate information about the vibration frequency is experimentally investigated and the results are presented. Also, for a composite beam undergoing deflections in the “simply - simply supported” configuration a theoretical method to predict the allowable maximum measurable vibration amplitude for any type of polarimetric sensor is derived in this study. It is envisaged that the results from the studies will provide significant information which can be used in composite material applications such as marine and aerospace, for selecting an appropriate type and length of a polarimetric sensor for vibration measurements in composite materials.

6.1.1 Introduction

In the majority of the composite material applications [6.4, 6.5] such as those in the aerospace, marine, aviation and civil engineering industries, composite structures are frequently subjected to vibrations over a variety of frequency ranges. This can lead to structural fatigue, natural frequency buckling, damage and/or catastrophic failures if the vibration frequency within the structure comes close to its natural frequency. Thus nondestructive SHM technologies for composite structures [6.6] are a key priority in order to ensure the safety and the durability of such structures.

Interferometric systems [6.7], are nondestructive and are successful in detecting damage in materials, but are too complex to be used for structures during operation as they involve a complex alignment process. Embedding OFS in composite materials [6.8-6.10] is a good practical approach because the size and weight of the optical fibers are comparable to those of the composite fiber reinforcement fabric, permitting them to act as a form of “nervous system” for a composite reinforcement fiber matrix structure. Optical fiber Bragg grating sensing [6.8- 6.11] have been widely used and the small gauge length of a typical FBG allows one to accurately determine point strain but the temperature cross sensitivity of FBG sensors is a disadvantage. Polarimetric fiber sensing [6.12, 6.13] technology is promising for vibration measurements in composite materials and within this class of sensors, polarization maintaining photonic crystal fibers (HB-PM-PCF) offer the lowest temperature sensitivity [6.14-6.16]. Furthermore, given the availability of a variety of polarization maintaining (PM) fibers and micro-structured highly-birefringent (HB) polarization maintaining fibers, such sensors can offer a wide range of sensitivities. Polarimetric fiber sensors, given their large gauge length, are suitable

for the measurement of average strain over an entire, potentially large, segment of a composite structure. we have previously reported a comparison study of both FBG and HB-PM-PCF sensors embedded in composite materials for vibration sensing [6.17]. In our earlier work, we have also reported the limitations of the Panda fiber based polarimetric sensor over HB-PM-PCF based polarimetric sensor during composite materials high amplitude vibration measurements [6.18].

At vibration frequencies close to the natural frequency of the composite beam such a beam experiences high amplitude vibrations. The influence of such high amplitude vibrations on a polarimetric sensor may affect the accuracy of the information provided by the sensors and has not been investigated to date. In practice composite beams are commonly employed in different types of configurations such as “simply supported”, clamped at both ends, and clamped at one end [6.19]. Each of the above mentioned configurations of the composite beam with an embedded polarimetric sensor needs detailed investigation during vibration measurements. In applications such as supporting structures (e.g., used in some bridges) “simply supported” composite beams are used [6.19]. As a case study in this work we investigate the influence of vibration amplitude of a high strain sensitive type and low strain sensitive type polarimetric sensors embedded in composite beams undergoing “simply supported” flexural vibrations. Moreover, here we have derived an analytical equation to find the maximum allowable vibration amplitude to be measured by a polarimetric sensor. Furthermore, a comparison between the analytically calculated maximum allowable vibration amplitude and experimental observations is also presented for different vibration amplitudes and vibration frequencies.

To analyze the influence of the sensor length on vibration measurements in

composite materials, glass reinforced composite material samples having different lengths with embedded HB-PM-PCF polarimetric sensors and Panda polarimetric sensors are fabricated and are subjected to a range of low frequency vibrations of up to 100 Hz, which is typical of the frequencies experienced by many composite structures [6.20]. Two different types of polarimetric sensors were used to allow for comparison. The vibration frequencies and amplitudes are measured using the embedded polarimetric sensors and then the results from both polarimetric sensor types are compared with the output from a non-optical reference. The principle of operation of the polarimetric sensors is explained in Section 6.1.2.A For a composite beam undergoing deflections in the “simply - simply supported” configuration a theoretical method to predict the linear response region of polarimetric sensor is derived in Section 6.1.2.B and Section 6.1.2.C. The fabrication of the composite material samples with embedded fiber optic sensors and the experimental arrangement are described in Section 6.1.3 and Section 6.1.4. A comparison of the measured vibration response of Panda and HB-PM-PCF is presented in 6.1.5.A. The dependence of sensor performance on sensor length for a polarimetric sensor is presented in Section 6.1.5.B. The determination and comparison of the maximum measurable vibration amplitude for Panda sensor presented in Section 6.1.5.C. The results and discussion are presented in Sections 6.1.6 and 6.1.7. The conclusions are presented in Section 6.1.8. The studies carried out in this work provide critical information for the SHM of smart composite materials in selecting of an appropriate polarimetric sensor type and polarimetric sensor that matches with the vibration amplitude range of interest to the end user.

6.1.2 Theoretical background of polarimetric sensors

A. Principle of operation of a polarimetric sensor

In polarimetric fiber sensing [6.21], a symmetric deformation effect in a single-mode fiber influences the propagation constant (β) for every mode because of the changes in the fiber length (L) and the refractive indices of the core and the cladding. Under the influence of the longitudinal strain (ε) at a constant temperature, for polarimetric sensors the change in the phase difference between two orthogonal polarisations of the propagating fundamental mode can be written as,

$$\delta(\Delta\Phi) = \frac{\partial(\Delta\beta)}{\partial\varepsilon} \delta L \quad 6.1$$

In the case of HB-PM-PCFs the influence of temperature on the birefringence of the fiber is very low [6.14, 6.21, 6.22] and can be neglected and hence the phase change in such a polarimetric sensor will only originate from the induced strain. The strain sensitivity of PM-Panda fibers is many times higher than that for a HB-PM-PCF [6.21]. The change in light intensity at the output due to the induced strain for a polarimetric sensor, at a wavelength λ , can be described by the formula:

$$I_s(\lambda) = \frac{I_0}{2} [1 + \cos(\Delta\Phi)] \quad 6.2$$

From the above equations it is clear that the output intensity signal of a polarimetric sensor is a periodic function of the external strain. The polarimetric sensor response is therefore only quasi-linear with respect to external strain if the strain induced phase change lies in the range between $-\pi/4$ to $+\pi/4$. Where a sensor is interrogated in the intensity domain using a polarization analyzer, any phase change outside of this range will lead to ambiguity. Thus for a polarimetric sensor operating in the

intensity domain, the linear response region of the sensor must be used for strain as well as vibration measurements [6.17]. When a polarimetric sensor is embedded in a composite material subjected to vibrations, it results in periodic variations of longitudinal strain on the sensor affecting the phase difference between the propagating modes (equation 6.1) which in turn results in periodic variations of the output light intensity transmitted by the polarimetric sensor at a certain wavelength (equation 6.2). If the changes in the output intensity of the polarimetric sensor caused by the vibrations occur within the quasi-linear part of the periodic dependency, the amplitude and frequency of such intensity variation can be used as a measure of the amplitude and frequency of vibrations applied to the composite material. However, if the changes in the output intensity of the polarimetric sensor caused by the vibrations occur outside the quasi-linear part of the periodic dependency, this will result in serious inaccuracies in the measurement of say an unknown vibration frequency and unknown vibration amplitude.

B. Linear response region of a polarimetric sensor

The range of external strain values, corresponding to the linear response region for a given polarimetric sensor depends on the strain sensitivity of the sensor [6.21]. The strain sensitivity (S) of a HB fiber section [6.21] with a length L can be expressed as follows,

$$S = \frac{2\pi}{T_\epsilon \cdot L} \text{ [rad/ (m}\epsilon \cdot \text{m)]} \quad 6.3$$

Equation 6.3 shows that the sensitivity increases with the sensor gauge length. T_ϵ is the strain value required to induce a 2π phase difference between the two polarizations of the fundamental mode. When the applied strain is increased from 0 to T_ϵ , one complete cycle of the periodic output intensity variation is observed

as per equation 6.2. For polarimetric sensors operating within the linear quadrature region, when the applied strain is less than or equal to one-fourth of the T_ε value, the output intensity of the polarimetric sensor varies almost linearly with the applied strain. The maximum possible applied strain for such a linearly responding polarimetric sensor T_{el} , and can be written as,

$$T_{el} = \frac{T_\varepsilon}{4} = \left[\frac{2\pi}{S \cdot L} \right] / 4 \quad 6.4$$

Also, as per above equation the T_{el} value is a constant for a constant length polarimetric sensor and only depends on its strain sensitivity. For low strain sensitive type polarimetric sensors the T_{el} is larger than that for high strain sensitive fibers. Thus, the advantage of PM fibers with lower strain sensitivity during vibration measurements is that for such low strain sensitive polarimetric sensors (for example, HB-PM-PCF sensors) the peak-to-peak output intensity variation is linear for a wider range of applied vibration amplitudes. I have found earlier that at high amplitude vibrations highly strain sensitive fibers (such as Panda fibers) showed multiple transmitted intensity peaks during one vibration cycle thus leading to inaccurate detection of the vibration frequency [6.18]. Thus for accurate vibration measurements using polarimetric sensors it is important to properly select the fiber types and lengths of the sensors to ensure their operation within the linear response region for the entire range of vibration amplitudes of interest.

C. Linear response region of a polarimetric sensor undergoing three – point bending

In this section the linear response region of polarimetric sensors is detailed for the polarimetric sensors embedded in a composite beam when subjected to three-point

bending induced strain. In the case of a “simply – simply supported” beam undergoing three-point bending the applied strain ε can be represented analytically by the formula [6.23]:

$$\varepsilon = \frac{6sd}{L^2} \quad 6.5$$

where L is the distance between the fixed ends of the composite beam and s is the deflection during the three-point bending, as shown in Figure 6.1.

d is the distance between the middle layer and the layer containing optical fibers [6.24] within the multilayer laminated fibre reinforced composite sample, shown in Figure. 6.2. For a constant bending deflection, an increase in the length of the composite beam results in the decrease in the applied strain proportional to $1/L.^2$

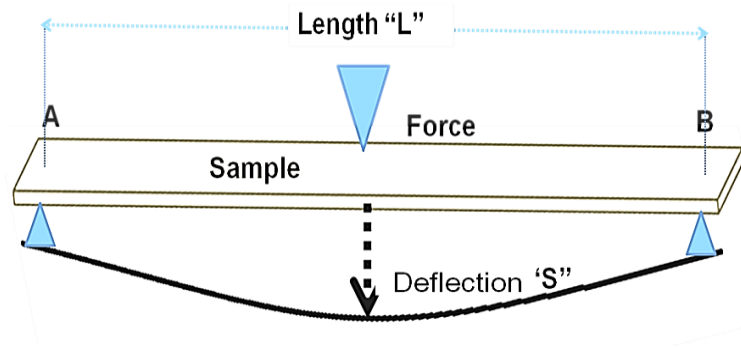


Figure 6.1 Schematic of three-point bending of the composite material sample

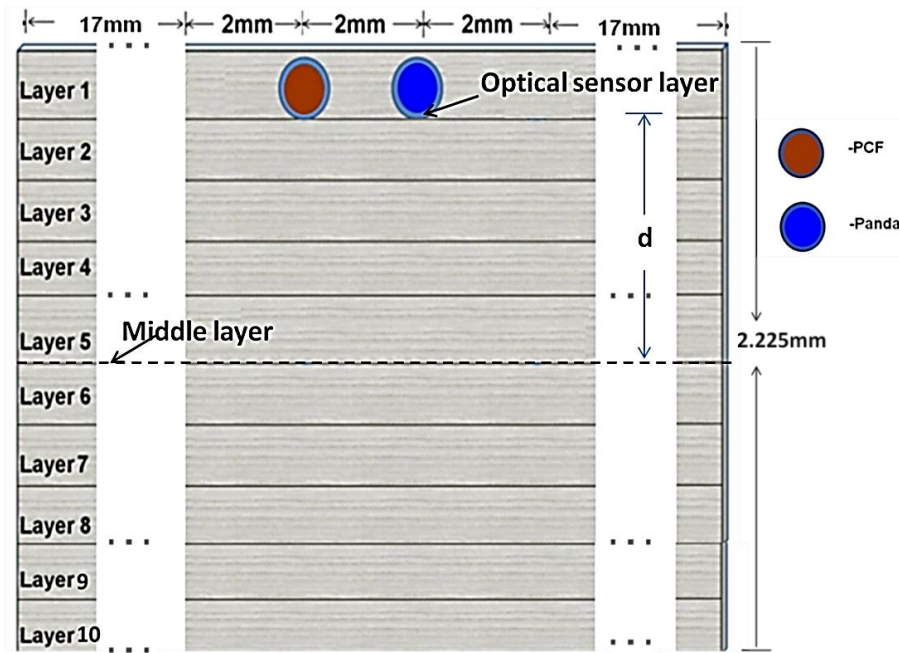


Figure 6.2 Schematic of cross sectional view of a composite material with embedded sensors

Due to the presence of a cosine function in equation 6.2, for polarimetric sensors subjected to three-point bending strain, in principle the output intensity periodically varies with applied strain. In section above section B, we have derived the maximum possible applied strain value T_{el} if a linear response is to be achieved for a polarimetric sensor and we have also demonstrated that this value is a constant for a polarimetric sensor of a constant length. Consequently, in the case of a polarimetric sensor embedded in a composite beam experiencing three-point bending deflections (s) a linear response from the sensor can only be achieved when the sensors operates in the linear quadrature region, that is if the three point bending deflection induced strain is limited to a value less than or equal to T_{el} . This corresponds to an increase of the three-point bending deflection from 0 to maximum of s_{el} . T_{el} can be related to s_{el} as using equation 6.5 thus,

$$T_{\varepsilon l} = \frac{6s_{\varepsilon l}d}{I_{\varepsilon l}^2} \quad 6.6$$

where s_{el} is the maximum value of three-point bending deflection for which given

polarimetric sensor provides linear output intensity variation. Therefore for accurate experimental vibration measurements a using polarimetric sensor the vibration amplitude must be limited from 0 to s_{el} . By substituting T_{el} from equation 6.4 to equation 6.6, the maximum allowable three point bending deflection s_{el} can be derived as,

$$s_{el} = \frac{\pi L}{12 S d} \quad 6.7$$

From equation 6.7 it is obvious that for a polarimetric sensor with a constant strain sensitivity, the maximum allowable bending deflection increases with an increase of the length of the composite beam. Since one can predict the maximum allowable bending deflection based on the end user application and the length of the composite part, thus a polarimetric fiber sensor can be designed to operate linearly by adjusting the sensor length as well as its sensitivity to strain, which is defined by the birefringence of the fiber (and thus fiber type). In general, for structural applications employing composite beam types other than a “simply supported” type such as cantilever type, for fixed – supported type and fixed- fixed type configurations the maximum allowable deflection can also be derived analytically, and therefore the sensor’s linear operating mode can be similarly achieved by properly selecting the fiber type and length for the sensor.

6.1.3 Fabrication of composite samples with embedded optical fiber sensors

The polarimetric fiber sensors used are realized based on two types of highly birefringent fibers: polarisation maintaining Panda fiber (PM–1500–HP) and HB-PM-PCF (PM–1500–01), having beat lengths of 5.0 mm and < 4 mm respectively

at an operating wavelength of 1500 nm. The PM-1500-HP fiber has a dual layer acrylate coating and the PM-1500-01 has a single layer acrylate coating with geometrical parameters as shown in Figure 6.3 (a) and Figure 6.3 (b) respectively.

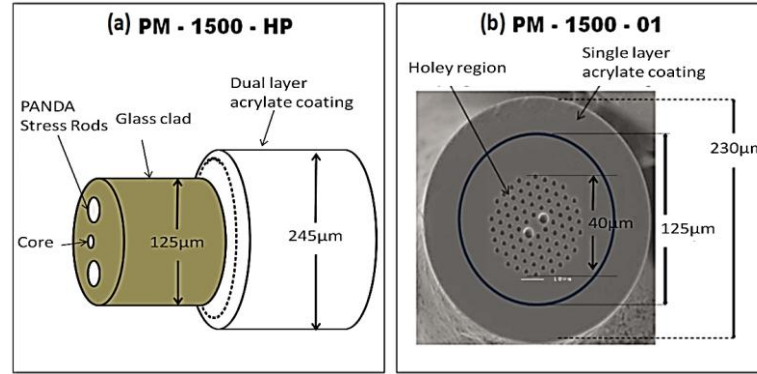


Figure 6.3 Cross sectional view of highly-birefringent fibers: (a) Panda fiber (b) HB-PM-PCF

The fiber glass reinforced composite materials for this study are fabricated by the hand lay-up method, with woven glass fiber fabrics as reinforcement bound together by resin. Samples were prepared with general purpose liquid resin Firepel K130 polyester having a viscosity of 400 cps, and with specific gravity of 1.29 at 25 °C. The woven glass fiber fabrics used have a density of 280 g/m². The fabrication process [6.17] is as follows: the mould surface is coated with a release agent of an anti-adhesive agent poly vinyl chloride, to prevent sticking of the moulded part to the mould surface. The liquid matrix resin is catalyzed 1% by volume. The first glass fiber reinforcing fabric is placed on the mould and using a brush the fiber fabric is impregnated with the resin. Then the second layer of the fiber reinforcing fabric is applied on the top of the resin and the process is repeated with stacked layers until the sample has ten layers of liquid resin and woven reinforcing glass fiber fabric oriented unidirectionally with respect to each other. In three point bending tests, if one considers compressive/tensile strain the top-

most or the bottom-most layers exhibit the maximum strain, higher than that in the inner layers. In the present experiment we have chosen the location in between the first layer and second layer as the placement layer for the optical fiber sensors in order to reduce the risk of breakage of the fragile optical fiber sensors due to high amplitude vibrations. The Panda fiber and PM-PCF were placed along the length of the composite sample, 2 mm apart from each other and are positioned approximately 19 mm from both the sides of the sample. During the process of embedding, a pre-strain is applied to the optical fibers positioned between the composite layers to make sure the optical fibers remain straight. The composite material sample is cured at room temperature for a day and then kept at a temperature of 60⁰ C for about 8 hours to evaporate excess moisture. The sample is then removed from the mould surface. The schematic of the cross section of the fabricated composite with embedded optical fiber sensors is shown in Figure 6.2, which shows the locations of the fiber sensors within the composite material. Six samples are prepared following the same procedure. Both HB-PM-PCF and Panda fiber sensors are embedded within each of the six samples, where the samples have lengths 21.5 cm, 29.5cm, 33.5 mm, 39.5 mm, 43.5 mm, and 47.5 mm. After curing, the samples are trimmed so they all have common width of 40 mm and are 2.225 mm thick as shown in the cross- sectional view of the composite sample in Figure 6.2. One of the fabricated samples is as shown in Figure 6.4.



Figure 6.4. Fabricated composite material sample

6.1.4 Experimental arrangement

The experimental arrangement for applying vibration to the composite materials embedded with optical fiber sensors is similar to a three-point bending set-up and is as shown in Figure 6.5.

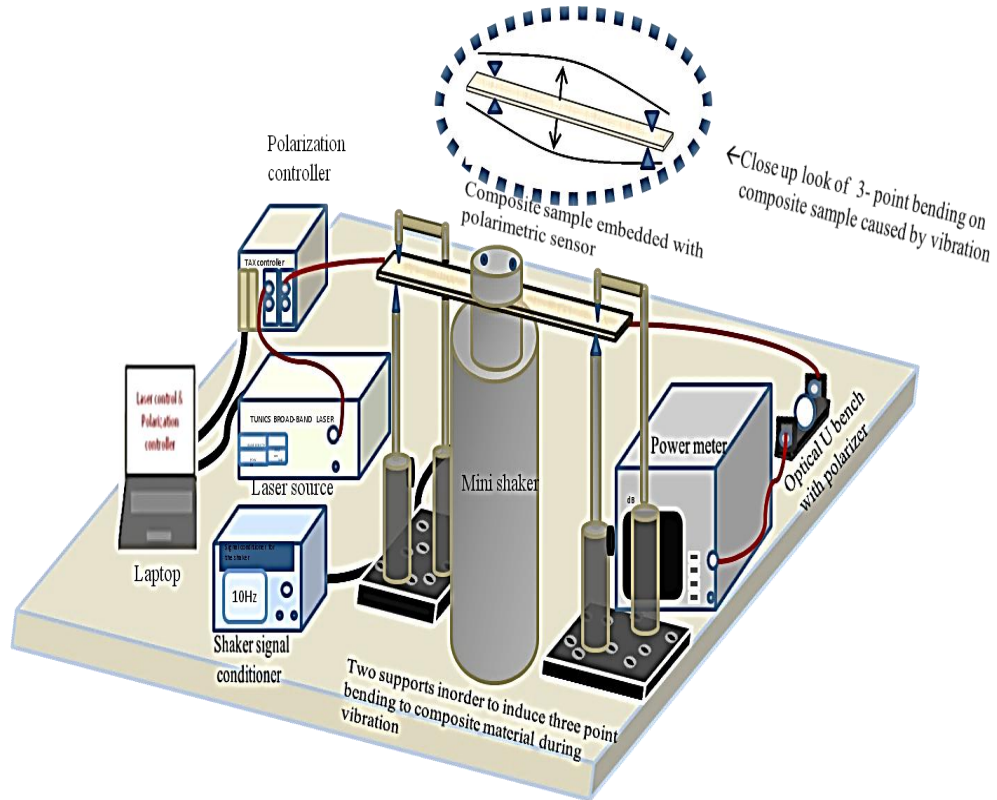


Figure 6.5. Schematic of the experimental arrangement used to apply vibration analogous to three-point bending on the composite material sample with embedded polarimetric sensors

The composite material sample is rigidly fixed at both ends and the middle of the composite sample beam is clamped on to the top of a vibration generator (a mini shaker, Model 1501 from Environmental Equipments Ltd). Input light from the laser source (1550 nm) is launched to the polarimetric sensors with its linear polarization at 45° relative to the slow axis of the optical fiber by using a polarization controller. The output fiber from the composite material is connected to a polarization analyzer, whose power output is then recorded by a high speed

optical power meter, which has the capability to measure 10,000 samples per second. The laser source and polarization controller are controlled by a computer running a LabVIEW instrumentation control program.

The mini-shaker is driven by a digital sine-wave controller (Environmental Equipments Model 1592), through which the frequency and lateral displacement of the shaker can be controlled. The amplitude and frequency of the shaker are also measured by an accelerometer, which provides a non-optical reference for the measurements obtained by the optical fiber sensors. In this study, we have applied vibrations to the composite material sample with frequencies ranging from 2 Hz to 50 Hz. It should be noted that the displacement of the shaker is a function of the applied frequency. The relation between the shaker frequency and shaker vibration amplitude follows a profile as shown in the Figure 6.6. The maximum displacement was set to 5.8 mm which occurred at 15 Hz (measured by the accelerometer), and thereafter the peak-to-peak displacement of the shaker head reduces as the frequency is increased. As per manufacturer's specifications, the natural frequency of the shaker suspension system is responsible for the peak in the vibration amplitude at 15 Hz [6.25, 6.26].

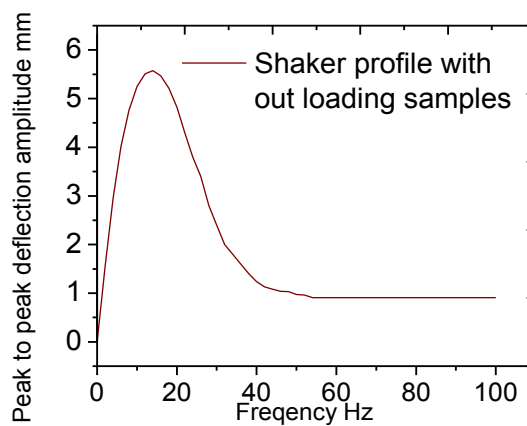


Figure 6.6. Shaker frequency response profile without loading samples measured using an accelerometer for applied frequencies from 0 to 100 Hz

6.1.5 Results and analysis

a) Panda and HB-PM-PCF vibration frequencies measurement at various vibration amplitudes

Vibration measurements on the composite material samples with embedded polarimetric sensors were carried out for a range of frequencies from 2-100 Hz for both a HB-PM-PCF and Panda fiber polarimetric sensors. The output signal intensity was measured using the high speed optical power meter with data recorded at a sampling speed of 1 kHz. The sample length was 21.5 cm and distance between the fixed end points of the “simply supported” beam was 18 cm. As expected the applied vibration causes periodic intensity variations in the output of the HB-PM-PCF and the Panda fiber sensors. The normalized intensity variations in the time domain and the FFT spectra for the HB-PM-PCF sensors for the applied vibration frequencies of 2 Hz, 10 Hz, and 20 Hz are shown in Figure 6.7.

To verify the accuracy of vibration frequencies measured using both types of sensors, the FFT spectra of the HB-PM-PCF sensor and the Panda fiber sensor are compared. From inspection of the time domain graphs (a, b, c) of Figure 6.7 for HB-PM-PCF and corresponding (a, b, c) graphs of Figure. 6.8 for Panda fiber, it is clear that HB-PM-PCF sensor response replicates input vibrations more accurately with less distortion than the Panda fiber sensors. The presence of significant distortion is problematic as it can make the accurate determination of the value of an unknown applied vibration frequency difficult.

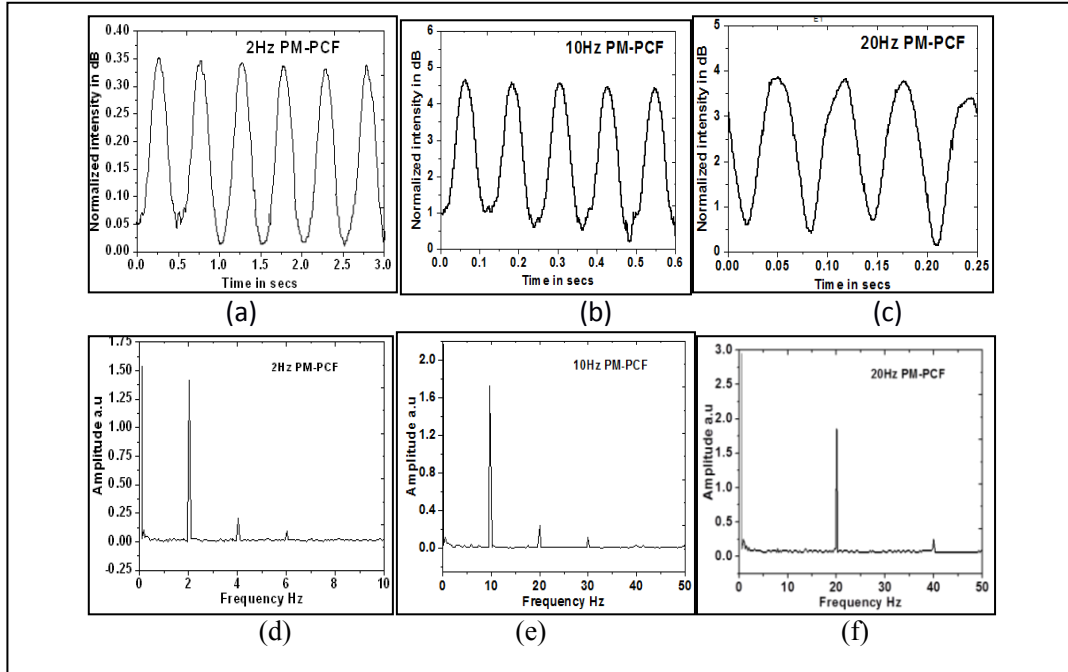


Figure 6.7. The time domain response (a), (b), and (c), and FFT spectrum (d), (e), and (f) of HB-PM-PCF fibers embedded in a 21.5 cm long composite sample at 2 Hz, 10 Hz, and 20 Hz vibration frequencies.

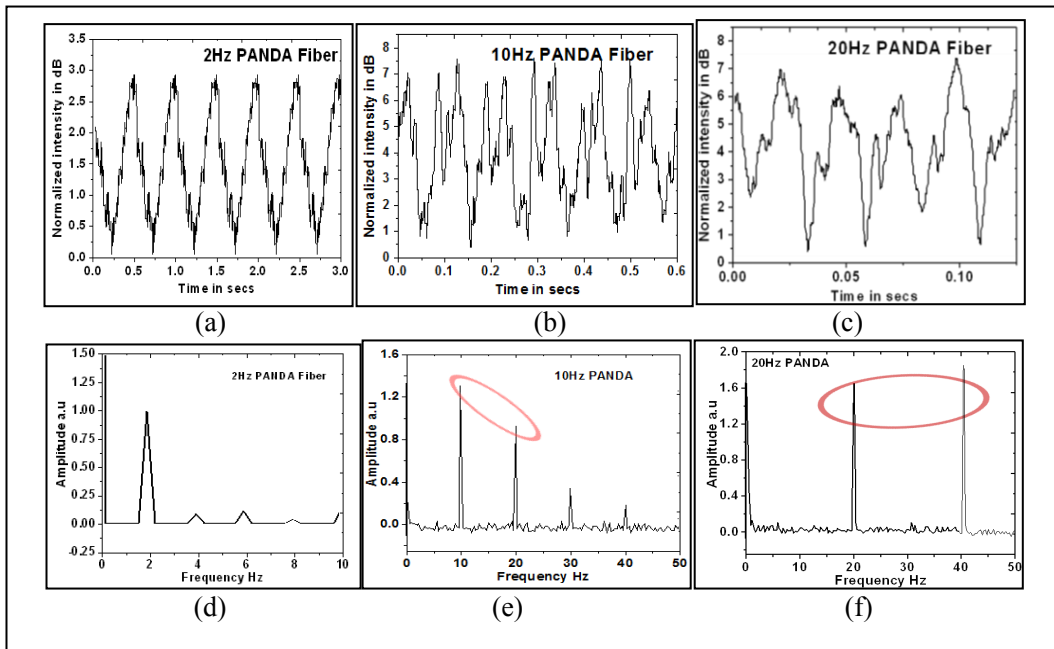


Figure 6.8. The time domain response (a), (b), and (c), and FFT spectrum (d), (e), and (f) of PM-Panda fibers in 21.5 cm composite sample at 2 Hz, 10 Hz, and 20 Hz vibration frequencies

This is best illustrated by considering the frequency domain equivalents (calculated using an FFT) of the time domain responses. The lower levels of distortion present for the HB-PM-PCF sensor are confirmed by the corresponding FFT graphs (d, e, f) of Figure 6.7 from which it can be seen that while some level of higher order harmonics of the applied vibration frequency are present in the FFT spectra, their amplitudes are significantly smaller than the main peaks corresponding to the applied vibration frequencies and thus the vibration frequency can easily be determined. However in the case of the Panda fiber polarimetric sensor, for applied sinusoidal vibrations, the sensor output showed highly distorted patterns in time domain, particularly at frequencies of 10 Hz and 25 Hz (Figure 6.8 (b) and Figure 6.8 (c)). The FFT spectra for the Panda fiber sensor shows the presence of substantial harmonic content for applied vibration frequencies of 10 Hz and 20 Hz. This would make the determination of an unknown vibration frequency difficult to accurately measure given the ambiguities created by high peak value second harmonic amplitudes (Figure 6.8 (e) and Figure 6.8(f)). For completeness the temporal response and FFT spectra for the 2 Hz case provided accurate information as shown in Figure 6.8 (a) and Figure 6.8 (d), respectively.

It is clear from the results above that exceeding the maximum measurable amplitude will result in serious inaccuracies in the measurement of say an unknown vibration frequency. Since sensor sensitivity depends on sensor length, it is very worthwhile therefore to experimentally investigate two issues: the dependence of sensor performance on sensor length and secondly the maximum allowable vibration amplitude, which will also be a function of the length of the sensor. These two topics are dealt with in the following sections.

b) Dependence of sensor performance on sensor length for a polarimetric sensor

The dependence of the peak-to-peak polarization state change (measured experimentally as a change in optical intensity) of both types of polarimetric sensors on the length of the sensor is studied in this section. This is done in order to later determine the maximum measurable vibration amplitude for a polarimetric sensor. It was reported earlier [6.18] that the amplitude of vibration can be determined by measurement of the peak-to-peak optical intensity variations of the temporal response of the HB-PM-PCF polarimetric sensors, assuming an appropriate calibration has taken place. In the frequency range from 0 Hz to 20 Hz, for a constant input amplitude the peak-to-peak vibration output amplitude of the shaker gradually increases from 0 to 5.8 mm and later decreases as verified by the non - optically measured vibration amplitude as shown in Figure 6.9 (a). This change over the frequency range is an inherent feature of the vibration shaker. The peak-to-peak optical intensity for different lengths of polarimetric sensor is measured and compared in this section. The composite sample fabrication process and experimental set up are as shown in Section 6.1.3 and Section 6.1.4, respectively. Samples with lengths of 21.5 cm, 29.5 cm, 33.5 cm, 39.5 cm, 43.5 cm, and 47.5 cm are tested. The vibration measurements were conducted using a three point bending type set-up. The distance between the fixed clamps placed 0.75 cm from the composite sample ends is effectively the sensor length and thus the assumed sensor lengths for each of the tested samples were 20 cm, 28 cm, 32 cm, 38 cm, 42 cm, and 46 cm. In order to verify the accuracy of the polarimetric sensors response, the amplitude of the vibrations of the composite material sample at different frequencies was also measured using a non-optical accelerometer as a

reference.

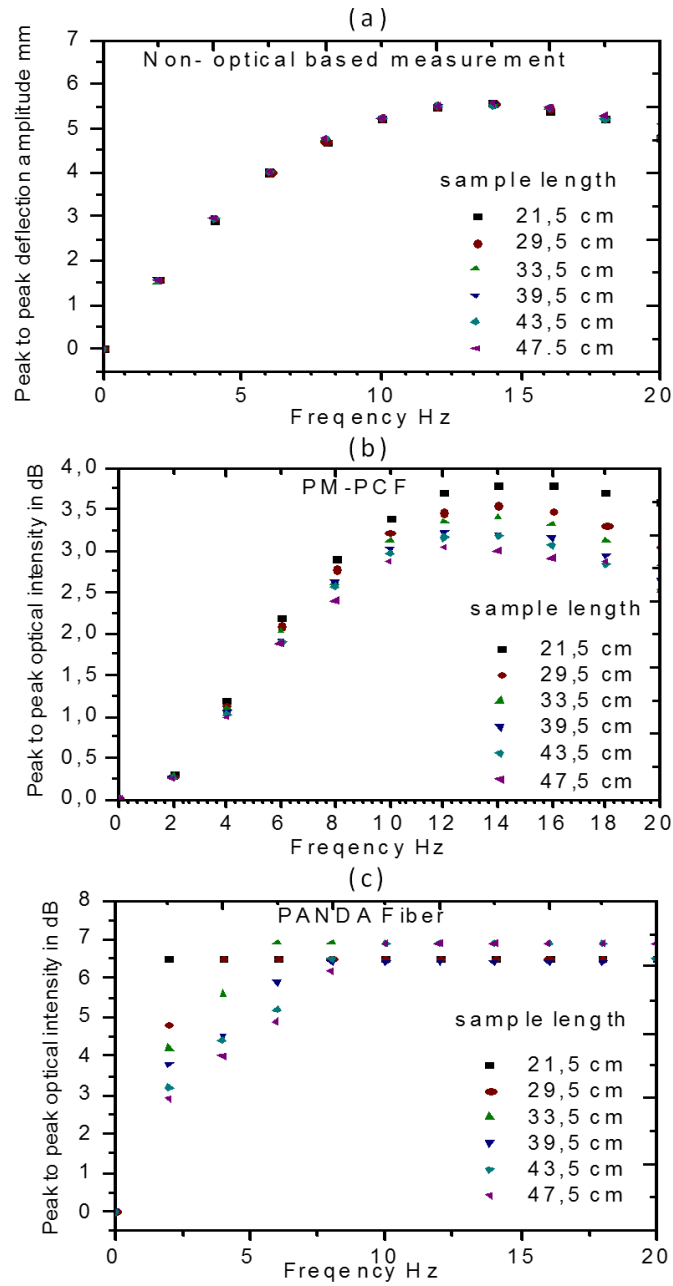


Figure 6.9. (a) The peak-to-peak vibration amplitude using non-optical measurement, the peak-to-peak output intensity variation of (b) HB-PM-PCF, and (c) Panda fiber for applied frequencies form 0 Hz to 20 Hz

The shaker vibration amplitude measured using the accelerometer versus applied frequency for different sample lengths is as shown in Figure 6.9 (a). The variation in the peak-to-peak optical intensity of the outputs of the HB-PM-PCF and Panda

fiber based polarimetric sensors with different lengths for applied frequencies ranging from 0 - 20 Hz is measured and is as shown in Figure 6.9 (b) and Figure 6.9 (c), respectively. From Figure 6.9 (b), it is clear that for all the samples the maximum peak-to-peak intensity variation of the HB-PM-PCF sensor output is observed at 15 Hz, corresponding to the highest vibration amplitude value 5.8 of mm and corresponding to the result determined from the accelerometer as in Figure 6.9 (a). Comparing the Figure 6.9 (a) and Figure 6.9 (b), it is observed that for all samples the amplitude of vibration measured by the HB-PM-PCF sensors is in a good agreement with the non-optically measured (based on accelerometer data) vibration amplitude profile as well as frequency response characteristics.

Again, for the HB-PM-PCF polarimetric case comparing the accelerometer measured vibration amplitude in Figure 6.9 (a) with the peak-to-peak output intensity variation of the HB-PM-PCF polarimetric sensors in Figure 6.9 (b), it is observed that for a constant vibration amplitude if the sample length increases the output peak-to-peak optical intensity decreases. For example, at 14 Hz, for a sample length of 21.5 cm, the peak-to-peak optical intensity variation is circa 3.6 dB, but decreases to circa 3 dB, when the length increases to 47.5 cm. This is due the fact that during three-point bending tests on the composite samples, the effective strain in the sample decreases with an increase in sample length as per equation (6.5). Thus in order to calculate the vibration amplitude from the HB-PM-PCF sensor peak-to-peak output intensity, an appropriate calibration is required for each sample length of the polarimetric sensor.

In the case of Panda sensors, the output peak-to-peak optical intensity is again found to decrease with an increase in a sample length. However, this can only be observed for composite samples having lengths of 33.5 cm, 39.5 cm, 43.5 cm, and

47.5 cm and only for applied frequencies ranging from 2 Hz to 7 Hz as shown in Figure 6.9 (c). This is because for short sample lengths of 21.5 cm and 29.5 cm or for higher vibration frequencies (implying higher amplitudes) the effective strain is such that it exceeds the maximum allowable vibration amplitude for the sensor, making measurement unreliable. This is in close agreement with our theoretical predictions (Equation 6.7).

c) Determination and comparison of the maximum measurable vibration amplitude for Panda sensor

This investigation is limited to Panda sensors, as this sensor type is the one that is most likely to place limits on the maximum vibration amplitude. For the HB-PM-PCF sensor the maximum measurable vibration amplitude is very high and thus is much less likely to place limitations on the use of the sensor. The strain sensitivity of the HB-PM-PCF polarimetric sensors after embedding into a composite material is found to be approximately 4 rad/m. mε [6.24]. For example, the maximum measurable vibration amplitude is theoretically 14.7 mm for the shortest sample length. In any event due to the mechanical performance characteristics of the shaker, the shaker we used for this investigation is limited to vibration amplitudes below a value of 5.8 mm and in turn restricts our vibration amplitude measurement range to less than 5.8mm. As a result, it is not possible to experimentally determine the maximum measurable vibration amplitude of the HB-PM-PCF sensor. For Panda sensors to determine the actual maximum measurable vibration amplitude of each sample length, here we compare the peak-to-peak optical intensity measured by a Panda fiber with non-optically measured vibration amplitude at different applied frequencies.

The maximum measurable vibration amplitude for a Panda fiber based polarimetric

sensor embedded in different sample lengths is measured by comparing and analyzing the vibration amplitude for applied frequencies from Fig. 6.9 (a) with the Panda fiber optical intensity variations corresponding to the applied frequencies from Figure 6.9 (c). The method is explained as follows: for each sample the applied vibration frequency for which the variation in the Panda polarimetric sensor's output intensity with frequency reaches a plateau is noted. Then the vibration amplitude corresponding to the noted frequency is extracted from the non – optical accelerometer data. For example, for a sample length 21.5cm, it is obvious from Figure 6.9 (c), that above an applied frequency of 2 Hz the output intensity variation of the Panda fiber no longer shows any variation with increase in the applied frequency. The vibration amplitude corresponding to 2 Hz calculated from the accelerometer data is 1.6 mm. Thus for 21.5 cm sample length vibration amplitude measurement, it can be concluded that a measurement of vibration amplitude in excess of 1.6 mm is unreliable for a Panda fiber polarimetric sensor. Similar for other samples lengths using the same method the maximum measurable vibration amplitude for Panda fiber vibration measurements is calculated and is shown in Table 6.1.

In addition, the experimentally measured results in Table 6.1 are compared with theoretical predictions. To do this the maximum allowable vibration amplitude calculated analytically using equation 6.7 is compared with the experimentally observed values. For this the strain sensitivity of the Panda fiber sensor is measured using a static strain applied in a three point bending setup. The applied strain is calculated analytically using equation 6.5 and thus the strain sensitivity is calculated by equation 6.3. The strain sensitivity of the Panda fiber polarimetric sensors after embedding into a composite material is found to be approximately 35.4 rad/m. mε.

This experimentally measured static strain sensitivity and the distance of optical sensor layer from the middle layer ($d \sim 0.89$ mm for all samples) are then substituted in the equation 6.7. The analytically calculated maximum allowable vibration amplitude values of all sample lengths are presented in Table 6.1.

Table 6.1. Comparison of experimentally and theoretically calculated values of the maximum measurable vibration amplitude of Panda fiber for different sample lengths

Length of the sample	Maximum measurable vibration amplitude (mm)		Error	Uncertainty in length measurement in %	Uncertainty in thickness of the sample in %	Uncertainty in embedded Panda fiber strain sensitivity in %	Total uncertainty in %	% deviation between theoretical and experimental
	Experimental	Theoretical						
21.5	1.7	1.66	0.04	0.023	0.561798	1.412429	1.997	2.37%
29.5	2.4	2.32	0.08	0.017	0.561798	1.412429	1.991	3.33%
33.5	2.7	2.65	0.05	0.015	0.561798	1.412429	1.989	1.85%
39.5	3.2	3.16	0.04	0.013	0.561798	1.412429	1.987	1.25%
43.5	3.55	3.49	0.06	0.011	0.561798	1.412429	1.986	1.69%
47.5	3.9	3.82	0.08	0.011	0.561798	1.412429	1.985	2.05%

The theoretically calculated maximum allowable vibration amplitude shows good agreement with experimental observations with a maximum deviation of 3.33 %, as shown also in Table 6.1, most likely as a result of unavoidable limitations in the experimental setup such as an error in the experimentally measured sensing region length (approximately ± 0.05 mm) and sample thickness measurement errors due to the non-uniform thickness (approximately ± 0.005 mm) of the fabricated composite beam. In addition, the lamination process slightly influences the Panda fiber strain sensitivity and thus uncertainty in the measured Panda fiber strain sensitivity after embedding into composite material is approximately 0.5 rad/m. mε. The error and uncertainty in the experimentally measured maximum measurable vibration amplitude is calculated taking in to account of the Guide to the Expression of

Uncertainty in Measurement (GUM) and is as shown in Table 6.1. It is observed that as the composite sample length increases the maximum measurable vibration amplitude increases. The reason for this is that the strain induced by the three point setup is inversely proportional to length and as per equation (6.6) as the length increases greater deflection can be applied to the sample to reach the maximum possible applied strain value for a linearly response for the polarimetric sensor.

One of the key reasons behind vibration measurements is to avoid exposure to high amplitude vibrations at frequencies close to the natural frequency of the composite structure. When a beam is allowed to vibrate close to its natural frequency, the amplitude of vibration will increase as the vibration frequency approaches the resonance frequency, which may lead to catastrophic damage to the beam. This makes vibration resonance tests an important mechanical test, but with the difficulty that to measure the natural frequency it will be necessary to sense potentially large vibration amplitudes close to resonance.

Using polarimetric sensors for this purpose as we discussed above is problematic, since if the unknown vibration amplitude is beyond the maximum measurable vibration amplitude of the polarimetric sensor then it is not possible to detect the natural frequency of the composite beam. Given the ability of a HB-PM-PCF sensor to deal with larger vibration amplitudes compared to a Panda sensor means that a HB-PM-PCF sensor is the better choice for such tests. To illustrate this in the case of composite sample having length 47.5 cm the simulated values of first two natural frequencies (using Ansys based mechanical simulations) are calculated to have values at 20.989 Hz and 84.013 Hz. In order to experimentally identify the vibration amplitude increase near the natural frequency and thus measure the natural frequency, the peak-to-peak optical intensity output intensity variation of

the HB-PM-PCF and Panda fiber based polarimetric sensors embedded in sample having a length 47.5 cm are measured for applied frequencies ranging from 0 - 100 Hz and is plotted in Figure 6.10. Also the vibration amplitude versus applied frequency for each sample length is measured using non-optical accelerometer and is plotted inside the graphs in Figure 6.10. The inset in Figure 6.10 shows that the non-optical accelerometer can detect the first and second natural frequencies at 21.45 Hz and 82 Hz. However, for the optical sensors the peak in vibration amplitude due to the first and second natural frequencies occurring near the frequency values of 21.45 Hz and 82 Hz are only visible in the response of the HB-PM-PCF as shown in Figure 6.10 but for the Panda fiber sensor the peak in the vibration amplitude near a frequency of 21.5 Hz is not seen visible as its vibration frequency is within the range where Panda sensor's output is distorted.

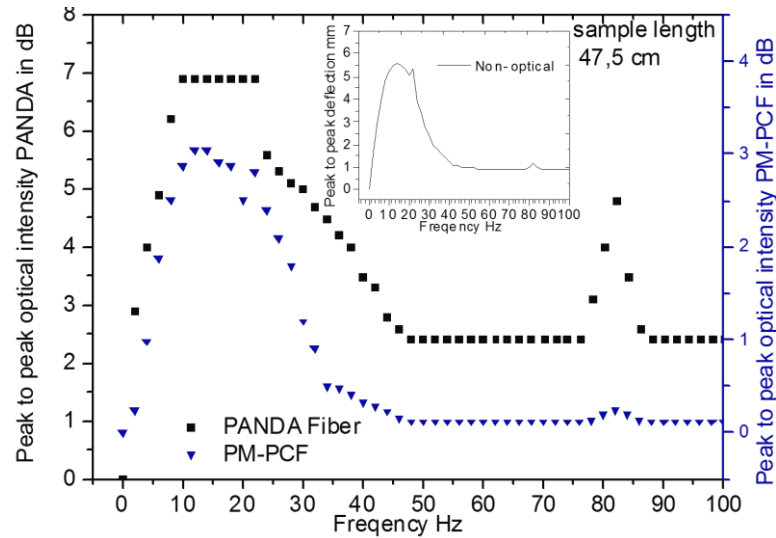


Figure 6.10. Comparison of the peak-to-peak intensity amplitude variation and applied frequencies for Panda and PM-PCF with non-optically measured response for sample composite sample having length 47.5 cm

6.1.6 Discussion

From our results it is observed that during vibration measurements the high strain

sensitive Panda fiber polarimetric sensor showed highly distorted in time domain intensity variations in response to the sinusoidal applied vibration oscillations, while for low strain sensitive HB-PM-PCF polarimetric sensors the intensity pattern accurately replicated the applied vibration frequency. This leads to the conclusion that when the strain sensitivity of the polarimetric sensors increases the maximum allowable amplitude of vibration decreases. Panda fibers of different length are compared for vibration measurements and from the results it is confirmed that the length of the polarimetric sensor influences the maximum allowable vibration amplitude. As the sensor gauge length increases the polarimetric sensor gives accurate vibration measurements for wider range of vibration amplitudes. The maximum allowable bending deflection for which the polarimetric sensor output intensity variations remain in the linear quadrature region can be predicted by using the analytical equation derived. The comparison of the theoretically and the experimentally measured maximum allowable vibration amplitudes measured by Panda fibers also shows good agreement with each other. This shows the feasibility of adapting this technique to estimate the maximum measurable vibration amplitude for embedded polarimetric fiber sensors, and thereby guarantee the reliability of using such sensors for composite materials.

6.1.7 Conclusions

The vibration amplitudes range over which the polarimetric sensors provide accurate information about the vibration frequency is studied. Low frequency vibration measurements from 0 Hz to 100 Hz are performed for glass fiber reinforced composite material samples embedded with two different polarimetric sensor types - a high strain sensitive Panda type fiber and a low strain sensitive

polarization maintaining photonic crystal fiber. we have derived an analytical expression to predict the allowable maximum vibration amplitude for any type of polarimetric sensor embedded in a composite beam undergoing deflections in a “simply - simply supported” configuration. The advantage of such an analytical calculation of the maximum allowable vibration amplitude that can be measured is that it allows end-users to choose a polarimetric sensor with appropriate birefringence and sensor length for accurate vibration amplitude measurements. Additionally, measurements for several glass fibers reinforced composite samples with different lengths embedded with polarimetric sensors are compared for different amplitudes of vibration frequencies. The experimental and theoretical results confirmed that as the sensor gauge length increases a polarimetric sensor provides accurate vibration measurements for wider range of vibration amplitudes. It is concluded that the strain sensitivity and sensor length of polarimetric sensors limits the vibration measurements to a certain range of vibration amplitudes. At high vibration amplitude vibration measurements, in order to ensure the output intensity of polarimetric sensor occurs within the quasi- linear region of the periodic dependency, the vibration measurements must be performed within the maximum measurable vibration amplitude of the particular polarimetric sensor type. For wide range of vibration amplitude measurement the best choice is a low strain sensitive polarimetric sensor such as a HB-PM-PCF fibers or a sufficiently longer length of high strain sensitive polarimetric sensor such as Panda fiber. The results of the studies provide critical information to the end-users for selecting an appropriate polarimetric sensor types and sensor lengths for vibration measurements in composite materials.

6.2 A photonic crystal fiber based polarimetric sensor for cure monitoring of magneto-rheological smart composite material¹⁶

Keywords: High birefringent photonic crystal fiber; fiber Bragg grating; Magneto-rheological; composite material; cure monitoring.

Abstract: A buffer stripped high birefringent photonic crystal fiber based polarimetric sensor is developed for monitoring the curing process of magneto rheological elastomer (MRE) smart composite material. Using the developed sensor, different phases of the MRE curing process are clearly visible from the phase shift variation of the embedded HB-PM-PCF sensor. During the curing process the buffer stripped HB-PM-PCF exhibits a stress/ strain induced phase shift variation from 0 to 1.98 radians. This is a significantly large phase change, which can be used to very clearly identify the different stages in the curing process. For comparison, a FBG sensor is also used for monitoring the internal strain during the curing process but its response does not allow one to reliably distinguish all the curing stages. The present investigation offers a simple nondestructive method to monitor the curing process of MRE smart composite material.

6.2.1 Introduction

Magnetorheological (MR) materials are a class of smart materials having mechanical properties that can be controlled by an external stimulus [6.27]. MR

¹⁴ M. Ramakrishnan, G. Rajan, Y. Semenova, Y. Zhou, S. Jerrams, and G. Farrell. "Photonic crystal fibre-based polarimetric sensor for cure monitoring of magnetorheological smart composite material." *Electronics Letters*, Vol 50(15), pp. 1083-1084, 2014 .

materials are solid or liquid materials composed of magnetizable (usually iron) particles suspended in a low permeability carrier matrix (usually rubber). Components made from such controllable MR materials have the distinct advantage that their stiffness, modulus and damping properties can be changed instantly and reversibly by applying an external magnetic field, making them a truly useful “smart material”. MR materials have potential applications in a variety of areas from medical to automotive and aerospace for controlled movement/motion in dampers, brakes and vibration absorbers [6.27]. However, in controlled movement applications, it is critical to have accurate control of the MR material properties. One reliable approach to realize this is by using embedded fiber optic sensors.

Compared to conventional non-destructive sensing techniques, optical fiber sensors have achieved wide acceptance due to their attractive properties such as small size, immunity to electromagnetic interference and low cost [6.28]. Optical fiber sensors embedded in various structures are very useful for applications such as structural health monitoring [6.28] using FBG while optical fiber based refractometers [6.29] have been reported for in – situ characterization of the cure process in composites. Highly birefringent fiber based polarimetric sensors [6.12] were reported earlier for structural health monitoring applications of fibre reinforced composite materials.

In this study we present a highly birefringent photonic crystal fiber based polarimetric sensor to monitor the internal stress/strain during the curing process of an MR material, in order to determine the rate of cure and the curing phases. The sensing element is a HB-PM-PCF with its buffer coating removed at the sensing area. Removing the buffer coating results in a sensor which exhibits good

sensitivity to both non uniform strain and stress variations. To the best of our knowledge the application of such a stripped photonic crystal fiber based polarimetric sensor is the first time an optical fibre sensor has been deployed for cure process monitoring of MR materials.

6.2.2 Experiment

In this work, we have fabricated a solid MR elastomer (MRE) sample by suspending ferromagnetic soft carbonyl iron particles (diameter $\sim 6.0 - 7.0 \mu\text{m}$, and density = 7.86 g/cm^3 from BASF, Germany) in a low permeability silicone rubber carrier matrix. The silicone rubber carrier matrix is formed by mixing a room temperature vulcanized (RTV) silicone rubber comprising a base elastomer (ESSIL 291 silicone resin) and a catalyst (ESSIL 291 catalyst) in the ratio 10:1. Further, carbonyl iron particles are incorporated into the silicone rubber carrier matrix in a concentration of 20 volume percent. After degassing, the mixture is poured into a mould. Before closing the mould, the optical fiber sensors were placed in the compound as shown in Figure 6.11 (a). The closed mould with compound and optical fiber sensors is allowed to cure in the presence of a magnetic field using a Halbach array, which is capable of providing a mean magnetic flux density of $400 \text{ mT} (\pm 5\%)$ over the 50 mm nominal diameters of the bore and is as shown in Figure 6.11 (b). For the present investigation, the orientation of the mould inside the Halbach array is such that during curing process the iron particles align parallel to the direction of optical fiber sensors. The cured sample with optical sensors has dimensions of $5 \text{ cm} \times 5 \text{ cm} \times 0.2 \text{ cm}$ and is as shown in Figure 6.11 (c).

Magnetic field lines

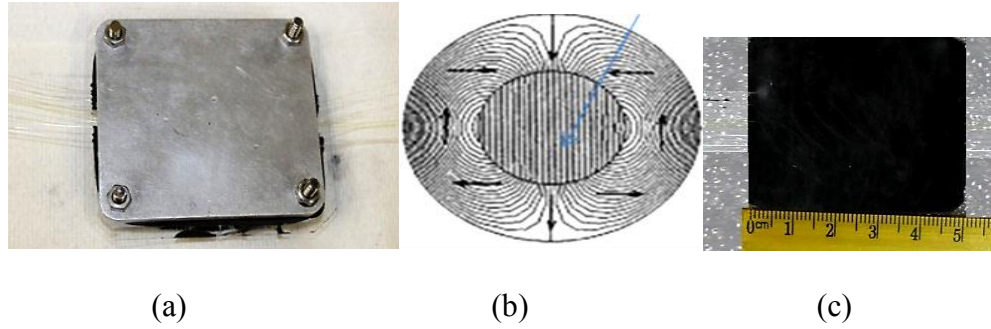


Figure 6.11. (a) Optical fiber sensors placed within mould; (b) Halbach Array; and (c) Cured MRE composite with optical fiber sensors

The polarimetric sensor used for this study is a buffer coating stripped HB-PM-PCF polarimetric sensor (PM-1550-01)). The HB-PM-PCF stripped sensing area is located within the 5 cm length of the MRE sample. For comparison, an FBG sensor is used for strain measurement within the MRE sample. It is a polyimide coated FBG having a 1550 nm peak wavelength and the 5 mm grating length placed.

The experimental arrangement for monitoring the curing process of the MRE using the polarimetric sensor and FBG sensor is as shown in Figure 6.12 (a). During the entire curing cycle, the mould filled with the MRE mixture with optical fibers is fixed inside a Halbach array. For polarimetric sensors, the variation in State of Polarization (SOP) is measured using a polarization controller and polarimeter (TXP 5004 from Thorlabs). Input light from the laser source (1550 nm) is launched into the polarimetric sensor with its linear polarization at 45° to the slow axis of the optical fiber by using a polarization controller. The output fiber from the MRE sample is connected to a polarimeter. During the curing cycle, the information about the phase shift variation of the HB-PM-PCF polarimetric sensor can be determined by evaluating SOP evolution and a more detailed description of this method is provided in reference [6.30]. For the FBG sensor, the peak wavelength

shift is recorded using an FBG interrogation system from Smart Fibers.

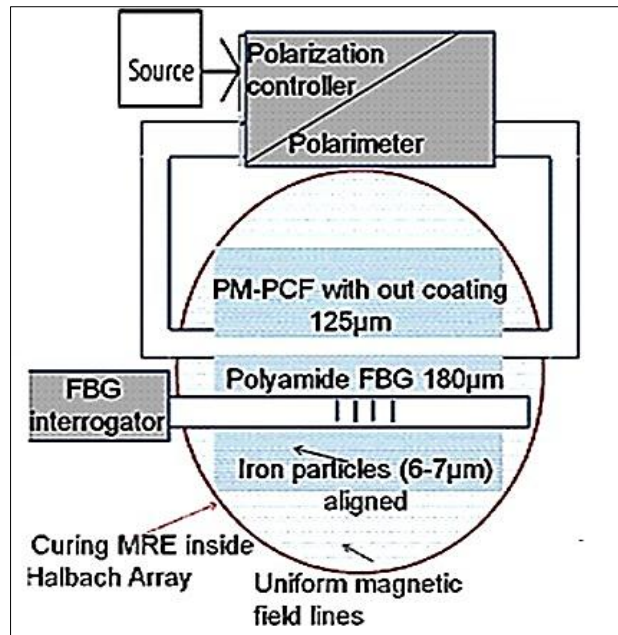
6.2.3 Principle

In the case of HB PM optical fibers, any symmetric deformation effect induced by strain influences the propagation constant of every mode propagating through the fiber optic fiber due to changes in fiber length and the refractive indices of both the fiber core and the fiber cladding [6.12, 6.30]. This leads to phase shift between the two polarizations of the fundamental mode.

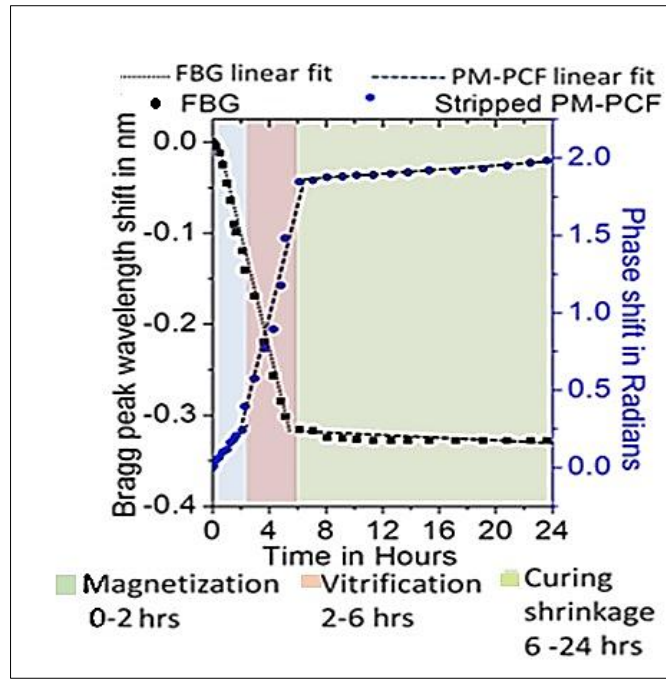
It was reported previously that for a PM-PCF sensor embedded in a composite material the presence of the buffer coating plays an important role in its temperature/strain sensitivity [6.30]. For stripped HB-PM-PCFs (such as PM-1550-01) the influence of temperature on fiber birefringence in free space is negligible [6.30]. However, as was reported earlier, the stripped HB-PM-PCF sensor shows an increased temperature induced response after embedding in the composite material [6.30]. This is due to the fact that the buffer stripped fibre is sensitive to both applied longitudinal strain and composite material thermal expansion induced non -uniform lateral strain/stress. Also, the typical strain sensitivity of a stripped HB-PM-PCF sensor in free space is 1.7 rad/m. mε. However, after embedding in an E-glass fibre reinforced composite material the stripped HB-PM-PCF showed elevated strain sensitivity due to the change in birefringence. For a buffer coating removed HB-PM-PCF polarimetric sensor such an additional variation in birefringence is created both by non - uniform lateral strain components as well as stress induced shape deformations of the optical fiber. For conventional FBG sensors the Bragg peak wavelength shifts in accordance with the applied longitudinal strain and temperature [6.28].

6.2.4 Results and discussion

A comparison of the responses of the buffer stripped HB-PM-PCF polarimetric sensor and the polyimide FBG sensor during the MRE curing process is carried out. For comparison with the FBG sensor, the real time changes in Bragg peak wavelength are also recorded using the FBG interrogator. Further, the polarimetric sensor's phase shift variation and the FBG sensor's Bragg peak wavelength shifts are plotted against curing time as shown in Figure 6.12 (b).



(a)



(b)

Figure 6.12. (a) Proposed experimental setup for cure monitoring of MRE (b) The MRE sample cure monitoring using HB-PM-PCF and FBG sensors

Considering Figure 6.12 (b), it can be seen that in the case of the stripped HB-PM-PCF sensor, an overall phase shift of 1.98 radians is observed during the 24 hour MRE curing process. Further inspection of the data in Figure 6.12(b) shows that the curing process response of the HB-PM-PCF sensor can be divided into three linear response regions with three different slopes. During the 24 hour curing cycle the FBG embedded in the same MRE sample showed blue Bragg wavelength shift from 0 to -0.32 nm but the overall the FBG response shows only two linear regions that are clearly visible as shown in Figure 6.12(b). The observed Bragg wavelength shift has a blue shift which indicates compressive strain. Considering the typical FBG stain sensitivity as $1.2 \text{ pm}/\mu\epsilon$, and thus the strain variation observed for FBG during curing process is fairly low with a value of $-0.386 \text{ m}\epsilon$. In order to differentiate between the separate stages of the curing process based on the HB-PM-PCF sensor response, we have calculated the slopes of the three linear

response regions of the HB-PM-PCF sensor response and listed them in Table 6.2. For comparison, the different slopes of the FBG sensor response are also detailed in Table 6.2.

Table 6.2: Rate of change of Phase shift for HB-PM-PCF sensor and rate of change of Bragg peak shift for FBG

Duration	Slope HB-PM-PCF response (Radians/ hour)	Slope of FBG response (nm / hour)
0 - 2 hours	~ 0.11	~ 0.055
2 - 6 hours	~ 0.37	~ 0.050
6 - 24 hours	~ 0.0155	~ 0.00551

The curing phase corresponding to a fluid to solid transition is called vitrification [6.30] and the associated solvent - matrix chemical reactions occur between the 2nd and the 6th hour of the curing cycle. The stress/ strain exerted at the vitrification stage are expected to be greater than in the initial magnetization stage (from 0 to 2 hours) in which the MRE mixture is not fully solidified and thus the aligned ferromagnetic iron particles within the mould will exert a comparatively low stress / strain on the embedded optical fiber sensors. From Table 6.2, it is obvious that the slope of the stripped HB-PM-PCF response during the second linear response region (from 2 to 6 hours of curing process) is higher than the first linear response region (from 0 to 2 hours). Finally, the slope of the third linear response region of the stripped PM - PCF sensor is very low as shown in Figure 6.12(b) and Table 6.2, indicating a low stress/ strain during this curing stage. During the first two hours the MRE mixture is in the form of a fluid and at this phase the ferromagnetic ion particles are free to align in the direction of the magnetic field - magnetization phase. Vitrification [6.28] occurs during the 2nd to 6th hours of the curing cycle. In the last phase of the curing cycle from the 6th to 24th hour the chemical process

ceases and a slow curing shrinkage takes place due to solvent evaporation. The measurements with stripped HB-PM-PCF sensor confirm that the phase shift variations observed are consequences of the strain and stress during the expected curing phases

Analyzing the response of the FBG sensor, it should be noted that the change in the slope of wavelength shift during the first two phases of curing is insignificant since we expect the slope of second phase higher than first. A clear weakness of the FBG sensor is that the response does not allow one to reliably distinguish between these two curing phases as shown in Figure 6.12(b). This difference in the curing response of the stripped HB-PM-PCF polarimetric sensor and FBG sensor is due to the fact that for buffer coating removed HB-PM-PCF polarimetric sensors there are two factors contributing towards the output phase variation. The first one is the birefringence variation caused by non - uniform lateral strain components resulted from shrinkage during curing. The second one is the birefringence variation of the HB-PM-PCF sensor caused by the deformation of stripped HB-PM-PCF sensor as a result of the alignment of ferromagnetic iron particles in the direction of the applied magnetic field. However, the Bragg wavelength shift from the FBG sensor does not adequately represent the change in such non-uniform lateral strain components and shape deformations of the optical fiber, and thus the FBG sensor fails to detected different phases of the MRE curing process. It can be concluded that a buffer stripped HB-PM-PCF polarimetric fiber sensor is a suitable candidate for identifying the curing stages by measuring the internal strain /stress components that evolved during MRE curing the process. The FBG measurements showed that the difference between the first two stages of curing process is not as pronounced as in the case of HB-PM-PCF sensor.

6.2.5 Conclusion

An embedded stripped HB-PM-PCF sensor is demonstrated for distinguishing different stages of the MRE curing process. The developed sensor identified the non-uniform strain/ stress components that evolve during different phases of the curing process. From the result we can conclude that more accurate cure monitoring is possible using stripped HB-PM-PCF sensors. Also we believe a buffer stripped HB-PM-PCF can be used for practical applications of MR smart composite material such as characterization of MR properties in presence of a magnetic field. Thus the proposed sensor has a wide range of applications in MR materials at all stages from fabrication to use in areas from medical to automotive and aerospace industries.

6.3 References

- 6.1 C. Ruddy, E. Ahearne and G. Byrne. "A review of magnetorheological elastomer properties and applications." 2012.
- 6.2 J. M. Ginder, M. E. Nichols, L. D. Elie, J. L. Tardiff. "Magnetorheological elastomers: properties and applications." *Smart Struct. Mater: Smart Mater. Tech. Proc. SPIE* 3675, 131–8, 1999.
- 6.3 W. H. Li, H. Du, N. Q. Guo, P. B. Kosasih. "Magnetorheological fluids based haptic device." *Sensor Review*, 2004
- 6.4 D.D.L. Chung. "Composite Materials: Science and Applications." 2nd Edition, Springer Publications, 2010.
- 6.5 D. P. Garg, M. A. Zikry, G. L. Anderson, X. E. Gros. "Current and potential

- future research activities in adaptive structures: an ARO perspective." *Smart Mater. Struct.* 10, 610-623, 2001.
- 6.6 D. Montalvão, N.M.M. Maia and A.M.R. Ribeiro. "A Review of Vibration-based Structural Health Monitoring with Special Emphasis on Composite Materials." *The Shock and Vibration Digest* 38, 295-324, 2006.
 - 6.7 J. Cordero, T. Heinrich, T. Schuldt, M. Ghlke, S. Lucarelli, D. Weise, U. Johann and Braxmaier. "Interferometry based high-precision dilatometry for dimensional characterization of highly stable materials." *Meas. Sci. Technol.* 20, 095301, 2009.
 - 6.8 V. Dewynter-Marty and P. Ferdinand. "Embedded fiber Bragg grating sensors for industrial composite cure monitoring." *Journal of Intelligent Materials Systems and Structures* 9, 785-787, 1998.
 - 6.9 Y. Fan and M. Kahrizi. "Characterization of a FBG strain gage array embedded in composite structure." *Sensors and Actuators A* 121, 297-305, 2005.
 - 6.10 B. A. Tahir, J. Ali and R. A. Rahman. "Strain Measurements Using Fibre Bragg Grating Sensors." *American Journal of Applied Science (Special Issue)*, Volume, 40-48, 2005.
 - 6.11 K. O. Hill and G. Meltz. "Fiber Bragg grating technology fundamentals and overview." *J. Lightwave. Technol* 15, 1263–1276, 1997.
 - 6.12 V. M. Murukeshan, P. Y. Chan, O. L. Seng and A. Asundi. "On-line health monitoring of smart composite structures using fiber polarimetric sensor." *Smart Mater. Struct* 8, 544-548, 1999.

- 6.13 Hegde, Asundi, A. "Performance analysis of all-fiber polarimetric strain sensor for composites structural health monitoring." NDT&E International 39, 320-327, 2007.
- 6.14 X. Dong and H. Y. Tam. "Temperature-insensitive strain sensor with polarization maintaining photonic crystal fiber based Sagnac interferometer." Applied Physics Letters 90, 151113 - 151116, 2007.
- 6.15 G. Rajan, K. Mileńko, P. Lesiak, Y. Semenova, A. Boczkowska, M. Ramakrishnan, K. Jędrzejewski, A. Domański, T. Woliński and G. Farrell. "A hybrid fiber optic sensing system for simultaneous strain and temperature measurement and its applications." Photonics Letters of Poland 2, 46-48, 2010.
- 6.16 H. V. Thakur. "All-fiber embedded PM-PCF vibration sensor for Structural Health Monitoring of composite." Sensors and Actuators A: Physical 167, 204–212, 2011.
- 6.17 G. Rajan, M. Ramakrishnan, Y. Semenova, A. Domanski, A. Boczkowska, T. Wolinski, G. Farrell. "Analysis of Vibration Measurements in a Composite Material Using an Embedded PM-PCF Polarimetric Sensor and an FBG Sensor." DOI: 10.1109/JSEN.2011.2172412, 2011.
- 6.18 M. Ramakrishnan, G. Rajan, Y. Semenova and G. Farrell. "Comparison of vibration measurements in composite materials using different types of polarimetric sensors." Proc. SPIE 8421, OFS2012 22nd International Conference on Optical Fiber Sensors, 842178, 2012.
- 6.19 P. Kishore, D. Dantala *et al.* "An etched fiber optic vibration sensor to monitor the simply supported beam." Proc. SPIE 8439, Optical Sensing and

Detection II, 84392F, 2012.

- 6.20 K. S. C. Kuang and W. J. Cantwell. "The use of plastic optical fibre sensors for monitoring the dynamic response of fibre composite beams." *Meas. Sci. Technol* 14, 736–745, 2003.
- 6.21 T. R. Wolinski, P. Lesiak and A. W. Domanski. "Polarimetric optical fiber sensors of a new generation for industrial applications." *Bulletin Of The Polish Academy Of Sciences Technical Sciences* 56, Page, 2008.
- 6.22 D. H. Kim and J. U. Kang. "Analysis of temperature-dependent birefringence of a polarization-maintaining photonic crystal fiber." *Opt. Eng* 46, No. 7, 2007.
- 6.23 G. Rajan *et al*, "Composite materials with embedded photonic crystal fiber interferometric sensors." *Sensors and Actuators A: Physical* 182, 57–67, 2012.
- 6.24 P. Lesiak, M. Szelać, D. Budaszewski, P. Robert, K. Milenko, G. Rajan, Y. Semenova, G. Farrell, A. Boczkowska, A. Domański and T. Woliński. "Influence of lamination process on optical fiber sensors embedded in composite material." *Measurement, Elsevier Science* 45, 2275-2280, 2012.
- 6.25 G. F. Lang. "Electrodynamic shaker fundamentals." *Sound and Vibration*, April 1997.
- 6.26 J. D. Whitney, G. H. Smerage, W. A. Block. "Dynamic analysis of a trunk shaker-post system." *Transactions of the ASAE* 33, 1066-1070, 1990.
- 6.27 J. M. Ginder, M. E. Nichols, L. D. Elie and J. L. Tardiff. "Magnetorheological elastomers: properties and applications." *Smart Mater. Tech. Proc. SPIE*, 1999, 3675, 131–138

- 6.28 L. Jinsong and A. Asundi, “Structural health monitoring of smart composite materials by using EFPI and FBG sensors.” *Sens. Actuators A, Phys.* 103, 103,330–340, 2003.
- 6.29 S. J. Buggy, E. Chehura, S. W. James and R. P. Tatam. “Optical fiber grating refractometer for resin cure monitoring.” *J. Opt. A, Pure Appl. Opt.* 9, 60, 2007.
- 6.30 M. Ramakrishnan, G. Rajan, Y. Semenova *et al.* “The influence of thermal expansion of a composite material on embedded polarimetric sensors.” *Smart Mater. Struct.* 20, 125002, 2012.

Chapter 7

Conclusions and Future Work

In this chapter, conclusions from across the thesis are reviewed and the contributions to current technology and knowledge from the whole thesis are discussed. Potential future research as an extension of this PhD thesis is also discussed.

7.1. Conclusions from the research

The hypothesis underpinning this research was identified in Chapter 1 as:


The hypothesis underpinning this research is that by careful selection of a combination of sensors that work in a complementary fashion, it is possible to measure multiple physical parameters, where the parameters being measured can also include complex indirect parameters.


The core aim of this research, based on the hypothesis above, is to investigate a hybrid sensing scheme that utilises sensors working in a complementary fashion to measure multiple physical parameters, where the parameters being measured include the complex indirect parameters thermal expansion and vibration, all in a composite material. In Chapter 1, a series of objectives were identified to meet the aim stated above. The conclusions presented and discussed here are divided into five sections based on the different objectives

and research strands investigated and reported in this thesis.

I. Conclusions regarding the influence of thermal expansion in a composite material on embedded sensors

In this thesis, one of the objectives was to study the important issues surrounding the influence of composite material thermal expansion on embedded polarimetric sensors for measurements of strain and temperature. Glass-fiber reinforced general purpose resin based composite samples are fabricated and characterized for this study. The two types of polarimetric sensors studied are based on polarization maintaining photonic crystal fiber and Panda fiber. The temperature sensitivities of the coated and coating-stripped HB-PM-PCF and Panda fiber polarimetric sensors are measured experimentally in free space and compared to those of the same sensors embedded in the composite material. The conclusions are:

 From the results it is concluded that a polarimetric sensor utilising an acrylate coated fiber embedded in a composite material shows the same response as the same sensor in free space, while a coating-stripped fiber polarimetric sensor shows a significant increase in temperature sensitivity when embedded in a composite material. This difference is due to the stress induced change in the fiber birefringence created by thermally induced strain.

 In the case of the coated fiber sensor, the effect of thermal elongation is largely eliminated by the coating. For Panda fibers the dependency on thermal expansion of the composite material is many times higher than that for HB-PM-PCF, because of the cross-sensitivity between temperature and thermal induced strain.



From an analysis, it is concluded that the influence of thermal expansion within the composite on the embedded fibers is the main source of errors during temperature and strain measurements using embedded polarimetric sensors. An acrylate coated fiber based polarimetric sensor embedded shows 9% deviation from free space. Whereas, an acrylate stripped fiber based polarimetric sensor embedded shows 100% deviation from free space.



Where significant thermal expansion is likely to occur for a sensorised composite component, it is asserted that 91% more accurate strain and temperature measurements can be obtained using buffer coated polarimetric fiber sensors.

II. Conclusions in regard to the measurement of thermal expansion induced strain in a composite using an embedded polarimetric sensor

The measurement of thermal elongation allows for the determination of the thermal expansion characteristics of the composite material. A novel method of measurement of thermal elongation induced strain in a composite material using a buffer stripped HB-PM-PCF sensor is reported in this thesis. For this purpose a composite material sample with an embedded buffer-stripped HB-PM-PCF based polarimetric fiber sensor is fabricated and characterized. A buffer-stripped PM – PCF is chosen since while this particular type of sensor has a very low temperature sensitivity in free space, it shows a significant phase change when embedded in a composite material due the thermal elongation of the composite material. The temperature induced phase changes of the buffer-stripped HB-PM-PCF polarimetric

sensors embedded in carbon-epoxy, E glass-epoxy and E glass-unsaturated polyester resin composite material samples are measured and the results are used to determine the thermal elongation induced strain in the temperature range from 0 °C to 65 °C. The conclusions are as follows:

✚ It can be concluded that a buffer-stripped HB-PM-PCF polarimetric fiber sensor embedded in a composite material shows significant phase change due to thermal elongation induced strain and is a suitable candidate for the measurement of thermal expansion in composite structures for practical applications.

✚ Using the sensors described, the experimentally observed thermal elongation induced strain values of carbon-epoxy, E glass-epoxy, and E glass-unsaturated polyester resin composite specimens are determined experimentally to be $3.648 \times 10^{-5} (\pm 0.0004) \text{ } \epsilon / ^\circ\text{C}$, $1.52 \times (\pm 0.00032) 10^{-5} \text{ } \epsilon / ^\circ\text{C}$, and $2.42 \times 10^{-5} (\pm 0.00036) \text{ } \epsilon / ^\circ\text{C}$ respectively.

✚ For comparison purposes a numerical analysis of the coefficient of thermal expansion for the specific composite configurations employed was conducted. The CTE values from the numerical analysis correlated well with those from experiments.

✚ The buffer stripped HB-PM-PCF sensor showed a higher temperature response in the carbon fibre reinforced composite material compared to that of the E-glass fibre reinforced composite because a carbon fiber reinforced composite has higher transverse thermal expansion coefficients.





✚ From the results one can conclude that more accurate determination

of thermal expansion is possible using stripped HB-PM-PCF sensors, assuming that expansions due to residual strain and moisture are taken into account.

III. Conclusions regarding the development of a novel hybrid sensor for simultaneous measurement of strain, thermal strain and temperature

In this thesis a novel hybrid sensor is demonstrated by combining polarimetric sensors together with an FBG sensor for simultaneous measurement of strain, temperature and thermal strain for a composite material. The hybrid sensor is interrogated in the intensity domain by converting the polarization and wavelength information from the polarimetric sensors and the FBG respectively into detectable linear intensity variations. A buffer-coated HB-PM-PCF polarimetric sensor, a buffer-stripped HB-PM-PCF polarimetric sensor and a polyimide coated FBG sensor are embedded in an E-glass-unsaturated polyester resin composite material sample and are characterized. Controlled fabrication conditions and post fabrication testing is adopted to ensure that residual strain and moisture induced expansion are absent in the fabricated composite samples. Thermal elongation induced strain sensitivity, axial strain sensitivity, and the temperature sensitivities of the individual sensors are measured and a characteristic sensitivity matrix for the hybrid sensor is developed based on these experimental results. Further, a miniaturized surface attachable interrogator for a hybrid sensor has been proposed and designed to realize as a flexible device compatible with surface mounting on a composite using post processing of platinum coated polyimide substrates. The corresponding

conclusions are:

-  A hybrid sensor system is developed for simultaneously sensing temperature, strain and thermal strain in composite materials and its operation is demonstrated by combining three different sensor types: a polarimetric sensor based on an acrylate-coated HB-PM-PCF, a coating-stripped HB-PM-PCF sensor, and a fiber Bragg grating sensor, embedded for the purpose of demonstration, in an E glass fiber reinforced composite material.
-  Temperature is sensed using the FBG sensor, strain is sensed using the acrylate coated HB-PM-PCF sensor and thermal strain is sensed using the coating stripped HB-PM-PCF. A characteristic sensitivity matrix for the novel hybrid sensor has also been experimentally determined.
-  Additionally an interrogation scheme for this hybrid sensor system is demonstrated that converts the polarization and wavelength information from the different sensors into the intensity domain. By detecting the outputs of the three sensors in the intensity domain, and by using the developed characteristic matrix of the novel hybrid sensor, information about temperature, axial strain and thermally induced strain can be simultaneously determined.
-  The design was completed for an interrogation module comprising of an AWG for FBG demodulation and an EO-MZI intensity modulator for the polarimetric sensors demodulation. Customized design procedures for the fabrication of the AWG and EO-MZI were used and the designed performance in simulation resulted in a wide

channel spacing of 5 nm, a low cross talk of -34 dB between adjacent channels for the AWG and a low V_π voltage of ± 1.5 V for the EO-MZI.









The fabricated flexible film type interrogation module can be compact, with an expected size of only 3.4 cm x 0.1 cm x 0.01 cm and could be integrated with photo detector arrays and wireless communication technology to enhance the applicability of a hybrid sensing scheme in smart sensing and SHM for composite parts in motion.

IV. Conclusions regarding polarimetric sensors for vibration measurements

The dependence of strain sensitivity and the length of polarimetric sensors on the vibration amplitude is investigated in this thesis. The vibration amplitude range over which the polarimetric sensors can provide accurate vibration measurement is derived analytically and verified through experiments. Low frequency vibration measurements from 0 Hz to 100 Hz are performed for glass fiber reinforced composite material samples embedded with two different polarimetric sensor types, a highly strain sensitive Panda type fiber and a low strain sensitive polarization maintaining photonic crystal fiber. An analytical expression to predict the allowable maximum vibration amplitude for any type of polarimetric sensor embedded in a composite beam undergoing deflections is derived for a “simply - simply supported” configuration of the composite beam. Vibration measurements for several glass fiber reinforced composite samples with different lengths embedded with polarimetric sensors are compared for different amplitudes




of vibrations. The conclusions are:

-  It is concluded that in the case of polarimetric sensors both their strain sensitivity and length are factors that limit the vibration measurements to a certain range of vibration amplitudes.
-  The experimental and theoretical results confirmed that a polarimetric sensor with a longer gauge length provides more accurate vibration measurements for wider range of vibration amplitudes.
-  For high amplitude vibration measurements, in order to ensure that the output intensity of the embedded polarimetric sensor occurs within the quasi-linear region of its periodic response, the measurements must be performed within a limited range of vibration amplitudes corresponding to the particular polarimetric sensor type.
-  For the widest possible range of vibration amplitude measurements the best sensor choice is a low strain sensitive polarimetric sensor such as a HB-PM-PCF fiber or a high strain sensitive polarimetric sensor such as Panda fiber with a sufficiently long gauge length.
-  At high amplitude vibrations the high sensitivity and low dynamic strain range of Panda type fibers result in a multiple-peaks intensity pattern within one vibration cycle which leads to ambiguous and thus inaccurate vibration frequency and vibration amplitude measurements.
-  An analytical calculation of the maximum allowable vibration amplitude has been carried out verified by experimental results and

provide critical information to end-users in selecting an appropriate polarimetric sensor type and sensor length for vibration measurements in composite materials.

V. Conclusions regarding the development of composite cure monitoring sensor

In this thesis to identify the most appropriate type of sensor for monitoring of the composite curing process, a study was undertaken of the performance of a polarimetric sensor and an FBG sensor both embedded in a magneto rheological elastomer (MRE) smart composite material during its curing process. During the curing process, the phase shift variation of the embedded HB-PM-PCF sensor and Bragg wavelength shift of an FBG are compared. The conclusions are:

-  During the composite curing process the phase shift variation of a stripped HB-PM-PCF is significant. Specifically it is concluded that during the curing process the buffer stripped HB-PM-PCF exhibits a stress/ strain induced phase shift variation from 0 to 1.98 (± 0.0008) radians, which can be used to clearly identify the different stages in the composite curing process.
-  During curing, there is no external strain applied, so an FBG sensor monitors only the internal strain during the curing process. The observed FBG wavelength shift is low and its response does not allow one to reliably distinguish all the curing stages.
-  The present investigation offers a simple non-destructive method to monitor the curing process of an MRE smart composite material based on buffer stripped highly birefringent photonic crystal fiber.

7.2. Overall conclusions from the research

Several useful topics on embedded fiber sensors in a composite material have been investigated in this thesis. The key overall conclusions are:

1. Embedded fiber sensors have been previously demonstrated by other researchers for measuring basic parameters for a composite material such as applied strain and temperature etc. In this thesis, it was successfully demonstrated that embedded fiber sensors can measure more complex indirect parameters such as thermal expansion, vibration etc.
2. The outcomes of this thesis provide key information for the composite manufacturing industry by further developing non-destructive methods based on embedded fiber optic sensors for the characterisation of composite material properties at different stages in their lifecycle, from fabrication through operation to predicting the onset of failure.
3. A novel hybrid sensor scheme is demonstrated for simultaneous discrimination of strain, thermal strain and temperature in a composite material. Furthermore, a compact miniaturised interrogation module is proposed that can interrogate the sensor outputs as a linear intensity variation for this hybrid sensing approach.
4. It has been demonstrated that it is possible to translate the knowledge and insights developed for sensing in traditional composite materials into techniques to monitor the fabrication of new smart materials, such as MREs, where physical properties can be tailored during

7.3. Future work

This thesis has described an experimental investigation of a hybrid sensor based on polarimetric sensors combined with FBGs for strain, temperature and thermal strain measurements in composite materials and their derived applications. There remain a number of unanswered research questions and challenges, including:

A) Determining the influence of the composite stiffness parameter on an embedded polarimetric sensor.

It has been reported that the composite lamination process and ply configurations play a very significant role in the transfer of applied strain and temperature to the optical fiber sensors [7.1, 7.2]. Preliminary insights into the differences in sensitivity of an optical sensor due to material hardness, the influence of the lamination process and the ply configuration of the composite material are presented in Appendix D¹⁷, which shows experimentally that a strain sensitivity variation from 0 to 30% is possible depending on the material hardness and ply configurations. It is important to quantify the dependence of the strain sensitivity of the embedded sensor on the material stiffness parameter, in order to improve the measurement accuracy of the embedded sensor. A suggested method to investigate the effect of material stiffness on embedded sensors is to measure the strain sensitivity of HB-PM-PCF sensors in different composite materials with different

¹⁵ Further, more details the dependence of strain sensitivity variation on the material hardness and ply configurations is presented in Appendix D. Appendix D is a published paper (Ramakrishnan. M, Rajan. G, Semenova. Y, and Farrell. G , " Composite Materials with embedded fiber sensors for in-situ structural health monitoring ", Workshop & International Conference on Smart Materials(WICSM), DCU, Sept. 2010.)

ply configurations, and derive a relationship between the stiffness parameter of the material and strain sensitivity of the HB-PM-PCF sensors. Such a future study on the effect of material stiffness on embedded sensor should not only improve the measurement accuracy but also should allow one to potentially develop a non-destructive method to measure the stiffness of a composite material.

B) Reducing errors associated with longitudinal thermal expansion

For most of the commercially employed fibre reinforced composites such as carbon and E- glass composites, the longitudinal CTE value is much lower than the transverse CTE value [7.3, 7.4], and further the effect of longitudinal CTE induced elongation is significantly reduced by the presence of the buffer coating for an embedded fiber sensor [7.5]. However during strain measurements in a composite material with a high longitudinal CTE there is a possibility of inaccuracy due to the strain induced by longitudinal thermal elongation of composite material. A suggested method to eliminate the inaccuracy in strain measurements is to measure the thermal elongation strain induced sensitivity of the buffer coated HB-PM-PCF after embedding in a particular composite material by applying only a temperature change in the absence of strain and to derive a correction factor from the measured thermal elongation strain induced sensitivity value for the strain measurements.

C) Implementing a wider range of strain / temperature measurements using an EO - MZI intensity modulator for polarimetric sensor demodulation

An EO - MZI intensity modulator can be configured so that it can be used to operate a polarimetric sensor in the linear response range of quadruple region of the sensor from $-\pi/4$ to $+\pi/4$. Thus whenever the phase change is greater than $\pi/2$ radians the relationship between the polarimetric sensor output intensity and strain/temperature is no longer linear. A possible solution, which needs further

research, in order to achieve strain and temperature measurements with a wider range, is by demodulating the output of the polarimetric sensor using a method based on the EOM voltage. The proposed method is outlined in a preliminary fashion in Appendix C. Here the phase change induced optical intensity variation in the output signal from the polarimetric sensor resulting from applied strain or temperature is nullified by the EOM by control of the EOM applied voltage [7.6]. The value of nullifying EOM voltage in turn provides information about the strain or temperature of the host composite material. The advantage of such an EOM interrogation scheme is that the linear relation between EOM voltage and strain / temperature of the polarimetric sensor can be realized for up to a π radians phase change.

D) Fabrication, characterization and packaging of the film-type interrogation module for the novel hybrid sensor

The film-type interrogation module designed in this thesis for the novel hybrid sensor could be attached to the surface of the composite part in motion with attached photo - detector arrays and wireless transmitters. The flexible interrogation module designed comprises an AWG for FBG demodulation and an EO - MZI intensity modulator for polarimetric sensor demodulation. While some work has been reported to date, one of the key areas of investigation that needs further work is the ingress / egress connections from the optical fiber sensor to the flexible waveguide device and its packaging for protection and to avoid disturbance from the environment. Overall further study that explores the packaging issues for the flexible interrogation module is required in order to increase the usefulness of the hybrid sensor in real-world applications.

E) Smart composite characterization method based on stripped HB-PM-PCF

sensor for MR materials

MR materials are a class of smart materials having mechanical properties that can be controlled by an external magnetic field [7.7]. As means of achieving controlled movement/motion of dampers and brakes, MRs are used in a variety of application areas from medical to automotive and aerospace [7.8, 7.9]. In such applications, it is critical to have accurate control of MR material properties [7.9, 7.10] and for this it is necessary to utilize sensors embedded in the MR materials. In this thesis the research presented regarding the MRE curing process concludes that a sensor based on high sensitive stripped HB-PM-PCF can identify different stages of curing process of a smart MR composite material. Further work is needed develop an optical fiber sensor based characterization method for MR smart composites to quantify stiffness variations during operation and thus achieve precise control of MR components, such as MR based brakes proposed for prosthetic limbs. A proposal to investigate magneto-rheological smart composite with embedded optical fiber sensors for medical applications was successfully approved as an SFI TIDA¹⁸ project for funding in 2014.

7.4. References

- 7.1 P. Lesiak, S. Mateusz., B. Daniel., P. Robert., M. Karolina., G. Rajan, Y. Semenova. et al. "Influence of lamination process on optical fiber sensors embedded in composite material." *Measurement*, , 45, 2275-2280, 2012.

¹⁶ Successful TIDA Proposal 13/TIDA/B2705 'Magneto-rheological Smart Composite With Embedded Optical Fiber Sensors For Medical Applications' has been approved for funding at a value of € 88,358 direct costs.

- 7.2 M. Ramakrishnan, G. Rajan., Y. Semenova., and G. Farrell. "Composite Materials with embedded fiber sensors for in-situ structural health monitoring. ", WICSM,-2010, Dublin.
- 7.3 S. R. Reid, and G. Zhou. "Impact behavior of fibre-reinforced composite materials and structures." CRC press October 31, 2000.
- 7.4 T Stolarski, Y. Nakasone. "A numerical study on the coefficients of thermal expansion of fiber reinforced composite materials." Composite Structures vol 78 pp 1-10, 2007.
- 7.5 M. Ramakrishnan, G. Rajan, Y. Semenova, et. al, "The influence of thermal expansion of a composite material on embedded polarimetric sensors." Smart Mater. Struct., 20, 125002, 2012.
- 7.6 M. Ramakrishnan, G. Rajan, Y. Semenova, and Gerald Farrell. "Electro-optic modulator based interrogation for a polarimetric fiber sensor for strain and temperature measurements", conference proceedings, Photonics Ireland - 2013, Belfast.
- 7.7 C. Ruddy, E. Ahearne and G. Byrne. "A review of magnetorheological elastomer properties and applications." 2012.
- 7.8 J. M. Ginder, M. E. Nichols, L. D. Elie, J. L. Tardiff. "Magnetorheological elastomers: properties and applications." Smart Struct. Mater: Smart Mater. Tech. Proc. SPIE 3675, 131–8, 1999.
- 7.9 W. H. Li, H. Du, N. Q. Guo, P. B. Kosasih. "Magnetorheological fluids based haptic device." Sensor Review, 2004

- 7.10 H. Herr, and A. Wilkenfeld, Industrial Robot. “User-adaptive control of a magnetorheological prosthetic knee”, Emerald, 30: 42–55, 2003.

Appendix A

Statement of Contribution

For the publications presented within this thesis, the co-authors listed below certify that:

1. Manjusha Ramakrishnan is the first author for all the publications.
2. As first author, Manjusha Ramakrishnana undertook all aspects of the research described in each publication, including preparation and submission of the publication and the preparation of any revisions requested by referees, with the support and advice of the co-authors.
3. The co-authors agree to the use of the publications in this thesis.



Dr. Gerald Farrell



Dr. Yuliya Semenova



Dr. Ginu Rajan



Dr. Poitr Lesiak



Prof. Andrzej Domański



Prof. Tomasz Woliński



Prof. Anna Boczkowska



Dr. Dean Callaghan



Yanfen Zhou



Stephen Jerrams

Appendix B

Basics of Polarimetric Sensor

An electromagnetic (EM) wave consists of two mutually coupled fields, an electric field and a magnetic field. Both of these fields have a direction and amplitude. Within the electromagnetic wave the two fields; electric and magnetic are oriented at precisely 90° to one another [A.1]. Consider the electric field to be oriented along the y-axis, and the magnetic field along the x-axis, then the direction of propagation is along the z-direction. For a completely polarized monochromatic EM wave with the direction of propagation along z-axis, the electric field can be presented as sum of two orthogonal components. Such a presentation of electric field is illustrated in Figure A.1 in which the two co-propagating orthogonal waves are oscillating along x-axis, y-axis and their sum along the z-axis. Further, the relative phase between these two waves in radians is ϕ , and the spatial displacement is [A.2]:

$$d = \lambda \phi / 2 \pi \quad \text{A.1.}$$

The state of polarization of an EM wave propagating along the z-axis can be described by the extremity of the electric field vector in the *xoy* plane. Figure A.1 shows the three separate state of polarization: linear, circular and elliptical.

In the case of linear polarization state is characterized by the extremity of the electric field vector traveling in the z-direction draws a straight line in the *xoy* plane. In general for linearly polarized EM waves, the components E_x and E_y have a phase difference given by [A.2],

$$\delta\phi = m\pi \quad \text{A.2.}$$

if $m=0, 2, 4, 6$, etc, the components are said to be in phase and if $m=1, 3, 5$, etc, the polarization line is orthogonally oriented compared to the previous one

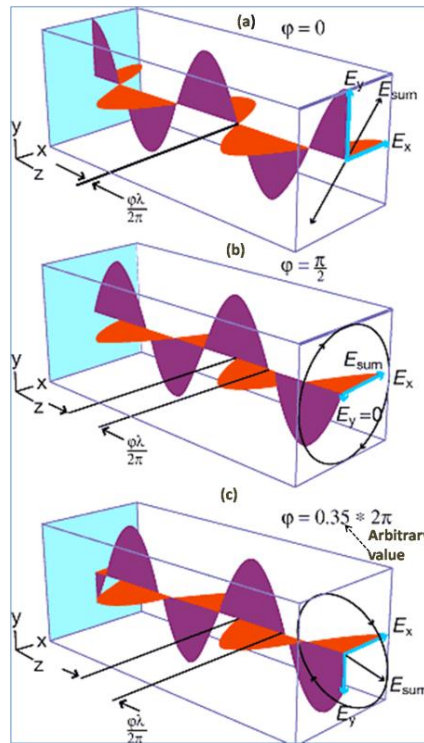


Figure A.1 Three state of polarization (a) linear; (b) circular; and (c) elliptical. [Courtesy: Guimond Stephen, and David Elmore. *Optical Design & Engineering Polarizing Views*. '30 May 2004, SPIE news room.]

Linear + 45° polarization state can be represented by a phase difference of $\delta\phi=0$ between the two orthogonal components along x-axis and y-axis and the resultant electric field E_{sum} oscillates about a line oriented at 45° in the xoy plane as shown in Figure A.1(a).

Circular polarization state is characterized by a phase difference of $\delta\phi=\pi/2$ between the two orthogonal components along x-axis and y-axis and the two components E_x and E_y having equal amplitudes. For circular polarization, the resultant electric field E_{sum} maintains a constant magnitude but rotates about the origin and traces a circle in the xoy plane either clockwise or anticlockwise- as represented in Figure

A.1(b). In general for circularly polarized EM waves, the components E_x and E_y have a phase difference [A.2],

$$\delta\phi = \pm \frac{\pi}{2} \quad \text{A.3.}$$

When electric field E_{sum} rotates in clockwise direction in the xoy plane, it is known as a right-hand circular polarization. For right-hand circular polarization the phase difference is given by [A.2],

$$\delta\phi = -\frac{\pi}{2} + 2m\pi \quad \text{A.4.}$$

and for left-hand circular polarization the phase difference is given by [A.2],

$$\delta\phi = +\frac{\pi}{2} + 2m\pi \quad \text{A.5.}$$

where, $m=0, \pm 1, \pm 2, \pm 3$, etc.

However, for elliptical polarization state, the amplitude of the electric field components E_x and E_y is not identical and their phase difference does not a characteristic value. The resultant electric field E_{sum} rotate in the xoy plane either in the clockwise or anticlockwise direction as represented in Figure A.1(c). Linear and circular polarizations are special cases of the elliptical polarization.

The most common methods of representing polarization states are Jones' matrix method, Muller matrix method, polarization ellipse, Stokes polarization parameters vectors, and Poincaré Sphere representation. In this thesis the output of polarimetric sensor is mainly interpreted using the Poincaré Sphere representation and is detailed in the following section

A. Jones' matrices formalism

There are various methods available for representing the polarization state as well as the transmission of light through a polarizing medium, such as a birefringent fiber [A.3]. Jones' matrices formalism is one of the efficient method that gives us

information about a polarization state which travels in a complex medium.

The two components of electric field can be represented using complex numbers.

The state of polarization can be approximated by using matrix algebra as given below [A.4],

$$a = \begin{bmatrix} Exe^{j\phi_x} \\ Ey e^{j\phi_y} \end{bmatrix} \quad \text{A.6.}$$

where Ex and Ey are the amplitudes and ϕ_x and ϕ_y are the phases of the components.

The above mentioned equation describes the general case of an elliptically polarized wave traveling in z -direction. In the case of a linear polarization which makes an angle θ with the x -axis the Jones matrix can be represented by [A.4],

$$a = \begin{bmatrix} Ex \cos \theta \\ Ex \sin \theta \end{bmatrix} \quad \text{A.7.}$$

An example of circular polarization Jones matrix can be represented by [A.4],

$$a = \begin{bmatrix} E \cos(\omega t) + i \sin(\omega t) \\ -E \sin(\omega t) + i \cos(\omega t) \end{bmatrix} \quad \text{A.8.}$$

Taking in to consideration only the real numbers out of each component,

$$\begin{aligned} Ex &= E \cos(\omega t) \\ Ey &= -E \sin(\omega t) \end{aligned} \quad \text{A.8.}$$

When $t=0$, the electric field vector, is given by $Ex=E$ and $Ey=0$. As t increases, Ex decreases but remains positive and Ey increases but remains negative, resulting a circle in clockwise direction.

For transmission of light through a diverse medium such as an isotropic absorbing medium, which weakens the amplitude but does not modify the state of polarization.

For such a medium Jones' matrix can be represented by [A.4]

$$A = \begin{bmatrix} \alpha & 0 \\ 0 & \alpha \end{bmatrix} \quad \text{A.9.}$$

where α is the weakening factor of the medium.

An ideal polarizer allows only one direction of the electric field to pass through and stops the others. For example, a polarizer oriented along the x -axis will have as a matrix [A.4],

$$A = \begin{bmatrix} 1 & 0 \\ 0 & 0 \end{bmatrix} \quad \text{A.10.}$$

when a wave passes through such a polarizer, the resulting wave has no component along the y -axis and is represented by [A.4],

$$\begin{bmatrix} 1 & 0 \\ 0 & 0 \end{bmatrix} \begin{bmatrix} E_x \\ E_y \end{bmatrix} = \begin{bmatrix} E_x \\ 0 \end{bmatrix} \quad \text{A.11.}$$

In general, the matrix of a polarizer whose transmitting axis is oriented at an angle θ with the x -axis in the xOy plane can be written as [A.4],

$$P = \begin{bmatrix} \cos^2 \theta & \cos \theta \sin \theta \\ \cos \theta \sin \theta & \sin^2 \theta \end{bmatrix} \quad \text{A.12.}$$

In particular, the matrix of a polarizer whose transmitting axis is oriented at an angle 45° with the x -axis in the xOy plane can be written as [A.4]

$$P = \begin{bmatrix} 1/2 & 1/2 \\ 1/2 & 1/2 \end{bmatrix} \quad \text{A.13.}$$

In Jones matrix formalism, the state of polarization of light coming out of a system made of several elements is found by multiplying the state of polarization when entering the system by the series of individual matrices of the different elements existing along the optical path.

An optical retarder is an element made of a birefringent material that changes the

state of polarization of any incident wave. When a wave enters in to the optical retarder, the wave is divided in to two in accordance with the two main axes of the medium, which are called ordinary axis and extraordinary axis. Then the two components will propagate through the birefringent material with different speeds defined by the ordinary refractive index n_o and the extraordinary refractive index n_e . Thus the outgoing wave from an optical retarder does not have the same phase differences and same states of polarization as the incident wave.

The relative phase difference $\Delta\phi$ between the ordinary and extraordinary axes is given by [A.4],

$$\Delta\phi = \frac{2\pi}{\lambda} d |n_e - n_o| \quad \text{A.14.}$$

where d is the thickness of the material and λ is the wavelength.

Thus in practical case the thickness of the birefringent material can be varied to produce the expected phase difference [A.3]. Examples of optical retarders are a half-wave plate and a quarter-wave plate. A half-wave plate rotates the direction of a linear polarization by 90° . A quarter-wave plate introduces a $\pi/2$ phase difference between the components of the light travelling along the ordinary and extraordinary axes.

B. Poincaré Sphere

According to Fresnel's theory, the optical field consists of two orthogonal components. The field components of the time varying optical disturbance can be described by the two wave equations [A.4],

$$\nabla^2 E_x(r,t) = \frac{1}{v^2} \frac{\partial^2 E_x(r,t)}{\partial t^2} \quad \text{A.15.}$$

$$\nabla^2 E_y(r,t) = \frac{1}{v^2} \frac{\partial^2 E_y(r,t)}{\partial t^2} \quad \text{A.16.}$$

$E_x(r,t)$ and $E_y(r,t)$ describe the optical field components, r is the vector point in space from the origin of the co-ordinate system, t is the time, v is the velocity of waves, and ∇^2 is the Laplacian operator.

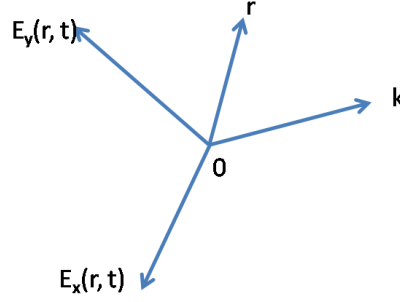


Figure A.2 Representation of optical field components in space

k is the wave number vector that describes the direction of propagation. The optical field components can be represented as given in Figure A.2.

The solutions of above wave equations are [A.4],

$$E_x(r,t) = E_{ox} \cos(\omega t - k \cdot r + \delta_x) \quad \text{A.17.}$$

$$E_y(r,t) = E_{oy} \cos(\omega t - k \cdot r + \delta_y) \quad \text{A.18.}$$

For a field propagating along z-axis, the above two components can be written as [A.4],

$$E_x(z,t) = E_{ox} \cos(\omega t - k \cdot z + \delta\phi_x) \quad \text{A.19.}$$

$$E_y(z,t) = E_{oy} \cos(\omega t - k \cdot z + \delta\phi_y) \quad \text{A.20.}$$

The equation of a polarization ellipse as given below [A.4],

$$\frac{E_x(z,t)^2}{E_{0x}^2} + \frac{E_y(z,t)^2}{E_{0y}^2} - \frac{2E_x(z,t)E_y(z,t)}{E_{0x}E_{0y}} \cos \delta\phi = \sin^2 \delta\phi \quad \text{A.21.}$$

where the phase shift between orthogonal polarization components, $\delta\phi = \delta\phi_y - \delta\phi_x$.

If the amplitudes E_{0x} and E_{0y} and the phase shift $\delta\phi$ are constants, the polarization ellipse remains fixed as the polarized beam propagates. The polarization ellipse in the rotated ξ - η coordinate system is as shown in Figure A.3.

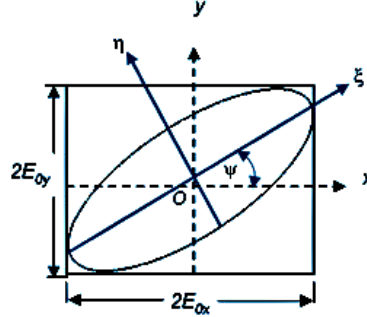


Figure A.3 Representation of polarization ellipse in the rotated ξ - η coordinate system

The degenerate polarization states are: (1) linearly horizontal/vertical polarized light (LHP/LVP), (2) linear $\pm 45^\circ$ polarized light (L+45P/L-45P), and (3) right/left circularly polarized light (RCP/LCP). The polarization states along with the mathematical conditions derived from polarization ellipse can be represented as given in Figure A.4.

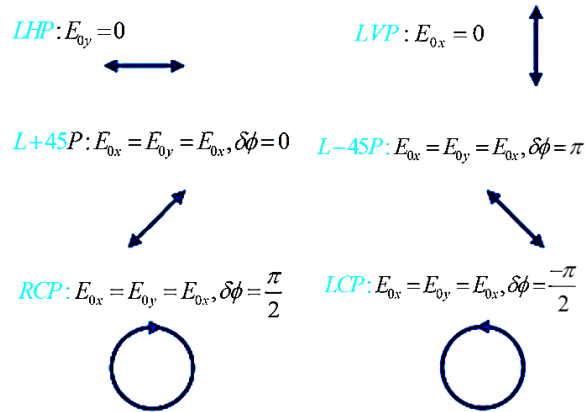


Figure A.4 Representation the degenerate polarization states with mathematical conditions

The polarization ellipse can be expressed in terms of two angular parameters: the orientation angle ψ , and the ellipticity angle χ . In of the parameters of the polarization ellipse these angles can be defined as [A.4],

$$\tan 2\psi = \frac{2E_{0x}E_{0y}}{E_{0x}^2 - E_{0y}^2} \cos \delta\phi, 0 \leq \psi < \pi \quad \text{A.22.}$$

$$\sin 2\chi = \frac{2E_{0x}E_{0y} \sin \delta\phi}{E_{0x}^2 + E_{0y}^2}, -\frac{\pi}{4} < \chi \leq \frac{\pi}{4} \quad \text{A.23.}$$

By introducing an auxiliary angle,

$$\alpha = \tan^{-1} \frac{E_{0x}}{E_{0y}}, 0 \leq \alpha \leq \frac{\pi}{2} \quad \text{A.24.}$$

the equations A.22, and A.23 can be rewritten as,

$$\tan 2\psi = (\tan 2\alpha) \cos \delta\phi \quad \text{A.25.}$$

$$\sin 2\chi = (\sin 2\alpha) \sin \delta\phi \quad \text{A.26.}$$

The conditions for the angles α , δ are $0 \leq \alpha \leq \pi/2$ and $0 \leq \delta\phi < 2\pi$, respectively.

The main drawbacks of the polarization ellipse are that the polarization ellipse is an instantaneous representation of polarized light, and neither the rotation angle ψ nor the ellipticity angle χ is directly measurable. Stokes polarization parameters can be used to overcome the limitation of polarization ellipse. This method involves numerical calculations by applying the time average definition to polarization ellipse equation.

The time average is defined by [A.4],

$$\langle E_i(z, t) E_j(z, t) \rangle = \lim_{T \rightarrow \infty} \frac{1}{T} \int_0^T E_i(z, t) E_j(z, t) dt \quad \text{A.27.}$$

where $i, j = x, y$ and T is total averaging time. Applying the time average definition to the polarization ellipse then yields the following equation [A.4],

$$S_0^2 = S_1^2 + S_2^2 + S_3^2 \quad \text{A.28.}$$

$$S_0 = E_{0x}^2 + E_{0y}^2 \quad \text{A.29.}$$

$$S_1 = E_{0x}^2 - E_{0y}^2 \quad \text{A.30.}$$

$$S_2 = 2E_{0x}E_{0y}c \cos \delta \quad \text{A.31.}$$

$$S_3 = 2E_{0x}E_{0y}s \sin \delta, \quad \text{A.32.}$$

and where $\delta = \delta y - \delta x$ and S_0 describes the total intensity P of the optical beam [A.4],

$$P = \sqrt{S_0^2} = \sqrt{S_1^2 + S_2^2 + S_3^2} \quad \text{A.33.}$$

S_1 describes the predominance of LHP light over LVP light, S_2 describes the predominance of L+45P light over L-45P light and, S_3 describes the predominance of RCP light over LCP light [A.4].

$$\text{Degree of polarization, } DOP = \frac{\sqrt{S_1^2 + S_2^2 + S_3^2}}{S_0} \quad \text{A.34.}$$

$$\text{Degree of linear polarization, } DOLP = \frac{\sqrt{S_1^2 + S_2^2}}{S_0} \quad \text{A.35.}$$

$$\text{Degree of circular polarization, } DOCP = \frac{S_3}{S_0} \quad \text{A.36.}$$

The quantities S_0 , S_1 , S_2 , and S_3 are the observables of the polarized field. They were introduced by Stokes and are called the Stokes polarization parameters. The Stokes parameters can be expressed in complex notation and can be explained as follows.

The optical components are expressed as complex variables [A.4],

$$E_x(t) = E_{0x} \exp(i\delta_x) \quad \text{A.37.}$$

$$E_y(t) = E_{0y} \exp(i\delta_y) \quad \text{A.38.}$$

The Stokes parameters then can be expressed in complex notation by suppressing

the propagator and are as given in following equations [A.4],

$$S_0 = E_x E_x^* + E_y E_y^* \quad \text{A.39.}$$

$$S_1 = E_x E_x^* - E_y E_y^* \quad \text{A.40.}$$

$$S_2 = E_x E_y^* + E_y E_x^* \quad \text{A.41.}$$

$$S_3 = i(E_x E_y^* - E_y E_x^*) \quad \text{A.42.}$$

where $i = \sqrt{-1}$ and * represents the complex conjugate.

The Stokes vector for elliptically polarized light can be written as follows [A.4]:

$$S = \begin{pmatrix} S_0 \\ S_1 \\ S_2 \\ S_3 \end{pmatrix} = \begin{pmatrix} E_{0x}^2 + E_{0y}^2 \\ E_{0x}^2 - E_{0y}^2 \\ 2E_{0x}E_{0y} \cos \delta \\ 2E_{0x}E_{0y} \sin \delta \end{pmatrix} \quad \text{A.43.}$$

The different Stokes vectors for the different degenerate polarization states can be derived by substituting corresponding amplitude as well as δ values to equation A.43. Such derived stokes vectors of the different degenerate states are given by [A.4],

$$\begin{aligned} S_{LHP} = I_0 \begin{pmatrix} 1 \\ 1 \\ 0 \\ 0 \end{pmatrix}, \quad S_{LVP} = I_0 \begin{pmatrix} 1 \\ -1 \\ 0 \\ 0 \end{pmatrix}, \quad S_{L+45P} = I_0 \begin{pmatrix} 1 \\ 0 \\ 1 \\ 0 \end{pmatrix}, \\ S_{L-45P} = I_0 \begin{pmatrix} 1 \\ 0 \\ -1 \\ 0 \end{pmatrix}, \quad S_{RCP} = I_0 \begin{pmatrix} 1 \\ 0 \\ 0 \\ 0 \end{pmatrix}, \quad S_{LCP} = I_0 \begin{pmatrix} 1 \\ 0 \\ 0 \\ -1 \end{pmatrix} \end{aligned} \quad \text{A.44.}$$

where I_0 is the intensity.

The Stokes method as well as polarization ellipse having drawback that just by viewing the polarization ellipse one cannot get information about the polarization states and thus tedious calculations required to determine the new angles of a

polarized beam [A.5] In order to overcome these difficulties Poincaré recommended using a sphere now known as the Poincaré sphere. The Poincaré sphere is a graphical representation of polarized light in a three dimensional space. The Poincaré sphere consists of spherical as well as Cartesian coordinates and is shown in Figure A.5.

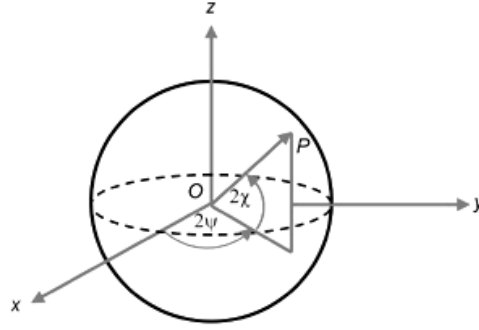


Figure A.5 Representation of the Poincaré sphere in Cartesian and spherical coordinates.

where P is a point on the surface of the sphere. Here x , y , and z are Cartesian coordinate axes, and ψ and χ are spherical coordinates. In a Poincaré sphere the angles are expressed as 2ψ and 2χ . The coordinates ψ and χ are same angles as mentioned in the previous section of the polarization ellipse, which are orientation angle and ellipticity angle respectively.

For a unit sphere the Cartesian coordinates and spherical coordinates are related by the following equations [A.4],

$$X = c \cos(2\chi) c \cos(2\psi), 0 \leq \psi < \pi \quad \text{A.45.}$$

$$Y = c \cos(2\chi) s \sin(2\psi), -\frac{\pi}{4} < \chi \leq \frac{\pi}{4} \quad \text{A.46.}$$

$$Z = s \sin(2\chi) \quad \text{A.47.}$$

where $x^2 + y^2 + z^2 = 1$ for a sphere of unit radius.

By relating Stokes polarization vectors with the orientation angle and the ellipticity angles, (ψ and χ) it is possible to determine the polarization states of the

propagating light. The relation between Stokes parameters and angles, ψ and χ is given by following equations [A.4],

$$S_1 = S_0 \cos(2\chi) \cos(2\psi) \quad \text{A.48.}$$

$$S_2 = S_0 \cos(2\chi) \sin(2\psi) \quad \text{A.49.}$$

$$S_3 = S_0 \sin(2\chi) \quad \text{A.50.}$$

$$\psi = \frac{1}{2} \tan^{-1} \left(\frac{S_2}{S_1} \right), \quad 0 \leq \psi \leq \pi \quad \text{A.51.}$$

$$\chi = \frac{1}{2} \sin^{-1} \left(\frac{S_3}{S_0} \right) \quad -\frac{\pi}{4} \leq \chi \leq \frac{\pi}{4} \quad \text{A.52.}$$

The values of the Stokes parameters (S_1, S_2, S_3), results in a point on the Poincaré sphere. For a propagating wave, the trace that obtained by plotting the continuous values of Stokes polarization parameters visually shows the changes in its polarization state.

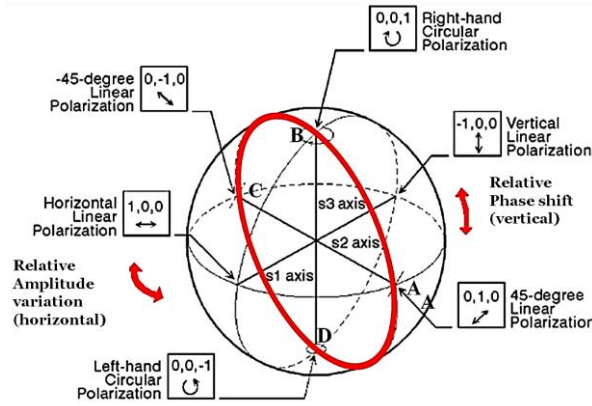


Figure A.6 Visual representation of degenerate state and SOP on the surface of the Poincaré sphere.

For all linear polarization states the trace of Stokes vectors on Poincaré sphere lie on the equator. For right and left circular polarization states the trace of Stokes vectors on Poincaré sphere are either at the north or south poles, respectively [A.4].

The visual representation of degenerate state on the surface of the Poincaré sphere is as shown in Figure A.6. Elliptically polarized states are represented everywhere else on the surface of the Poincaré sphere and the degenerate states are represented at polar / equator of the Poincaré sphere as shown in Figure A.6. In this thesis, a light having SOP 45-degree linear polarization (L+45P) is used as the input light to a polarimetric sensor and any changes in the SOP at the output of polarimetric sensor are analyzed by evaluating the trace of the output SOP on the Poincaré sphere. If a L+45P light undergoes a relative phase shift without any amplitude change, then the corresponding SOP trace of the light will complete a circle as shown in Figure A.6. Such a circle starts from the point A on the equator of the Poincaré sphere and then passes through points, B, C, D which represent degenerate states RCP, L-45P, LCP, respectively as shown in Figure A.6. By extracting the information about the Stokes vectors from the Poincaré sphere trace it is possible to calculate orientation angle and ellipticity angles by using equations A.51 and A.52. The relation of orientation angle and ellipticity angles (ψ and χ) with phase shift ($\delta\phi$) between orthogonal polarization components are represented by equations A.22 and A.23. In this thesis for polarimetric sensor based strain / temperature measurements, a linearly polarized light oriented at an angle 45° is used as input and thus the two orthogonally polarized states are similarly excited. Consequently, equation A.52 can be written as,

$$\sin \delta\phi = \sin 2\chi \quad \text{A.53.}$$

$$\delta\phi = \sin^{-1}(\sin 2\chi) \quad \text{A.54.}$$

The conditions on the angles χ and $\delta\phi$ are and $-\pi/4 \leq \chi < \pi/4$ and $0 \leq \delta\phi < 2\pi$,

respectively.

C. References

- A.1.K. Arun, A. K. Ghatak. "Polarization of light with applications in optical fibers." Vol. 246. SPIE Press, 2011.
- A.2. P. M. Varnham, et al. "Polarimetric strain gauges using high birefringence fibre." Electronics Letters 19.17, 699-700, 1983.
- A.3. T. S. Yu Francis, Y. Shizhuo. "Fiber Optic Sensors." Marcel Dekker Inc., New York ,2002.
- A.4. C. Edward. "Field guide to polarization." Vol. 15. Bellingham, WA: SPIE press, 2005.

Appendix C

Electro-Optic Modulator Based Interrogation for A Polarimetric Fiber*

This paper presents an electro-optic modulator (EOM) as the basis of an interrogation scheme for a polarimetric fiber sensor, used for strain/temperature measurements in the composite materials. In a polarimetric fiber sensor a symmetric deformation effect or temperature etc, lead to phase difference between both polarizations of the fundamental mode [A.5].

For conventional polarizer/analyzer based polarimetric sensor strain/temperature measurements, the linear response range is limited to the quadruple region from $-\pi/4$ to $+\pi/4$ so whenever the phase change is greater than $\pi/2$ radians the relation between the polarimetric sensor output intensity and strain/temperature is no longer linear, as shown in Figure A.7(a). The interrogation scheme presented here involves processing the output of the polarimetric sensor using an EOM. The phase change induced optical intensity variation in the output signal from the polarimetric sensor resulting from applied strain or temperature are nullified by the EOM by control of the EOM applied voltage (V_A) and is as shown in Figure A.7(b). The value of V_A in turn provides information about the applied strain or temperature of the host composite material. The advantage of the EOM interrogation scheme is that the linear the relation between EOM voltage and strain / temperature of the

¹⁶ Manjusha Ramakrishnan, Ginu Rajan, Yuliya Semenova, and Gerald Farrell, “Electro-optic modulator based interrogation for a polarimetric fiber sensor for strain and temperature measurements” Poster Presentation at the photonics Ireland, Belfast, 04-06 September 2013.

polarimetric sensor can be realized for up to a π radians phase change.

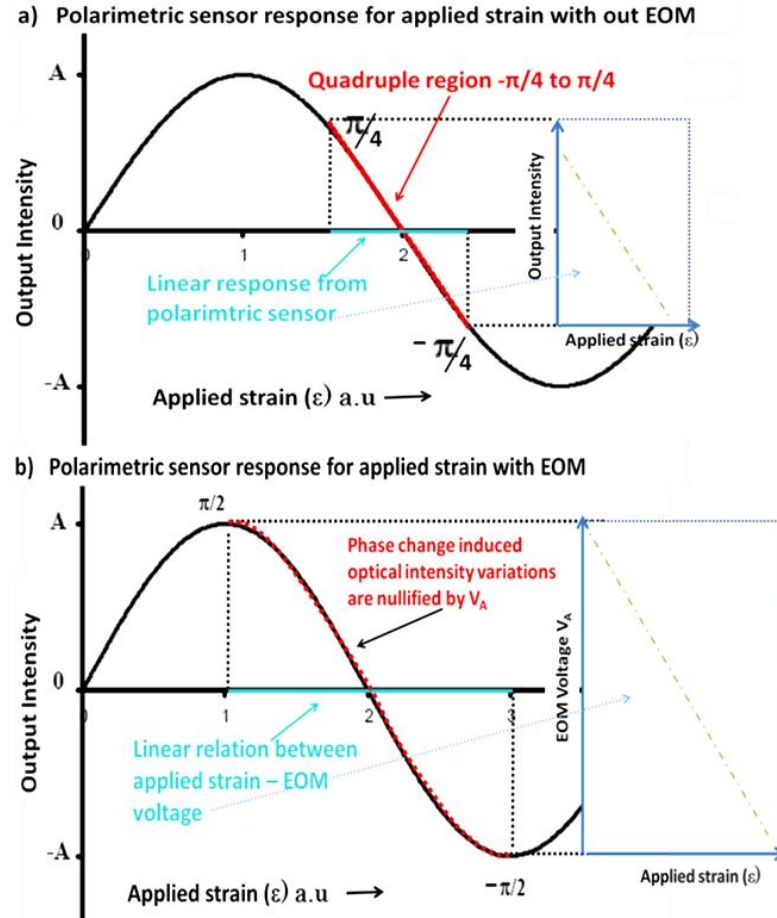


Figure. A.7 (a) polarimetric sensor response without an EOM, and (b) polarimetric sensor response with an EOM.

In addition, the EOM scheme makes it possible to differentiate between the tensile strain and compressive strain, or a decrease or increase of temperature in the composite material. An EOM based scheme was reported earlier for polarimetric sensors working in reflection mode [A.6]. To the best of our knowledge, this is the first time an EOM scheme is demonstrated for a polarimetric sensor for a linear response during the strain/ temperature measurements of composite materials.

During our experimental demonstration, to assure that polarimetric sensors have no phase shift at the constant temperature and at zero applied strain conditions, the initial settings are done by shifting the output intensity of the polarimetric sensor

to the middle of the linear quadruple region. Once the initial setting is done, any positive phase shift observed at the polarimetric sensor output induced by applied strain / temperature is nullified using an applied positive EOM voltage (V_A), having a value which lies within 0 V to $V\pi/2$ V. Also, any negative phase shift is nullified using an applied negative EOM voltage ($-V_A$), having a value which lies within $-V\pi/2$ V to 0 V.

In the case of HB-PM-PCF strain measurements, a linear response for strain versus EOM voltage is for an applied strain from $-4150 \mu\epsilon$ to $+4150 \mu\epsilon$, as. In conclusion this polarimetric sensing system with a linear response to strain has significant potential for sensing in smart composite materials.

References

- A.5. T. R. Woliński, P. Lesiak, and A. W. Domański. "Polarimetric optical fiber sensors of a new generation for industrial applications." *Technical sciences* 56.2, 2008.
- A.6. R. Claverie, et al. "New versatile and linear optical sensor based on electro-optical modulation and compensation." *Review of Scientific Instruments* 79.12: 123103, 2008.

Appendix D

Composite Materials with Embedded Optical Fiber Sensors for in Situ Structural Health Monitoring*

Keywords: Fiber optic sensors, composite materials, hand lay-up method, embedded sensors

Abstract: In paper presents experimental results on strain and temperature measurement by fiber optic sensors embedded in composite materials for the purpose of in-situ structural health monitoring. The objective of this study was to determine the optimal position for the placement of an optical fiber sensor in a multi- layer composite structure to obtain efficient strain transfer and accurate temperature measurement and also to study the influence of the hardness of the composite material on the strain and temperature response of the embedded optical fiber sensor. A novel hybrid fiber optic sensing system is used which combines two optical fiber sensors, a polarimetric sensor based on a photonic crystal fiber (and a Panda fiber in the second case) and a fiber Bragg grating sensor (FBGs). The advantage of using this hybrid approach is that it is possible to monitor strain and temperature simultaneously within the composite structure. Several samples of fibre glass reinforced composites are fabricated by the hand lay-up method. Two

* Manjusha Ramakrishnan, Ginu Rajan, Yuliya Semenova and Gerald Farrell," Composite materials with embedded optical fiber sensors for in situ structural health monitoring", Proceedings of WICSM 2010, 22-24 September 2010, Dublin, Ireland

different reinforcing fiber ply configurations are considered, 0/0 and 0/45 and the optical fiber sensors are embedded at different layers in each configuration. A number of fiber glass reinforced composite material structures with different hardness are fabricated by using different resins such as general purpose resin Polyester and Encore. The fabricated structures are subjected to different loading conditions with an applied strain of up to 4,000 $\mu\epsilon$ and a temperature range from 0 to 70 $^{\circ}\text{C}$. The strain and temperature response of the fiber optic sensors embedded at two distinct layers, in two different composite materials and two ply configurations of multi-layer composite structures are presented.

A. Introduction

Smart composite structures with embedded fiber optic sensors have a wide range of applications due to their in-situ health monitoring capability. The laminated composite material comprises several layers, each of which contains continuous reinforcing fibers moulded using homogenous, linearly elastic materials such as resin/ epoxy [A.7]. The embedded optical fiber sensors within these structures can measure stain and temperature, which can provide valuable information regarding deformation and aging of these materials. However, the accuracy of measurement of these parameters depends on the placement of the optical fiber in the multilayered structure, the material hardness and the orientation of reinforcing fibers within the composite layers. In this part of thesis we present an investigation of sensor response by embedding sensors in various layers and 0/0, 0/45 fiber reinforcing ply configurations by using two types of general purpose resin Encore 30 and Firepel K-130 polyester. weI present a new method for simultaneous strain and temperature measurement by using a hybrid approach which combines two

types of sensors: highly birefringent polarimetric fiber sensors; a Panda fiber and HB-PM-PCF sensors and FBG sensors [A.8].

B. HB-PM-PCF-FBG hybrid sensor

In a polarimetric sensor, symmetric deformation influences the propagation constant for every mode because of the changes in fiber length and the refractive indices of the core and the cladding, which leads to changes in the phase difference between the two polarizations of the fundamental mode [A.9]. In the FBG sensor the Bragg wavelength shifts arise due to both applied strain and temperature [A.10]. The two types of polarisation maintaining (PM) fibers used in the polarimetric sensing system are Panda fiber and HB-PM-PCF. In the case of the Panda fiber both temperature and strain lead to a phase difference between both polarizations of the fundamental mode LP_{01} [A.9], while in the case of HB-PM-PCF the phase difference arises only from strain, since HB-PM-PCF fibers are proven to be temperature insensitive. In applications where localized strain and temperature information is needed, multiple FBG sensors can be used in addition to the polarimetric sensors, to obtain a combined temperature and strain information. The polarimetric sensors measure average strain and temperature, whereas the FBG sensors measure localized strain and temperature. The influence of temperature on the FBG sensors can be eliminated by using the temperature information from the polarimetric sensor assuming that temperature is constant across the sample. Consequently these two types of sensors work in a complimentary manner to provide localized and average strain and temperature information for the composite material.

C. Composite fabrication

Samples have been prepared with two types of general purpose liquid resin Encore 30 and Firepel K130 polyester having viscosity 230 cps and 400 cps, and with specific gravity at 25⁰ C, of 1.09, and 1.29 respectively.

The fibre glass reinforced composites are fabricated by the hand lay-up method. During the sample preparation a 2D fabric sheet is laid on the top of an epoxy resin layer and this process is repeated for multiple layers. To embed optical sensors a pre-strain is applied to the optical fibers positioned between the composite layers. To protect these optical sensors from external perturbations and to avoid breakage during the fabrication process at least one layer of 2D fabrics and epoxy is applied on the top of the layer with the optical sensor. The fabricated composite material sample was 215 mm long, 40 mm wide and 1.8 mm thick. Each sample consists of 8 layers and all the three above mentioned types of fibre sensors embedded inside the composite structure 5 mm apart from each other, in the second and the third composite layers (Figure A.8.) of 0/0 and 0/45 fiber ply configurations.

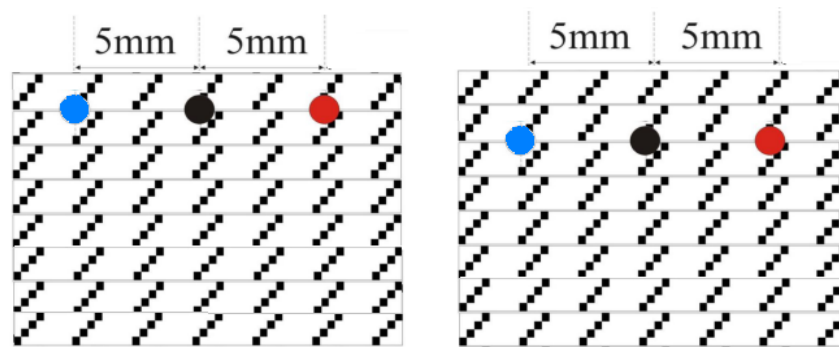


Figure A.8. Multilayer composite layout



Figure A.9. Fabricated composite samples with embedded sensors.

D. Experimental arrangement

The polarimetric sensor is fabricated from Panda fiber (PM-1550 HP) and HB-PM-PCF (PM 1550-01). A laser source at a wavelength of 1550 nm is used as an input source. The strain sensitivity of the polarimetric sensors is measured using a polarimeter and polarization control system, TXP 5004. The schematic of the hybrid sensor using polarimetric sensors and FBG sensors is as shown in Figure A.10. To introduce strain in the composite material sample a force is applied in the middle region to bend the sample as shown in Figure A.11. The average strain experienced by the sample is calculated analytically [A.11].

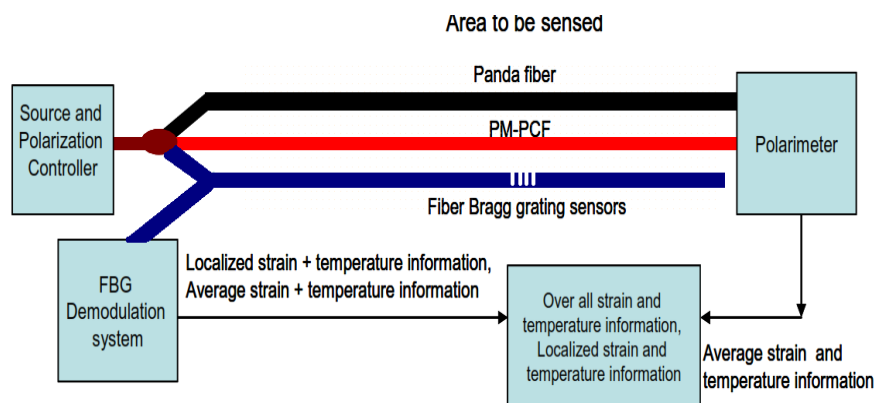


Figure A.11. Schematic of the hybrid sensor using polarimetric sensors and fiber Bragg grating sensors

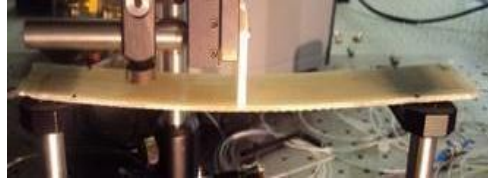


Figure A.11. Experimental setup to apply strain to the composite material

E. The strain and temperature sensitivity analysis

a) Strain analysis

In the polarimetric sensor, strain induces polarization variation measured by the polarimeter. The Poincare sphere graphically represents the polarization transformations. The Poincare sphere is a graphical tool in real, three dimensional space in which the polarization can be uniquely represented by a point on or within a unit sphere centered on a rectangular (x,y,z) coordinate system. The coordinates of the point are the three normalized Stokes parameters describing the state of polarization [A.11]. Because a state of polarization is represented by a point, a continuous evaluation of polarization can be represented as a continuous path on the Poincare sphere. Thus strain and temperature response of the polarimetric sensor can be drawn out by the evaluation of the Poincare sphere. For example, if the strain and temperature applied to obtain one complete circular path Poincare sphere i.e., 2π radians, the strain and temperature sensitivity can be measured.

In this part of thesis the convention employed to label the samples used involved specifying in a fixed order: the material ply configuration plus the number of the layer with an embedded optical fiber sensor in brackets. For example, a sample prepared from a Polyester general purpose resin, fabricated in 0-0 ply configuration with optical fiber sensor embedded in the third layer is labeled as Polyester 0/0 ply(3).

The HB-PM-PCF used was 15.5 cm long and the ends were spliced to standard

single mode (SM-28) fibers using a conventional fusion splicer. The samples are subjected to strain of up to 4000 $\mu\epsilon$. The strain induced phase difference is measured from the Poincare sphere of the polarimeter as shown in Figure A.12 and Figure A.13 respectively. The strain applied to obtain 2π variation in the Poincare sphere is measured to determine strain sensitivity of the samples. It has been observed that the HB-PM-PCF strain sensitivity is less than that of a Panda fiber as shown in Figures A.12, A.13 and in Table A.1.

The localized strain information is obtained from FBG sensors with a length of 10 mm embedded in the centre of the composite, where applied strain is maximum. The peak wavelengths of the FBGs used are 1560 nm for Polyester 0/0 ply (3) and 1550 nm for Polyester 0/45 ply (3) configurations. The results are as shown in Figure A.14.

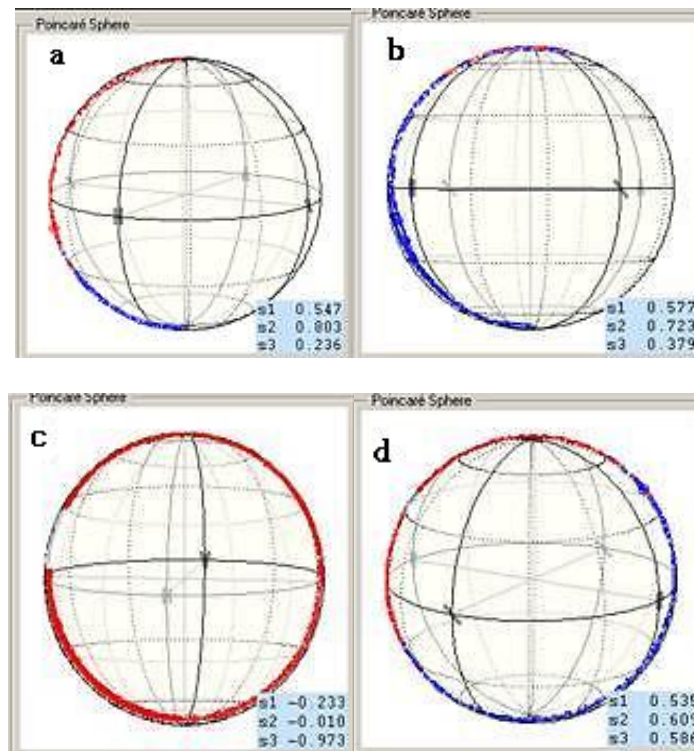


Figure A.12. Observed phase change in the Poincare sphere for Panda fibres with applied strain of 1500 $\mu\epsilon$ (a) Encore- 0/0 ply(3); (b) Polyester-0/45 ply(3); (c) Polyester 0/0 ply(3);

and (d) Polyester 0/0 ply(2)

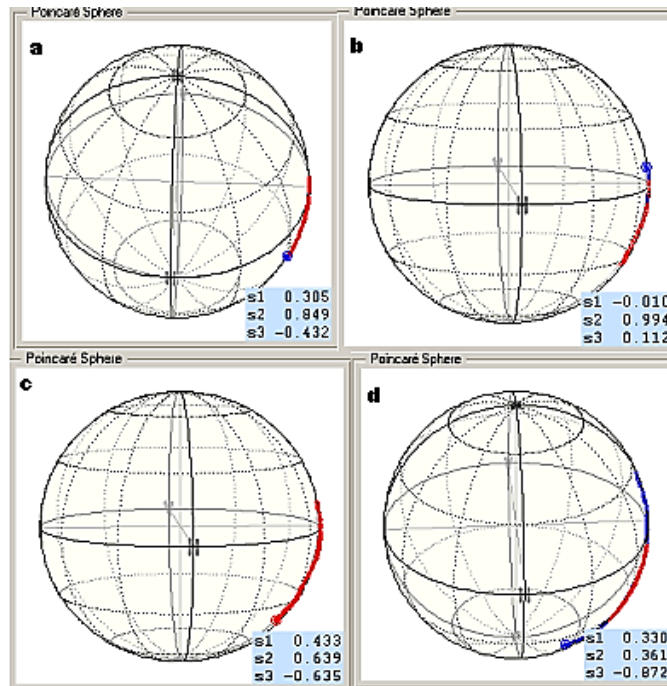


Figure A.13. Observed phase change in the Poincare sphere for PCF fibres with applied strain of 1500 $\mu\epsilon$; (a) Encore 0/0 ply (3), (b) Polyester 0/45 ply (3), (c) Polyester 0/0 ply (3), (d) Polyester 0/0 ply (2).

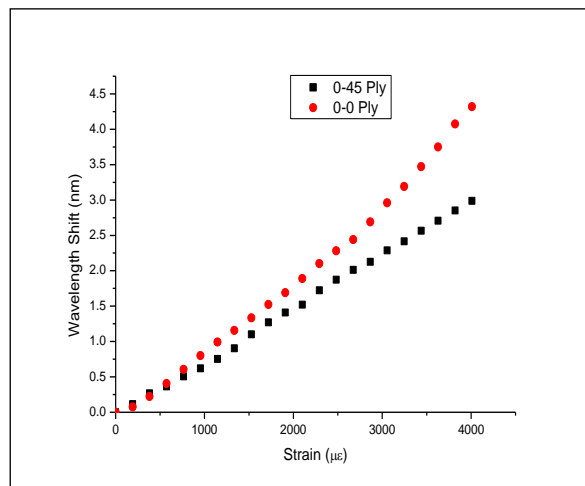


Figure A.14. Measured FBG wavelength shift with applied strain for different ply configurations

b) Temperature analysis

In the Panda fiber based polarimetric sensor both temperature and strain induce polarization variations. To analyze temperature sensitivity the Panda fiber samples are subjected to temperature variations without applying any strain. The temperature applied to achieve 2π rotation in the Poincare sphere is used to evaluate temperature sensitivity of the samples.

The HB-PM-PCF are found to be temperature insensitive [A.12], with small fluctuations as shown in Figure A.16, which arise due to the temperature sensitive nature of the acrylate coating of the HB-PM-PCF fibers. A complete temperature independence can be obtained by using a buffer stripped HB-PM-PCF. Thus, by cross evaluating the HB-PM-PCF and Panda fiber sensor responses the strain induced variation can be nullified for a Panda fiber based polarimetric sensor, and the average temperature information of the composite samples can be obtained.

The Panda fiber polarimetric sensor results are shown in Figure A.15.

By embedding FBGs with different peak wavelengths at different positions in the composite sample the localized temperature is obtained. In the present samples FBG is embedded at the centre of optical fiber sensor layer. The samples are subjected to temperatures from 0 °C to 70°C at an interval of 5 °C. The results are as shown in Figure A.17.

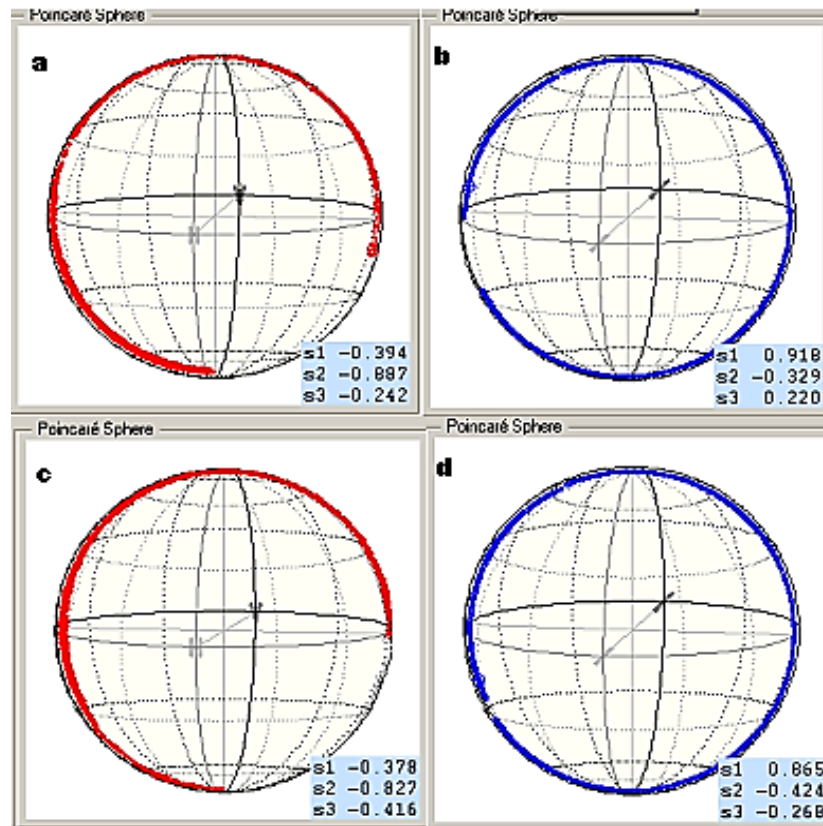


Figure A.15. Observed phase change in the Poincaré sphere for Panda fibres for temperature variation from 0 °C to 45 °C (a) Encore 0/0 ply (3); (b) Polyester 0/45 ply (3); (c) Polyester 0/0 ply (3); and (d) Polyester 0/0 ply (2).

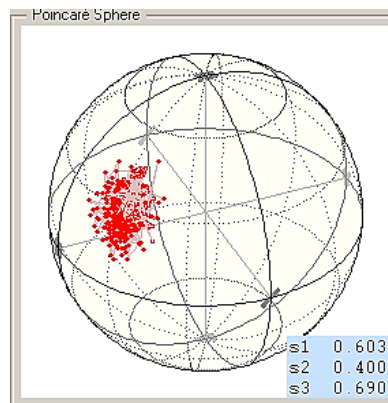


Figure A.16. Temperature response of the HB-PM-PCF fiber polarimetric sensor

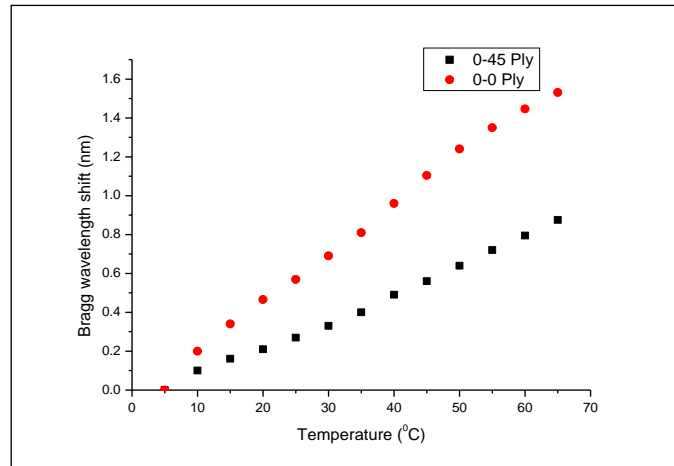


Figure A.17. Measured FBG wavelength shift with applied temperature for different ply configurations

F. Results and discussions

Composite samples with the optical fiber sensors in the second layer show the maximum compressive strain response and temperature response, due to the fact that the strain and temperature gradually increase in the direction from the middle layer towards the top layer [A.12]. Moreover, material stiffness also alters the effective strain transfer, due to Poisson mismatch between layers [A.13]. The 0/45 angle ply laminate structure offers no Poisson mismatch and maximum shear coupling [A.14]. Thus material stiffness, ply orientation and placement layer of embedding fiber play vital role in the overall strain and temperature response of the composite structure as shown in Tables A1 and A.2. From the samples tested the FBG sensor shows a linear variation with strain and temperature. Moreover, the variation in the slope indicates that the transfer of applied strain and temperature in to the embedded FBG sensor also varies with the composite ply configuration.

Table A.1. Comparison of strain sensitivity of the composite samples

Material	Ply	Number of the layer with embedded fiber sensor	Strain sensitivity, radians/mε	
			PCF	PANDA
Polyester	0/0	2	0.4405	3.1306
Polyester	0/0	3	0.3712	2.7074
Polyester	0/45	3	0.3141	2.3479
Encore 30	0/0	0	0.2798	2.0515

Table A.2. Comparison of temperature sensitivity of the composite samples

Material	Ply	Number of the layer with embedded fiber sensor	Temperature sensitivity of PANDA fiber, radians/°C
Polyester	0/0	2	0.1378
Polyester	0/0	3	0.10827
Polyester	0/45	3	0.1231
Encore 30	0/0	0	0.1185

G. Conclusions

From the tested samples the following concluding remarks can be summarised as follows: the maximum strain and temperature response is achieved by embedding optical fiber sensors in the top layer or bottom layers of the multi-layer composite structure. The ply configurations play remarkable role in the applied strain and temperature transfer to the optical fiber sensor, since the fiber reinforcement direction has a great effect on the composite material mechanical properties. The stiffness of the composite material is also important since the mismatch between composite laminate structures yields inefficient strain and temperature transfer to the region with embedded sensor, consequently giving inaccurate strain and

temperature information. The difference in sensitivity of the optical sensor varies from 0 to 30% due to material hardness and ply configurations.

F. References

- A.7. S. R. Reid, Stephen Robert, and Gang Zhou, eds. Impact behaviour of fibre-reinforced composite materials and structures. Elsevier, 2000.
- A.8. K. O. Hill, M. Gerald. "Fiber Bragg grating technology fundamentals and overview." Journal of lightwave technology 15.8: 1263-1276, 1997.
- A.9. T. R. Woliński,, P. Lesiak, A. W. Domański. "Polarimetric optical fiber sensors of a new generation for industrial applications." TECHNICAL SCIENCES 56.2, 2008.
- A.10. T. L. Yeo,, T. Sun, K. T. V. Grattan. "Fibre-optic sensor technologies for humidity and moisture measurement." Sensors and Actuators A: Physical 144.2: 280-295, 2008.
- A.11. D. H. Kim, J. U. Kang. "Analysis of temperature-dependent birefringence of a polarization-maintaining photonic crystal fiber." Optical Engineering 46.7 : 075003-075003, 2007.
- A.12. C. Edward. "Field Guide to Polarization, SPIE Field Guide vol. FG05.", 2005.
- A.13. A.W. Domanski, et al. "Comparison of Bragg and polarimetric optical fiber sensors for stress monitoring in composite materials." Acta Physica Polonica-Series A General Physics 116.3 : 294, 2009.
- A.14. M. Grassi, Z. Xiang M. Michele. "Prediction of stiffness and stresses in z-fibre reinforced composite laminates." Composites Part A: applied science and manufacturing 33.12 : 1653-1664, 2002.

- A.15. E. S. Ardic, C. Bolcan, A. Kayran. "A method of strain and stress analysis for failure prediction in laminated composites." Proceedings of the Institution of Mechanical Engineers, Part G: Journal of Aerospace Engineering 209.1 : 43-51, 1995.

